2019

FATIGUE CRACK GROWTH OF RECYCLED RUBBER IN NATURAL RUBBER/BUTADIENE RUBBER BLENDS

Binti Abang Ismawi Hassim, Dayang Habibah

UNIVERSITY OF PLYMOUTH

FATIGUE CRACK GROWTH OF RECYCLED RUBBER IN NATURAL RUBBER/BUTADIENE RUBBER BLENDS

by

DAYANG HABIBAH ABANG ISMAWI HASSIM

A thesis submitted to the University of Plymouth in partial fulfilment for the degree of

DOCTOR OF PHILOSOPHY

School of Engineering, Computing and Mathematics

September 2019

Abstract

Fatigue Crack Growth of Recycled Rubber in Natural Rubber/Butadiene Rubber Blends

By

Dayang Habibah Abang Ismawi Hassim

Ground rubber from waste tyres may be added to elastomers to provide economic and environmental benefits. Both untreated and treated fillers have been investigated in different types of virgin rubber matrix. A principal concern is their crosslinked structure and large particle sizes. These additional fillers introduce flaws corresponding to micro-crack initiation sites especially under dynamic loading. Smaller particles, incorporated at a suitable concentration, may alleviate reduction of key mechanical properties.

Many studies involving recycled rubber powder (RRP), untreated or treated materials, focus mainly on the quasi-static mechanical properties; generally few works examine the fatigue life and fracture morphology. In this study, two different RRPs: (i) crumb rubber powder (denoted as CRP400 ~400 µm nominal diameter) and (ii) micronised rubber powder (denoted as MRP074 ~74 µm nominal diameter), from ambient and cryogenic production respectively, were characterised. The effect of RRP on the cure characteristics, mechanical properties (tensile strength, crescent tear, and abrasion resistance) and fatigue crack growth (FCG) were studied in Natural Rubber (NR)/Butadiene Rubber (BR) blends. This study includes a filler-matrix interface study using 'network visualisation' via transmission electron microscopy of the unfilled NR or BR matrix (without carbon black filler). Lorenz-Park, Cunnen and Russel, and Kraus equations based on an equilibrium swelling study were used to investigate the extent of interaction between RRP and rubber matrix. The study provides understanding of the adhesion between filler-rubber matrices, which partially contributed to the crescent tear strength.

For fatigue crack growth performance, the energy balance approach for the crack growth analysis could provide a better approach for RRP evaluation. Determination of absolute and relative hysteresis loss during FCG testing was conducted under constant displacement amplitudes, while compensating for permanent set throughout the fatigue cycles. Different trends in relative hysteresis loss suggest that an additional energy dissipation mechanism due to multiple new crack surfaces at the crack tip contributes to the FCG of the RRP. Higher

absolute and relative hysteresis loss, at higher tearing energy, are slightly detrimental to the crack growth rates of the RRP compounds. Fracture morphologies at different tearing energies for NR/BR and RRP filled compound were discussed. Differences in the surface fracture topography at various tearing energies revealed the dependency of the crack growth microstructure on the tearing energies. The different rankings were displayed for MRP074 or CRP400 filler using conventional rubber test standards and fracture mechanics. Although the average CRP400 particle diameter is approximately a factor of five larger than that of MRP074, the CRP400 compound exhibits a lower crack growth rate in the technically important low strains/tearing energies region. The “rougher”/irregular surface of CRP400 appears to be a more important factor than the particle size of MRP074 for the FCG performance, especially at lower strains. The findings offer a different approach in evaluating RRP for application in the elastomeric matrix.

Acknowledgements

First and foremost, Thank you and Alhamdullilah to Allah (S.W.T) for granting this opportunity and with His provision the strength, patience and motivation to complete this thesis. I gratefully acknowledge the funding received towards my PhD from Malaysian Rubber Board (MRB), Malaysia. I'm highly indebted to my former Director of Technology and Engineering Division and currently Director General (DG) of MRB, Dato' Dr. Zairossani Md Nor for his encouragement to pursue this PhD study and Deputy DG (Research and Development), Dr. Amir Hashim for his support. To former TARRC CEO, Dato' Dr. Kamruddin Malek and current CEO, Dr. Fauzi Md Som, thank you to access facilities described in this thesis and accommodation at TARRC. I would like to extend thanks to Dr. Stuart Cook, the Director of Research of TARRC with suggestions and technical discussion on 'network visualisation' technique.

I would like to express my sincere gratitude to my director of studies, Dr. Frank Abraham for introducing new area of studies for my PhD study, his time, support, guidance, discussion and patience throughout completing my thesis. Equally, I am grateful to my second supervisor, Prof. Dr. John Summerscales who actively involved in the technical discussion and also his patience in correcting my paper and thesis. I also appreciate technical advice and some discussion from my third supervisor Paul Brown.

The facilities and compounding materials for the present research work provided by Tun Abdul Razak Research Centre (TARRC), Hertfordshire, UK, MRB, Malaysia and School of Engineering, University of Plymouth (UoP). My deep appreciation also to Paul Gladwin, Kenneth Halls, James Sandilands, Jonathan Clark, Jaymini Patel, Jean-Louis Poisson, Vincenzo Orlando, Robert Picken and Che Muhd Firdaus Che Mat (crosslink density experiments) for all their help on some of the experimental work.

Many thanks to Dr. Andy Chapman for some technical discussions, Charles, Sarah, Cath, Ruth & Glynis for physical testing, Dr. Robin Davis and Kathy Lawrence for microtome and transmission electron microscopy work, Collin Hull for composition analysis. Other staffs from TARRC, MRB, UoP, Global Testing and Consultancy for Rubber ($GTAC_R$), MRB who contribued to some part of my thesis were also acknowledged.

I would like also to extend my thanks to my fellow PhD students, Sahar, Fan, Rabiu, Mohamed and Muhsin; former post-graduate students, Toshi, Bin Yang and Huang for their friendship.

The help and support from various technical laboratory personnel of the School of Engineering and Plymouth Electron Microscopy Centre (PEMC), UoP is also appreciated. Many thanks go especially to Terry Richards for his continuous support and help for the lab work in particularly fatigue testing. Thanks also to Sam Thorpe, Bob Williams, Dr. Richard Cullen, Neil Fewings, Pete Bond and Glenn Harper for their kind support.

I am deeply thankful for all the help from Norain Tyler and family, her food and company during my stay in Hertfordshire. Not forgetting to my other lovely friends in Hertfordshire, Umar and family, Sarah and Zalia. All have made my short stay in Hertfordshire, busy but cheerful.

For my former program head and also as my dearest friend, Mazlina: Thank you for staying in touch and being very supportive. My thanks also go to my Malaysian friends and other PhD colleagues in the UK especially, Iskandar, Teku, Rohaidah, Salina, Suhawati and Rohani who were always helpful in numerous ways.

To my Malaysian friends in Plymouth, especially Kak Ros and family, An and family, Azie, Quin, Anis, Hana, Huda and all their family. Thank you all especially during festive gathering, lovely food and friendship during our stay in Plymouth.

Finally, the most important is appreciation to my family: my parents, sisters and brother as well as to my in-laws for their prayers, love and support. To my husband for his love, continued patience, sacrifice and endless support throughout this study is immensely appreciated. May Allah bless you! My dearest children, Aliya, Ariff, Aisyah and Afiq, who give me challenge, sad and fun at the same time, thank you for being very patient. I love you all!!!

Author's declaration

At no time during the registration for the degree of *Doctor of Philosophy* has the author been registered for any other University award without prior agreement of the Doctoral College Quality Sub-Committee.

Work submitted for this research degree at the University of Plymouth has not formed part of any other degree either at the University of Plymouth or at another establishment.

I declare that this thesis has been presented is based on my own original work except as specified in the acknowledgement. This research work has not been submitted, in whole or in part, in any previous application for a degree. Any literature or figures from work of others are explicitly referenced within this thesis.

Word count of main body of thesis: 42000

DAYANG HABIBAH ABANG ISMAWI HASSIM

Signed:……...

Date:……..

Conference/Poster proceedings/Journal

- Mechanical and fatigue properties of rubber compounds containing rubber powder made from waste tyres. Postgraduate society conference series 5th December 2016 at University of Plymouth (oral presentation)
- Mechanical, dynamic and morphology properties of Natural rubber (NR)/Butadiene rubber (BR) blends with recycled rubber powder. Poster presentation KHK2016, 22-24th November, 2016 at Hannover, Germany
- Presentation on "Fatigue Properties and Fracture Morphology of Micronised Rubber Powder (MRP) from Waste Tyres in unfilled Elastomer", 2018 2nd European Conference on Materials, Mechatronics and Manufacturing (ECMMM 2018), February 10-12, 2018 Krakow, Poland
- Abang Ismawi Hassim, D. H., Abraham, F., Summerscales, J. and Brown, P. (2018). "Fatigue Properties and Fracture Morphology of Micronised Rubber Powder (MRP) from Waste Tyres in Unfilled Elastomers," *International Journal of Materials, Mechanics and Manufacturing* vol. 6, no. 4, pp. 281-285.
  DOI: http://dx.doi.org/10.18178/ijmmm.2018.6.4.392
  PEARL (OA): http://hdl.handle.net/10026.1/11429
- Abang Ismawi Hassim, D. H., Abraham, F., Summerscales, J. and Brown, P. (2018). Oral Presentation on **"**The influence of tyre fine waste particles as filler in elastomer matrix, on tear strength, abrasion and interface morphology**",** RubberCon2018, 10-11 May 2018, Intercontinental Istanbul, Turkey.
- Abang Ismawi Hassim, D. H., Abraham, F., Summerscales, J. and Brown, P. (2018). Abrasion resistance and fatigue crack growth independence of recycled tyre filler content and the interface morphology, Paper conference, Presented by Dr. Frank Abraham, 13th Fall Rubber Colloquium, Hannover, Germany, November 6-8.
- Abang Ismawi Hassim, D. H., Abraham, F., Summerscales, J. and Brown, P. (2019). The effect of interface morphology in waste tyre rubber powder filled elastomeric matrices on the tear and abrasion resistance, Express Polymer Letters, 13(3), pp. 248-260.
  DOI: http://dx.doi.org/10.3144/expresspolymlett.2019.21
  PEARL (OA): http://hdl.handle.net/10026.1/13003

Table of Contents

List of Figures

List of Tables

Abbreviations and Acronyms

6PPD	N-1,3-dimethylbutyl-N’ phenyl-p-phenylenediamine
BET	Brunauer–Emmett–Teller
BIIR	Bromobutyl rubber
BR	Polybutadiene rubber
BS	British standard
CB	Carbon black
CIIR	Chlorobutyl rubber
CR	Chloroprene rubber
CRP400	Crumb rubber powder (nominal particle size 400 μm)
dia	Diameter
DMFC	DeMattia flex cracking
DBP	Di-n-butyl phthalate/ dibutyl phthalate
DPDS	Diphenyl Disulphide
EB	Elongation at break
ELVRT	End Life Vulcanised Rubber Tyres
ELVR	End Life Vulcanised Rubber
ELT	End-of-life tyres
EPDM	Ethylene-Propylene-Diene Polymer
EU	European Union
FCG	Fatigue crack growth
FTFT	Fatigue-to-Failure Tester
FTIR	Fourier Transform Infrared
GTR	Ground tyre rubber
GRP	Ground rubber powder
HAF	High-abrasion furnace carbon black
HPHTS	High-pressure high-temperature sintering
IIR	Isobutylene-isoprene rubber/ butyl rubber
ISO	International Organisation of Standardisation
JIS	Japanese Industrial Standard
LSCM	Laser Scanning Confocal Microscope
MRP074	Micronised rubber powder (nominal particle size 74 μm)
NR	Natural rubber

NBR	Acrylonitrile-butadiene rubber/Nitrile rubber
N234	Carbon black grade (Intermediate Super Abrasion Furnace-Low Structure)
NR/BR	Blend Natural rubber and Butadiene rubber
pphr	Parts per hundred of rubber
RRP	Recycled rubber powder
RP	Recycled powder
ROI	Region of interest
SEM	Scanning Electron Microscope
SMR	Standard Malaysian Rubber
SENT	Single-edge Notched Tensile specimen
SBR	Styrene Butadiene Rubber
SIC	Strain induced crystallisation
SSSE	Solid-state shear extrusion
TARRC	Tun Abdul Razak Research Centre
TBBS	N-tert-butyl-2-benzothiazole sulphenamide
TEM	Transmission electron microscopy
TGA	ThermoGravimetric Analysis
TMTD	Tetramethly thiuramdisulphide
TMQ	2,2,4-trimethyl-1,2-dihydroquinoline
uv	Ultraviolet
t_{95}	Cure time
t_{s2}	Scorch time

Nomenclature (list of symbols)

a, b, C, m	Constant (Chapter 7)
C_f	Concentration of recycled rubber powders (Chapter 5)
c	Crack length
ν_c	Crosslink density (Chapter 2)
dc	Increment in crack length
dc/dN	Crack growth rate per cycle
ρ	Density of recycled rubber powders (Chapter 5)
ρ_s	Density of solvent
ρ_p	Density of polymer
λ	Extension ratio
F	Force applied (N)
F_{min}	Minimum force/load
Hy	Hysteresis
H_r	Relative hysteresis
H_{abs}	Absolute hysteresis
k	Constant (function of strain)
kc	Kilocycles
M100	Modulus at 100% elongation
M_H	Maximum torque
M_L	Minimum torque
M_{tot}	Total mass of all ingredients including rubber for each compound/formulation (in pphr) – Chapter 5
M_H- M_L	Torque difference
ΔM	Torque difference
ML(1+4)	Mooney viscosity after 1 minute preheating and 4 minutes testing, measured with a large rotor
MU	Mooney units
1/Q	Apparent crosslink density
Q	Swelling value/index
Q_f	Swelling value for filled rubber compound
Q_g	Swelling value for gum/unfilled rubber compound
T	Tearing energy (kJm^{-2})

T_{tot}	Total volume of all ingredients including rubber for each formulation
T_c	Catastrophic tearing energy (Chapter 3)
Tg	Glass transition temperature
Tan δ	Loss factor
T_0	Threshold tearing energy at initiation
T_z	Threshold tearing energy at initiation, unproctected (no antiozonants)
tM_H	Time at maximum torque
t_{95}	Time at 95% of the maximum torque rise
t_{s2}	Time for torque to rise 2 units above M_L
U_a	Total work done under cyclic loading
U_s	Total work done under cyclic unloading (from load (N) *vs* displacement curve)
σ	Stress (MPa)
ε	Strain
ε	Dynamic strain amplitude (Chapter 8)
$\dot{\varepsilon}$	Strain rate (Chapter 8)
V_r	Volume fraction of rubber in swollen gel
V_{ro}	Volume fraction of rubber in unfilled/gum compound
V_{rf}	Volume fraction of rubber in filled compound
η	Viscosity
w	Initial mass of sample (before swelling)
w_1	Swollen vulcanisates (after swelling)
w_2	Deswollen vulcanisates (Dried sample)
W_{min}	Energy at the minimum load level
W	Strain energy density/Elastic energy (Chapter 3 and Chapter 8)
W_t	Total energy (Chapter 8)
t	Time (Chapter 8)
W_a	Work of deformation for a unit volume (cyclic loading)
W_s	Work of deformation for a unit volume (cyclic unloading)
ø	Volume fraction of filler
z	weight fraction

Chapter 1 Introduction

1.1 Background

Rubber has a predominant role in our daily life from general rubber to industrial rubber goods. Rubber products are made up of elastomers, commonly a mixture of natural and/or synthetic rubber, filler, plasticisers and a variety of chemical additives depending on the application. To combine the entire ingredients into a useful product, a vulcanisation process is necessary. "Vulcanisation is defined as the process of rubber crosslinking normally in the presence of heat utilising mostly sulphur or sulphur containing compound, an irreversible process discovered by Charles Goodyear in 1839" [1,2]. After the crosslinking process, the uncured rubber changes to an elastic state, which gives rubber its typical properties including, flexibility, strength, impermeability to gases and resistance to abrasion, chemical action, heat and electricity. As such, vulcanised rubber blends of Styrene Butadiene Rubber (SBR) with Butadiene Rubber (BR) or SBR with Natural Rubber (NR) exhibit high frictional properties which are indispensable for tyre applications.

Despite the benefit of a cross linked structure, a key issue is that it is not biodegradable even when buried in soil. Another challenge is that vulcanised rubbers are highly complex engineering structures comprised of many dissimilar materials. Each product possesses different properties. Rubber as a raw material is blended or compounded with other materials, including synthetic polymers, to meet the needs of different applications [3]. One manufacturer may produce various products of different composition. Currently, there is no ideal single process to break down vulcanised rubber to its original form. This creates a tremendous problem in waste disposal and rubber recycling at the end of the service life of a rubber component.

The increasing use of rubber in many applications results in a growing volume of rubber waste. The disposal of waste automotive tyres in particular is an increasing environmental problem worldwide due to the ever increasing numbers of vehicles on the road. Figure 1-1 shows that major uses for vulcanised rubber are vehicle tyres, tubes and conveyor belts, which taken together, make up about 72% of all production [3]. According to statistics, about 26 million tonnes of rubber were produced in year 2015 [4], about 60% devoted to making

vehicle tyres. On the other hand, it is also estimated that 800 million tyres are discarded around the world annually and this figure is expected to increase by 2% every year [2,5]. Elsewhere, statistics predicting over one billion waste tyres generated per year have been reported [6,7].

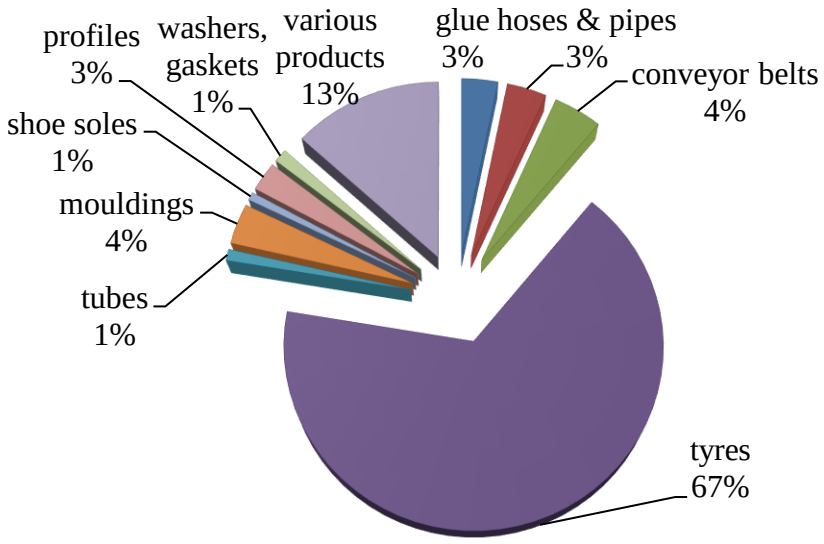

Figure 1-1 Distribution of Rubber Production by Product Group [3].

To address the problems associated with tyre waste, recycling and reclaiming has been a subject of interest for some time and is seen as the preferred method compared to other methods of disposal. Inclusion of rubber powder made from End of Life Vulcanised Rubber tyres (ELVRT) into new rubber products will be of significant environmental and economic benefit, provided it does not considerably affect the quality of the product. Throughout this work, ELVRT is used interchangeably with ground tyre rubber (GTR), rubber powder (RP), crumb rubber powder (CRP), end-of-life tyres (ELT), recycled rubber powder (RRP) or recycled rubber (RR) which are normally found in other literature. However, it is also recognised that the rubber compounds produced by traditional recycling methods have inferior mechanical properties compared to new rubber. During the reclaiming process, apart from breaking sulphur-crosslinks, the main polymer chains are also broken down which affects the quality of the recycled rubber [8]. In other cases, surface modifications of the ELVRT might be necessary to enhance the adhesion between the ELVRT and other polymer

matrices. At present, on-going research seeks innovative techniques of surface treatments in order to improve the key properties of materials containing ELVRT.

To date, most rubber or non-rubber companies are able to produce ground rubber from tyre waste but the main issue is relatively low quantities being used in the manufacturing of new high performance products or re-used in new tyres. The targeted amount of recycled content added into tyres is from 5%-10% without deteriorating the tyres' original properties [9,10], whereas for non-tyre applications, the tolerated amount maybe up to 25% [10]. Blumenthal [9] also reported that the use of more than 5-10% of recycled content material in new tyres resulted in a product exhibiting greater heat build-up which increased the energy dissipation and consequently increased rolling resistance. This increases fuel consumption and could cause the tyre to wear faster which limits its usage. Therefore, current applications are mainly into secondary products such as asphalt, aggregate for cement, flooring materials, footwear, athletic and recreational materials, such as running tracks and playground surfaces, dock bumpers, patio decks and railroad crossing blocks [11]. The often poor quality of the existing recycled rubber powder restricts its use in more dynamic applications such as body seals, bushings and gaskets for non-tyre applications and also as a filler in new tyres [10]. This implies a need for more research to create advances in technology towards properties improvement.

Intensive research [12-17] has been conducted on the basic mechanical properties of materials containing ELVRT or surface treated ELVRT and on the optimisation of their incorporation, but very limited research was conducted into the fatigue behaviour of the materials. In dynamic applications, it is essential to understand the fatigue behaviour of such materials to predict the fatigue lives of these rubber products and thereby ensure the necessary service life which are usually exposed to extended periods of cyclic loading. It is unusual for rubber failure to occur in a single loading cycle for engineering applications, hence common tests such as tensile and tear strength are not suitable for predicting failure. At present, the fracture mechanics approach is often used to characterise the strength of rubber under dynamic applications. As fatigue failure may commence from inherent flaws which grow as a result of repeated stress, it is also assumed that inclusion of large rubber particles would reduce fatigue life. The relationship between filler particle size (or flaw size) and flaw density in standard elastomers has been investigated by Abraham [18], using glass spheres as

artificial flaws. That author concluded that the inherent flaw size is a highly important factor in fatigue behaviour.

1.2 Aims and chapter outline

This thesis provides different approaches for evaluating ELVRT or optimised treatments for use in the rubber matrix. Most of the evaluation of treated ELVRT did not include dynamic testing that would replicate actual service conditions. Quasi-static tests are relatively useful for comparing the performance of fillers in rubber matrices, but those tests do not reflect the performance under dynamic applications for real world products.

The overall aim of this project is to investigate the mechanical and crack growth behaviour with incorporation of ELVRT in Natural and Butadiene rubber blends. The question is, how does the particle size of ELVRT influence the crack growth rates of the rubber compound?

In this study, two types of recycled rubber powder (RRP), smaller size particles (~ 74 µm) produced by the cryogenic method and common commercial particles sizes (~ 400 µm) from ambient ground production are incorporated in rubber compound as recycled filler. Compounds containing both of the recycled rubber powders were evaluated for their quasi-static properties (tensile, hardness, tear, abrasion resistance) and also their dynamic properties testing. Chapter 1 gives a brief overview of the importance of rubber and addresses the issues related to waste tyres recycling.

Chapter 2 gives a short introduction of tyres and the composition of rubber. This is to provide insight into the challenges for recycling tyres. Chapter 2 also reviews the ELVR from waste tyres, the handling options of “End-of-life tyres” and the benefits of utilising the product. Many researchers have worked to address the recycling issues, modified ELVRT for better use, and discussed properties of virgin rubber containing unmodified or modified ELVRT.

Chapter 3 reviews the literature on the mechanical fatigue of rubber. It is important to understand properties of rubber under cyclic deformation and the influence of various factors affecting the fatigue behaviour of rubber in order to achieve maximum fatigue life. The

rubber characteristics, and the response of rubber properties under dynamic loading and the influence of rubber formulation, environmental conditions and other factors were discussed.

Chapter 4 describes the characterisation of the recycled rubber powder used for particle size distribution, morphology structure and the constituent composition using ThermoGravimetric Analysis (TGA) and Fourier Transform Infrared (FTIR) spectroscopy analysis. It is crucial to ensure compatibility between RRP and the rubber when incorporated into a new rubber formulation. Corresponding mechanical and dynamic properties are also dependent on the characteristic/properties (method of production, particle size, morphology structure, etc.) of the ELVRT incorporated.

Chapter 5 presents the preliminary study of the mechanical and fatigue properties of unfilled (without the addition of carbon black in the host matrix) NR, BR and NR/BR blends compound with and without CRP400 or MRP074 filler. This ensured that the reinforcement by the carbon black filler did not compromise the individual assessment of the RRP filled compound. The mechanical properties tests included tensile, tear strength and hardness tests conforming to standard methods used in the rubber manufacturing industry. Fatigue-To-Failure tests (FTFT) were conducted to evaluate their dynamic behaviour.

"Network visualisation" using TEM was successfully used for studying the compatibility at the interfaces between two different polymers or matrices. Chapter 6 provides the interface study of NR and BR (without carbon black) containing RRP produced either using ambient or cryogenic methods using "Network visualisation" techniques.

Wear and fatigue life properties are important in dynamic applications. Generally, little work has been conducted on the effect of untreated or treated recycled rubber powders on the fatigue life of rubber compounds. Chapter 7 evaluates the effect of CRP400 or MRP074 in carbon black filled NR, BR and NR/BR compounds on mechanical (tensile, hardness, crescent tear, abrasion) and fatigue life (FTFT) properties. The investigation of fatigue life was focused on NR/BR compounds containing CRP400 or MRP074 since the blend compound is commonly used in the rubber industry. The extent of interaction between RRP and the rubber matrix was studied using Lorenz-Park, Cunnen and Russel, and Kraus

equations based on an equilibrium swelling study to correlate with crescent tear strength results.

Chapter 8 is of practical importance since recycled rubber powder may potentially be used in applications exposed to dynamic loadings. The effect of an artificial sharp cut on the fatigue crack growth rate in carbon black filled NR/BR containing CRP400 or MRP074 was investigated in detail. The fracture mechanics approach was used in the crack growth measurement which relates crack growth rate (*dc/dN*) and strain energy release rate (T, also called tearing energy). Single-edge notched tensile specimens (SENT) were used and crack growth rates were monitored during cyclic deformation with different tearing energies. The dynamic behaviour of RRP in filled rubber compounds was studied in terms of absolute and relative hysteresis loss.

This chapter also includes the analysis of fracture morphology after fatigue crack growth (FCG) tests. The fracture morphology is important for understanding the fatigue crack growth mechanism within rubber materials. Using SENT specimens, the mechanism from the crack initiation until fracture was observed and this was useful in predicting the location of failure in rubber products.

Chapter 9 states the main findings of this study and presents recommendations for future work.

Chapter 2 Review on End of Life Vulcanised Rubber (ELVR) from waste tyres

2.1 Tyres composition and characterisation

Tyres continue to be the dominant rubber product with approximately 60% of world rubber production. Global rubber consumption is expected to rise by 2.5 % from 29.39 million metric tonnes in 2018 to 30 million metric tonnes in 2019, stimulated by the growth of the tyre industry [19]. Figure 2-1 shows the important elements in a cross section of a tyre, where the compounded rubber is carefully layered with different parts of rubber sheets, metal and textile layers for reinforcement. The complex structure, with different compound formulations and durabilities due to presence of metal and textile, make them difficult to recover/recycle and thus they require a special process. In general, tyres consist of 40–45 wt% of rubber, 25–35 wt% of carbon black (CB) as reinforcing filler, 14-15% steel [20] and the remainder are accelerators, antiozonants, textiles and other fillers. These figures are based on the percentage of the total weight of a complete tyre.

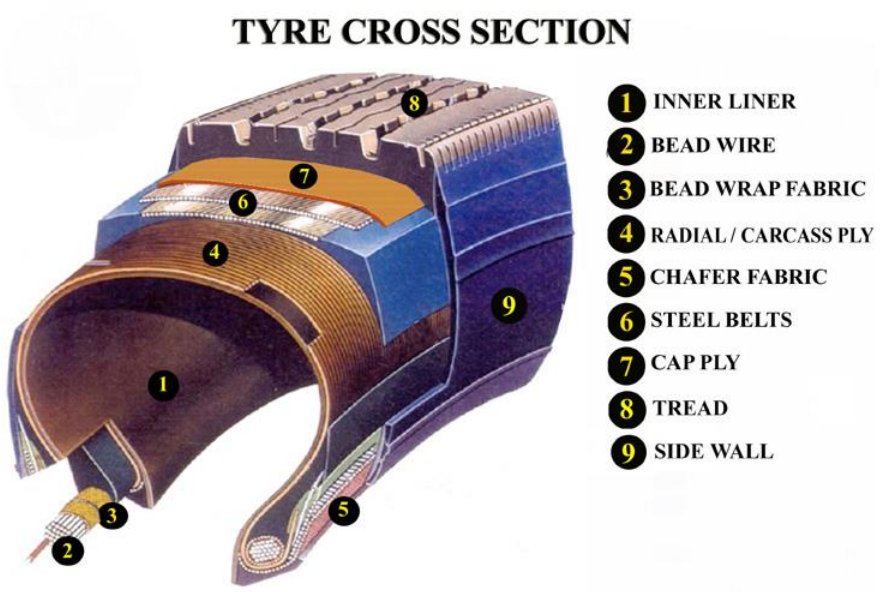

Figure 2-1 Tyre cross section [21].

Table 2-1 [8] shows the possible blends of rubber used in different parts of tyre construction. The most important types of rubber in vehicles tyres (both passenger and truck) are natural rubber (NR), styrene butadiene rubber (SBR) and butadiene rubber (BR) which are normally used for the tread, sidewall, and carcass compound followed by isobutylene-isoprene rubber (IIR) for the inner liner. Due to heavy loads and usage (long distance, frequent loading, etc.), truck tyres have higher NR content than passenger car tyres as shown in Table 2-2 and this also varies with the functionality of each type of the tyre for different vehicles (motorcycle, off road tyres, etc.).

Table 2-1 Possible blends of different types of rubber for different component of tyre construction [8].

Component	Polymers
Tread	SBR, BR
Belt	NR
Sidewall	NR, BR
Carcass	SBR, NR, BR
Bead	NR
Apex	SBR, NR, BR
Cap-ply	NR, BR
Inner liner	SBR, NR, IIR

A new trend in tyre composition is the inclusion of “green” materials such as silica filler, usually as a partial replacement of carbon black for lower rolling resistance and a corresponding increase in fuel efficiency. However the exact compositions depend on the individual tyre producer and recipes are normally held as proprietary formulations. For each tyre, manufacturers use up to 10 different rubber blends to produce specific tyre characteristics. Rubber compounds for winter tyres are entirely different to those for summer tyres. Winter tyres are specifically designed with more grip to enable them to work at temperatures below 7°C due to their lower glass transition temperature (Tg) [22]. Racing car

tyres are designed to have higher friction coefficients and withstand high forces and temperatures. In addition, they demand a very lightweight construction that can augment movement, speed, and support quick manoeuvres therefore, a “soft” rubber compound is required so that they adhere to the smooth racing tracks [23]. Additionally to the choice of material or ingredients, the pattern design and tyre build-up also plays an important role in the performance of each tyre.

Table 2-2 Main components of passenger car and truck tyres [24].

	Truck (in %)	Car (in %)
Rubber	45	47
Carbon black[1]	22	21.5
Metal	25	16.5
Textile	-	5.5
Zinc oxide	2	2
Sulphur	1	1
Additives	5	7.5
Type of rubber [25]		
Natural rubber	60-80	30-40
Synthetic rubber (BR, BR)	20-40	60-70

[1]Silica replaces part of the carbon black in certain types of tyres

Referring to the choice of material, the viscoelastic properties of tyre rubber contribute significantly to the grip properties. A material that exhibits both viscous and elastic characteristics is said to exhibit viscoelastic behaviour. In viscoelastic materials, part of the energy is elastically stored while the viscous component will dissipate energy as heat (hysteresis) when a load is applied and then removed (see section 3.2.2). This behaviour is associated with the mobility of filler structures, within the polymer matrix, when subjected to deformation. The components attributed to the viscoelastic behaviour of rubber are the dynamic storage modulus (E’) and dynamic loss modulus (E”). The ratio of the E” to the E’ (E”/E’) is a measure of the energy dissipation derived from the viscous to elastic response defined as the loss factor or tan δ.

Understanding the relationship between energy dissipation and other important elastomer properties, i.e. modulus and their dependency on stress, frequency and temperature is

important for each and every application. Figure 2-2 (a) shows energy loss and modulus versus temperature [26,27]. As the temperature increases, the compound modulus is low and in a rubbery state and thus the tendency to relatively dissipate energy decreases. Near the glass transition temperature, the rubber attains its maximum loss factor (tan δ) which could indicate maximum grip. Figure 2-2 (b) shows the characteristic difference between winter and summer tyre compounds, where tread rubber compounds in winter tyres are designed for maximum relative dissipated energy, besides flexibility at low temperatures (frequency 10Hz). A detailed discussion however is beyond the scope of this work and can be found elsewhere [26,27]. Hence, the compounding ingredients and proportion of elastomer, reinforcing fillers, sulphur or other additives in tyre compositions determine the ability of compounds to dissipate or restore the deformation energy. The viscoelastic behaviour has been shown to significantly influence the fatigue life of certain elastomers [28].

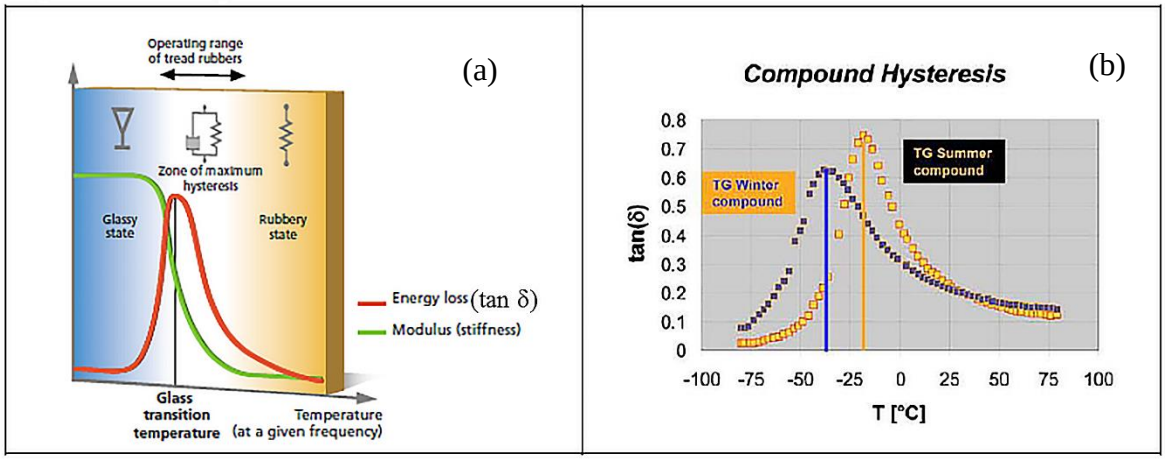

Figure 2-2 a) Effect of temperature on hysteresis of elastomers subjected to deformation b) Energy loss comparison between winter and summer compounds shown by tan δ [26,27]. Copyright © Société de Technologie Michelin, 2001

2.2 End of Life Vulcanised Rubber Tyres (ELVRT)

Meeting the high demand for quality recycled rubber derived from waste tyres is important for both economic and environmental benefits. Despite the difficulties faced by the rubber industries in obtaining the appropriate solution, there is still a great interest in the recycling of waste tyres. There are a large number of published works [12,14,15,17,29-32] on recycled rubber and several reviews [2,33-35] regarding ELVRT. The following section briefly gives

an overview of the production of ELVRT, the methods of waste tyre recycling/utilisation and discusses the current trends of the technology.

Figure 2-3 illustrates various possibilities for the end of life cycle of tyres. "*An end-of-life tyre is a used tyre that cannot or is not reused for its originally intended purpose and is not retreaded*" [36]. At this point, the management of ELVRT must be handled according to national waste management, as well as international legislation. Although the aspect is not discussed in this work, several directives influence the disposal method chosen by recyclers; from ways of collection, processing, product development and marketing [37]. There are various levels of treatments available in transforming ELVRT into a usable recycled material. Landfill disposal is not included in the diagram (Figure 2-3) since many countries have banned the route due to burning risk, pollution and breeding grounds for mosquitoes from accumulated waste tyres. In European Union countries, for example, the landfill directive (1999) [37] banned the landfilling of whole passenger car and truck tyres as from 2003 and tyre by-products from 2006. Nevertheless landfill accounts for only 5% among other possible routes of recovery in the European Union (EU) based on the 2010 statistics which reduced tremendously by approximately 49% from year 1996 [34]. The 2016 statistics [38] showed an increase of approximately 25% for the material recycling route.

Waste tyres are divided into two main categories i.e. part worn tyres and ELVRT. Part worn tyres are still capable of being used on roads; however lower tread depth levels raise concern over safety for driving on wet roads. Other applications for whole tyres are reuse as crash barriers, playground equipment [11], and sound barriers [37].

Retreading is a process where old tread is removed from a worn-out tyre and then a new tread is applied. In practice, passenger car tyres are not usually retreaded due to difficulties in supply of retreadable casings, competition with cheap non-retreadable tyres and customer concerns about the quality of the retreaded tyres [8]. Truck and aircraft tyres are regularly retreaded up to three times, provided they still have a good casing. The benefit is that it extends the tyre life span and significantly reduces the amounts of rubber waste [34]. After the life span of the part worn tyres have elapsed, eventually the path will return to the ELVRT and further handling of these waste tyres will be discussed in the following section.

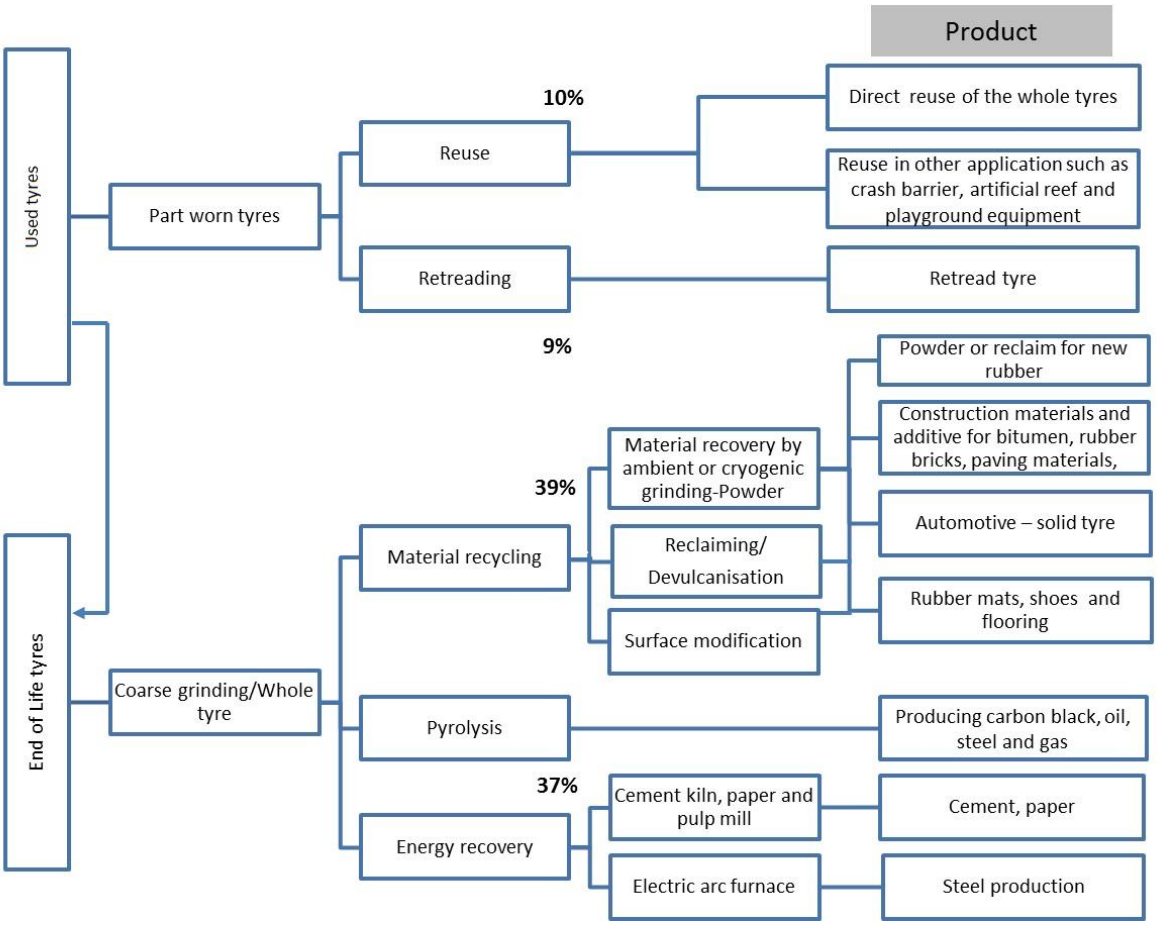

Figure 2-3 Various possibilities for the life cycle of waste tyres [2,8,34] and percentage of recovery routes in the European Union (EU) for year 2010 [2,39].

2.2.1 Downsizing waste tyres

"Rubber recycling in general is a multistep process that begins with grinding the rubber material, separating contaminants and reinforcing material, and possibly upgrading the rubber powder by surface treatment or reclaiming" [32]. Prior to grinding to smaller particle sizes, the tyre is cut into relatively large pieces and then shredded into smaller portions. In a subsequent step, the coarse material of ELVRT will be transformed into a finer rubber granulate or powder using different grinding processes. These processes can also be regarded as "downsizing" or "down-cycling" [33]. The grinding process is usually a preparation stage for the granulated rubber to be used in either different applications (i.e. rubber compounds, rubberised asphalt, etc.) or the next processing step of material recycling (i.e. reclaiming, surface activation). Currently, there are various sources available for granulate rubber

generated from different types of used tyres. The basic and most common grades are granulates made from mixed whole tyres, then from either entirely car tyres or truck tyres, and finally granulates made from tread buffings (by-product of retreading) [40]. Therefore it is important to identify the source of material, since it will determine the quality and properties of the final product, especially given the wide variety of formulations used by different tyre manufacturers for each type of tyre.

The selection of grinding process is also important in determining the characteristics of the ELVRT, such as particle size and particle size distribution, morphology of the particles, and purity of the rubber powder. The technology used for grinding of rubber is based on cutting, shearing, or impact, in different grinding conditions (ambient, wet or cryogenic grinding) employing from simple to specialized equipment (knife, shredder, granulator, extruder, disc grinder or impact mill) [32]. The advantages and disadvantages of various methods of waste tyre downsizing were compiled by Ramarad *et al.* [2] are shown in Table 2-3.

A comparison was also made by Jacob and De [41] on different techniques of grinding. For the production of 100 µm particle sizes, cryogenic grinding was considered more economical than ambient grinding, due to the easier pulverisation at cryogenic compared to ambient temperatures. Moreover, the cryogenic process produces a smaller particle size powder and a higher level of separation [15]. Thus, this would significantly reduce the wear and tear on the machinery and subsequently the maintenance costs [41].

The surface structure under microscopic examination [32] showed that cryogenically ground powder was smooth with a lower specific surface area (lower total surface area of a material per unit of mass) than ambient ground material which makes it difficult to bond to the polymer. Due to properties limitations using current grinding methods, recently, researchers [42,43] have reported an investigation of the solid-state shear extrusion (SSSE) process which utilise high pressure and shear force as it can produce controlled particle size powder through a continuous process. In addition, this new mechano-chemical process causes chemical bonds to rupture, which leads to partial devulcanisation of the rubber; however the exact mechanism is still under exploratory study [42].

Table 2-3 General methods of waste tyre downsizing [2].

Methods(size)	Description	Advantages	Disadvantages
Ambient (0.3 mm rough, irregular)	Repeated grinding following shredder, mills, knife, granulators and rolling mills	High surface area and volume ratio	Temperature could rise up to 130 °C Oxidation on the surface of granulates Cooling needed to prevent combustion
Wet ambient (100 μm rough, irregular)	Grinding suspension of shredded rubber using grindstone Water cools granulates and grindstone	Lower level of degradation on granulates High surface area and volume	Requires shredding of tires before grinding and drying step
Water jet (rough, irregular)	Used for large size tires (trucks and tractors) Water jet of >2000 bar pressure and high velocity used to strip rubber	Environmentally safe, energy saving, low level of noise and no pollutants	Requires high pressure and trained personnel
Berstorff's method (rough, irregular)	Combines a rolling mill with specially designed twin screw extruder in a line.	Small grain size, large specific area and low humidity	Not disclosed
Cryogenic (75 μm sharp edge flat/smooth)	Rubber cooled in liquid nitrogen and shattered using impact type mill	No surface oxidation of granulates and cleaner granulates	High cost of liquid nitrogen

2.2.2 Properties of ELVRT

As mentioned earlier, it is recognised that the source and the quality of ELVRT has to be determined/characterised to relate the final properties of the rubber products. The challenge is that the whole tyre contains different types of rubber from different parts of tyre components compared to single parts of the tyre such as tread buffings or sidewalls. The reduction in the level of contamination (steel, textile) is important [33]. Moreover, it has been shown that the tensile strength of NR [31] or NR blend [30] compounds is decreased with increased size of the ELVRT. Therefore, in practice, the classification according to the particle size fraction is usually carried out in accordance with the ASTM D 5644 and the particle size and distribution is given in mm (or mesh size) [33].

The properties of ELVRT are also classified in terms of the chemical composition such as ash, acetone extract, carbon black, and hydrocarbon content. Figure 2-4 shows the high resolution thermogravimetric analysis/differential thermal gravimetric analysis (TGA/DTGA) [44] as useful tools for the accurate determination of ELVRT composition under N_2. The first weight loss (200-300°C) is attributed to any volatile components such as processing aid or oil. The second weight loss corresponds to NR decomposition (350°C) and subsequently SBR at a 474°C peak. Switching to oxidative atmosphere (O_2), allows the identification of carbon blacks in the range of 500-600°C. The final residues are probably metallic oxides and/or silica. The simple technique of TGA/DTGA is however subject to a limitation as it cannot determine the styrene butadiene ratio; nevertheless this can be done by FTIR analysis.

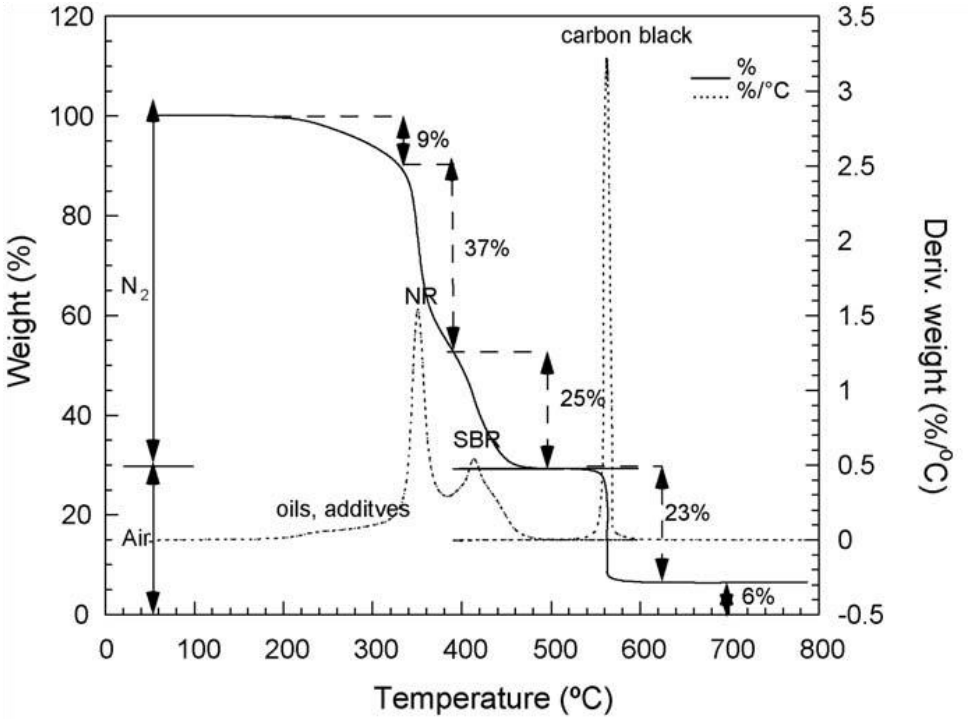

Figure 2-4 Hi-Res TGA/DTGA curves of NR/SBR (40/60) vulcanisates. Image reproduced from [44] with permission from Elsevier. Copyright © 2006 Elsevier B.V.

2.2.3 Modification of ELVRT

The addition of ELVRT without any modification or surface treatment normally leads to a decrease in mechanical properties of rubber formulations. It is reported [33,45] that ELVRT content in vulcanisate rubber cannot go beyond the 10 wt% threshold and it merely acts as non-reinforcing filler. At present, modification to the ELVRT is required when incorporating into virgin polymer or specifically rubber vulcanisates, to achieve environmental benefits, cost savings and improved properties.

In general, the properties of compounds containing ELVRT are governed by the particle size, surface area of the ELVRT and its size distribution. Other variables that can affect the mechanical properties of these compounds are the granulate composition, method used for grinding, type of rubber matrix and its composition and curing conditions during the compound preparation [46].

It is also recognised that insufficient interfacial bonding between ELVRT and the virgin matrix [2,47] is the cause of a reduction of mechanical properties. Therefore many efforts have been given to enhancing the polarity of the ground rubber surface. The approaches are physical and chemical surface modification. Kim *et al.* [15] used trichloroisocyanuric acid (TCI) to chlorinate ELVRT in a silica filled compound. Comparison of untreated and surface chlorinated ELVRT showed enhancement of mechanical performance (modulus and tear strength) of treated ELVRT with a polar nitrile-butadiene rubber (NBR) matrix, but surprisingly reduced the tear strength of NR compounds. Thus, the authors concluded that chlorination of the crumb rubber caused a decrease in adhesion to nonpolar substrates, due to the increased polarity of the ELVRT surface.

A simple and cost effective method for surface modification of ELVRT powders in NBR compound was studied by Zhang *et al.* [48]. The authors applied plasma treatment by atmospheric pressure dielectric barrier discharge (DBD) method using a commercial parallel plate dielectric barrier discharge reactor. They found a similar observation to the previous results [15] for NBR containing chlorinated ELVRT. Plasma treatment of ELVRT caused an improvement in the interfacial bonding between the modified ELVRT and polar NBR matrix. The result is expected for a polar matrix and it would be interesting to conduct similar experiments on NR-based materials.

Fuhrman and Karger-Kocsis [49] studied the photochemical grafting of methacrylic acid onto ELVRT, which was applied to polyamide-6, epoxy resins and polyurethane elastomers. Similarly, the concept was to create a new polar group on the surface of ELVRT and thus increase the interfacial adhesion between the ELVRT and the polymer matrix. A modest improvement in fracture strength of polyamide-6 and epoxy resins was observed probably due to ineffectiveness of surface grafting for larger particle size of ELVRT. However, they claimed a promising result in polyurethane elastomers with grafting yield up to 16% with no deterioration in their mechanical properties compared to 20% reduction of tensile strength of untreated ELVRT.

A similar problem was also faced by Yehia *et al.* [13] where a partial replacement of high-abrasion furnace carbon black (HAF) with larger particle size (100 – 500 μm) of ELVRT caused dilution and a decrease in the mechanical properties of the rubber vulcanisates. They

treated the ELVRT with nitric acid (HNO_3) and 30% hydrogen peroxide (H_2O_2) and achieved the highest tensile strength values of the vulcanisates compared to the untreated rubber powder using 20% HNO_3 and 30% H_2O_2. It was also suggested that it should be used in combination with 10-30 pphr (parts per hundred of rubber) of carbon black for properties improvement.

A commercial product known as *Surcrum* introduced by Vredestein Rubber (The Netherlands) appears quite beneficial compared to other treatments [50]. It was claimed that the compound was applicable as a partial or complete substitute of virgin compounds. The technology was established by surface activation whereby the ELVRT was coated with crosslinkable polymers, containing vulcanising chemicals. The manufacturing processes were conducted at a low temperature including the grinding process, were environmentally friendly and therefore claimed to have no degradation effect on the surface activation processes. In addition, Surcrum exhibited homogeneous coating system in terms of chemical composition and is suitable to all varieties of rubber including whole tyre crumb. However, the inconsistency in quality and composition of the used tyres is the main drawback. NR or SBR-based Surcrum can achieve a tensile strength between 8 MPa and 12 MPa. Interestingly, Surcrum based on SBR, with up to 25 pphr is also found not to be detrimental on the flex-fatigue resistance (DeMattia tester) of an SBR-based compound.

Compatibilisers such as aliphatic hydrocarbon resin are essential for coherent bonding between the crumb and the matrix. The compatibiliser enhanced the tensile strength in polar NBR but not in NR [15]. Due to the difficulty of incorporating high amount of ELVRT in rubber, researchers tend to incorporate ELVR in thermoplastic, thermoplastic elastomer (TPE) and thermoplastic vulcanisates (TPV). In TPV, it is envisaged that the success of dispersing vulcanised particles in the plastic matrix could be applied to TPV containing ground rubber tyre. It is a challenge, however, to meet the necessary requirement, i.e to achieve nano particles (less than 1µm).

2.2.4 Reclaiming/Devulcanisation

Reclaiming is a process, after ELVRT has undergone the downsizing process, for the material to be further treated, processed and transformed into a reprocessable/reusable material. At

this stage, it can be revulcanised alone or with virgin rubber using the conventional curing process. Higher energy input (mechanical shearing, heat and light) during the breakdown of the rubber network, caused broken sulphur cross-links and scission of the carbon-carbon bonds of the polymeric chain. The broken polymer chains generated in the reclaiming processes influence the properties and reduce the quality of the recycled material. Contrarily, devulcanisation is the process of selectively opening sulphidic crosslinks (C-S_x-C, when x can be 1, 2, 3….) of vulcanised rubber [8]. An ideal devulcanisation process is a reverse vulcanisation without damaging the main polymer chain. In the preferred method, only sulphur cross-links are broken, while the main polymer chains remain intact [8]. Consequently, the devulcanisate is expected to be as close to the original raw material both in structure and quality. Figure 2-5 differentiates the processes that occur in reclaiming and devulcanisation.

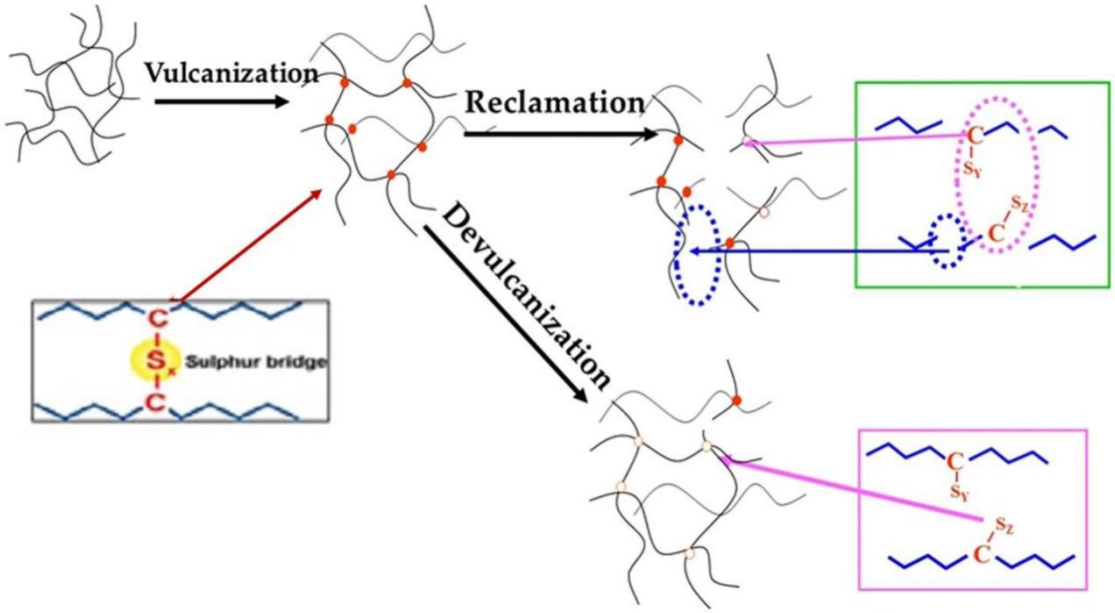

Figure 2-5 Simplified scheme of the two reactions occurring during rubber recycling processes: reclamation and de-vulcanisation [8].

Although devulcanisation is the most promising way to achieve high quality recycled material, it is also obvious that an efficient devulcanisation process is the critical challenge for the production of high quality materials. Therefore, at present, reclaiming is still widely practiced, however, the carbon-carbon bond cleavage process needs to be minimised. This is feasible considering the energy to break a carbon-carbon bond is higher compared with breaking sulphur bonds [2].

Adhikari *et al.* [45] and Myhre *et al.* [35] have given a comprehensive summary of various methods of reclaiming and devulcanisation. The processes can be carried out using physical or chemical processes. The physical process methods encompass thermomechanical, thermochemical, ultrasonic, microwave and other processes while the chemical processes are; radical scavengers, nucleophilic additives, catalyst systems and chemical probes. Currently industry prefers chemical reclaiming agents for the devulcanisation process at elevated temperature [51]. The commonly used chemical is diphenyl disulphide (DPDS), but the main drawback is the unpleasant odour released during processing. Alternatively, tetramethyl thiuramdisulphide (TMTD) is used; however TMTD is identified as generating nitrosamine which is considered carcinogenic. Thaicharoen *et al.* [52] studied thiosalicylic acid as a devulcanising agent during mechano-chemical processing, and claimed that the efficiency of the devulcanisation using thiosalicylic acid under certain conditions was comparable to that of the widely used DPDS. Mandal *et al.* [53] used safe multifunctional rubber additives, tetra benzyl thiuram disulphide (TBzTD) as an alternative option for SBR/reclaimed rubber. The authors identified that 20 wt% reclaimed rubber can be used to substitute virgin SBR, with no significant reduction in physical properties, thermal, and exhibited higher ageing resistance compared to the virgin SBR rubber at 40 pphr loadings.

The continuous process of microwave devulcanisation of ELVRT requires microwave energy between 915 and 2450 MHz. The properties of the reclaim are reported to be better than those of rubber obtained by other reclaiming methods [45]. The advantage of this technique is the energy used is sufficient to cleave crosslink bonds but insufficient to cleave polymer chains. In addition, it does not require the use of chemicals and little grinding. However, the limitation is the waste material must be polar in order that the microwave energy will generate the heat necessary to devulcanise [45]: EPDM and IIR are particularly suitable for this process.

The continuing effort in improving the quality of reclaims has seen devulcanisation using extruders or modified extruders become the focus of interest. Isayev *et al.* [54] applied ultrasonic devulcanisation on ELVRT, using model compounds based on SBR and other types of rubber. They established optimal conditions of the die geometry, amplitude of oscillation, pressure, temperatures and residence time which affect the degree and rate of

devulcanisation. Several papers related to the processing parameters and resultant properties [55], crosslinking density and gel fraction measurement [56], were also published. Although there is evidence for selective sulphur bond cleavage, they also identified some carbon – carbon bond cleavage, which needs further attention. A further study by Levin *et al.* [57], proposed a possible mechanism of the revulcanisation process using ultrasonically devulcanised SBR. They found larger amount of sulphidised molecules in the devulcanised rubber, which were ready for crosslinking and approximately 85% of the accelerator remained which attributed to a decrease or disappearance of the induction period in the cure curves.

Other approaches for reclaiming/devulcanisation are the combination of one or two types of treatment. For example, De *et al.* [17] treated ELVRT using mechanochemical reclaiming using tetramethyl thiuramdisulphide. An improvement in the tensile properties of SBR was reported to up to 60 pphr inclusion of reclaim ELVRT and this could be enhanced with additional carbon black. Lee *et al.* [58] studied the combination of ozone and ultrasonic treatments and reported that a 21% improvement in tensile properties of revulcanised rubber was achieved, compared to single treatments, i.e. 7% for ozone and 12% for ultrasonic.

Adhikari *et al.* [45] found that the air ageing performances in an oven at 70°C (24, 48 and 72 hour), with blend containing an optimum ratio of reclaimed material, were better than those of the virgin compound. Similar results were obtained by other researchers [17] and probably suggest that rubber products containing reclaim do not require the addition of antioxidants, as they are already in the original tyre formulation, which would probably explain the good ageing properties. Another advantage of using reclaim is the ease of processing due to the broken molecular chains and eventually lower mixing time. The use of reclaim material during the extrusion process also provides a higher dimensional stability and lower shrinkage rate due to the presence of crosslinked gel in the reclaim [45].

2.2.5 Other related work

Farris [59] and Morin *et al.* [60] presented an interesting work on a High-pressure high-temperature sintering (HPHTS) recycling technique that enables the recycling of vulcanised rubber powders made from scrap tyres only by the application of heat and pressure. The

advantage of this process is the use of 100% recycled rubber and using conventional rubber mouldings equipment. However, Bilgili *et al.* [61] who argued that the HPHTS method is part of their second stage patented technology. The authors have developed a method of pulverising waste granulates into small particles using the solid-state shear extrusion process and subsequently compression moulding the material in the absence of virgin rubber. They also proposed a physico-chemical mechanism of bonding waste rubber particles in the absence of virgin rubber while Farris [59] presented the chemistry of the particle bonding. In addition, they also pointed out that higher temperatures and pressures generally improved the bonding of the particles, whereas a high crosslink density and the presence of large amount of coarse particles inhibited the particle bonding.

Gugliemotti [62] explored the HPHTS technique using different variations of sizes of ELVRT and moulded large pads to assess tensile properties, dynamic mechanical and thermal analysis of the final products. These investigations showed that higher ultimate tensile properties was obtained using smaller particles (~0.4 mm) and also with combination with medium size particles (~1.2 mm), without additional treatments or incorporation of virgin material and additionally maintained the reduction in cost of production. Despite these benefits, this concept is limited, as the product yields are of low quality and are only suitable for low end secondary products such as carpet underlays, sport field surfaces, etc. Thus it is necessary to further improve the adhesion in order to upgrade this technology to the next level.

Kojima *et al.* [63] developed a devulcanisation process that utilises supercritical CO_2 ($scCO_2$) as a devulcanisation reaction medium in the presence of a devulcanising reagent. They stated that CO_2 was the most advantageous medium for the current purpose because of its chemical inactivity, nontoxicity, non-flammability, and low cost. They found that the addition of 40 pphr of devulcanised material, by this method, retained about 90% of the original tensile strength of filled NR containing carbon black. This finding was attributed to less scission of the polymer main chain due to the absence of intensive mechanical shearing.

2.2.6 Energy recovery

It was reported [34,45] that burning the ELVRT, produces a higher caloric value (32 MJ/kg) compared to coal (18.6–27.9 MJ/kg). In the cement industry, whole and shredded tyres can be used as a fuel source and residues are used as filler in cement. The high temperatures above 1200°C the oxidising atmosphere in the kiln and more combustible matter in the ELVRT gave the advantage of complete combustion and lower emissions compared to coal. Clauzade [64] demonstrated the viability of using ELVRT as a replacement of anthracite (type of coal) which is normally used as carbon and additional heat source together with scrap metal and other ingredients in an electric arc furnace, for steel making industry. Although the energy contributed by the ELVRT had not been accurately accessed, it provided an alternative solution in handling waste tyres. Therefore ELVRT is a suitable choice of fuel source in steel production, cement, pulp and paper kilns. Consequently, the utilisation of this recovery method in the EU was seen to increase from 1996 at 20% to 37% in 2012 [2].

2.2.7 Pyrolysis

Although recycling and energy recovery methods are the most appealing to waste tyre consumers [2], the pyrolysis technique has also received more attention recently. It is a technique of thermal degradation of waste tyres in the absence of oxygen to generate gas, oil, carbon black and steel (in the form of wires). From rubber technologies perspective, recovered carbon black (rCB) is often used in rubber compounding as a cost reduction alternative. The rCB from tyres usually contains blend averaged weight of different grades of carbon black, which was left in the waste tyres and does not represent the original type/grade of reinforcing carbon black used in new tyres [65]. Thus, it is likely that these rCB do not reinforce as well as virgin CB. Through research and technology, it is not possible to produce rCB equivalent or better than the N700 series [65].

A recent development is the recovery of silica filler from waste rubber compounds (rSilica), using pyrolysis in order to meet the sustainability challenges of ‘green’ tyre compounds. The main focus was to study the effect of rSilica in comparison with virgin silica for their physical properties, abrasion resistance and dispersion performance in the tyre tread formulations [66].

2.2.8 Microbiological method

A considerable interest has been shown into the devulcanisation of ELVRT using both bacteria (eg. bacteria species such as *Rhodococcus rhodochrous, Corynebateria spp., Pseudomonas spp., and Escherichia coli*) and fungi (*Recinicium bicolour*) [67]. The technique of biological devulcanisation removes the sulphur crosslinks in vulcanised rubber by the sulphur-oxidising activity of enzymes. The activity conducted in anaerobic conditions (no oxygen) prevents hydrocarbon oxidation, therefore produces higher quality material than the aerobic processes (with oxygen). Similarly for fungi, several species of white rot fungi (efficient lignin-degrading enzymes) have been successful in increasing the susceptibility of rubber to biodegradation and eventually devulcanised the ELVRT [67].

A review by Stevenson *et al.* [67] reported that extensive research has been carried out in rubber metabolism and many microbial species which are responsible for rubber biodegradation and their enzymes have been identified. The authors [67] also disclosed that further development on molecular and biochemical studies on rubber degrading enzyme were needed before efficient recycling and bio-chemical processes can be proposed. Li *et al.* [68] concentrated on microbial desulphurisation of ground rubber (GTR) by Thiobacillus ferrooxidans and revulcanised the product and compared it with untreated ground rubber in NR compound at various concentrations. The authors have demonstrated that desulphurised ground tyre filled NR composites had slightly better mechanical properties and lower crosslink densities than the untreated GTR at similar concentrations in NR composites. This microbiological treatment may become the method of the future.

2.3 Characterisation of quality of ELVRT

After reclaiming or devulcanising ELVRT, it is necessary to characterise the quality of the material, in the sense that the efficiency of each treatment can be determined and compared. Therefore, characterisation before and after treatments is essential to understand factors contributing to the enhancement or reduction in the physical properties (e.g. tensile strength, modulus and hardness). The sol-gel experiment is used to quantify the devulcanised portion, as a section will become partially soluble and another remain in the gel state. The desirable portion is higher sol, where the crosslinked structure is destroyed and this can be determined

by extraction using the Soxhlet apparatus [69] and corresponding swelling test [70]. Prior to the determination, low molecular weight components, such as processing aids, were extracted by acetone, before the swelling test. The cross-link density, ν_c, was then calculated according to the Flory-Rehner equation, Eq. 2-1 [71] by using swelling test data.

$$\nu_c = \frac{-\left[\ln(1-V_r)+ V_r + \chi_1 V_r^2\right]}{\left[V_S\left(V_r^{1/3} - V_r/2\right)\right]} \quad \text{(Eq. 2-1)}$$

where V_r, χ_1 and V_s are rubber volume fractions in the swollen sample, rubber-solvent interaction parameter and molar volume of the solvent respectively. In order to calculate the percentage of devulcanisation, the value of the parameter is given: χ_1 equal to 0.37 for the system SBR/toluene, 0.34 for the system BR/toluene or 0.39 for the system NR/toluene [69], while V_s equal to 106.2 x 10^{-6} m^3/mol for toluene [72]. The mass of the swollen vulcanisates was measured before and after the swelling test. Thus, percentage of devulcanisation was calculated according to Eq. 2-2 where ν_1 and ν_2 are the cross-link densities of the samples before and after devulcanisation [70], respectively:

$$\text{Percent of devulcanisation} = \frac{\nu_1 - \nu_2}{\nu_1} \times 100 \quad \text{(Eq. 2-2)}$$

The sol fraction percentage was calculated according to Eq. 2-3:

$$\%\ \text{Sol fraction} = \frac{w - w_1}{w} \times 100 \quad \text{(Eq. 2-3)}$$

where w is the mass of the sample before the swelling test and w_1 is the mass of the sample after the removal of toluene. The melt processibility of ELVRT after treatment can be characterised by using a Mooney Viscometer. A higher viscosity of ELVRT could lead to an incompatibility of blending with the virgin polymer and improper dispersion of compounding ingredients. On the other hand, a too low viscosity of ELVRT creates a problem of sticking during mixing and processing.

The cure properties are characterised by various torque rheometers and physical tests, such as tensile strength, modulus and hardness have been used to determine the quality of ELVRT. Again, tests under repeated stress, such as fatigue tests, are largely absent from the literature.

2.4 Blends of ELVRT in rubber vulcanisates and current technology of interest

Although blending is a common practice to mix ELVRT in rubber vulcanisates, the incompatibility between the blend components often results in poorer mechanical properties compared to the virgin rubber. Rattanasom *et al.* [16] reported that the addition of tyre tread reclaimed rubber to virgin NR caused a decrease in the mechanical properties of both conventionally and efficiently cured materials. Sreeja *et al.* [14] also showed similar results on the cure characteristics and mechanical properties of NR with whole tyre reclaims. A reduction in tensile strength has been observed with the addition of 20 pphr of reclaims. In contrast, Grigoryeva *et al.* [12] have shown that inclusion of 20% of partially thermochemical devulcanised ELVRT in a tyre formulation did not significantly affect the tensile properties of the compound. However, an increasing content of devulcanised ELVRT in the range of 40-80 wt% leads to a significant decrease of the elasticity of the revulcanisates and some reduction of the tensile strength values.

Several exhaustive reviews of ELVRT [2,33,73,74] in polymer blends suggest different areas for future developments. The influence of ELVRT size, concentration, modification, crosslinking and mechanical and thermal properties of rubber containing ELVRT were discussed by Ramarad *et al.* [2]. The authors highlighted that research interest in thermal, dynamic mechanical, fatigue, ageing and swelling studies seem to be lacking. A comprehensive review by Karger-Kocsis *et al.* [33] indicated that incorporation of ELVRT in fresh rubber stocks remains a promising recycling route. Nevertheless, in order to achieve a significant incorporation of ELVRT in rubber compounds, the ELVRT need to be subjected to chemical treatments via devulcanisation/reclaiming or otherwise the value is limited to less than 10 pphr. They also suggested special extruders for continuous processes whereby any form of ELVRT could be used without producing fine powder. Additionally, they needed to enable sufficient co-reactions, between macro radicals from molecular chains scission and reclaiming additives, in the extruder to avoid using traditional batch mixers. In terms of

application, ELVRT can generate inhomogenous crosslinked structure of rubbers and rubber-like materials which can be used as excellent sound absorbers [33].

Bandyopadhyay [73] reviews published studies on ELVRT in thermoplastics and rubbers. The recent review by Myhre *et al.* [74] described various rubber recycling approaches in terms of chemistry, processing and applications and discussed possible future directions. The authors also defined the terminology between reclaiming and devulcanisation. As stated earlier, devulcanisation still remains an important method of recycling rubber, but special equipment is needed to make it more efficient and economically feasible by enabling higher output. Thus, a modified extruder has been recently utilised, although normal extruders have been used for recycling scrap rubber for a few years [75]. Economic feasibility is another crucial aspect of the current reclaiming process.

Isayev *et al.* [54] developed a devulcanisation method for waste tyres using high power ultrasonics (900 W, frequency 20 kHz). In a recent work [76], they carried out devulcanisation using ultrasonically (40 kHz) aided extrusion in an attempt to use industrial scale equipment. They used two different sizes of ELVRT i.e. 10 (2000 μm) and 30 mesh (~600 μm) and found that 30 mesh exhibited higher tensile strength than 10 mesh after revulcanisation.

Maridass *et al.* [29] performed a series of studies on thermo-chemical shear extrusion (TCSE) for decrosslinking of waste rubber powder. In their preliminary study, they emphasise the extruder design, extruder parameters, i.e. temperature and screw rotation speed and also the addition of DPDS as devulcanising agent. These factors are important in determining the quality of the extrudate. Uncontrolled process conditions and inappropriate extruder design could cause hard, charred and burnt odour extrudate. They managed to produce an extrusion processed ELVRT (EPELVRT) blended with NR at 70/30 ratio (70E/30N), filled with 15 pphr carbon black resulting in a tensile strength of about 16 MPa and elongation at break (EB) of 370%. These results are equivalent to devulcanisate material produced by different types of treatment by Myhre *et al.* [77]. In addition, they found the addition of DPDS improved the EB to 460%. Maridass *et al.* [75] also further investigated the optimum content of carbon black and curatives of 70E/30N compound at an extruder screw speed of 30 rpm and a temperature of 170°C. Maridass and Gupta [78] also modified the length to diameter (L/D)

ratio of the extruder from 10 to 8. They optimised the mechanical properties using experimental designs (relationship between response functions and process variables) and reported that the optimum tensile strength was achieved at a barrel temperature of 197°C and screw speed of 25 rpm. It was observed that with higher temperature and screw speed, the properties were declining. This was possibly due to the degradation of NR and hardening for SBR, followed by excessive chain break down of ELVRT, which resulted in a low quality of extrudate.

2.5 Summary

1. Various methods of handling waste tyres have been reviewed as alternative solutions to the tyre recycling issues. Further work is important to ensure the solutions are viable and there is a need to explore more recent technology advancements for future benefit.

2. The problems associated with ELVRT have been discussed and they are due to crosslink structure, large particle size and incompatibility with the matrix. The modified surface methods have yet to achieve the desirable properties. The improvement so far is marginal and most of the research work is still at the laboratory scale level. Various improvements in material recycling showed the potential of such measures as a combination of physical and chemical treatments and a continuous devulcanisation combination using a modified extruder for mechanical properties optimisation. Commercialisation means higher output and using a continuous devulcanisation process appears to be an appropriate way of meeting this objective.

3. There has been little discussion on the evaluation of untreated or treated ELVRT with regard to the fatigue behaviour in fresh/virgin rubber formulations.

4. The use of Thiobacillus ferrooxidans appears an interesting route for research but is beyond the scope of this thesis.

Chapter 3 Review on mechanical fatigue of rubber

3.1 Introduction

Rubber products can offer many special properties to meet demanding requirements, even under severe conditions, through precise compound formulation and sophisticated rubber manufacturing technologies. In terms of long-term durability, rubber components can deteriorate due to various factors: mechanical stress, heat, uv light, chemicals, and ozone plus heavy metal contaminants such as iron and copper cause changes to properties. The changes are usually undesirable as they affect the function and durability of rubber components during service. From all factors that affect rubber performance in service, fatigue failure due to dynamic loading are of great interest in the context of many real-world applications. Fatigue failure in rubber components can be seen as tread groove cracking or tread and ply separation in tyres, failures in torsion springs, engine mounts, O-ring seals and numerous others [79].

Fatigue failure can be described as the tendency of a material to fracture by means of crack propagation under cyclic stress which ultimately leads to failure. Beatty [79] has defined fatigue in rubber as the reduction of a physical property causing failure, which results in service unreliability due to physical and chemical properties changes. Important factors known to influence fatigue behaviour of rubber are the nature of the base polymer, antioxidants/antiozonants, reinforcing fillers and their dispersion, crosslinking density and nature of the crosslink structures; service/test conditions, such as temperature, strain level, strain rate/frequency and dissipative aspects of stress-strain behaviour of rubbers, etc. Some of these factors have been reviewed by Mars [80]. In this thesis, rubber characteristics and the response of rubber properties under dynamic loading and the main compounding ingredients in rubber formulation are elaborated to understand their effects related to fatigue behaviour.

3.2 Elastomer behaviour

3.2.1 General properties of rubber

The typical stress-strain behaviour of rubber can be described as non-linear viscoelastic as shown in Figure 3-1 (a). Therefore, unlike metals and ceramics, rubber does not follow

Hooke's law, meaning the strain is not proportional to the applied stress resulting in different material behaviour especially at larger deformation levels. Rubber has unique properties, especially its ability to undergo large deformation/strains at smaller stresses (~0.3 MPa). It has a low elastic modulus compared to ceramics and metal but can have excellent strain energy absorption characteristics [81]. Hence rubbers are used in many engineering applications, especially for vibration damping control.

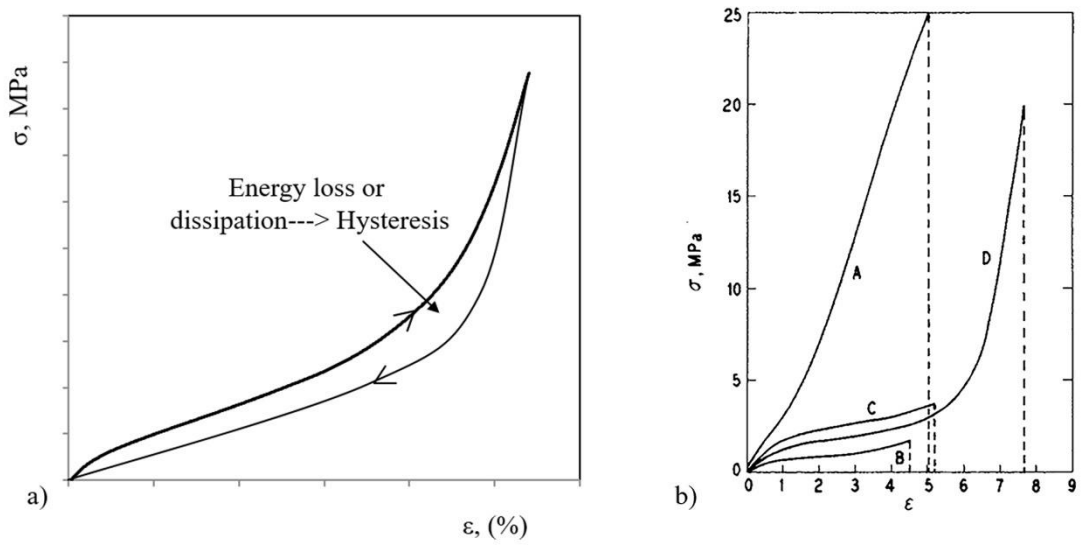

Figure 3-1 a) Non-linear viscoelastic stress-strain curve b) Typical stress-strain of an amorphous elastomer, (A)-carbon black filled compound, (B)-unfilled vulcanisates, (C)-filled with large particle inert filler, (D)-filled with graphitised carbon black [82].

The shape of the stress-strain curve is also dependent on the type of rubber, crosslinking system, filler (Figure 3-1 (b)) [82], curing temperature and time, operating temperature, environment, loading history and loading rate [83]. In cyclic loading, the mechanical response of filled rubber material displays different dissipative aspects (e.g. strain induced crystallisation, Mullins effect and viscoelastic) of stress-strain behaviour, which can affect the fatigue behaviour of rubber materials [80,84].

3.2.2 Viscoelasticity

Rubber compounds exhibit both viscous and elastic characteristics when subjected to cyclic loading. This behaviour is attributed to interaction of the neighbouring molecules due to forces of attraction and physical entanglements in the elastomer network [85]. The response of the arrangement of those molecules and their mobility under different strain/stress, frequency and temperature determines the dynamic properties of the rubber. From the stress-strain curve, energy losses or hysteresis is the area between the loading and unloading stress on the curve (Figure 3-1 (a)), occurred during deformation. The ratio of energy dissipated to the energy stored/input is a function of the viscoelasticity of the rubber. Figure 3-2 [26] shows the viscoelastic properties, when represented by a dash-pot and spring assembly. The diagram also showed that viscoelastic properties are dependent on temperature and frequency/strain rate. Higher energy loss around the glass transition temperature (Tg) was observed at a certain frequency/strain rate, or temperature, and this also depends on the choice of different types of rubbers.

Relationships between hysteresis (or available energy in the cycle) and fatigue properties have been reported by many researchers [80,86,87]. The Tg of polybutadiene rubber (BR) increases as the vinyl structure content increased. The delays in fatigue failure for high vinyl compared to lower vinyl content in BR are due to higher viscoelastic energy dissipation [28]. Persson *et al.* [88] presented a qualitative discussion on the contribution of viscoelastic energy dissipation at the crack tip related to the resistance of polymers. The contribution arises from the bond-breaking processes at the crack tip and from the bulk viscoelastic dissipation. The authors also highlighted the dependence of the tearing energy, T, on the crack velocity and temperature around the vicinity of the crack tip.

For unfilled single component rubber, Qazvini *et al.* [89] have demonstrated that the fracture energy is controlled by the viscoelastic losses and decreases as temperature increases. For blend systems, a counter-balance to the viscoelastic loss arises from the coupling parameter between polymer phases and the network residual stress and this is dependent on the miscibility of the rubber blends.

The crack growth behaviour in carbon black (CB) filled SBR compounds is governed mainly by viscoelastic effects [90]. Kar *et al.* [91] showed that carbon black filled NR or SBR compound under static deformation contributes significantly to hysteresis loss, even when the samples are swollen in xylene and paraffin oil. They reported that the hysteresis loss also increases with an increase in strain rate and strain level within the examined strain rate/strain range [91]. The higher the carbon black concentration, the higher the temperature developed due to more breakage of the carbon black structure in the rubber network and increases the hysteresis loss [92].

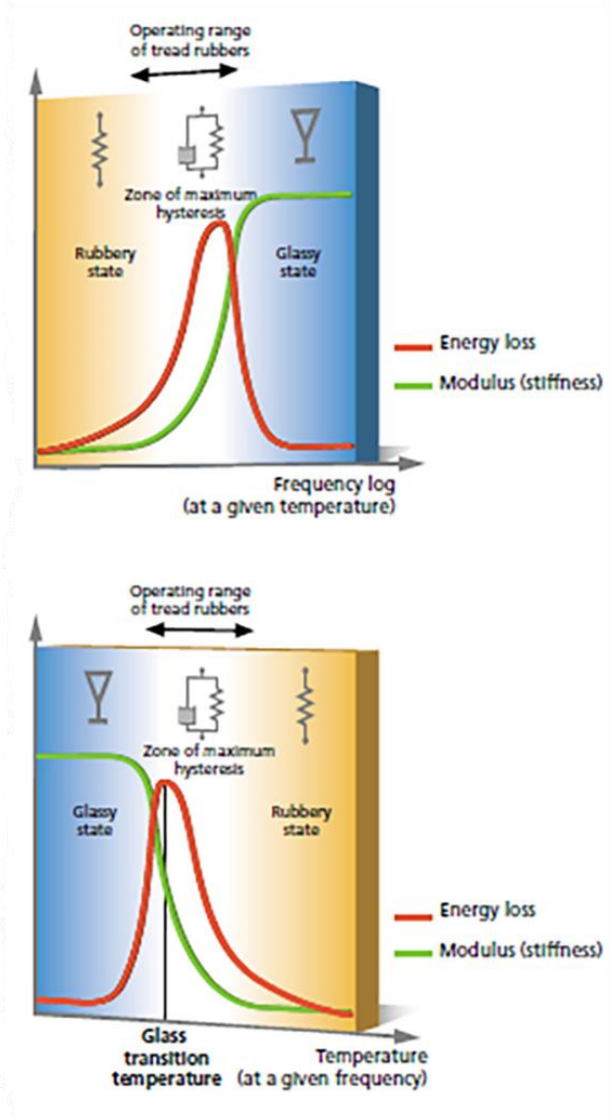

Figure 3-2 Hysteresis response as a function of frequency or temperature. Reproduced from [26] Copyright © Société de Technologie Michelin, 2001

3.2.3 Mullins and Payne effect

'Cyclic stress relaxation' or stress softening can be described as a decrease in rubber stiffness due to cyclic deformation. The stress reduction occurs primarily on the first and second cycles after which it reaches a quasi-equilibrium stress-strain relation after a few cycles [85]. When the extension exceeds the maximum extension previously applied, the material stress-strain response during the first deformation is little affected (comparison of cycle A and cycle B in Figure 3-3 by previous stretching. This phenomenon is normally referred to as the "Mullins effect" [93]. The stress softening increases progressively with increasing maximum stretch and is dependent on the maximum load. Under displacement controlled tests, stress–softening reduces the load and results in a much less damaging effect [80]. Thus the choice of conditions in fatigue crack growth tests could produce different results, using similar materials.

'Stress-softening' is much more pronounced in carbon black filled, than unfilled, compounds. At higher strains, the hysteresis loss increases, due to greater breakdown of filler–filler and rubber–filler bonds and produces higher energy dissipation.

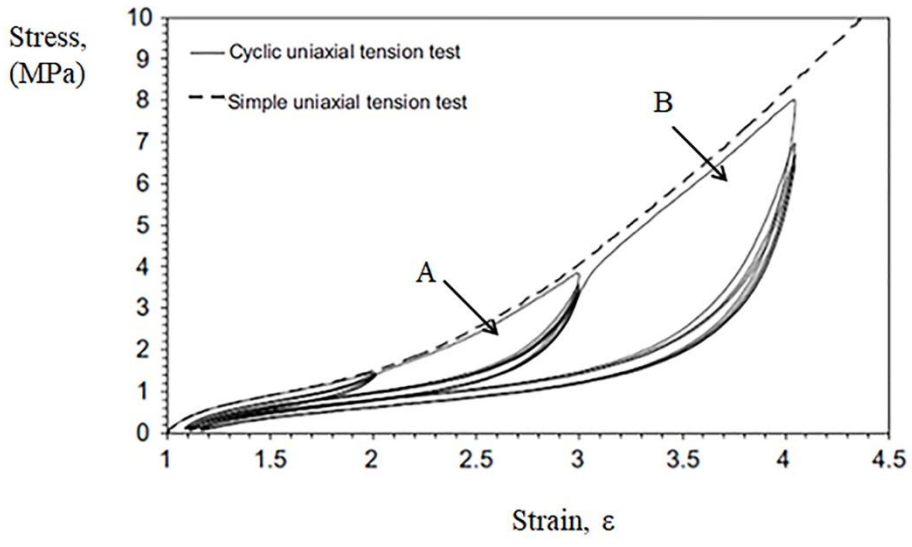

Figure 3-3 Stress-strain responses in simple or cyclic uniaxial tension tests and the Mullins effect for a SBR filled with 50 pphr CB at low constant strain rates of 10^{-3} s^{-1}. Image reproduced from [94] with permission from Elsevier. Copyright © 2006 Elsevier B.V.

The dependence of dynamic modulus on strain amplitude was published by Payne [95]. When the dynamic strain amplitude increases, the decrease in the elastic modulus was attributed to the breakdown of the carbon black structure or filler-filler networks. The strain independent contributions of modulus are the combination of polymer network, hydrodynamic reinforcement effects and from the polymer-filler interaction. Further study by Fröhlich [96] examined in detail the dynamic behaviour of carbon and silica filled rubber and used a rubber process analyser to understand the basic filler structure and related Payne effects, under a wide range of shear amplitudes. The authors concluded that the stress softening at small amplitudes (<5%) is attributed to the breakdown of the inter-aggregate in the filler network [96]. The higher surface activity of the filler creates competitive processes between filler-filler and polymer-filler interaction. At much higher strain (>30%), the filler structure in the in-rubber state, including the occluded rubber-rubber contribution and the surface activity of the filler, plays an important role.

3.2.4 Strain induced crystallisation (SIC)

The high resistance to crack growth in NR is partly attributed to the ability of NR to crystallise under strain. This is normally associated with the high regularity of the macromolecular structure (cis-configuration) in NR, during stretching. The schematic model of crystallisation by the high orientation of the crosslinking network chain during deformation has been illustrated by Tosaka *et al.* [97] and is shown in Figure 3-4. The unidirectional increase in modulus and enhancement in tensile strength as result of strain induced crystallisation (SIC) is evident using simultaneous synchrotron X-ray diffraction measurements. A comprehensive review of SIC of NR during static deformation and X-ray diffraction was given by Huneau [98], who suggested X-ray investigation of the SIC effect should be carried out during fatigue life measurement.

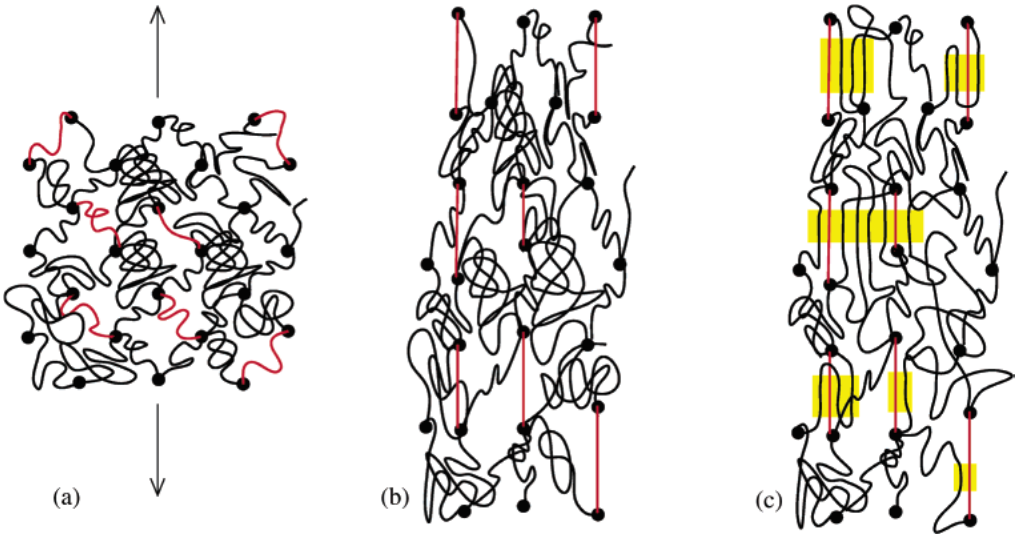

Figure 3-4 Model of nucleation and crystallisation in vulcanised NR. Relatively short chains (red lines). Filled circles represent cross-links. (a) Before deformation: cross-links are distributed uniformly (b) After deformation: short chains are fully stretched (c) The fully stretched chains act as nuclei of crystallites (yellow parts). Image reproduced from [97] with permission from the publishers).

The SIC effect in strain-crystallised rubber is a dominant influence on crack growth behaviour. Lindley [99] investigated the relation between hysteresis and dynamic crack growth resistance of NR. The author concluded that hysteresis in unfilled NR is due to the effect of SIC. The application and increase of a minimum load showed a significant increase in fatigue lifetime, which has been observed by many researchers [83,100]. The improvement was attributed to the SIC, which did not diminish when the material was unloaded. In addition, the strain energy available for crack propagation was less when the minimum load or strain was not zero [83]. In SIC rubber, crystallisation in the region of the crack tip created anisotropic material which attributed to an oriented crosslinking network chain in a direction parallel to the applied load and caused crack deviation when the crack propagation path crossed the aligned orientation network [101,102]. For higher crack growth rates or at higher strain rates [103], it appears that strain crystallisation was suppressed when there was not sufficient time for the material to crystallise resulting in a fracture energy reduction [101].

The addition of carbon black (CB) probably increases crystallinity by increasing the size of the crystallised zone at the stressed crack tip, which can inhibit propagating cracks [101]. Although there are conflicting explanations for how CB affects the crystallinity of the rubber, a review by Huneau [98] concluded that CB amplifies the local strain of the chains, which allows SIC to start at lower macroscopic stretch ratios. The strain crystallisation at the crack tip is increased at higher strain levels contributing to higher crack growth resistance in NR [84,98].

3.3 Fracture approach

The traditional method for engineers in predicting fatigue life of a component is often represented by a "Wöhler" curve also known as the S-N plot. Plotting amplitude by maximum stress, (S), against the number of cycles to failure, (N), to estimate the fatigue life of a material is shown in Figure 3.5. The data are usually displayed on a log linear plot. There is often a considerable amount of scatter in the fatigue data; therefore to determine the actual S-N line representing the mean of the data several tests per testing condition is conducted. Although the S-N curve is very useful in determining the fatigue limit or stress that causes failure at certain cycles, it does not describe directly the crack behaviour of a material.

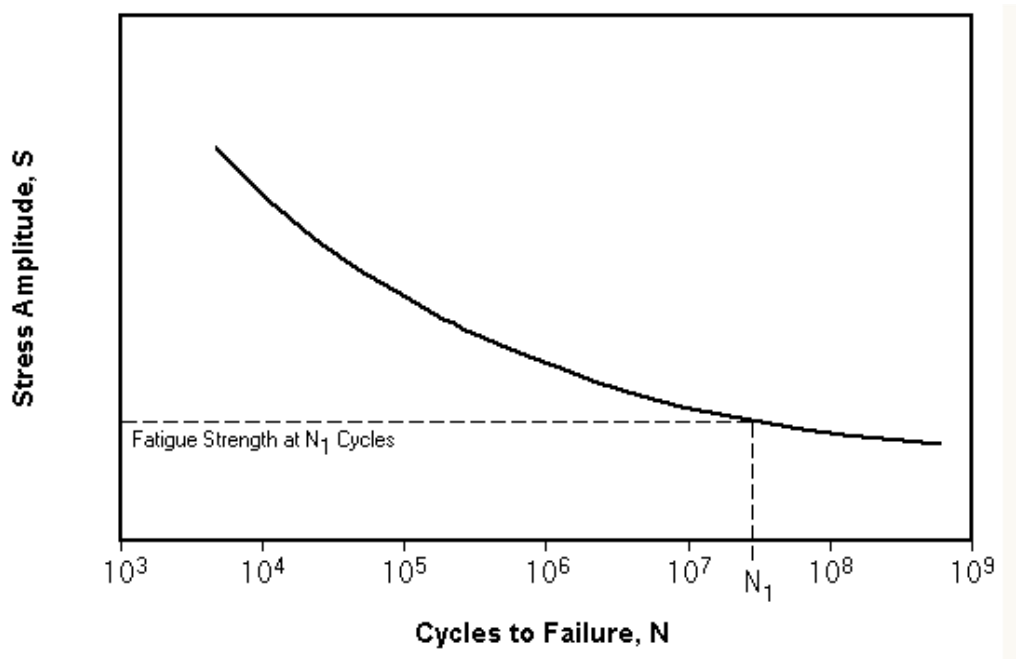

Figure 3-5 S-N curve of material.

Fatigue failure process comprises of both crack initiation and propagation of cracks due to a repetitive cyclic loading. There are two main approaches typically used by engineers to obtain fatigue life predictions, that is crack nucleation (initiation) and crack growth (propagation) analysis. Mars and Fatemi [104] have discussed both approaches and quantification parameters associated with the analysis. In the crack nucleation approach based on Wöhler curves, the fatigue life was defined as the number of cycles required to cause the appearance of a crack of a certain size. The maximum principal strain and strain energy density parameters were used for the nucleation phase.

For the crack growth analysis, Lake [105] and Gdoutos [106] stated that all materials contain pre-existing defects in the form of small flaws or voids in the material resulting from material imperfections, such as impurities or inhomogeneities due to various rubber compounding variables and poor manufacturing processing. Higher stress concentration at the crack tip compared to the adjacent material is often responsible for lowering the strength of the material and initiated fatigue crack growth. Thus, it is vital to evaluate the crack behaviour and predict the fatigue life of a material, using parameters as close as possible to the actual service conditions. In the following section, fatigue crack growth analysis based on fracture mechanics are briefly discussed.

3.3.1 The tearing energy fracture criterion

Theoretical approaches for predicting fatigue failure have been discussed and applied for more than six decades. The energy necessary for crack growth is supplied either by the strain energy in the deformed rubber, or the applied forces, or both. By applying Griffith's criterion of energy balance of fracture in hard solids, Rivlin [107] experimented on rubber vulcanisates and used the energy balance to predict the force required to rupture test pieces. Eq. 3-1 gives the Tearing energy (T) as the energy released per unit area of crack surface growth [107,108]; where W is the elastic/strain energy density stored in specimen and A, the area of one fracture surface of the crack. The tearing energy 'T' has the same definition as 'G' the "strain energy release rate" which is used for plastics and metals [83].

$$T = (\partial W / \partial A)_I \qquad \text{(Eq. 3-1)}$$

The subscript l implies that the specimen is held under constant displacement, so no external work is done on the system during propagation. Note that the energy release rate is independent of the specimen type [107]. Table 3-1 presents the Equations with associated sample geometries to calculate tearing energy.

Table 3-1 Tearing energy related to specific test pieces used for tear measurement of rubber [107].

Shape	Mathematical equation	Notation definition (units)
a) Tensile strip 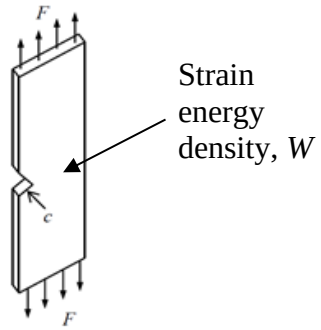	T = 2kWc	T = Tearing energy (N/mm) k = Function of strain (-) W = Strain energy density (N/mm^2) c = Crack length (mm)
b) Trouser 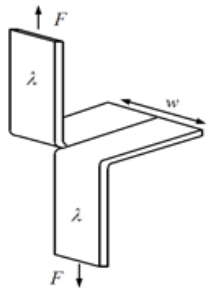	T = 2Fλ/h - wW	T = Tearing energy (N/mm) F = Force applied (N) λ = Extension ratio(-) h = Thickness of rubber sheet (mm) w = Width (mm) W = Strain energy density (N/mm^2)
c) Pure shear 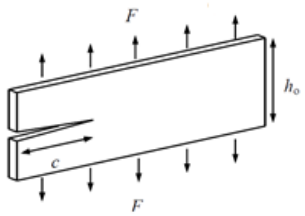	T = Wh$_o$	T = Tearing energy (N/mm) W = Strain energy density (N/mm^2) h_o = Unstrained height (mm)

Subsequent works by Gent *et al.* [109] also showed that different geometries produced consistent results in terms of crack growth rate versus tearing energy. According to Hamed [86], the agreement was better when the elastomer was rather highly crosslinked and more elastic compared to cases in which the vulcanisates were highly dissipative. With regards to problems associated with unsteady tearing such as stick-slip and knotty tearing especially in carbon black filled vulcanisates, split-tear test pieces were proposed [110].

Figure 3.6 [90] shows the schematic tearing force-time curves and crack path using a trouser test piece displaying smooth, steady, stick-slip and knotty tearing. The knotty crack growth is caused by the anisotropic behaviour of the elastomer in the region perpendicular to the direction of the crack [111].

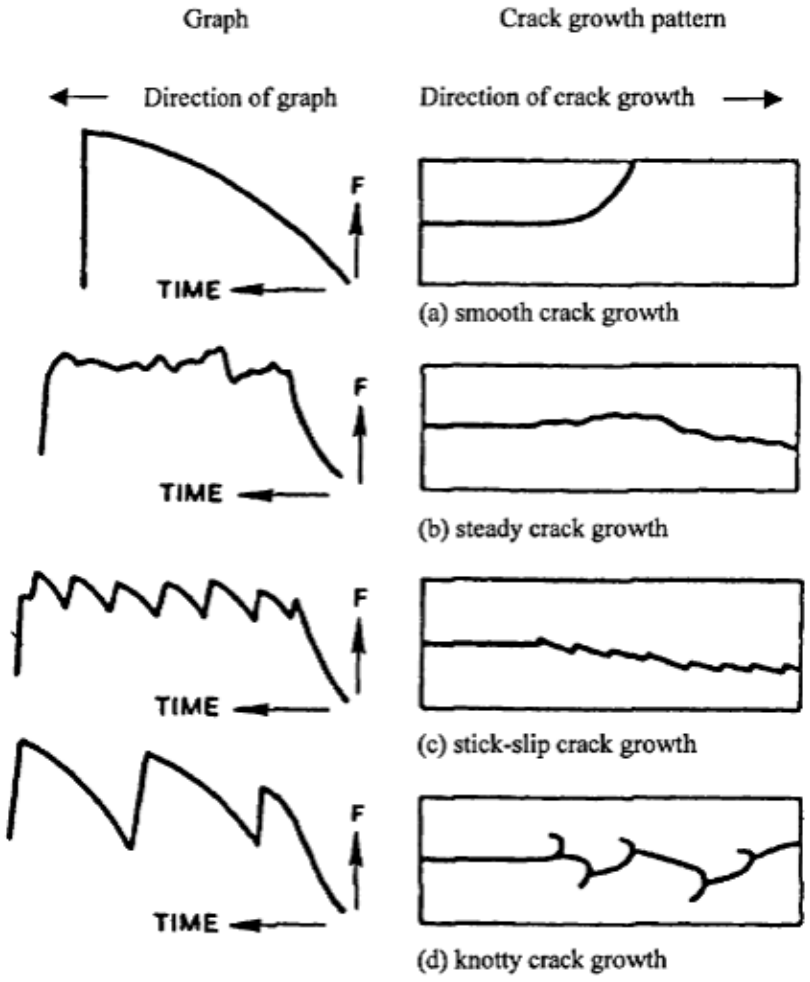

Figure 3-6 Schematic tearing force-time curves and crack path patterns of different types of crack growth. Image reproduced from [90] with permission from the publishers).

Since the tearing energy is independent of the geometry used, the relationship of crack growth rate and tearing energy, for given conditions, can represent a characteristic property of vulcanisates. Fatigue crack propagation (FCP) testing allows the comparison of different materials across a spectrum of tearing energies, rather than at only a single point [112]. The crack growth per cycle can be represented by Equation 3.2 [113]:

$$\frac{dc}{dN} = f(T) \qquad \text{(Eq.3.2)}$$

where c is the crack length in the unstrained state, n the number of cycles, T represents the maximum tearing energy attained from each cycle and obtained experimentally. It was established that during fatigue cracking, there are four regions (see Figure 3-7) associated with several development stages of crack: crack initiation, stable or incremental crack growth, and rapid, catastrophic crack growth [114,115] which are described as the following:

I: Low tearing energies: $T<T_0$, T_0 = fatigue threshold, limit below which there is no mechano-oxidative crack growth
II: Above threshold: $T_0<T<T_l$, crack growth is dependent on both environmental (ozone, uv, etc.), and mechanical factors
III: Stable crack growth region: $T_l<T<T_c$, T_c = level of tearing energy which is before critical tearing begins
IV: When the tearing energy, T, reaches the critical value, T_c ($T>T_c$), rapid crack growth will occur.

In region III, referring to Figure 3-7, between the tearing range of T_1 and T_c, the crack growth rate follows the power-law relationship in Equation 3.3:

$$\frac{dc}{dN} = B(T)^F \qquad \text{(Eq.3.3)}$$

B and *F* are constants depending on the material, frequency, temperature and environment.

Experimental results indicate that the value of tearing energy at crack initiation, T_0, is a characteristic property of the material and strongly dependent on the rubber material. Halladay and Krakowski [112] have shown that fatigue crack propagation is important for the rubber compound development in dynamic applications. The authors demonstrated that formulations with similar base elastomers (NR/BR) exhibiting similar modulus, (but differing in cure systems, carbon black grade and type of polybutadiene) behaved differently in the region between T_0 and T_c.

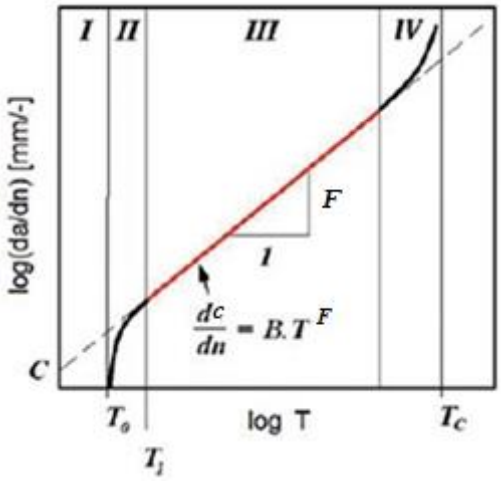

Figure 3-7 A plot of crack growth rate *dc/dN* versus tearing energy, T for a rubber material. Image reproduced from [116] with permission from Elsevier. Copyright © 2013

Non-strain-crystallising elastomers, such as SBR, can suffer from mechanical crack growth even under static load, normally referred to as time-dependent (steady) crack growth. Under cyclic loading, as a function of T, the crack growth rate can be computed as the sum of steady and cyclic contributions to the crack growth rate. Changing the cyclic frequencies also changed the strain rate, i.e. time under deformation for each cycle [117]. In non-SIC rubbers, the test frequency has a larger effect on the cyclic growth of the rubber compared to SIC rubbers which is attributed to the time dependent continuous crack growth, associated with the viscoelastic behaviour [117]. As for SIC rubbers such as NR, crack growth only occurred above a given applied tearing energy and therefore the fatigue crack growth of NR appeared to be not time dependent. The fatigue crack growth of NR showed less frequency dependency over the range of 10^{-3} to 50 Hz [117].

Tsunoda [90] found that the energy loss increased with an increasing strain rate (0.41, 4.16, 41.6 s^{-1}) for an unfilled SBR, however, for 50 pphr of CB filled SBR, the energy loss was much less sensitive to the similar strain rate. Lake and Thomas [118] reported that carbon black fillers could substantially reduce the time-dependent crack growth in non-crystallising rubbers.

3.4 Effect of rubber formulations on fatigue behaviour

3.4.1 Base polymer/polymer type

The susceptibility to fatigue is significantly different between strain induced crystallising (SIC) and non-crystallising rubber. Rubbers that exhibit SIC include (homopolymer) natural rubber (NR), isoprene rubber (IR) and polychloroprene (CR), while (co-/ter) polymers exhibiting little or no crystallisation include styrene-butadiene rubber (SBR), polybutadiene (BR), butyl rubber (IIR), NBR and ethylene-propylene rubber (EPDM) [80]. The viscoelastic behaviour of the elastomer plays an important role in inhibiting crack growth especially once the threshold limits of tearing energy, T_0 are exceeded [113]. Thus, at high strain, higher energy dissipation is desirable to inhibit mechanical crack growth. For SIC rubber, the effect of high hysteresis is more pronounced due to strain crystallisation. (see section 3.2.1)

Figure 3-8 shows a comparison of crack growth behaviour for different elastomers. At low tearing energy, CR displayed a lower fatigue crack growth rate compared to NR, EPDM and NBR. In contrast, at higher tearing energy, NR exhibited lower crack growth than CR. This implies that over the whole tearing energy range (T_0 to T_c), no single material has the best fatigue life properties [117]. Young [114] used power law fatigue growth constants to differentiate between different rubbers and their blends as shown in Table 3-2 [80]. The data showed that NR exhibits a smaller fatigue crack growth exponent, F in Equation ($da/dN = BT^F$) and high tearing energy due to strain crystallisation. F is dependent on the elastomer used and can be affected by both strain level and strain rate. It also indicates that proper blending between rubbers [119] and secondary factors, such as compounding ingredients [117], can contribute to lower F.

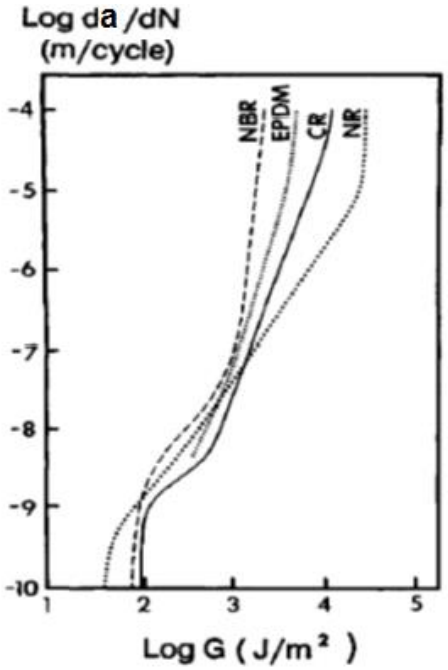

Figure 3-8 Fatigue crack growth rate as a function of tearing energy at 22°C for various elastomers [117]. (Figure reproduced as original [120]: *da/dN* = *dc/dN*, G = T)

Table 3-2 Fatigue Crack Growth Properties of Various Filled Elastomers, da/dN = BT^F [80,119]. (Note: da/dN = *dc/dN*)

Elastomer	B (m/cycle)/(x10^{-18} J/ m^2)^F	F
NR	4460000	1.35
45/45/10 CIIR/NR/EPDM Blend	33900	1.91
50/50 NR/BR Blend	13800	2.12
60/35/5 CIIR/NR/EPDM Blend	9500	1.96
BR	12.0	3.44
CIIR	0.85	3.31
BIIR	0.12	3.42

3.4.2 Filler

Generally, fillers are classified into three groups, reinforcing, semi-reinforcing and non-reinforcing. Rubber reinforcements' effectiveness is dependent on the characteristics of the filler such as, particle size, surface area, surface activity, crystal structure, structure (for

carbon black) and volume fraction. The most frequent reinforcing fillers are carbon black (CB), precipitated silicas, and nanofillers (clay, nanotubes), which have attracted much attention recently [121]. The addition of active fillers results in a substantial increase in stiffness, tensile strength, and resistance to abrasion and wear of unfilled rubbers. Furthermore, the effect is pronounced especially in non-crystallising rubber. Mars and Fatemi [80] have described possible multiple mechanisms, due to the inclusion of filler which potentially affect the fatigue properties, which include:

i) pronounced changes induced by fillers on stiffness and hysteresis properties;
ii) crack tip blunting, deviation and branching, induced by inhomogeneity of the rubber-filler composite, at the crack tip;
iii) agglomeration of filler particles, resulting in increased effective initial flaw sizes.

Hence, well-dispersed filler is extremely important in providing energy dissipation, the ability to deflect or arrest crack growth, thereby delaying the onset of catastrophic crack growth [122]. Although the dissipative process is not fully understood, as it involves several mechanisms as previously mentioned, the role of molecular mechanisms on fatigue and fracture of rubber is given by Hamed [102,122]. The effect of CB structure and concentration on fatigue life of SBR has been studied by Dixon *et al.* [123] and Auer *et al.* [124] respectively. Carbon blacks are characterised by their grape-like structure comprised of particles fused together as rigid structures termed aggregates. High structure carbon black exhibits a higher range of particle aggregation meanwhile low structure carbon black consists of individual spherical carbon particles and less aggregates. Finer carbon black produces better fatigue life compared to the coarser grades. Additionally, similar to filler reinforcement, optimal concentration of filler is required to achieve maximum crack growth resistance. Beyond optimal concentration, the fillers tend to agglomerate and contribute to the increase of the effective flaw size, resulting in lower fatigue lives [28,80]. The fatigue life is also found to increase with structure level and decreases with higher specific surface area of the carbon black [28]. The structure level and surface area of carbon black can be determined by the dibutyl phthalate (DBP) absorption number and Nitrogen surface area respectively.

Nie *et al.* [125] investigated the influence of different furnace carbon blacks on the fatigue crack growth of NR, in relation to the material properties. The authors found that carbon

black grade; N330-filled NR (filler particle size, 28-36 nm) had the lowest crack growth rate at a given value of tearing energy, thus, the higher resistance to crack growth, whereas N770-filled NR (filler particle size, 61-100 nm) had the lowest crack-growth resistance. Therefore, better fatigue properties in carbon-black NR filled vulcanisates are obtained using high structured CB compared to low structure CB. This finding is consistent with previous research [28].

3.4.3 Crosslink density and structure

It is recognised that crosslink density determines the physical properties of rubber as depicted in Figure 3-9. As the crosslink density increases, modulus and hardness increase whereas elongation at break, and permanent set, decrease. On the other hand, tear, tensile strength and fatigue resistance pass through different maxima, and then decrease. It is also well understood [115,117], that the polysulphidic type networks confer high levels of fatigue resistance to accelerated sulphur cure systems, relative to monosulphidic crosslink networks, for natural rubber vulcanisates. The ability of the polysulphidic chain to break and reform when overloaded redistributes the stress to neighbouring areas contributing to the superior properties [80]. In this case, conventional and semi-EV (efficient vulcanisation) processes are often selected for longer fatigue life. However the superiority of polysulphidic crosslinks changes as rubber is exposed to thermal oxidative conditions (presence of oxygen and high temperatures). For SBR passenger car tyre, when more polysulphidic links are present in the network, reduction of the groove crack resistance is observed [126].

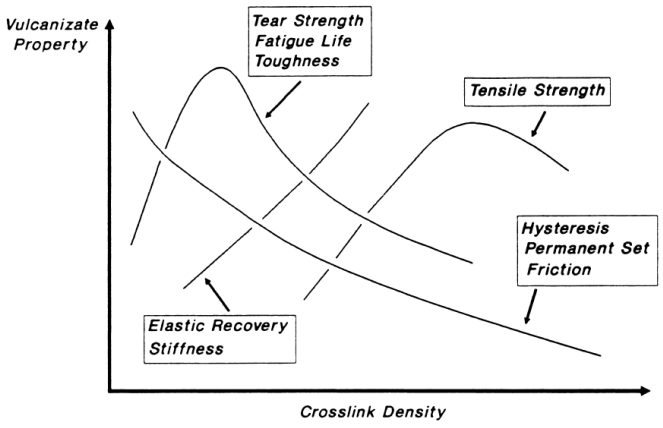

Figure 3-9 Effect of crosslink density on rubber vulcanisates [127].

Kim [128] revealed that heat ageing in air caused changes in crosslink density and structure resulting in higher FCP rates. It appears that conventional systems exhibit higher FCP rates compared to other type of crosslinking systems due to a poorer resistance to heat ageing. There is an optimum crosslink density for each type of crosslinking system to achieve maximum fracture resistance [80,102]. Nevertheless the effect on the type and degree of crosslinking is less pronounced than the choice of elastomer.

Scott [129], pointed out that the involvement of sulphur compounds contributed to the anti-fatigue behaviour. Therefore, he emphasised the contribution of sulphur in fatigue resistance and suggested vulcanisates with other crosslinking agents, in order to achieve high levels of fatigue resistance.

3.4.4 Environmental effects

3.4.4.1 Oxygen

The principal mechanism of oxygen attack is an autocatalytic, free radical reaction as reported elsewhere [130,131] and results in reduction of tensile strength and elongation properties. Degradation by oxygen results in hardening or softening depending on the microstructure of a diene elastomer [131]. Rubber compounds exhibit dominant chain scission during ageing, and generally become softer and sticky. However, most rubber compounds eventually harden and embrittle during oxidation as the consequence of a dominant crosslinking reaction [130]. The high degree of unsaturation in the backbones of "diene" rubbers (such as NR, SBR, NBR) and chloroprene rubber (CR)) makes them prone to oxygen and ozone attack. On the other hand, saturated rubbers such as acrylic rubber (ACM), chlorinated polyethylene (CM), fluoroelastomer (FKM) and silicone rubber (Q) are much less sensitive to oxidation than diene rubbers [131].

Experimental results conducted in air and vacuum showed that oxygen plays an important role in fatigue crack growth. Thus, the threshold, T_0, for the initiation of mechanical crack growth is much lower in the presence of oxygen [113].

Antidegradants (antioxidants and antiozonant) can be added to rubber compounds to protect rubber products against oxygen and ozone attack, either physically or chemically. Physical protectors such as microcrystalline waxes in rubber compounds migrate to the surface, providing a physical barrier between rubber and the degradants. Datta [131] highlighted however, under dynamic conditions, wax gives no protection and may accelerate failure by concentrating ozone attack at flaws in the surface film created by flexing. Improvements in fatigue life can also be obtained through the addition of antioxidants, which appear to reduce mechano-oxidative crack growth. Common types of antidegradant are aromatic amines, phenolics and phosphites. The success of N-isopropyl-N'-phenyl-p-phenylenediamine (IPPD) compared to other types of antioxidant is undisputable. Scott [129] revisited the fundamental work of antidegradants development and provided comparisons of detailed mechanism of antioxidants and antifatigue agents. It is an interesting finding that different types of antioxidants can provide different antifatigue efficiency for rubber compounds. This is mainly dependent on the role of these additives to remove or involve the trapping of alkyl and alkyl proxy radicals during rubber degradation at various temperatures/conditions [132].

3.4.4.2 Effect of temperature and oxidative ageing

At constant strain, a significant drop occurs in the fatigue life of SBR gum vulcanisates, while only a small variation is observed for gum NR vulcanisates as the temperature increases from 0°C to 100°C [105]. The effect of temperature is greater for amorphous than crystallised rubber and the temperature dependence can be reduced by filler incorporation.

The oxidative ageing (combined effect of oxygen and temperature) effect involves chemical and physical changes of the rubber network and results in reduced resistance to fatigue crack growth. Crack growth rates increased in oxidised rubber. For example in tyres, cracks propagated between the belts, potentially resulting in tread separation [133]. The effect was greatest at elevated temperature. Hamed and Zhao [134] also observed that carbon filler in NR and SBR promoted stiffening during ageing. This would ultimately contribute to a reduction in resistance to cut growth and flexing in rubber.

Legorju-Jago and Bathias reported [135] that the crack growth rate of natural rubbers increases when the temperature increased. The authors also concluded that fatigue damage

depended on three basic mechanisms: chemical (composition, crystallisation), environmental (oxygen) and mechanical (stretching, triaxial stresses). In addition to the mechanical damage, an important chemical damage occurred due to the presence of gaseous oxygen in the air. This chemical damage was more extensive at higher temperatures, caused by the acceleration of the oxidation reaction. Hu *et al.* [136] found similar results with a pronounced deterioration in tensile and tear strength at higher temperature for carbon black filled NR.

3.4.4.3 Ozone

The initiation of crack formation on strained samples can become more severe in the presence of ozone, leading to faster fatigue failure. It was reported [137] that only about tens of parts per billion (ppb) ozone in the atmosphere, activated by sunlight/uv, can cause severe cracking of rubber. The effect of ozone on elastomers can occur during constant and cyclic deformation. Referring to the power law dependence of crack growth rate, which is valid only over a limited T range, it is found that below the mechanical fatigue threshold, T_0, the mechanical crack growth is absent and therefore ozone attack is the single source of crack growth. In this region, for unprotected rubber, the tearing energy threshold (due to ozone), T_z is approximately 0.1 J/m^2 [80]. This value however depends on the presence of antioxidants and antiozonants. The rate of crack growth can also be influenced by the polymer type and is directly proportional to the ozone concentration. However, once T_0 is exceeded, increasing tearing energies, the ozone influence quickly becomes negligible at normal atmospheric ozone concentrations since the mechanical crack growth is much more rapid. The T_0 reported for vulcanisates, including NR and SBR is about 50 J/m^2 [118]. A detailed discussion on ozone cracking was given by Lake [138].

For a rubber compounder, the economical way to protect rubber from ozone attack under both static and dynamic conditions is the addition of antiozonant chemicals to the rubber compound. However, careful selection is required, taking into account the diffusion coefficient of the antiozonant as the protection mechanism of each antiozonant also varies. Typically, para-phenylenediamines (PPDs) are effective in reducing ozone cracking in diene rubbers [130]. Antiozonant protection via physical methods such as microcrystalline wax can be used, by blooming to the surface, to form a protective film which is impermeable to ozone. Under dynamic conditions, however, physical methods alone are not as efficient. Hence, the

combination of protective film formation and scavenging is the most preferable mechanism [131]. The efficient scavenging mechanism required the antiozonant to rapidly migrate to the surface of the rubber to react with the ozone's attack on the double bond of the rubber chains. This process is strongly dependent on the diffusion rate of the antiozonant chemicals.

3.4.5 Anti-reversion agent/chemical

Datta [131] investigated anti-reversion chemicals such as Thiuram, dithiophosphates accelerator, zinc soap acitivators (struktol A73), silane coupling agent, disodium hexamethylene bisthiosulphate (DHTS), Perkalink® 900 and 1,6 –bis (N,N-dibenzylthiocarbamoyldithio) hexane (BDTCH, Vulcuren KA 9188) to improve the thermal stability during overcure or exposure to heat, under limited supply of air, which can affect the mechanical properties of the elastomer. With respect to fatigue life and applicability to truck tyre tread compound, the author concluded that DHTS, in typical NR formulation, significantly improved fatigue life before and after ageing, while Perkalink® 900 and Vulcuren KA 9188 provided marginal improvement due to the heat stability offered by the network formed. The addition of thiuram, dithiophosphates accelerator and zinc soap activator however, decreased the fatigue properties. The approach, which reduced sulphur and increased accelerator level, resulted in a network with a higher proportion of monosulphidic crosslinks compared to polysulphidic crosslinks.

3.4.6 Blends

Blending can offer a set of properties that have great potential of providing application areas not possible with either of the polymers comprising the blend [139]. However, compatibility between blends is important to achieve targeted properties to exploit the full potential of both materials' intrinsic properties. Suitable blending improves overall performance such as reduced tread wear. The common examples for blends in tyre manufacturing are tread, side wall and carcass formulations. For industrial applications such as conveyor belts, balanced properties like fatigue, ozone, strength and flame resistance requirement may be obtained by appropriate blending. Beatty [79] has demonstrated several combinations of blends used in tyres. The author drew general conclusions from fatigue tests, particularly at fully relaxing

conditions that either BR or SBR, depending on the blend composition, improved the flex-fatigue of NR. As for crack growth tests, he also concluded that BR improved crack growth resistance in both SBR and NR and observed some correlation between fatigue results and crack growth.

A study by Kim and Hamed [140] concluded that a blend of NR and BR was suitable for passenger car sidewalls due to their good crack growth resistance. The blends possess advantageous features of NR and BR which are probably due to the co-continuity phases of a 50/50 blend. Similarly, an investigation [141] of CB filled (50 pphr) NR/BR blends compound, showed the increase in BR ratio led to faster crack growth at higher tearing energies. Blend ratios with higher NR content showed higher crack resistance due to the strain-induced crystallisation of the NR. The authors described that the lower crack growth resistance of BR at high tearing energies was attributed to chip and cut mechanism. The FCP behaviour of NR and NR/BR blends (different ratios) using double-notched pure shear specimen was studied over a wide range of tearing energies [142]. The authors highlighted the contribution of higher BR content toward reduced crack growth rate of NR/BR blends in a range of 20-35 % strain, but reversal ranking was observed above a transition strain level. The effect of temperature, R ratio, waveform and cure system in NR and NR/BR (60/40) was also discussed.

Apart from carbon black, reinforcing silicas have been widely used in tyre compositions for reducing rolling resistance. In this case, the addition of coupling agents was necessary to improve the rubber filler interactions. Menon *et al.* [143] studied phosphorylated cardanol prepolymer as a coupling agent compared to traditional silane coupling agents. This study showed that uniform distribution of fine particles of filler with a high degree of polymer–filler interaction played an important role for improvement of the mechanical properties. They found that vulcanisates containing phosphorylated cardanol prepolymer showed higher tear strength and greater resistance to fatigue-crack growth at various deformation ratios.

3.5 Effect of ELVRT on the fracture properties of rubber

Karabork and Akdemir [144] mentioned that many documented publications concentrated on the mechanism and mechanical properties of devulcanised rubber-virgin rubber composites.

This is consistent with the review in Chapter 2 of this thesis. There is very little discussion on the fatigue performance of ELVRT, untreated or treated, when incorporated in a virgin/fresh rubber compound. A few reports on the fatigue and crack behaviour of the ELVRT compound will be discussed in this section. The authors also suggested that further investigations related to the influence of different devulcanisation methods, devulcanised rubber content, morphology and state of crosslinking on devulcanised rubber filled with different virgin rubber were necessary to provide more insight into the friction and wear behaviour of revulcanised/recycled compound. Although, friction and wear behaviour are beyond the scope of this review, wear of rubber is mainly caused by fatigue or tearing of the rubber compound due to frictional forces [145].

Han *et al.* [146] studied the crack growth and fatigue life of NR and SBR filled vulcanisates with the addition of various sizes of ground rubber powder (GRP) and different concentrations. They reported that crack growth was reduced with increased concentration and decreasing particle size of the ground rubber powders. Similar results were obtained for fatigue life and the effect was more prominent for SBR vulcanisates compared to NR. Comparing the fatigue growth rate, NR vulcanisates possess a lower crack growth rate than SBR due to its SIC properties [105]. In the case of filled vulcanisates containing GRP, Han *et al.* [146] observed that the crack growth rate of SBR and NR were quite similar and assumed that the SIC of NR probably did not occur. They stated that the presence of ground rubber particle *in situ* at the crack tip might suppress the SIC effect. The authors [146] used DeMattia flex cracking (DMFC) for crack growth rate measurement. Findings by other researchers [112,117,142] highlighted the contradictory performance of rubber compounds at different tearing energies. This suggests that the energetic approach for crack growth analysis would be appropriate for the GRP evaluation.

Bandyopadhyay *et al.* [30] incorporated different particle sizes of ELVRT; 40, 80 and 100 (~150 μm) mesh, in NR/BR blends of light commercial vehicle tyre tread compounds. Similarly, with the previous study [146], it was observed that fatigue life (fatigue to failure properties tests at 100% strain) of the vulcanisate improved with smaller particles size and decreased with higher ELVRT concentrations. The crack growth property using DMFC, however, did not produce any clear trend.

Previous studies [147,148] have reported that poor adhesion between ELVRT and rubber matrix cause deterioration in the mechanical properties. Kumar *et al.* [149] highlighted the need to study not just the adhesion between matrix and ELVRT, but also cohesion within ELVRT. The authors developed a modified Intrinsic Flaw Sizes (IFS) using corner cuts on a tensile dumbbell specimen instead of edge cuts in SBR compounds (unfilled and filled carbon black) using ELVRT granulates from model compounds. They then examined the interfacial strengths between matrices and granulates and between the granulates using trouser tearing and peel energy test. They found that the granulates increased the defect size and, as expected, the bonding was also weaker. In addition, the granulate-granulate interface was much weaker than the matrix-granulate. This finding is consistent with the previous statement on ELVRT that without appropriate surface modification or reduction in size, the level of incorporation will be limited and reduces mechanical properties.

Investigation by Phadke *et al.* [148] offers important insights to the evaluation of ELVRT in rubber compounds. Higher sulphur content and the addition of carbon black compensated for losses in the physical properties of cryogenic ELVRT (400 μm) filled NR compound. The researchers used DMFC to measure the fatigue life of the vulcanisates.

Stoček *et al.* [150] have demonstrated how the addition of waste rubber powders from truck tyres could positively influence the fracture mechanics of a rubber-polymer-blend-system. It is, however difficult to conclude since the source of the ELVRT, the blend system and the preparation method were not reported adequately.

3.6 Summary

1. Designing rubber formulation for longer fatigue life is challenging since there are many factors that may affect the performance of the rubber. Effects of various compounding ingredients such as the base elastomers, fillers, oil, curing system and type of crosslinking play an important role in determining the strength of the rubber. In addition, different service environments, the effect of oxygen, ozone, temperature, heat ageing and the combination of these factors need to be taken into consideration. Incorporation of suitable antioxidants and antiozonants is necessary to ensure the durability of the rubber.

2. Material imperfections, such as impurities, flaws or inhomogeneities act as stress initiators/raisers which can initiate cracks. The development of cracks can weaken the strength of rubber under repeated stress, leading to failure. The size, shape and concentration of the flaws are factors that could affect the crack growth behaviour. To add to the complexity, the modes of deformation, frequency, temperatures, and stress acting on the rubber influence the mechanical fatigue life of rubber during service.

3. Additionally, the dynamic and fracture behaviour of filled rubber also changes with the dissipative aspects from the stress-strain behaviour (e.g. strain induced crystallisation, Mullins effect, cyclic stress softening and viscoelastic) of rubber. Therefore, thorough assessment related to rubber containing ELVRT should take into accounts all of the aforementioned factors. Currently, the fracture mechanics approach based on a tearing energy fracture criterion is described as the most acceptable approach to predicting the failure of rubber components.

Chapter 4 Recycled Rubber Powder (RRP) characteristics

4.1 Introduction

The method of production of RRP, such as cryogenic or ambient temperature milling of the End of Life Vulcanised Rubber Tyres (ELVRT), affects the morphological structure and size of the particles. In addition, characteristics of the particle i.e. Brunauer–Emmett–Teller (BET) surface area, surface roughness, morphology, particle size distribution etc. have a huge influence on the particle-matrix interaction [41]. The ambient process produces a coarse structure, whereas the cryogenic process results in smooth textures [2,32,33]. Based on the irregular structure resulting from ambient method, Dierkes [32] emphasised that the cavities on the surfaces allow penetration of polymer chains and thus provided good physical bonding. Therefore, the ambient ELVRT-filled rubber compound was claimed to provide better mechanical properties than cryogenic milled filler compound. In contrast to Dierkes, Ayyer *et al.* [151] claimed that the cryogenic particles had higher surface area due to a greater proportion of finer particles compared to ambient particles, for all nominal particle sizes.

Despite the advantages of ambient ELVRT, the commercial scale process for ambient ground rubber is only able to produce ≥ 400 μm particles (see Chapter 2.3 for advantages and disadvantages of different textures of ELVRT resulting from different methods of grinding). Thus, the emergence of smaller sized ELVRT produced using cryogenic methods in micronised form certainly appear to have great potential for many applications. Composition of the ELVRT used (type of rubber, carbon black content, etc.) is also important to ensure the compatibility of new rubber formulations and to further understand their effects on the vulcanisate properties. Thus, in this work, particle size distribution, morphology and the composition of two different commercial available types of ELVRT were analysed before incorporating them in new rubber formulations.

4.2 Experimental procedures

4.2.1 Materials

Crumb rubber powder (CRP400) entirely made from truck tyres, with a 40 mesh or ~ 400 µm maximum nominal particle size, was supplied by Crumb Rubber Ltd., Plymouth. Micronised Rubber Powder (MRP074-Polydyne^{TM} 200) supplied by Lehigh Technologies of Georgia, US is recycled rubber material also from truck tyres, 200 mesh (at < 74 µm). CRP400 and MRP074 recycled materials were from different batches of tyres. In this study, Recycled Rubber Powder (RRP) refers to both MRP074 and CRP400 filler.

The morphology of the raw RRPs were observed using a JEOL JSM-6610 LV Scanning Electron Microscope (SEM), operating at 15 kV accelerating voltage. The specimens were gold coated prior to analysis to avoid electrical charging.

The MRP074 particle size distribution was analysed using the ImageJ [152] (open source image analysis software from the US National Institutes of Health, http://imagej.nih.gov/ij) package. The images of MRP074 from SEM were transformed to binary images before the analysis was done (see Appendix A for detail procedures). The analysis set 100 µm^2 as the particle lower limit and estimation of the apparent average particle size diameter was based on a circular equivalent area, irrespective of any shape appearing in the region of interest. An approximate diameter of the particle size (d) was calculated using, $d = 2\sqrt{(A/\pi)}$, where area (A) automatically measured by the software). The calculations may overestimate the actual particle size due to the irregular structure of the RRP. Comparing the binary to the original image is important to avoid unnecessary stray pixels. Overlap particles need to be separated using the watershed function in ImageJ.

Due to overlapping and irregular structures, CRP400 were characterised by means of sieve distribution analysis using an Endecott test sieve shaker with different sieve aperture (500, 355, 250, 180, 125, 90 µm), as shown in Figure 4-1. All the selected sieve sizes were stacked accordingly and mounted in the Endecott test sieve shaker and subsequently shaken for approximately 15 min [153]. The last pan collects any particles smaller than 90 µm. 50 g of CRP400 powder was used for each sample within a similar batch to provide more

representative data. The measurement was made three times. Once the sieving was completed, any powder rubber retained on a specific sieve was weighed. The percentage of individual retained and cumulative passing of the CRP400 were calculated.

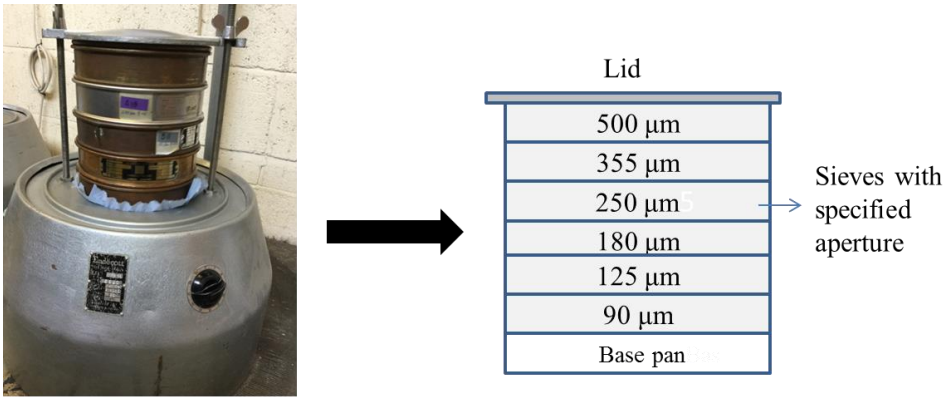

Figure 4-1 Particle size distribution using an Endecott mechanical shaker and schematic diagram of the sieves arrangement.

4.2.2 Particle composition analysis

The composition analysis of RRP (CRP400 and MRP074) was performed using ThermoGravimetric Analysis (TGA) and Fourier Transform Infrared (FTIR spectroscopy). These tests were conducted at Tun Abdul Razak Research Centre (TARRC), Hertfordshire, UK. The precision for the polymer ratio was ±5 wt%, while for the TGA analysis was ±0.9 wt%. Prior to analysis, samples were acetone extracted overnight at ~56°C. The extraction was performed to remove low molecular polar substances such as remaining accelerator and curatives [8]. Thermal weight loss measurements were made using a PerkinElmer Pyris1. Extracted samples of approximately 10-15 mg were heated from ambient temperature with a heating rate of 30°C/min in a nitrogen atmosphere and switched to oxygen atmosphere at around 550°C. For the FTIR, portions of each extracted sample were pyrolysed in a test tube, under standards conditions at 515°C ± 10°C and the released liquid was analysed using a PerkinElmer Spectrum 100 FT-IR Spectrometer.

4.3 Results and Discussion

4.3.1 Characterisation of raw recycled rubber powder

Figure 4-2 shows the morphology of micronised powder rubber (MRP074) from the cryogenic production with a nominal particle size of 74 µm (Lehigh Technologies product specification). It is clear that the structure of cryogenic powder from waste tyres is microscopically smooth and angular, consistent with reports from other authors [32,151]. The morphology of ambient crumb rubber was seen to be rough texture and also containing some smooth surfaces as shown in Figure 4-3.

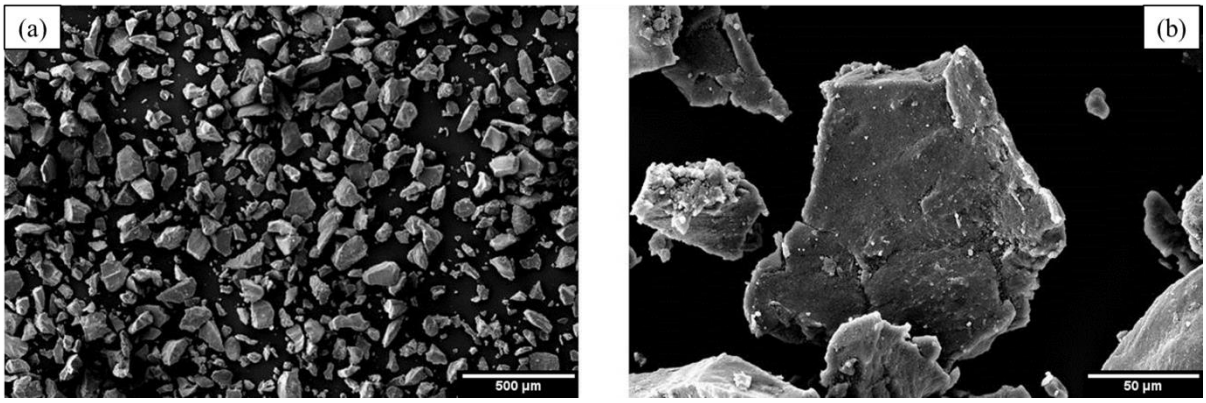

Figure 4-2 Micronised powder rubber (MRP074) from the cyrogenic method (~74µm), (a) white scale bar represents 500 µm (b) white scale bar represents 50 µm.

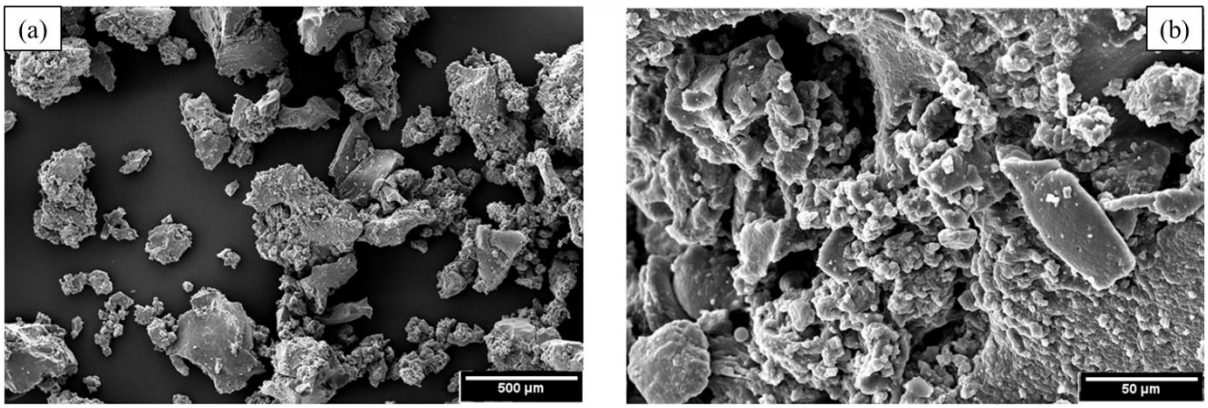

Figure 4-3 Crumb rubber (CRP400) from ambient ground tyre (~400 µm), (a) white scale bar represents 500 µm (b) white scale bar represents 50 µm.

The two-stage weight loss in the TGA analysis (Figure 4-4) is related to the decomposition of NR and SBR/BR respectively. The first major weight loss (D1) occurs at a maximum rate of approximately 400°C. This is assigned to the decomposition of NR and the second weight loss (D2) at a maximum peak decomposition temperature around 455°C is assumed to be the butadiene-based rubbers. This is consistent with the findings of other authors [44,154]. When the N_2 atmosphere was switched to O_2, the carbon black reacted with the oxygen and contributed to the weight loss above 550°C. The solid residue commonly called 'ash', due to inorganic fillers, remained in the pan after cooling.

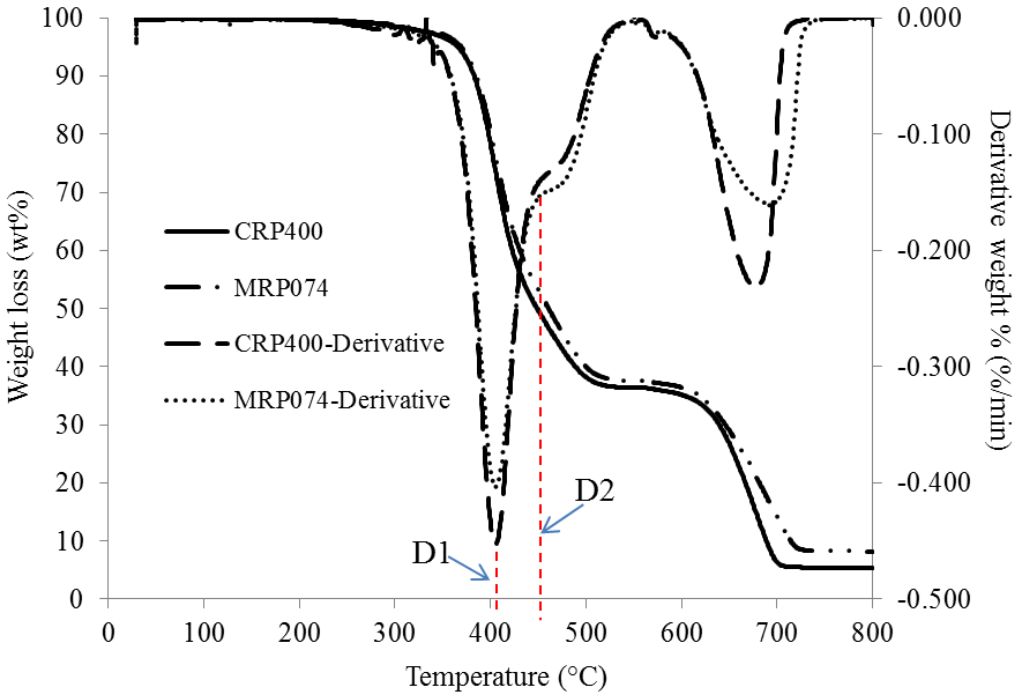

Figure 4-4 TGA weight loss and weight loss derivative curves as a function of temperature of RRP.

FTIR analysis was conducted to confirm the blend compositions. The IR absorbance peaks of MRP074 or CRP400 are shown in Figure 4-5. The peak absorbance at around 890 cm^{-1} is assigned to the NR structure. Other peaks related to typical polyisoprene are present around absorbance peaks of 1454 and 1377 cm^{-1} for δCH_2 deformation. The peak absorbances at around 967 cm^{-1} assigned to aromatic C-C stretching of Styrene Butadiene Rubber (SBR), was observed. These positions agree well with other reported research [44,154] although the intensities of the peaks change due to different blend compositions.

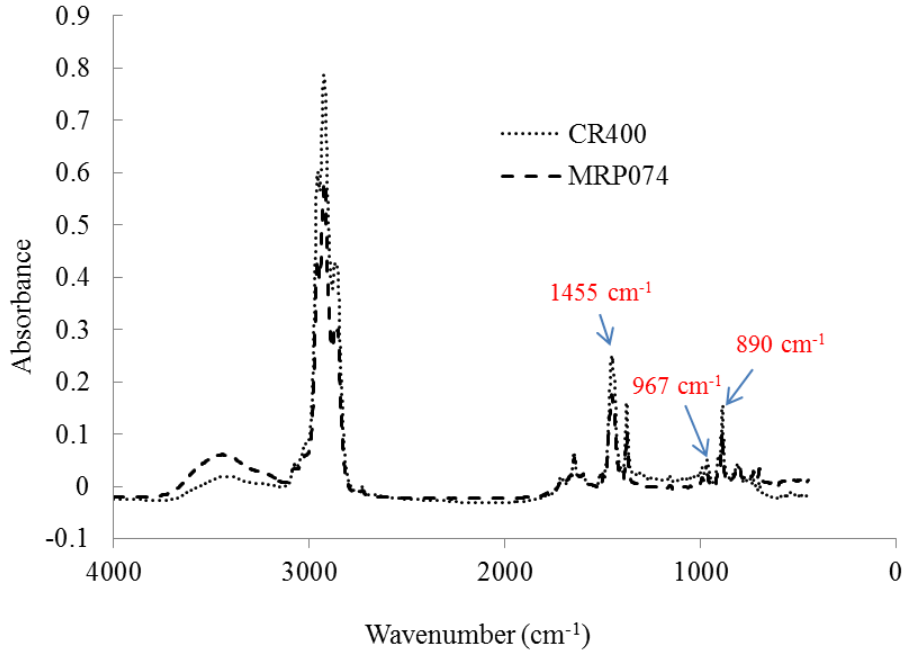

Figure 4-5 FTIR absorbance of CRP400 and MRP074.

The composition analysis from TGA, complemented by FTIR spectroscopy, is given in Table 4-1. The polymer ratios in NR/SBR/BR RRP are based on calibration curves using SBR with 23.5% styrene. The identification of NR to SBR/BR polymer ratio in both powders is about 80:20 by weight (NR:SBR/BR). SBR and BR show similar structure in the FTIR footprint, so this method could not distinguish between them. The main composition was not significantly different after taking into account the precision of the measurement, except that MRP074 had a slightly higher ash value, compared to CRP400. This was probably a result of excess talc added to prevent the rubber surfaces from sticking together during the cryogenic grinding process and storage.

Table 4-1 Composition of recycled rubber powder after analysis.

	Composition (wt%)		
	CRP400	MRP074	Change from CRP400
Rubbers	60.9	59.6	(-1.3)
Carbon	28.8	27.2	(-1.6)
Ash	5.0	7.6	(+2.6)
Extract	5.3	5.6	(+0.2)

4.3.2 Particle size distribution of RRP

The average result of the particle size distribution of CRP400, by sieve analysis, is displayed in Table 4-2. Since the powder is 40 mesh grading, it is expected that 100% of the particle size would pass through the 500 μm sieve size. In this case, some of the powder was slightly agglomerated and did not pass through the sieves. For the MRP074 particles, the distribution showed about a 20% fall between 0-30 μm, 48% between 30-60 μm, 26% between 60-90 μm, and 6% between 90-120 μm as shown in Figure 4-6 (a). The higher particle sizes, above 100 μm, are probably due to agglomeration or overlapping particles, which are difficult to separate during image analysis measurement.

Table 4-2 Average particle distribution of a 50 g CRP400 sample using sieve analysis.

Sieve size (μm)	Mass retained (g)	Individual retained (%)	Cumulative passing (%)
500	0.15	0.30	99.70
355	18.08	36.81	62.89
250	15.32	31.18	31.70
180	12.11	24.64	7.06
125	3.22	6.55	0.51
90	0.25	0.51	0.00
Pan	0		
Total	49.12*	100.0	

*A small loss in the total mass of powder compared to the original was probably due to a loss in air during sieve transfer or sticking to the mesh sieves

Figure 4-7 shows the cumulative frequency of apparent particle size of MRP074 (µm) and the cumulative passing of CRP400 particles, using a sieve analysis. The median apparent particle size diameter (50% of the value in cumulative distribution) for CRP400 was approximately 300 µm, while for MRP074 was approximately 60 µm.

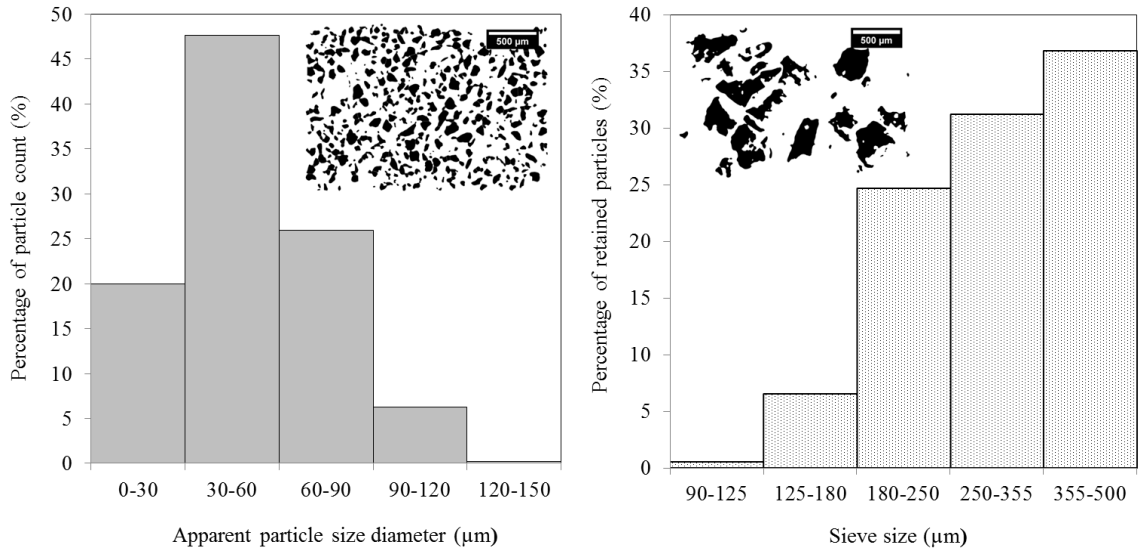

Figure 4-6 Histogram of (a) percentage particle count MRP074 versus apparent particle size diameter (µm) (b) percentage of retained particles of CRP400 using sieve method.

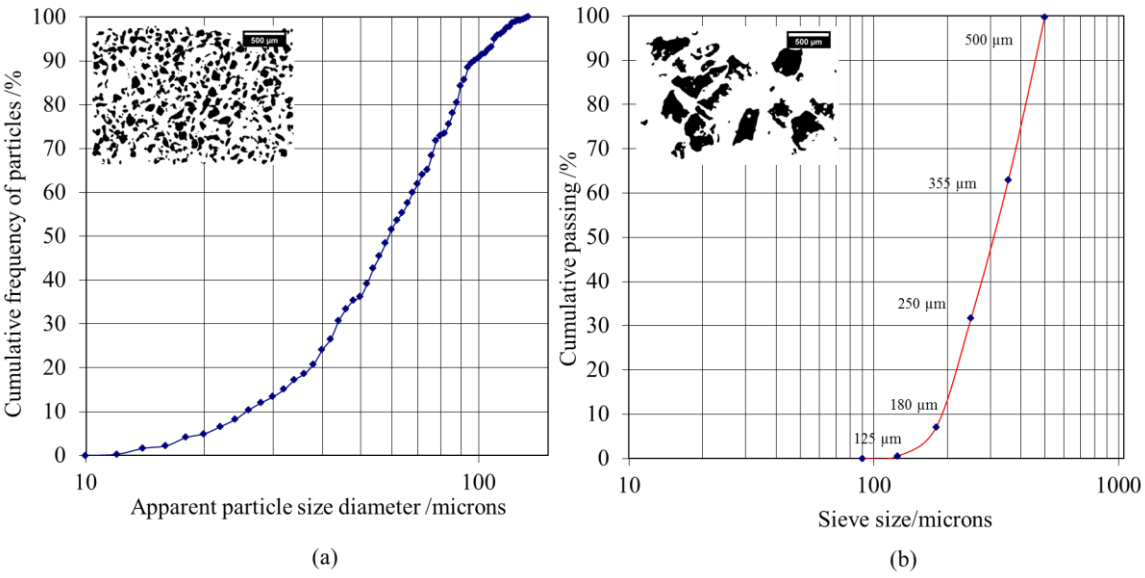

Figure 4-7 Particle distribution of (a) MRP074 (Cumulative frequency using image analysis) (b) CRP400 (Cumulative passing by sieve).

4.4 Summary

The difference between CRP400 and MRP074 resulted from the method of production, where CRP400 were ambient milled particles and MRP074 were cryogenic milled particles. The material compositions of both powders were quite similar for rubber/type, carbon black and extract content. The MRP074 however contained a slightly higher ash content compared to CRP400. The median apparent particle size diameter for CRP400 was approximately 300 μm, while for MRP074 it was approximately 60 μm.

Chapter 5 Effect of Recycled Rubber Powder (RRP) filler on mechanical properties and fatigue life of unfilled NR, BR and NR/BR compound

5.1 Introduction

Untreated or treated End of Life Vulcanised Rubber Tyres (ELVRT) were investigated in different types of virgin rubber matrices [2,33]. ELVRT used to replace virgin material can reduce the overall product carbon footprint and waste tyre disposal problems. Less energy is consumed in the production and utilisation of recycled rubber products than in production using virgin raw rubber material [45]. A saving of ~4.6 litres of oil/tyre can be achieved by incorporating 10% of recycled rubber [155]. A principal concern which limits ELVRT potential for a partial replacement of virgin rubber, is their crosslinked structure and large particle sizes.

Larger particle sizes, as produced by ambient ground ELVRT (>400 μm), reduce the physical properties (tensile strength, elongation at break, abrasion resistance index, heat-build up, etc.) [7,148]. These property changes have been attributed to either poor adhesion to the matrix [156] or 'crosslinked' crumb particles acting as discontinuities and stress-raising flaws [157] and thus initiating crack propagation at the weak crumb-matrix interface, especially under dynamic loading. Cryogenic ground MRP074 particles have a smooth surface [32,147] which restricts their potential bonding and also leads to a decline in physical properties [148]. Fine powders (<20 μm) [158] improve the key properties and could provide many positive benefits in various engineering applications, relative to coarse particles. Smaller particles than 400 μm for ambient ground ELVRT, are currently only produced in small batches, so not readily commercially available, with the only source being cryogenic ground production. Hence, demand for high quality ELVR from waste tyres is important for both economic and environmental benefits.

A preliminary study in this Chapter investigates the influence of ambient-ground Crumb Rubber Powder (at < 400 μm denoted CRP400) or Cryogenic-ground Micronised Rubber Powder (at < 74 μm denoted MRP074) on cure characteristics, tensile strength, fatigue life

and fracture morphology of unfilled NR, BR and NR/BR (70/30 ratio) compounds. The cure characteristics of the unfilled material are discussed, along with carbon black filled compounds in Chapter 7. The incorporation of carbon black (CB) compensated for the reduction of mechanical properties (tear resistance and hysteresis behaviour) of compounds containing recycled rubber with mechanical treatment, as reported by Phadke *et al.* [159]. Hence, in order to assess the performance of the Recycled Rubber Powder (RRP), additional carbon black was not added in the host matrix. In this chapter, RRP refers to both MRP074 and CRP400 filler.

5.2 Experimental procedures

5.2.1 Materials

CRP400 and MRP074, as described in Chapter 4, were used. Natural rubber was Standard Malaysian Rubber (SMR) 10 and cis-1,4 polybutadiene rubber (Europrene Neo cis-BR-40). An NR/BR ratio of 70/30 was selected [160] to balance properties such as abrasion resistance, strength, fatigue and crack growth resistance for tyre tread formulation. Driven by their targeted properties, other authors have used NR/BR ratios of 50/50 [140,161] or 60/40 [162]. Chemical ingredients, as defined in Table 5-1, were of commercial grade.

Table 5-1 Masterbatch rubber formulations (pphr).

Masterbatch			
Rubber (NR, BR or NR/BR blends)	100	100	100
Zinc Oxide	3.5	3.5	3.5
Stearic Acid	2.5	2.5	2.5
Antilux 654 wax	1	1	1
6PPD antioxonant	2.5	2.5	2.5
Flectol TMQ antioxidant	1	1	1
CRP400/MRP074	0	10	30

6PPD: N-1,3-dimethylbutyl-N’ phenyl-p-phenylenediamine
TMQ: 2,2,4-trimethyl-1,2-dihydroquinoline

The curatives, 1.2 parts per hundred rubber (pphr) sulphur and 1 pphr TBBS (N-tert-butyl-2-benzothiazole sulphenamide) were added during final mixing. All rubber and chemical ingredients were supplied by the Tun Abdul Razak Research Centre (TARRC).

5.2.2 Mixing

NR was masticated to reduce the viscosity to a nominal value of 60 Mooney units (ML(1+4) at 100°C), using a Bridge cracker mill, (406 mm dia x 508 mm length) then a two-roll mill (Francis Shaw-50kg capacity). Two master batches of each NR, BR or NR/BR compounds were prepared using a Polylab 2000E internal mixer with Banbury rotors (390 cm^3 and fill factor of 0.75). For NR/BR blend compounds, the raw NR and BR were mixed simultaneously before adding RRP and other compounding ingredients. The mixing of the masterbatch was carried out with a starting temperature of 40°C and rotor speed of 80 rpm. The mixing cycles started with a mastication of each rubber or blend for 1 min, followed by the addition of, firstly half RRP mixed for 1 min, then the second half of RRP and finally all masterbatch ingredients were added. The total mixing time was approximately 5 min. The masterbatches were allowed to cool overnight before the curatives were added separately using a two-roll mill. A band of rubber was formed as a continuous sheet on the mill. Once the curatives had all been added, the banded rubber was cut and rolled three times from each side of the mill; alternating from the left and from the right. After that, the entire compound was removed as a roll and passed through a tight nip for three passes, not allowing the rubber to band but taking off as a roll. The number of cuts and passes is kept low to minimise degradation of the rubber matrix whilst ensuring good dispersion of the curatives. Finally, each mix was then sheeted out at approximately 4-5 mm thickness. (see Appendix B for mixing process outline)

5.2.3 Preparation of test pieces

Test pieces from each mix were produced using a Bradley and Turton Ltd. (Kidderminster, UK) steam press at a temperature of 160°C and pressure of 8 MPa. The 229 mm square sheets of 2 mm thickness and cylindrical test pieces of 13 mm diameter with 6 mm thickness (image analysis test specimens) were compression-moulded using their respective optimum

cure times, t_{95}, while the hardness buttons, cylindrical discs of 25 mm diameter and 6 mm thickness, were cured at t_{95} + 5 mins. (see Appendix C for images of the respective mould)

5.2.4 Cure characteristic and Mooney viscosity

The curing characteristics of the samples containing RRP were obtained at 160°C for 30 min, using a Monsanto MDR 2000 rheometer with a 0.5° arc, in accordance with BS ISO 6502:2016 standard. The respective optimum cure time, t_{95} (time at 95% of the maximum torque), scorch time, ts_2 (time for viscosity to rise 2 units above minimum torque (M_L), maximum torque (M_H), etc., were determined from a rheograph or cure curve. The viscosity of the samples was measured using the Wallace MK III Mooney viscometer at 100°C, according to BS ISO 289-1:2014. Sample masses were approximately 25-30 g. The results were expressed using ML (1+4), where M stands for Mooney, L = large rotor, 1 for 1 minute reheat and 4 min testing.

5.2.5 Mechanical properties

Dumbbell samples for tensile tests were cut from a 2-mm-thick moulded sheet, as shown in Figure 5-1. The tensile properties were determined according to BS ISO 37:2011 (type 2 test pieces). An Instron 5567 universal testing machine with a 1 kN load cell was used at a crosshead speed of 500 mm/min. Equivalent strain rate can be defined as crosshead speed divided by gauge length and thus, the equivalent strain rate for the tensile test is 0.42 s^{-1}. The tensile strength was taken as the maximum force at break divided by the initial cross-sectional area of the narrow test piece. The Shore A hardness measurement was conducted in accordance to BS ISO 7619-1:2010. The median of five readings was recorded from both the tensile and the hardness tests with an average then taken from tests on the two hardness buttons.

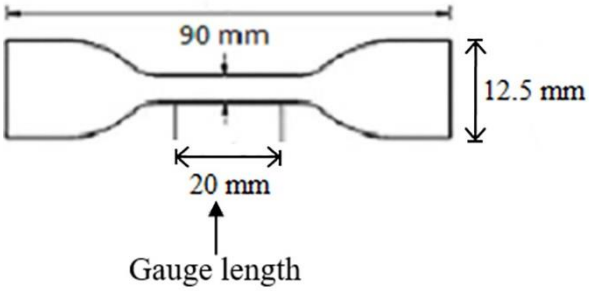

Figure 5-1 Type 2 dumbbell specimen.

5.2.6 Apparent crosslink density using equilibrium swelling test

Apparent crosslink density of the vulcanised compound, containing various concentration of CRP400 or MRP074, was determined using the equilibrium swelling method, using toluene as the swelling agent. Two vulcanised samples of each compound were weighted between 0.2 and 0.25 g having an accuracy of 0.0001 g and were allowed to swell in 25 ml toluene, at ambient temperature, for about 72 h. The solvent was changed after 24 h. At equilibrium, the swollen vulcanisates (w_1) were quickly blotted with tissue paper and weighed immediately in a covered glass vial. The sample was then immersed in acetone for 30 min to remove excess of toluene and dried to constant mass (w_2). The swelling index, Q of the rubber was determined using Eq. 5-1. Q is defined as amount of solvent absorbed by 1 g of rubber, where w is initial mass of the sample before swelling and M_{tot} is total mass of all ingredients including rubber (in pphr) [163].

$$Q=\left(\frac{w_1 - w_2}{w}\right) \times \left(\frac{M_{tot}}{100}\right) \qquad \text{(Eq. 5-1)}$$

The apparent crosslink density in the rubber matrix was calculated as the reciprocal swelling value, 1/Q; the smaller the value, the lower is the degree of crosslinking.

5.2.7 Fatigue testing

Eight tensile dumbbells (BS ISO 37:2011 Type 2) were cut from each cured sheet. Two test pieces were used for each compound during the test set-up. The test pieces were each marked

with a 20 mm gauge length on the narrow part. Some adjustment was necessary to achieve the required separation indicated by the gauge lines to achieve the maximum strain value (of 100%), and this was measured using a Mitutoyo digital Vernier calliper. The distance between clamps was set to the required strain and the samples were then tightly clamped between the grips to avoid slippage. The fatigue test setup is shown in Figure 5-2 (a) and each specimen holder attached to an individual 100 N load cell. The fatigue test was conducted at TARRC and more details of the testing machine layout was published by Kamaruddin [164].

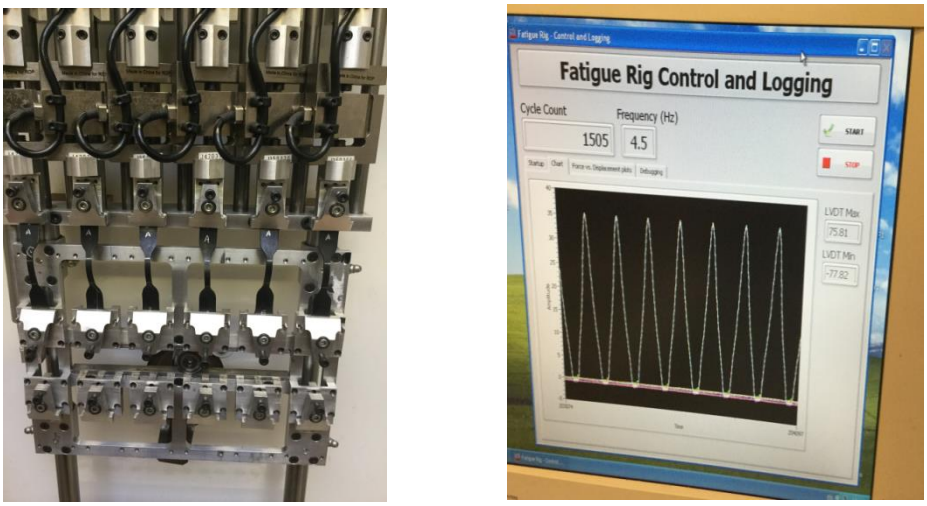

(a) (b)

Figure 5-2 (a) Fatigue set-up with samples at fully-relaxing conditions and (b) force and time plot for 6 samples running simultaneously.

Figure 5-2 (b) shows the plot for all 6 samples of force versus time during one of the tension fatigue tests. The specimens were cycled at a frequency of 4.5 Hz (maximum frequency limits of the fatigue set-up) to a maximum strain of 100% until failure under fully relaxing conditions, i.e. minimum strain was zero, and the numbers of cycles to failure were recorded.

5.2.8 Image analysis

The two cured cylindrical test pieces were prepared for optical microscopy. The samples were cut with one stroke using a cutter, each time with a new sharp razor blade. The surface of the RRP, within the rubber matrix, was captured using an Olympus BX60 microscope with reflective and polarised modes and the contrast of the image was optimised. Further analysis used Olympus Stream phase image analysis software (SM04733).

5.2.9 Fatigue fracture morphology

Prior to analysis the samples were cut about 3 mm from the surface fracture and all specimens were gold coated before viewing. Fracture surface specimens were observed using JEOL JSM-6610 LV Scanning Electron Microscope (SEM), operating at 15 kV accelerating voltage.

5.2.10 Laser Scanning Confocal Microscope technique

An Olympus LEXT/OLS 3000 Laser Scanning Confocal Microscope (LSCM) was used to examine the fatigue fracture surface of selected rubber compounds. LSCM can reconstruct three-dimensional (3D) topography maps of the fracture surfaces of the rubber matrix. The technique used was the confocal scanning mode at 50× magnification. The presence of a pinhole in the detection light path produces improved depth of focus relative to conventional optical microscopy [165]. Thus, reduction of the out-of-focus background, from in-focus signal focal plane, enables sharp images. The fatigue fracture sample from SEM observation was used for the 3D reconstruction.

5.3 Results and Discussion

5.3.1 Mixing behaviour

The incorporation of 10 pphr of either CRP400 or MRP074 did not give a significant effect on the final mixing torque due to low concentration and ease of processing in NR, BR and NR/BR compounds, as shown in Figure 5-3. Increasing the RRP concentration to 30 pphr reduced further the deformable part in the rubber matrix which is known as the dilution effect [166]. Thus, a very slight increase in the mixing torque with a higher concentration was observed. Comparing CRP400 and MRP074, there is little change in their final torque value. BR exhibited higher torque values compared to NR and NR/BR compounds. This clearly indicated that the mixing behaviour is directly related to the compound viscosity.

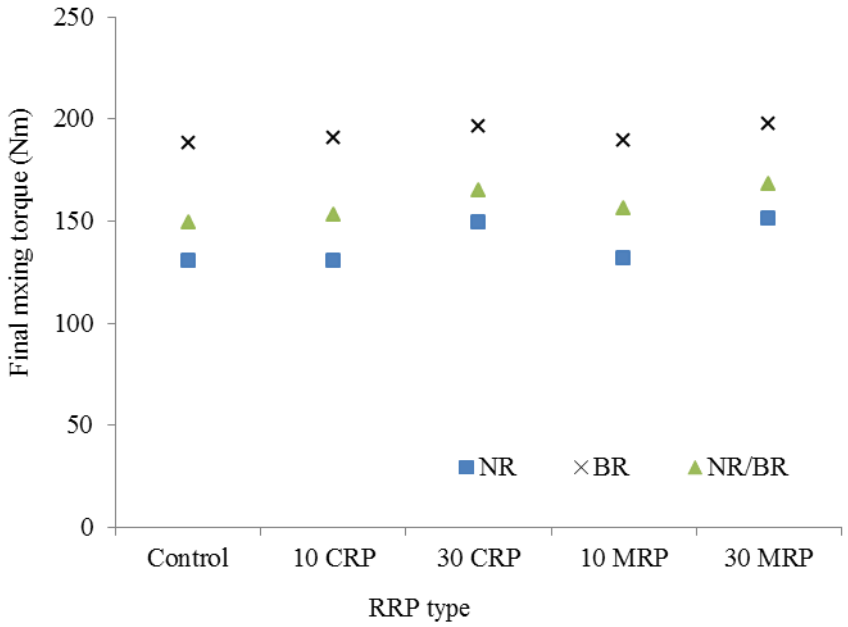

Figure 5-3 Final mixing torque of NR, BR and NR/BR compounds containing RRP.

5.3.2 Mooney Viscosity

Both of the powders increased the minimum torque (M_L) which also indicated an increase in the viscosity of the compound. The higher viscosity was expected partly due to the hydrodynamic reinforcement effect of the filler. The contribution of particulate filler in the matrix was to increase the viscosity and stiffness of the elastomeric material, is based on Einstein's theory (Eq. 5-2) [167] of the effect of a low concentration of rigid spheres suspended in fluid. The Einstein equation assumed that the particles were spherical and there was no interaction between the particles. Therefore, the Eq. 5-2 became invalid when the volume fraction of filler, $ø > 0.02$ [168] and represented by the following:

$$\eta = \eta_0 (1 + 2.5\, ø) \qquad \text{(Eq. 5-2)}$$

where, η is the viscosity of rubber containing RRP filler, η_0 is the viscosity of the unfilled rubber and $ø$ is the volume fraction of the spherical particles/RRP filler.

Since recycled powder is used in a low concentration, ignoring filler-filler interaction and occluded rubber, the Einstein equation is superior in prediction of the viscosity of rubber compounds, compared with the Guth-Gold equation, as reported by Gibala *et. al* [167]. Although this model is not perfect as the recycled fillers are not typically spherical in shape, it is still broadly applicable and the researchers also demonstrated that both equations (Einstein and Guth-Gold) and Mooney viscosity values have no dependency on the particle size. As CRP400 and MRP074 have a large variation in size, the viscosity of compounds containing both fillers in NR, BR and NR-BR blends was also predicted by the Einstein equation and comparison with the experimental values are shown in Figure 5-4.

The values for RRP volume fraction used in this study were calculated using Eq. 5-3.

$$ø = \frac{\rho\, C_f}{V_{tot}} \qquad \text{(Eq. 5-3)}$$

where, ø is the volume fraction, ρ is the density of the RRP, C_f is concentration of RRP in pphr, and V_{tot} is total volume of all ingredients including rubber for each compound. Gibala *et al.* [167] showed the differences in the morphology of the ambient and cryogenic method produced in Mooney viscosity values, with higher viscosity exhibited by irregular shape from ambient ground production. However, in this work, at 10 pphr concentrations, it was observed that the viscosity of CRP400 filled NR had negligible difference compared to the MRP074 filled compound. Similar trends were also seen in BR and NR/BR blends. However, a slightly higher viscosity for CRP400 filled NR or BR than MRP074 was observed at 30 pphr concentrations. The viscosity prediction using Einstein equation showed good correlation for individual NR or BR compounds particular CRP400 in NR whereas MRP074 in BR compound. However for both CRP400 and MRP074, the viscosity prediction by Einstein equation overestimated the experimental value of their viscosities in NR/BR blends.

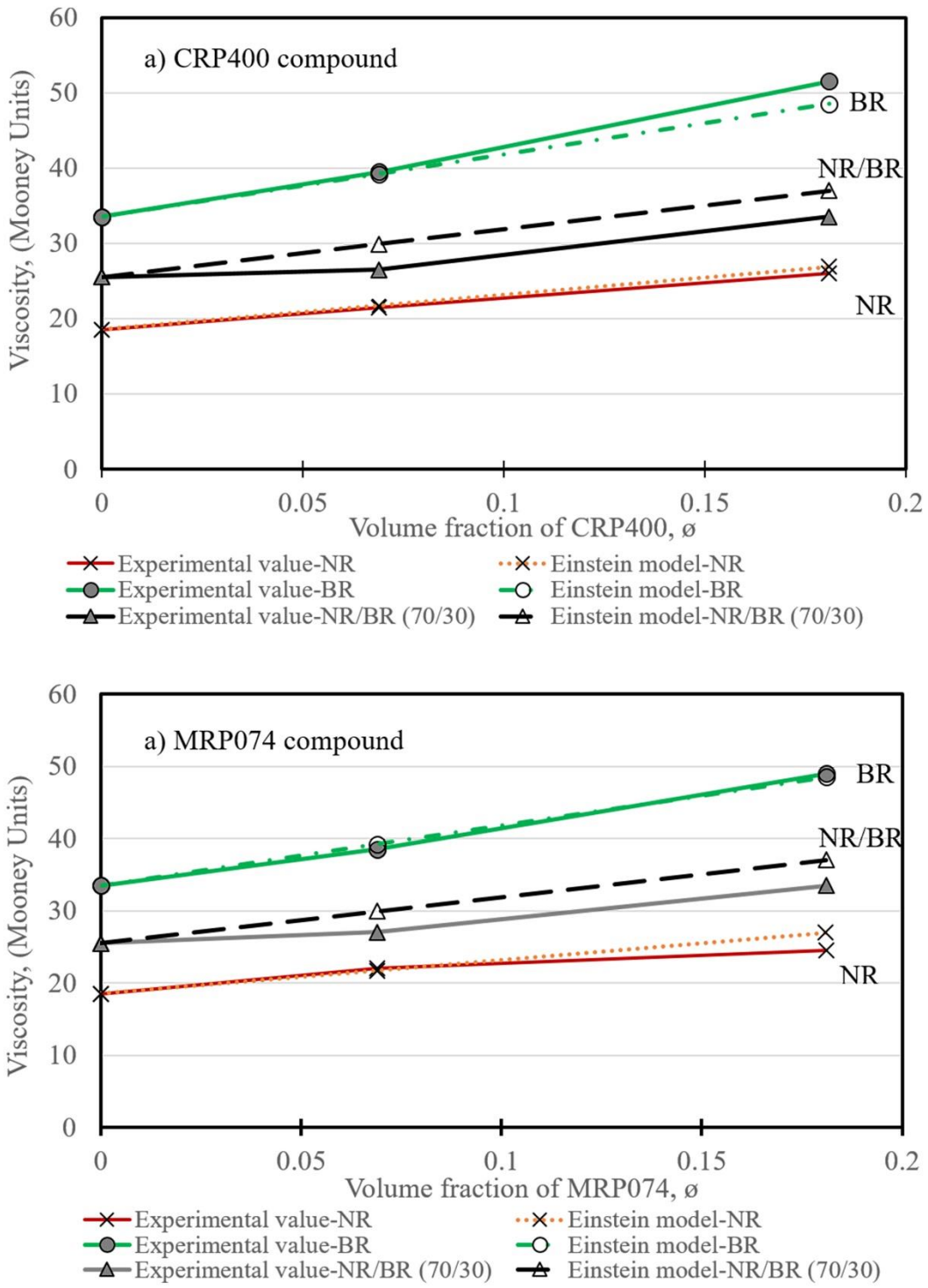

Figure 5-4 Effect of volume fraction of RRP fillers on viscosity of NR, BR and NR/BR (70/30 ratio) compound – comparison of theoretical and experimental values.

5.3.3 Mechanical and fatigue life properties

5.3.3.1 Tensile strength

Figure 5-5 shows the mechanical properties of NR, BR and NR/BR containing either MRP074 or CRP400 at 10 and 30 pphr. The higher tensile strength (Figure 5-5 (a)) of NR is attributed to strain induced crystallisation (SIC) during stretching. For NR, as expected, the tensile strength reduced with increases in either CRP400 or MRP074 concentration. The reduction of tensile strength with MRP074 is not very pronounced, relative to CRP400 filled NR. Larger particles of CRP400 acted as critical stress-raisers that initiated fracture and lowered the strength [157]. In NR/BR compounds, the MRP074 filled compound at 10 pphr exhibited higher tensile strength in comparison with the control compound. However, failure at the machine grip for all the control samples indicated only a lower bound of tensile strength. Altogether, 10 samples were tested and all fractured at the machine grip. A similar trend to NR, a severe reduction (about 55%) in tensile strength was observed at higher concentrations for CRP400.

Due to its high stereoregularity, BR has the capability to SIC. A study by Gent and Zhang [169] showed that under strain, BR exhibits a lower degree of crystallinity than NR. Kang *et al.* [170] revealed that high cis-BR (98% content) did not show any crystallisation but could retard the SIC, in NR compounds, as the blend ratio increased. This probably explains the low tensile strength of the unfilled BR and NR/BR compounds compared to NR. For BR, the addition of 10 or 30 pphr of CRP400 did not have a significant effect on the tensile strength. In contrast, for MRP074, the tensile strength and the elongation at break (EB) of the BR compound (Figure 5-5 (c)) increased as the MRP074 concentration increased. This probably indicated some degree of bonding between the MRP074 particles and BR matrix.

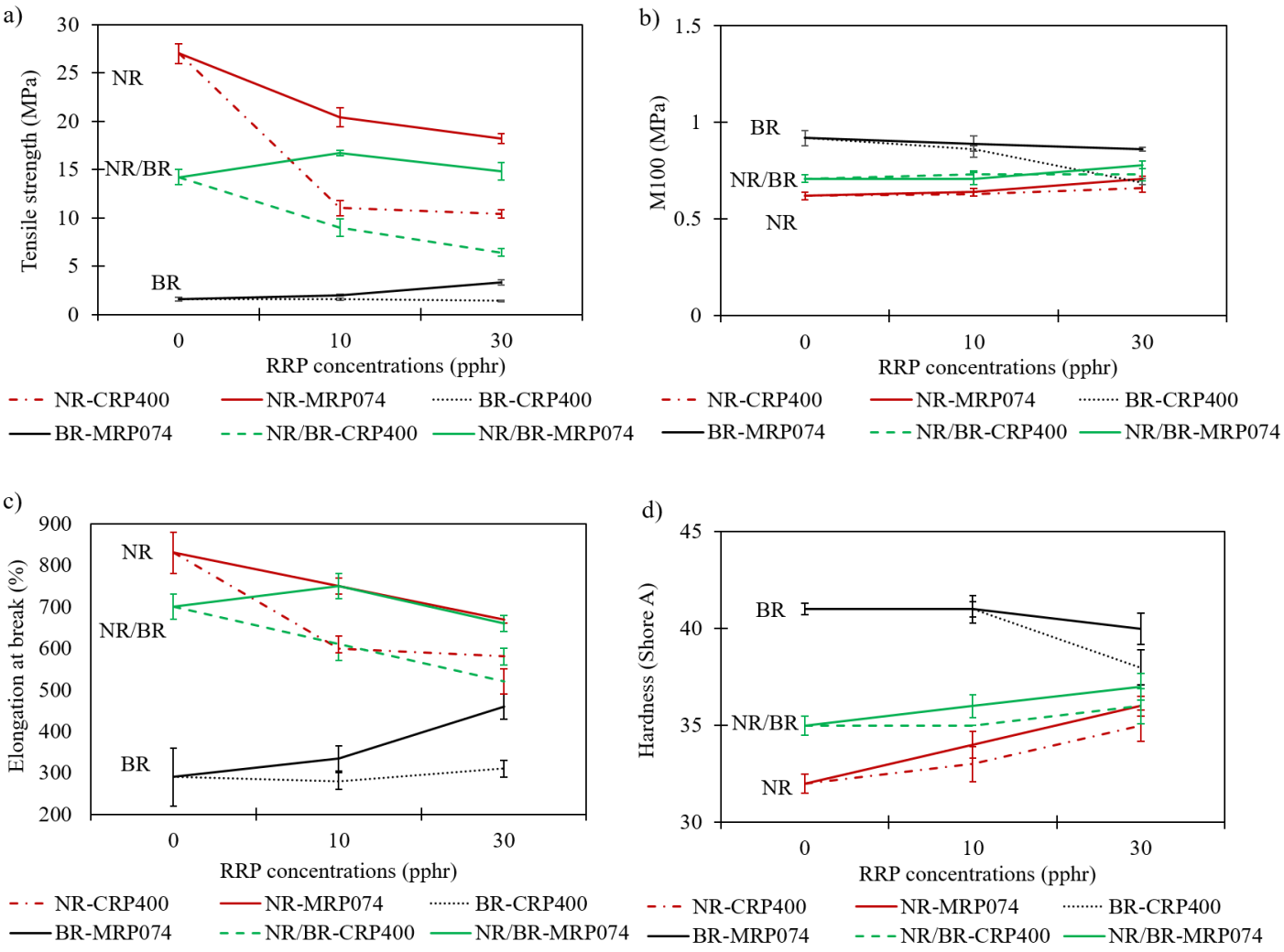

Figure 5-5 Mechanical properties of unfilled rubber (NR, BR and NR/BR (70/30 ratio) containing CRP400 and MRP074: a) Tensile strength, b) M100, c) Elongation at break and d) Hardness.

Figure 5-6 shows the apparent crosslink density of either MRP074 or CRP400 filled NR, BR or NR/BR compounds measured using the swelling index, Q. The reciprocal of the swelling index (1/Q) is a relative measurement of the degree of crosslinking in a rubber matrix; the smaller the value, the lower is the degree of crosslinking. The addition of either filler reduced the crosslinking density of the rubber matrix, most likely due to sulphur migration from the virgin compound to the RRP [171]. This will be discussed in detail in Chapter 7.

The elastic modulus at 100% elongation (M100) was related to the crosslinking density of the rubber compound. For NR and NR/BR compounds, the M100 and hardness (Figure 5-5 (b)

and (d)) showed little change with the addition of 10 pphr of either CRP400 or MRP074. The incorporation of 30 pphr RRP further increased the modulus and hardness but reduced the EB. The competition between the reduction of crosslinking and stiffening [172] of both RRP filler explains the opposite trend in the behaviour of M100 for NR or NR/BR.

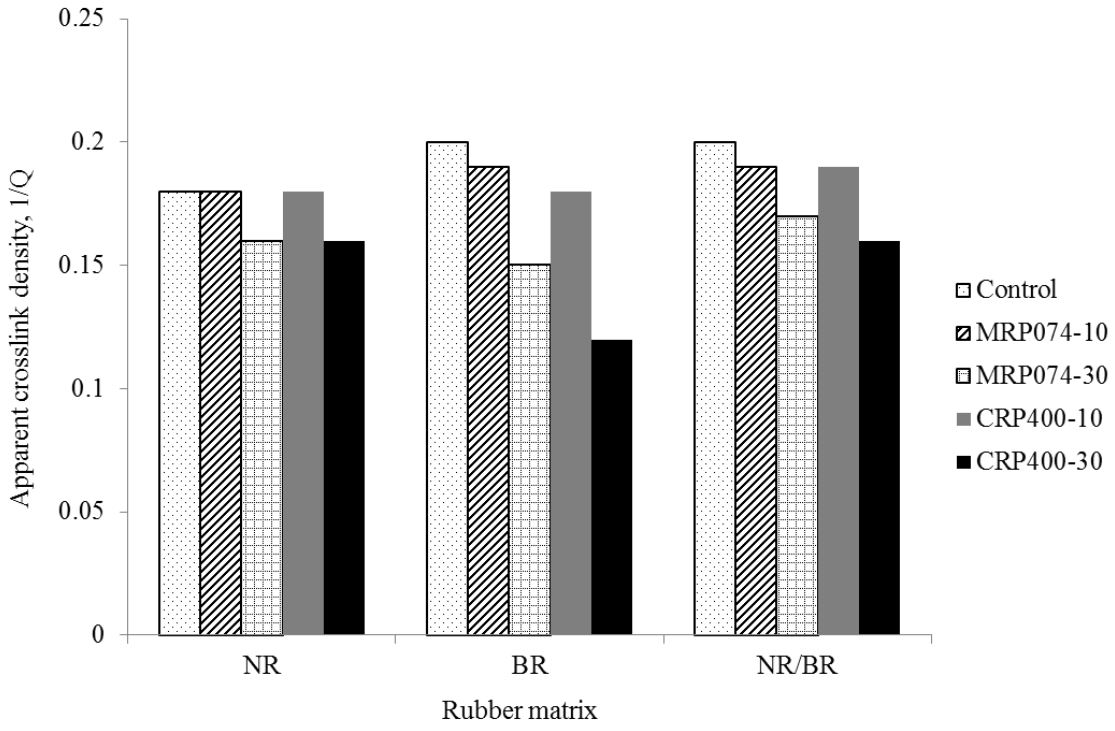

Figure 5-6 Apparent crosslink density of unfilled NR, BR and NR/BR blend compounds containing MRP074 and CRP400 filler.

The higher modulus of BR corresponds to higher apparent crosslink density by comparison with NR or NR/BR compound. The reduction of M100 is pronounced in BR compounds with the incorporation of CRP400 or MRP074 at 30 pphr concentrations. The hardness slightly reduced but increased the elongation at break (EB) of BR compounds. The sulphur migrations, mentioned earlier, reduced the crosslinking density of the BR matrix, hence permitting greater molecular chain mobility under a tensional force.

5.3.3.2 Fatigue life

It is well-known that mechanical properties under quasi-static loading do not represent the strength exhibited in dynamic applications. The fatigue life of rubber compounds is a

complex subject due to the influence of many factors which could affect the behaviour; including mechanical loading history, rubber formulation, effect of environmental conditions and dissipation aspects from the stress-strain behaviour of individual rubbers [80]. Many laboratory fatigue experiments, such as fatigue-to-failure tests (FTFT), DeMattia flex crack tests, Wallace ring fatigue tests, etc., often do not correlate with actual service life [112]. However, they are still popular among rubber technologists and in industry, due to time and equipment constraints and provide useful comparative information. In this study, the fatigue life of rubber compound is defined as kilocycles (kc) to failure and a median of the six measurements was reported. Figure 5-7 shows the fatigue life for unfilled and RRP filled NR, BR and NR/BR compounds.

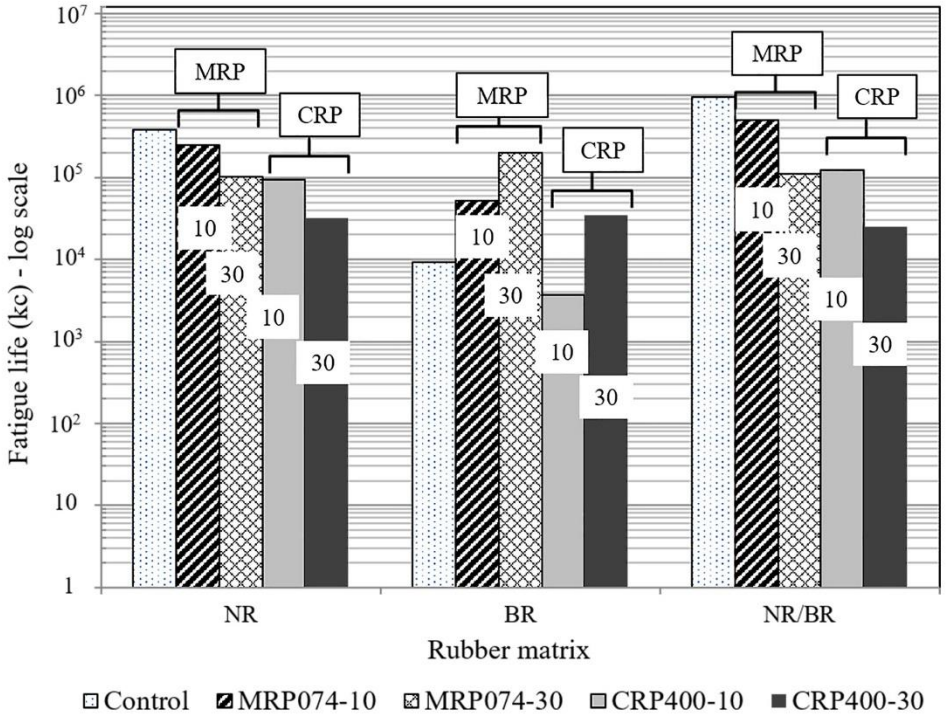

Figure 5-7 Fatigue life (at 100% strain) of unfilled NR, BR and NR/BR containing MRP074 or CRP400 at 0, 10 and 30 pphr filler concentrations.

For NR, the compound containing RRP exhibited reduced fatigue life in cycles to failure compared to the control compound. This may be partially attributed to a reduced ability to SIC at the crack tip [146]. The fatigue life decreased with an increase in the RRP filler

concentrations. MRP074 filled NR exhibited less reduction in fatigue lives compared to the CRP400 filled compound.

NR/BR compounds possessed a better fatigue life, in terms of cycles to failure, than the NR compounds. These results showed the benefit of blending, where the fatigue of NR was enhanced with partial replacement of BR. The possible reason could be due to higher crack initiation resistance in NR/BR compounds. The blends possessed advantageous features of NR and BR which were probably due to the co-continuity of both phases [140]. For the effect of RRP in NR/BR, a similar trend to NR compounds was observed. The inclusion of CRP400 at 10 pphr reduced the fatigue lives by approximately one-eighth relative to the control compounds. The reduction of fatigue life is in agreement with another study regarding the inclusion of recycled tyre material [30] in NR/BR compounds. Increasing concentration of 30 pphr further deteriorated the fatigue life of RRP (either CRP400 or MRP074) of NR/BR compounds. MRP074 filled NR/BR at 10 pphr exhibited better fatigue life compared to CRP400 filled blend compounds. The homogenous distribution of smaller particles in MRP074 filled NR or NR/BR, as observed in the optical image analysis (Figures 5-8 and 5-9, respectively), partially contributed to the longer fatigue life of MRP074, compared to the CRP400 filled compounds.

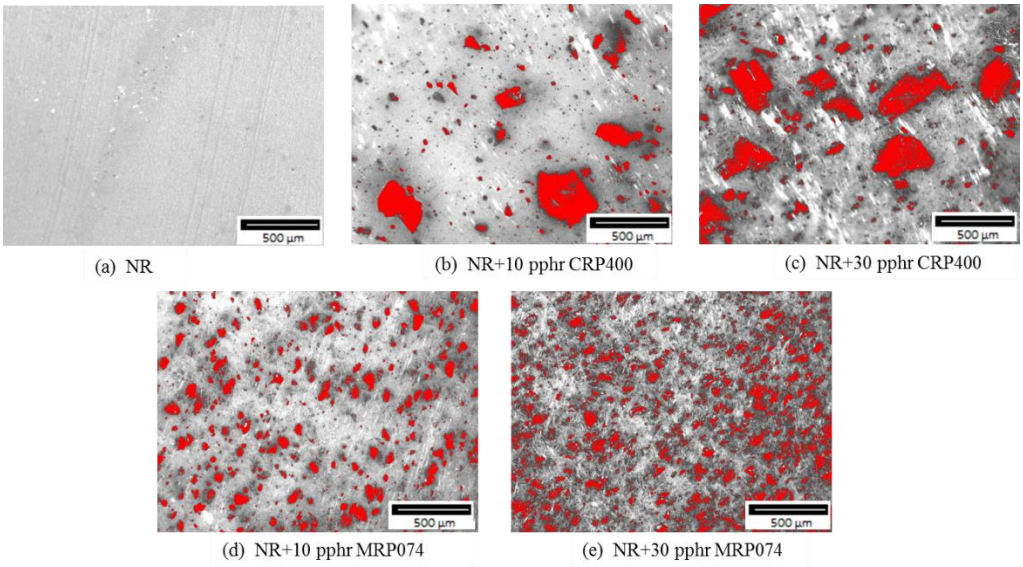

Figure 5-8 Phase analysis of NR containing CRP400 or MRP074 filler.

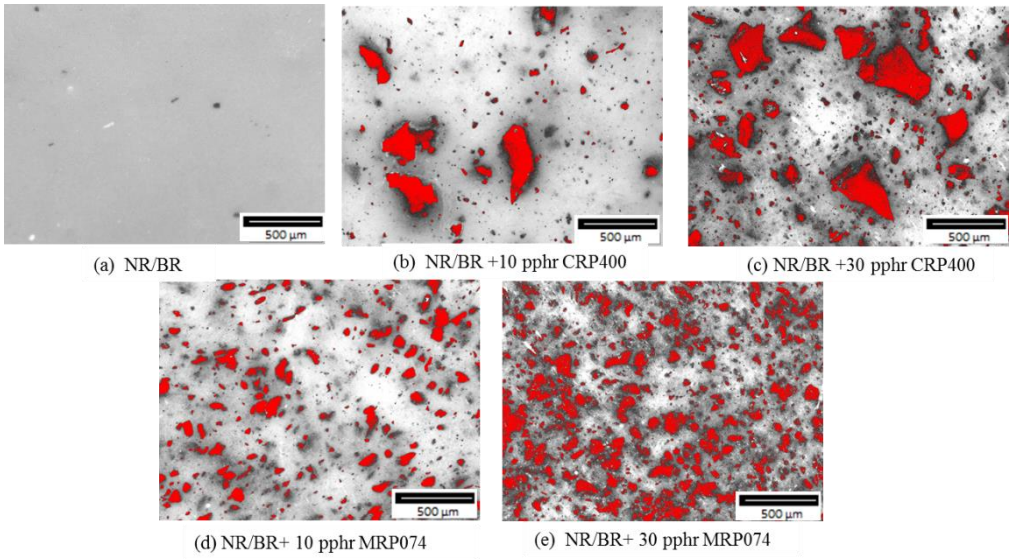

Figure 5-9 Phase analysis of NR/BR containing CRP400 or MRP074 filler.

The behaviour of BR appears to resemble non-crystalline rubber characteristics such as those of Styrene Butadiene Rubber (SBR). Han [146] showed that the fatigue life of SBR increases with decreases in average particle size and with an increasing concentration of the recycled rubber. The addition of up to 30 pphr MRP074 to the BR compound increases the fatigue life of the vulcanisates. The possible explanation for the increase in fatigue life for BR containing higher RRP filler is enhanced energy dissipation attributed to more tear path deviation [146]. This would reduce the energy available for the crack growth, resulting in slower crack growth rates. CRP400 filled BR at 10 pphr clearly exhibited deterioration in fatigue life compared to the control compound with the larger CRP particles again probably acting as the critical stress-raisers in the matrix. At 30 pphr concentration, higher fatigue life was observed in CRP400 filled BR, compared to the control compound. It is assumed that with increased CRP400 concentration, there would be more filler particles present per unit volume to deflect or deviate an advancing crack as shown schematically in Figure 5-10. Similar to NR or NR/BR, homogenous distribution of smaller particles of MRP074 filled BR compounds as observed in the optical image analysis (Figure 5-11) partially contributed to the longer fatigue life of MRP074 compared to CRP400 filled compounds.

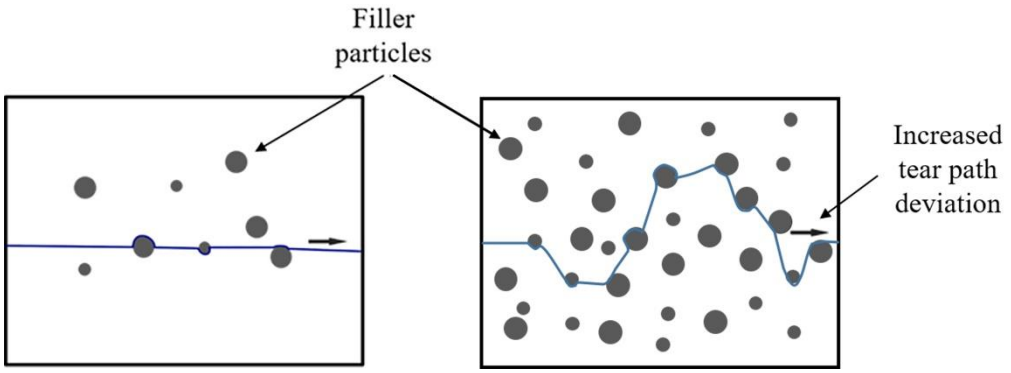

Figure 5-10 Schematic of increased tear path deviation in filled rubber matrix

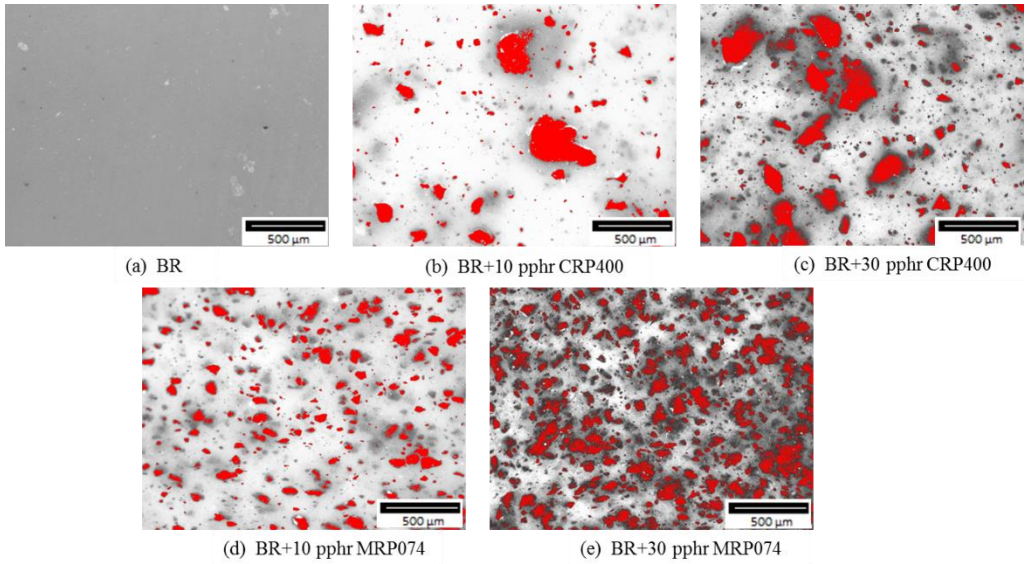

Figure 5-11 Phase analysis of BR containing CRP400 or MRP074 filler.

5.3.4 Surface morphology of fatigue fracture samples

Figure 5-12 is a typical fracture surface morphology of rubber showing three distinct region/phases based on unfilled NR compound. Phase/area 'I' is a microscopic rough surface and textures consist of multiple layers of cracks. Since the FTFT tests used an un-notched specimen, the exact location of the crack initiation is unknown, however, it is believed that the crack initiation commenced from phase 'I' [173]. In phase/area 'II', the crack growth was much faster and crack lines appeared to be much broader 'fracture leaves' and rougher on a macroscopic scale. Finally phase/area 'III', is macroscopically smooth which indicated the final fatigue failure.

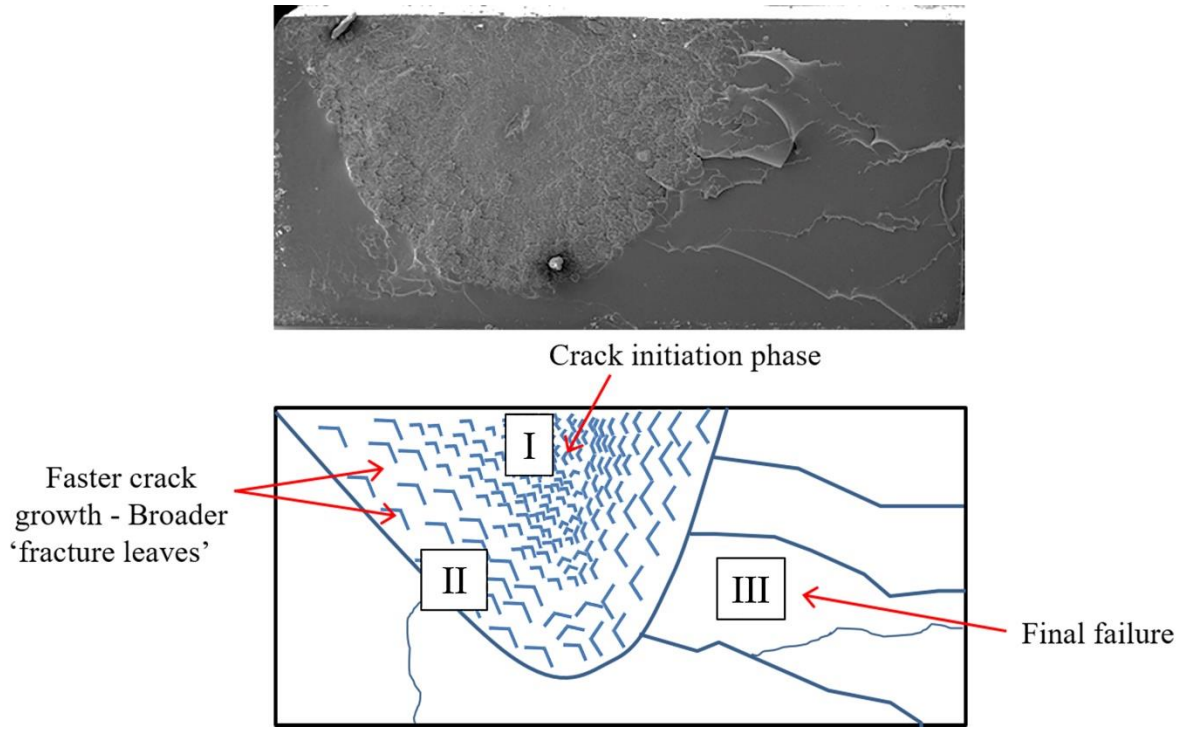

Figure 5-12 Typical fracture surface morphology of unfilled NR compound

Beurrot *et al.* [174] attribute the fracture "leaves" as the secondary crack branching, during fatigue crack propagation, for carbon black filled NR. The creation of new fracture surfaces attributed to tear path deviation/crack branching reflected an enhanced energy dissipation. This would reduce the energy available for the crack growth, resulting in slower crack growth rates. The fracture 'leaves' or scale-like texture provide a greater resistance to the dynamic load and correspond well to the fatigue life result (Figure 5-7). Munoz *et al.* [175] have reported that crack growth velocities are well connected to fracture morphology. The rougher phase (I) at the crack initiation phase probably indicated a low velocity of crack growth.

As the crack progresses, at a certain stage the stress distribution in the matrix is no longer uniform and cannot arrest the crack propagation. Hence, there is a transition between the two phases (II & III) before tearing. The higher velocity of crack growth is believed to lead to catastrophic failure (region 'III'), resulting in the formation of a relatively smoother failure surface. Details of the morphology of fracture fatigue surfaces from a crack tip initiation was discussed in section 8.4.4.

Depending on the type of rubber matrix, unfilled or filled compound and structure/properties of fillers, there are different textures in the surface fractures between CRP400 and MRP074 filled NR, BR and NR/BR compounds and their control compounds. The SEM images of NR, BR and NR/BR vulcanisates, after fatigue failure, are shown in Figures 5-13, 5-14 and 5-15 respectively.

In NR, the 'fracture leaves' in region 'I' and 'II' for MRP074 or CRP400 filled compound at 10 pphr (Figure 5-13 (b) and (c)) appear to be broader than in the control compound (Figure 5-13 (a)) which probably relates to the reduction of the fatigue life. Although the fatigue life of NR is decreased with MRP074 filler, the overall morphology fracture surfaces are much rougher compared to the control and CRP400 compound. The presence of MRP074 is presumed to provide additional energy dissipation and thus may inhibit catastrophic failure. This will create a longer crack path around RRP particles and hence additional new surface energy compared to unfilled compounds (without RRP).

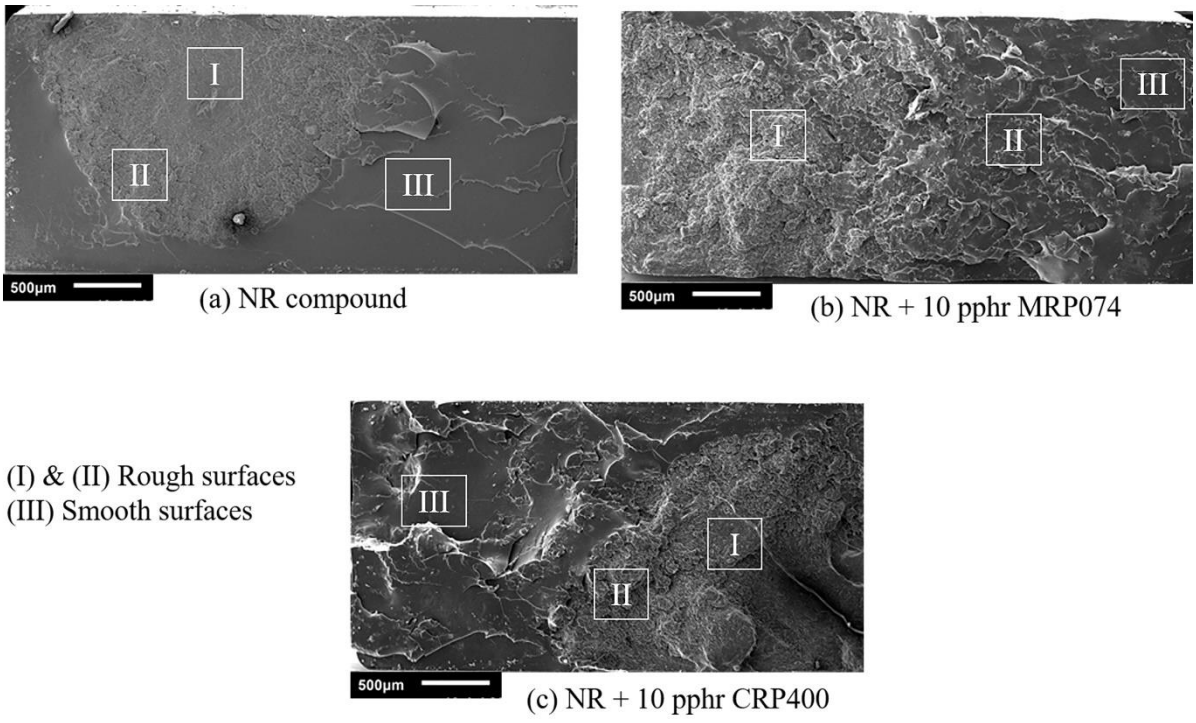

Figure 5-13 SEM micrograph of fatigue fracture surfaces of NR compound containing 10 pphr of CRP400 or MRP074.

In the BR control compound, the rough surface (I & II) region in Figure 5-14 is less obvious. Overall, BR showed much smoother surfaces without the addition of the MRP074. This texture shows that fracture easily occurs across the BR matrix, without considerable resistance, which resulted in a reduced number of fatigue to failure cycles i.e. average value about 10,000 cycles at 100% strain. The topography map achieved by confocal laser technique (Figure 5-16 (a)) clearly indicates a 'brittle structure' where the cracks propagate through the matrix. Similar structures were observed as 'mud-cracks' by Agarwal *et al.* [176] where many individual crack lines propagated through the matrix and interconnected. This morphology structures were also found in the tensile fracture surface of unfilled ethylene-propylene rubber [177].

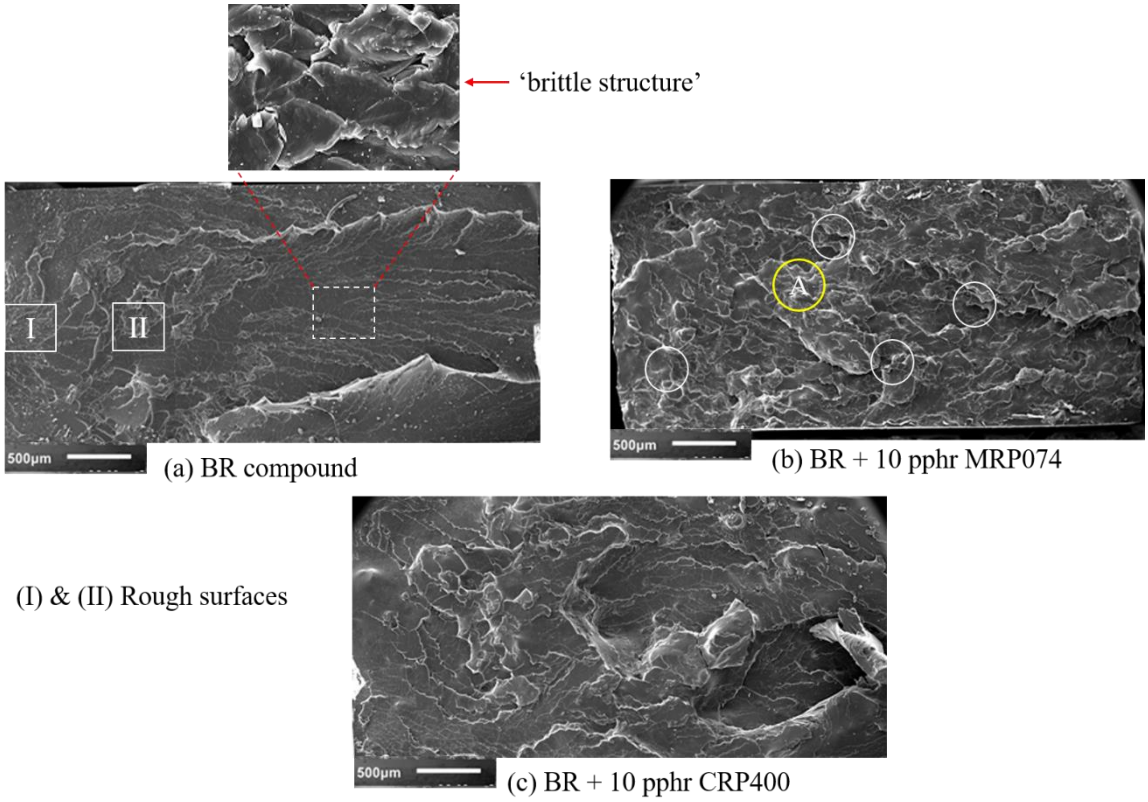

Figure 5-14 SEM micrograph of fatigue fracture surfaces of BR compound containing 10 pphr of CRP400 or MRP074.

For NR/BR blends, a similar texture to NR was observed. However, the proportion of 'I' and 'II' largely dominates the failure surface compared to the NR compound. This observation supports the enhancement of fatigue life of NR/BR vulcanisates, relative to the individual NR

compound. The 3-D topography image shown in Figure 5-16 (b) displays the transition from rough to smooth failure phase for an NR/BR compound marked with a T in the region circled in Figure 5-15 (a). Uneven fracture planes correlate well to the 'scale-like' features.

For MRP074 or CRP400 filled NR/BR blends, it is clear that the rough surface morphology region tends to decrease (Figure 5-15 (b) and (c)) by comparison with unfilled NR/BR compounds (Figure 5-15 (a)). This morphology trend is in good agreement with the decrease in fatigue life of RRP filled NR/BR compounds. Several voids due to detachment of larger particles were detected in the CRP400 filled material which contributed to lower fatigue lives of NR/BR when compared to MRP074 filled blend compounds. This could probably explain lower fatigue life at 30 pphr concentrations for the RRP filled compounds.

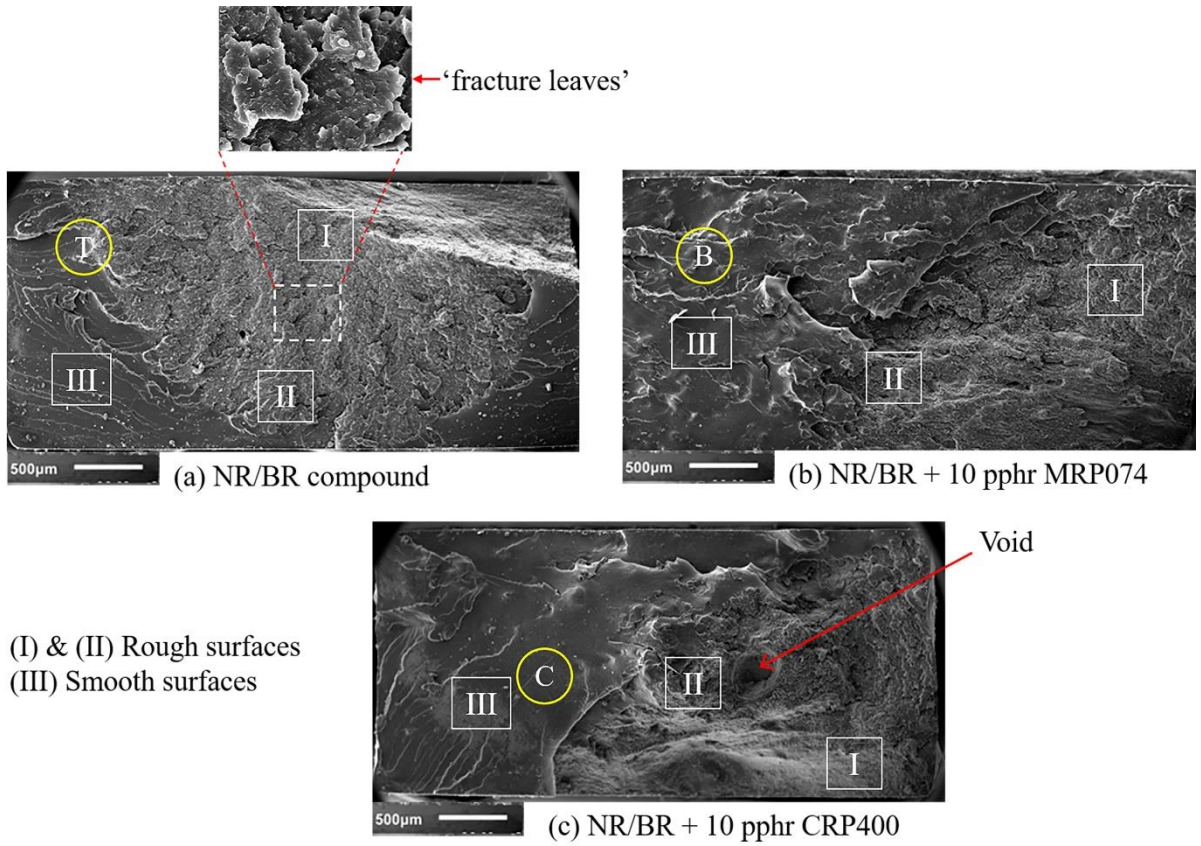

Figure 5-15 SEM micrograph of fatigue fracture surfaces of NR/BR compound containing 10 pphr of CRP400 or MRP074.

The incorporation of 10 pphr MRP074 in the BR compound produced much rougher surfaces as designated by 'A' (Figure 5-14 (b)) compared to the control compound. More fracture

"leaves" and distinct disordered crack lines are observed as indicated by the circles. The cracks are believed to be deflected by the recycled particles producing rougher crack surface regions. Clearly, the crack deflection is responsible for the increase of surface roughness. MRP074 filled BR showed more homogenous and consistent roughness than the CRP filled compound, corresponding to the improvement in fatigue life of BR compounds. The higher probability of finding a large flaw in 10 pphr of CRP400, compared to MRP074 filled BR, leads to more frequent material fracture under a given stress concentration. Rougher textures compared to the control was also observed, however the 'fracture leaves' are much broader than for MRP074. Considering the factors described in this section, CRP400 filled BR has a lower fatigue life compared to MRP074 filled compound.

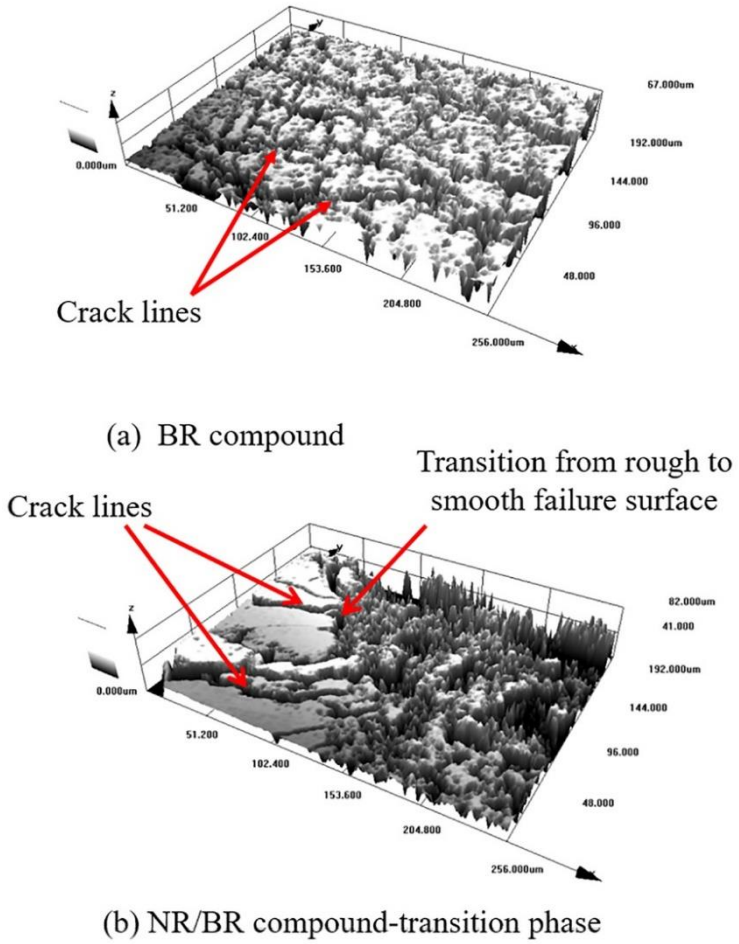

(a) BR compound

(b) NR/BR compound-transition phase

Figure 5-16 Dimensional image construction of topography map of fatigue fracture surface of BR and NR/BR compounds in a specific region.

5.4 Summary

The tensile strength result is directly dependent on the particle size of RRP and type of rubber matrix. Tensile and fatigue life properties of NR are reduced by the incorporation of either MRP074 or CRP400 filler. MRP074 filled compound showed higher tensile strength compared to CRP400 filled compound for NR, BR or NR/BR blend compounds. The behaviour of BR resembles the behaviour of non-crystallising rubber. The addition of up to 30 pphr MRP074 to the BR compound increases the tensile strength and fatigue life of the vulcanisates. Partial blending of NR with BR showed an enhancement in fatigue life of the NR/BR (70/30 ratio) blend compound. Fatigue to failure test seems to favour homogeneous distribution of filler particles in a matrix. Higher fatigue life was obtained for MRP074 filled NR, NR/BR or BR compounds compared to CRP400 filled compounds, at equivalent filler concentrations.

The SEM images of the fracture surface of the control rubber compounds and their MRP074 or CRP400 filled variants following fatigue testing showed different textures depending on rubber phase/ratio and particle size concentration. The roughness of the fracture surfaces qualitatively indicated a greater resistance to the dynamic load, which confirmed the fatigue life result. The roughness texture largely dominated the surface failure of NR/BR compared to the NR compound. This observation supports that the enhancement of fatigue life of NR/BR vulcanisates is better than for individual NR compounds.

The fatigue life of NR or NR/BR reduced with increasing filler concentration of MRP074 or CRP400. Despite the fatigue life reduction, the transition from smooth to rough surface fracture morphology, compared to the control compound, showed advantages of inhibiting catastrophic failure. The creation of new fracture surfaces attributed to tear path deviation reflected an enhanced energy dissipation. This would reduce the energy available for the crack growth and delayed crack growth rates. MRP074 filled material appeared to be rougher compared to CRP400 at similar concentration for NR, BR and NR/BR compounds. The rougher morphology of MRP074 filled NR, BR and NR/BR correlated well with achieving longer fatigue life than in CRP400 compound.

Chapter 6 Interface morphology between RRP filler and rubber matrix using TEM "network visualisation"

6.1 Introduction

In a filled rubber, apart from primary particle size, good matrix-filler bonding and enhanced filler network structure are essential for optimum reinforcement. The overall performance of the rubber/blend compound is governed by the strength of the filler-filler or rubber matrix-filler interfaces [178]. Other factors such as distribution of filler, phase morphology, crosslinking system, and density are often studied to understand the properties of rubber and their blends. Several techniques for the measurement of the rubber-filler interaction strength have been briefly described in the previous literature [179], including the dynamic mechanical method [178,179]. Cook and co-workers [180,181] applied the "network visualisation" [182] technique to measure crosslink density and qualitatively assess the interface strength between two different phases in rubber blends. This technique polymerises styrene in the swollen rubber-filler matrix, causing weak rubber-filler surfaces to debond and become visible in Transmission Electron Microscopy (TEM), due to the formation of extended polystyrene regions called 'voids/vacuoles' around the particles/interface as shown schematically in Figure 6-1.

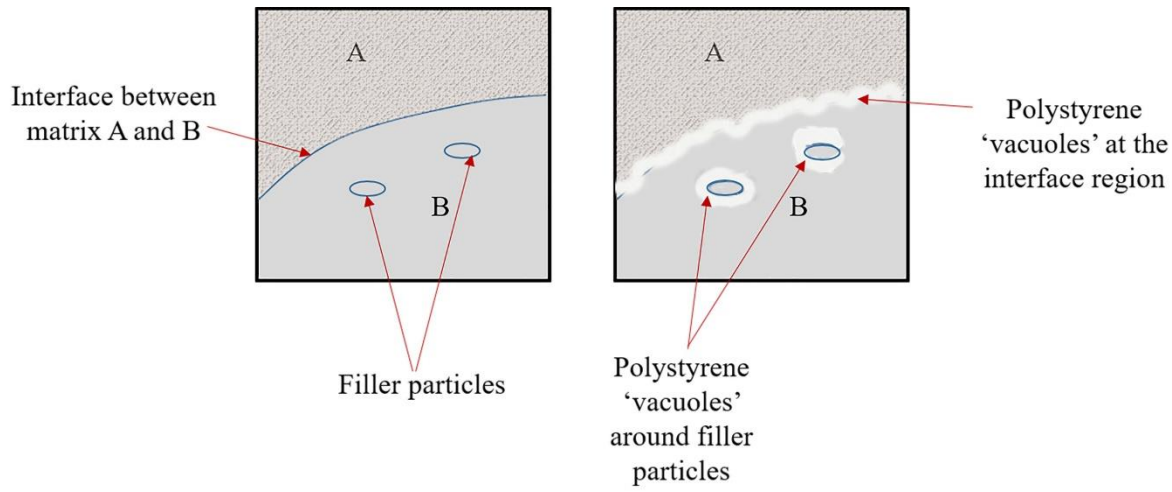

Figure 6-1 Schematic diagram of polystyrene 'vacuoles' at the interface region and around filler particles showing poor/weak rubber-rubber and rubber-filler interaction.

This technique is also used in silica-filled rubber to analyse the morphology of filler to rubber interaction. Vacuoles were observed around silica particles, in the absence of a coupling agent, as a result of a weak rubber-filler interaction [163,183]. This indicates that there is less rubber chains interaction between the rubber and filler which could restrict the mobility of the rubber molecules on the filler surfaces. Martin *et al.* [184] used the same techniques to analyse rubber wear surfaces.

The method is time consuming, but does provide insight into the interface morphology that allows for correlation with the corresponding mechanical properties. TEM "network visualisation" was carried out to investigate the interface morphology between RRP filler and each of the NR and BR matrices, using similar techniques to Cook *et al.* [180]. Cryogenic ground Micronised Rubber Powder (at <74 μm denoted MRP074) and ambient-ground Crumb Rubber Powder (at <400 μm denoted CRP400) were compared.

6.2 Experimental procedures

6.2.1 Materials

For ease of preparation and observation, samples of unfilled NR and BR, containing 10 pphr of micronised rubber powder (MRP074) and crumb rubber powder (CRP400) were selected. All rubber samples were from the compounds described in Chapter 5 (Table 5-1).

6.2.2 TEM 'network visualisation' sample preparation

Samples of approximately 10x4x2 mm were cut from dumbbell specimens and wrapped into 40x50 mm lens tissue and labelled accordingly. The selected samples were acetone extracted at 56°C using a Soxhlet-extraction apparatus overnight, then dried under a fume hood to remove residual solvent, before further drying in a vacuum oven overnight. The samples were cut to about 4x5 mm and put into a small test tube with 3 ml of pre-mixed modified [184] styrene solution containing about 30-100 mg benzoyl peroxide (cure initiator) and 50-200 mg di-n-butyl phthalate (DBP) (plasticiser) and allowed to swell to equilibrium over 1 to 2 days. The modified styrene solution was used to inhibit premature styrene polymerisation. The swollen samples (triplicates) were then further trimmed before encapsulation in a gelatine

capsule (Figure 6-2) with a fresh styrene solution, as described above. These capsules were heated to about 50°C, inside a metal block, to polymerise the styrene. After about 7 days, the samples were hard enough for TEM sectioning.

Figure 6-2 Some stages of "network visualisation" samples preparation.

Ultrathin (~ 100 nm) sections of the samples were prepared using an RMC PowerTome PC ultra-microtome, at room temperature, with a diamond knife. The sections were floated on a water-filled trough and relaxed with xylene vapour before collecting on TEM grids. Sections were then stained with osmium tetroxide (OsO_4) for one hour and observed, using a Philips CM12 TEM operating at 80 kV, to reveal the rubber network. TEM micrographs were acquired at higher magnifications using JEOL 1400 TEM at 120 kV.

6.3 Results and Discussion

The MRP074 or CRP400 particles are seen as a matrix containing carbon black particles in all TEM micrographs. In the unstained micrograph of MRP074 filled NR (Figure 6-3(a)) and BR (Figure 6-3(c)), a distinct line of small particles is visible at the interface between the MRP074 and the rubber matrix.

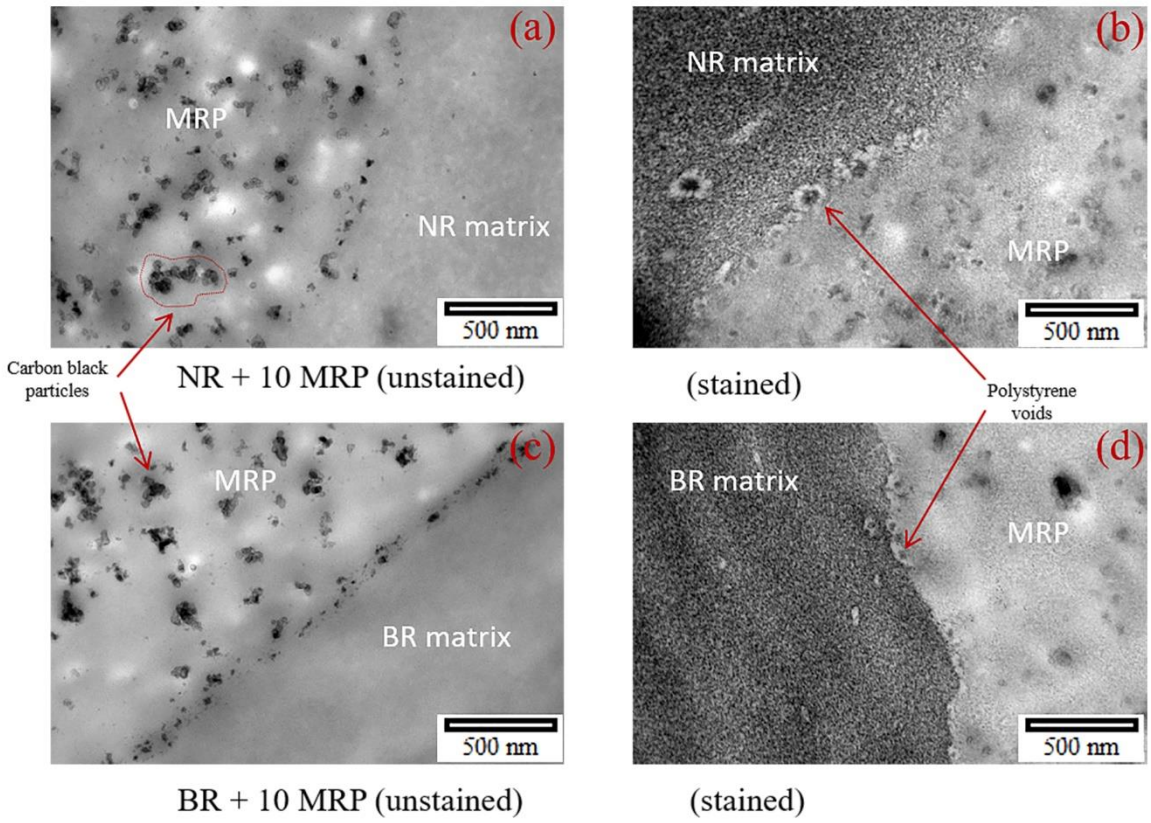

Figure 6-3 TEM ‘‘network visualisation’’ micrographs of (a) NR+10 pphr MRP074 (unstained) (b) NR+10 pphr MRP074 (stained) (c) BR+10 pphr MRP074 (unstained) (d) BR+10 pphr MRP074 (stained) sectioned from unfilled rubber vulcanisates.

The mesh structure of the rubber network can be distinguished from the polystyrene region in the stained samples. The OsO_4 vapour staining method enhances contrast in regions of the network with different levels of saturation. The stained network causes the mesh structure to appear darker than the polystyrene region. The stained samples (Figure 6-3 (b), (d)) show several areas of the interface with currently unidentified particles, that are surrounded by ‘polystyrene voids’, present in NR and BR. It is assumed that the unknown particles were probably a result of talc (hydrated magnesium silicate) added by the manufacturer to prevent the rubber particles from sticking together during the cryogenic grinding process and storage. Thus, in Chapter 4 (Table 4-1), the higher ash content in the MRP074 composition was most likely attributed to the extra added talc.

Higher magnification TEM micrograph sections of MRP074 filled NR and BR matrix interface containing polystyrene 'voids' are highlighted (thin red line) in Figure 6-4. The relatively weak interface interaction between the rubber-MRP074 networks may have enabled the polystyrene to penetrate between the rubber and those particles. The number of these particles at the interface is assumed to increase with the MRP074 content and create further stress concentrations, leading to de-bonding and eventually detachment of the particles. This could have resulted in reduced mechanical properties which are discussed in Chapter 7.

Figure 6-5 shows the TEM micrograph of stained CRP400 filled NR (top) and BR (bottom) respectively. The irregular surface of CRP400 (highlighted red line) is very pronounced in both NR and BR compound. Small particles are observed at the interfaces of MRP074 filled NR or BR, but these are not visible at the interface of the CRP400 filled NR or BR. However, the 'voids' are randomly present in the recycled matrix.

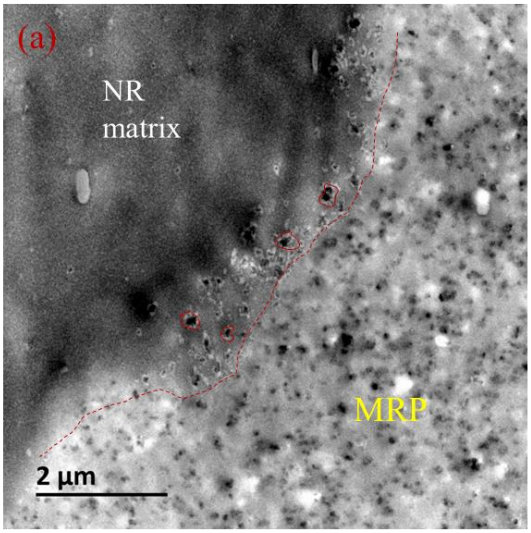

NR + 10 pphr MRP

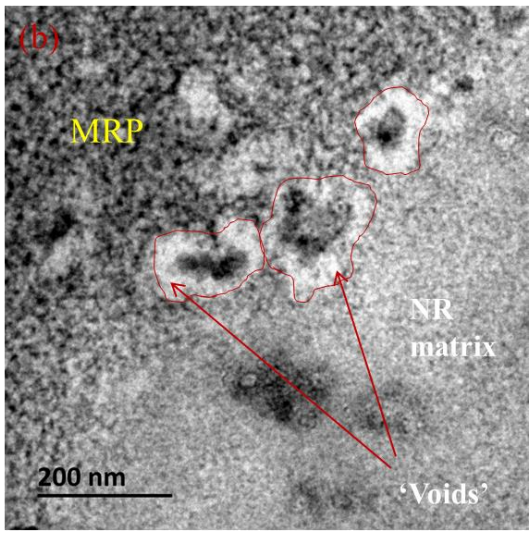

NR + 10 pphr MRP

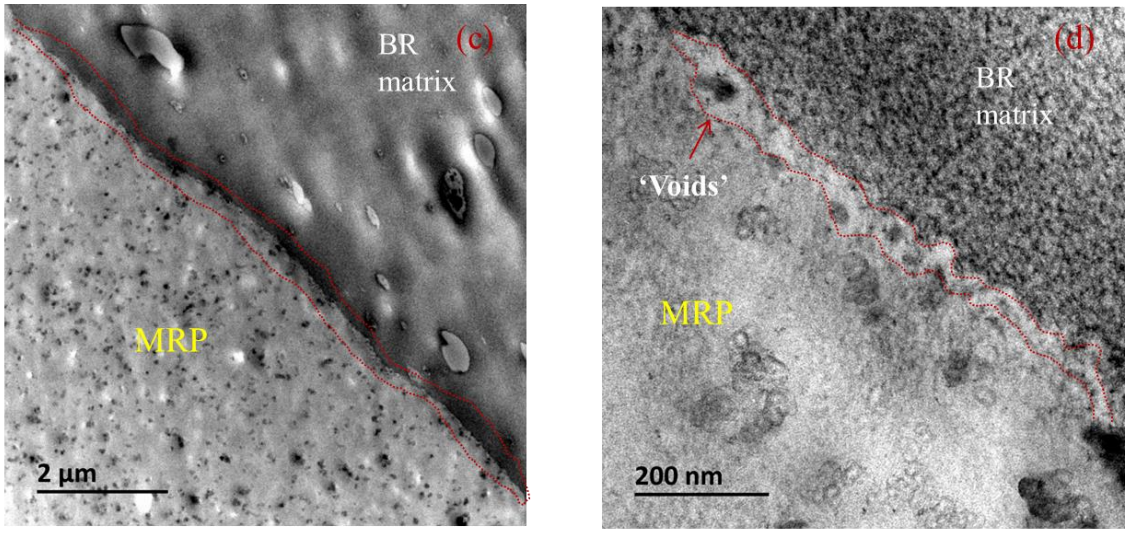

BR + 10 pphr MRP BR + 10 pphr MRP

Figure 6-4 TEM ‘‘network visualisation’’ micrographs of (a) NR+10 pphr MRP074 (stained) (b) NR+10 pphr MRP074 (stained) (c) BR+10 pphr MRP074 (stained) (d) BR+10 pphr MRP074 (stained) sectioned from unfilled rubber vulcanisate.

The interface morphology showed that CRP400 provided more developed structures or ‘irregular interfaces’, which probably suggests a stronger interface strength of the CRP400 with the rubber matrix. The strong physical bonding between the rubber matrix and CRP400 network is clearly associated with the irregular shape, compared to the microscopic smooth surface structure of MRP074 particles. The irregular shape on the surfaces results in an additional area to allow further penetration/entrapment of polymer chains and thus provided good physical bonding [32,185]. The relationship of the interface morphology with tear strength and abrasion resistance are discussed in Chapter 7.

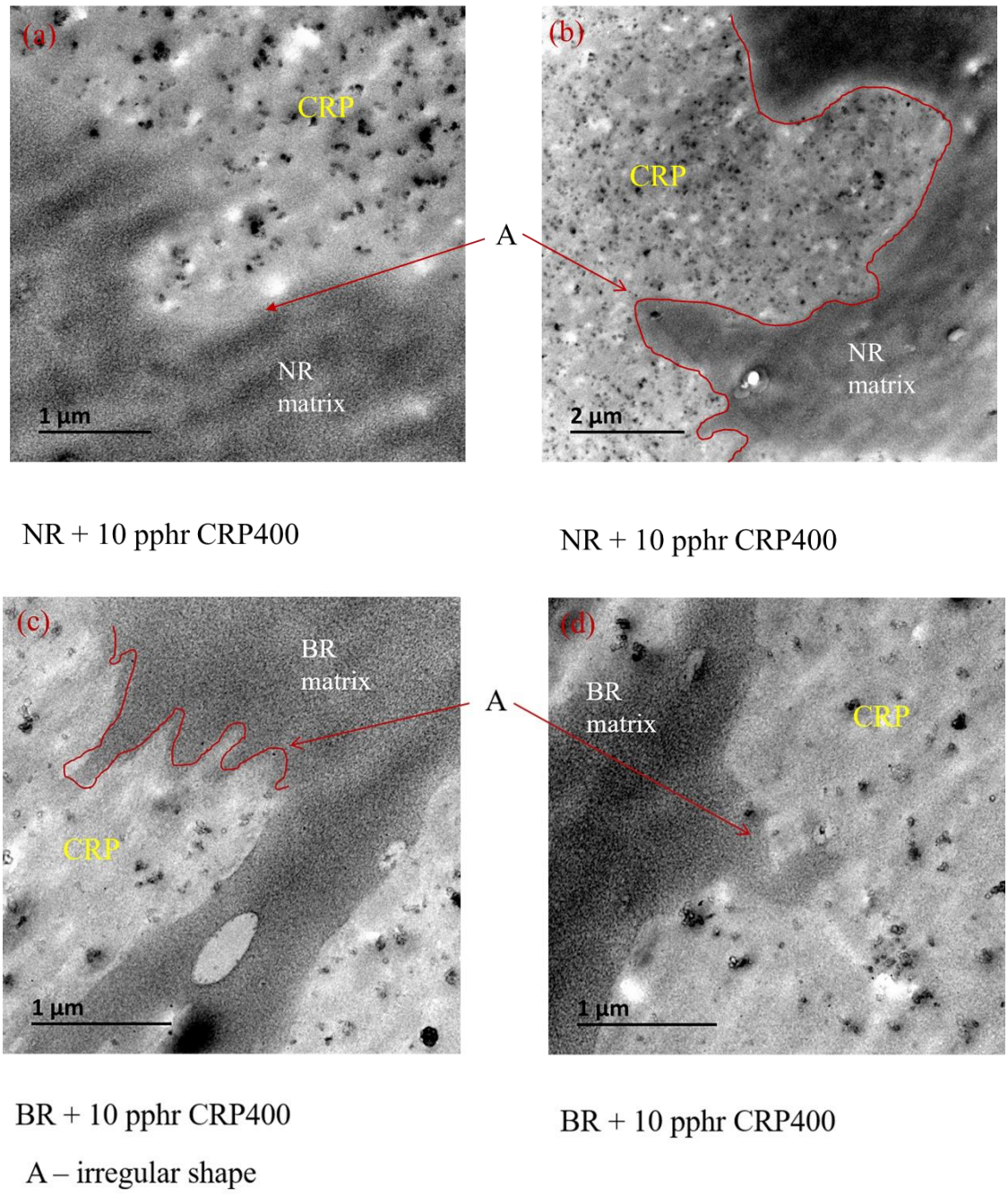

Figure 6-5 TEM ‘‘network visualisation’’ micrographs of (a) NR+10 pphr CRP400 (stained) (b) NR+10 pphr CRP400 (stained) (c) BR+10 pphr CRP400 (stained) (d) BR+10 pphr CRP400 (stained) sectioned from unfilled rubber vulcanisates.

6.4 Summary

The weak interaction at the interface between the MRP074 particles and the rubber network matrix was visualised as polystyrene ‘voids’ around particles, using the TEM ‘network

visualisation’ technique. A more regular shape in the TEM micrographs of MRP074 compared to CRP400 was identified. This confirmed the lower physical bonding between the MRP074 particles networks to the rubber matrix by comparison with that for the CRP400 particles.

Chapter 7 Effect of Recycled Rubber Powder filler on cure characteristics, tear strength, fatigue life and abrasion resistance of carbon black filled NR, BR or NR/BR compounds

7.1 Introduction

In the rubber industry, carbon black (CB) fillers play an important role for rubber reinforcement, and are considered to be a more effective reinforcing filler for rubber tyre treads than silica, especially when the silica is used without a coupling agent [186]. Phadke *et. al* [148] found that carbon black incorporation can minimise the loss of mechanical properties of recycled NR compound containing cryogenic ground powder. The authors used recycled rubber powder of about 400 µm particle size and both curing and mechanical properties (tensile, tear, hardness, flex resistance, etc.) were discussed. The effect of commercial cryogenic micronised rubber powder has not been widely studied, although it is reported that the mixing behaviour and the mechanical performance of the vulcanisate improved with the increased surface area of particles, using particle sizes below 250 µm [147]. Swor *et al.* [158] demonstrated that ultrafine recycled powder of 20 µm, produced from their exploratory study using a mechanical process at the ambient temperature, led to no significant decline in the tensile strength of NR and Styrene Butadiene Rubber (SBR) compound. The authors also showed that the fatigue life in terms of number of cycles to failure was enhanced by ultrafine powder, in an SBR compound. However, no data was reported for fatigue life when using NR matrix. Unfilled NR, BR and NR/BR compounds in Chapter 5 showed that an MRP074 filled compound gave better tensile strength and fatigue life (fatigue-to-failure tester (FTFT)-100% strain) compared to a CRP400 filled compound. The interface study in Chapter 6 showed that CRP400 exhibited an irregular shape and stronger interface interaction than the MRP074 filled compound.

This Chapter describes an investigation into recycled rubber powder (RRP) particles in carbon filled NR, BR and NR/BR compounds. The cure characteristics and mechanical (tensile, hardness, tear, and abrasion) of MRP074 or CRP400 carbon black filled NR, BR and NR/BR compounds were investigated. In addition, the investigation of fatigue life focuses on NR/BR compounds containing CRP400 or MRP074. A common tear strength method,

crescent tear, was used to assess tear resistance, while DIN and Akron tests determine the abrasion resistance. In this chapter, the cure characteristics and tear strength of the unfilled compounds from Chapter 5 are discussed in comparison with the carbon black filled compounds.

7.2 Experimental procedures

7.2.1 Materials

All rubbers and ingredients were as described in Table 5-1 (Chapter 5). N234 carbon black is a high reinforcing carbon black and 30 pphr were incorporated in every mixing. Experiments using 50 pphr of N234 were only carried out for the NR/BR-MRP074 filled compounds (0, 10, 30 and 50 pphr MRP074 concentrations).

7.2.2 Mixing

NR was masticated to reduce the viscosity to a nominal value of 60 Mooney units (ML(1+4) at 100°C), using a Bridge cracker mill, (406 mm dia x 508 mm length) then a two-roll mill (Francis Shaw-50kg capacity). Three master batches of each NR, BR and NR/BR compound were prepared using a Polylab 2000E internal mixer (390 cm^3 and fill factor 0.72). For NR/BR blend compounds, the raw NR and BR were mixed simultaneously before the addition of carbon black, RRP and other compounding ingredients. The masterbatch mixing was carried out with a starting temperature of 40°C and a rotor speed of 60 rpm. Total mixing time was 6.5 min. The CB filled BR required a slightly longer mixing time of 7 min. The masterbatches were allowed to cool overnight before the curatives were added separately using a two-roll mill. A band of rubber was formed as a continuous sheet on the mill. Once the curatives had all been added, the banded rubber was cut and rolled three times from each side of the mill, alternating from the left and from the right. After that, the entire compound was removed as a roll and passed through a tight nip for three passes, not allowing the rubber to band but taking off as a roll. The number of cuts and passes is kept low to minimise degradation of the rubber matrix whilst ensuring good dispersion of the curatives. Each mix was then sheeted out at approximately 4-5 mm thickness (see Appendix B for mixing process outline). Preparation of the compounds to this strict regime was chosen to keep the

processing of each compound as similar as possible to reduce the effect of processing variability on the rubber vulcanisate properties.

The NR/BR compound with 50 pphr carbon black, was prepared using a Farrel OOC Banbury internal mixer (4300 cm^3 and fill factor of 0.75) but the MRP074 was added subsequently in a Farrel BR Banbury internal mixer (1570 cm^3 and fill factor of 0.75).

7.2.3 Preparation of test pieces

The 229 mm square sheets of 2 mm thickness were prepared according to the experimental description in Chapter 5. DIN abrasion specimens (cylindrical discs of 15 mm dia and 8 mm thickness) were moulded using their respective optimum cure times, t_{95} (time at 95% of the maximum torque rise). The Shore A hardness button (a cylindrical disc of 25 mm dia x 6 mm thickness) and Akron abrasion moulded discs (64 mm dia x 12.5 mm thick) with a centre hole of 12.7 mm dia were cured at t_{95} + 5 mins. (see Appendix C for images of the respective mould)

7.2.4 Cure characteristics and mechanical properties

The cure characteristics and mechanical properties testing (tensile strength, elongation at break and hardness) were carried out according to the experimental methodology described in Chapter 5. The tear strength was determined according to ISO 34-1:2015 (Method C for crescent test pieces). Test pieces for the crescent tear test (Figure 7-1) were cut from a 2-mm-thick moulded sheet. An Instron universal testing machine (Model 5567) was used, with a 1kN load cell at a crosshead speed of 500 mm/min. The tear strength (kN/m) was taken as the maximum force required for the tearing of the specimen, divided by the thickness of the test piece and the median force was determined from tests on five specimens.

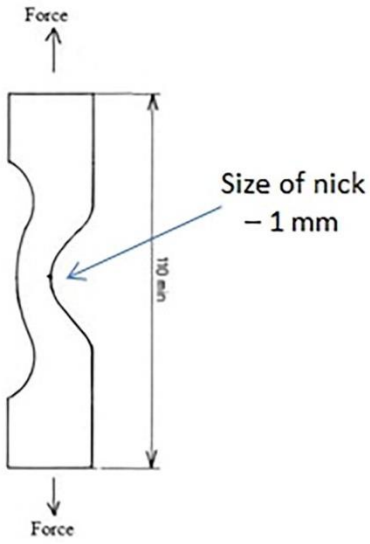

Figure 7-1 Crescent tear piece.

The DIN abrasion resistance (BS ISO 4649:2010) for carbon black filled NR, BR and NR/BR compounds was measured by abrading the rotating vulcanised test specimens against a surface of an abrasive sheet, prepared to the standard specification. The specimen was mounted on a revolving drum (40 rpm) at a constant force (10 N) and speed (0.32 m/s). The abraded distance was nominally 40 m. Each compound was tested using 3 different specimens. The Akron Abrasion Laboratory wear testing was adapted from BS 903: A9: 1988 (Method B) followed an in-house procedure of Tun Abdul Razak Research Centre (TARRC, Hertfordshire, UK). The position of the samples was set to a slip angle of 15º. Carborundum and Fuller's earth dust (2:1) were applied to remove debris and reduce stickiness. The specimens were pre-abraded for 500 revolutions before testing and repeated 5 times at 1000 revolutions, to achieve stable conditions. The mass loss was measured (mg) after every 1000 revolutions and the average of the third-to-fifth measurements were recorded. The abrasion resistance for the Akron and the DIN tests were expressed as volume loss, calculated from the mass loss and the density of the compound. The ratio of the sample mass in air and the volume (sample mass difference in the water and in air) was determined for density measurement.

The standardised Fatigue-To-Failure Tests (FTFT) was carried out using a TARRC Universal Crack Growth Machine to measure the fatigue life of the compound containing RRP in NR/BR carbon black filled compound only and the total number of cycles to failure was

reported. The systems were configured and testing conducted at TARRC. These type of tests used an un-notched specimen, thus involved both fatigue initiations and crack propagation of the total fatigue life. Six dumbbells (type 2 of BS ISO 37:2017) were die-stamped from moulded 2 mm rubber sheet and cycled under fully relaxing conditions, at a frequency of 5 Hz and a fixed strain of 100%. The fatigue life was calculated based on the accepted Japanese Industrial Standard (JIS) average, which was determined from the four highest values recorded using the following equation [187]:

$$\text{JIS average} = 0.5A + 0.3B + 0.1\,(C+D), \qquad \text{(Eq. 7-1)}$$

where A is the highest value followed by B, C, and D. Fatigue life for unfilled NR/BR (Chapter 5) was determined based on the JIS average for trend comparison.

7.3 Results and Discussion

7.3.1 Cure Characteristics

All rheometer curves and basic cure characteristics for unfilled and CB filled NR, BR and NR/BR compounds containing RRP (CRP400 and MRP074) are shown in Appendix D. Figure 7-2 shows a comparison of the change in torque, ΔM (ΔM = maximum torque (M_H) – minimum torque (M_L)) for MRP074 and CRP400 concentration of unfilled or CB filled NR, BR or NR/BR compound. The ΔM value usually indicates the crosslink density and stiffness of the rubber vulcanisates [188]. Hence, the addition of up to 30 pphr RRP decreased the crosslinking of unfilled BR compound. These results agree with work by Gibala and Hamed [171], who found that migration of sulphur from the virgin compound to the RRP led to additional crosslinking of the RRP, while decreasing the crosslinking density of the matrix. Overall stiffness of RRP filled compounds was dominated by the matrix, which reduced ΔM. Modifying the formulation by increasing sulphur and reducing accelerator for RRP compounds may have restored crosslink density to be comparable to the control compound [7].

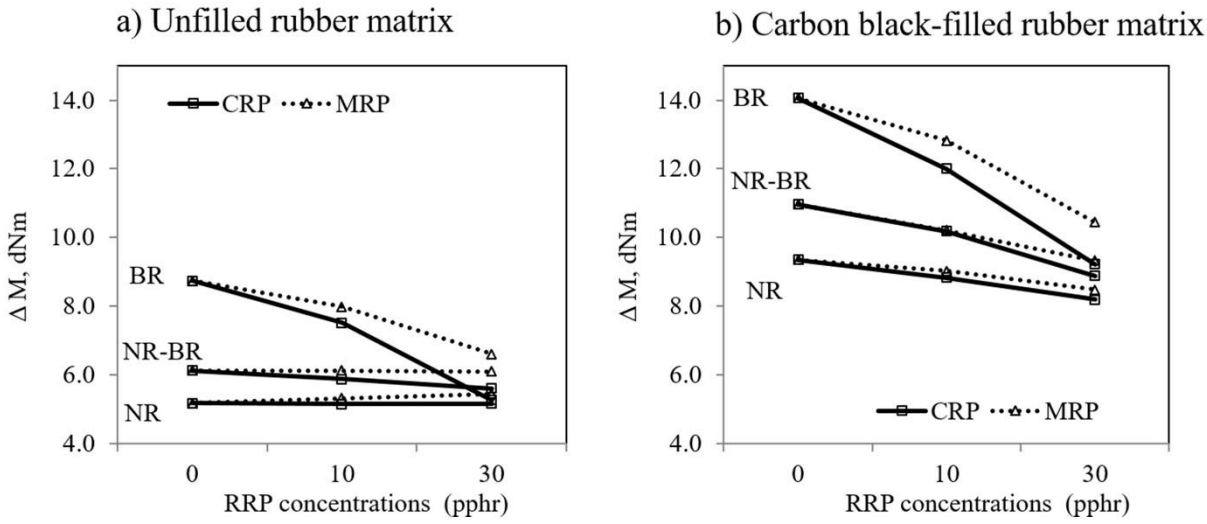

Figure 7-2 Comparison of ΔM for MRP074 and CRP400 concentration of a) unfilled, and b) carbon black filled NR, BR and NR/BR compound.

The effect on ΔM of either CRP400 or MRP074, up to 30 pphr concentrations, is marginal for unfilled NR and NR/BR blends. Competing factors between reduction of crosslinking and stiffening effect of RRP (original composition was NR/BR filled carbon black) explains the trends in torque behaviour of NR and NR/BR compound. At similar concentrations, MRP074 filled NR/BR exhibited higher torque than CRP400 filled compounds. This may be attributed to smaller particles of MRP074, which provided slightly higher hydrodynamic reinforcement compared to CRP400. In addition, the increased solubility of curatives in BR than in NR [189] probably allowed more diffusion of curatives from virgin BR to the RRP phase which could explain the much larger drop in ΔM. The extent of sulphur migration is also affected by the particle surface area of RRP filler [172]. It appears that sulphur migration is higher for CRP400 than for MRP074 at 30 pphr concentrations, probably due to irregular surfaces of CRP400 providing more contact surface area to the BR matrix. This explains a larger drop in ΔM for CRP400 compared to MRP074 filled BR compounds.

As expected, in the carbon black (CB) filled compounds, the addition of carbon black increases ΔM through restriction from physical absorption and/or crosslinks between rubber molecules and CB surfaces [190]. The presence of carbon black in the RRP compound appeared to affect the apparent crosslink density of the rubber matrix. The reciprocal swelling value, 1/Q (Eq. 5-1) which relates to the apparent crosslink density of the vulcanisates

(Figure 7-3) corresponded with the variation in the ΔM with the exception of NR compounds containing 10 pphr CRP400. As with the unfilled NR and NR/BR compound, the competition between the reduction of crosslinking and stiffening of each RRP filler explains the trends in torque behaviour of NR and NR/BR compound. The ΔM reduction is more obvious in CB filled than unfilled NR or NR/BR compounds. The ΔM reduction could also be associated with the 'dilution effect' of RRP filled NR, BR and NR/BR matrices, which are less stiff compared to respective CB filled compounds (without RRP) [191]. In this case, ΔM was not suitable for the indication of the crosslink density of rubber but was more affected by the stiffness of the rubber matrix.

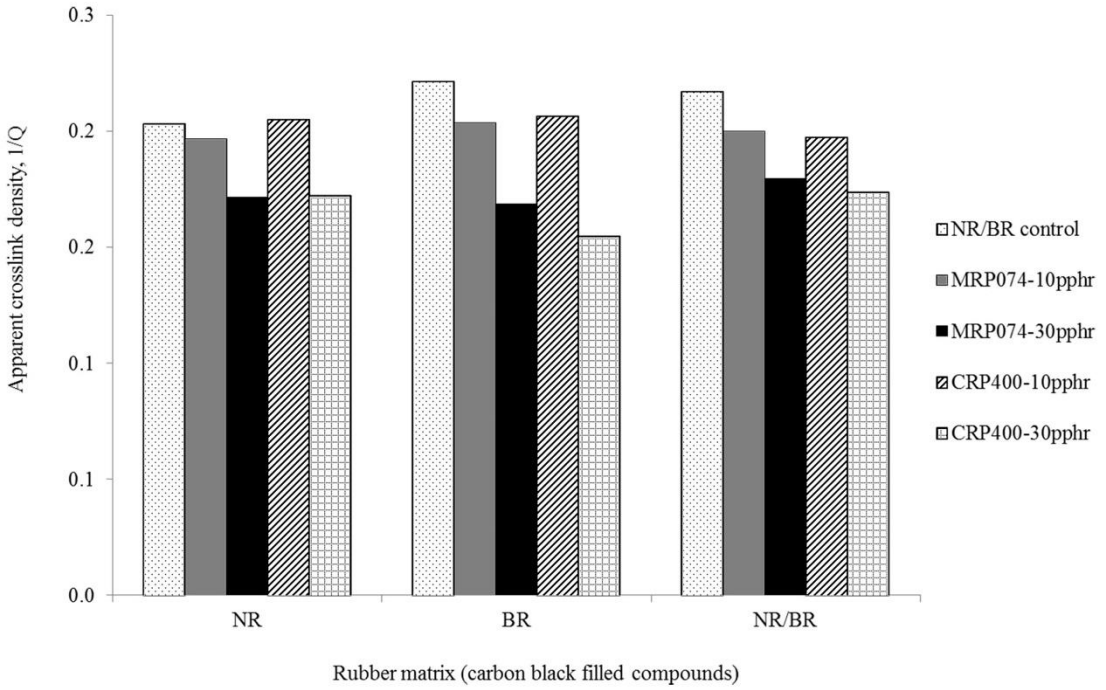

Figure 7-3 Apparent crosslink density of carbon black filled NR, BR or NR/BR blend compound containing MRP074 or CRP400 filler.

Gibala and Hamed [171] additionally found that unreacted accelerators, bound to the RRP network, can be released due to the sulphur migration into the rubber crumb. This reduces the cure time of the compounds containing CRP400 and MRP074, as shown in Figure 7-4 (a) for unfilled NR, BR and NR/BR compounds with the single exception of CRP400 filled BR at 30 pphr concentration. An observed increase in the cure time suggests that sulphur migration in CRP400 was faster than in MRP074 filled BR leading to a rapid depletion of the accelerator

fragments (unreacted accelerators) in the blends. In carbon black filled compound, the accelerator fragments may have been absorbed by the carbon black [148] leading to a marginal reduction of the cure time, compared to the unfilled compound (Figure 7-4 (b)). The trend for CRP400 and MRP074 filled compounds was similar, thus the cure time for CB NR, BR and NR/BR blend compound was not significantly affected by the particle size of the RRP.

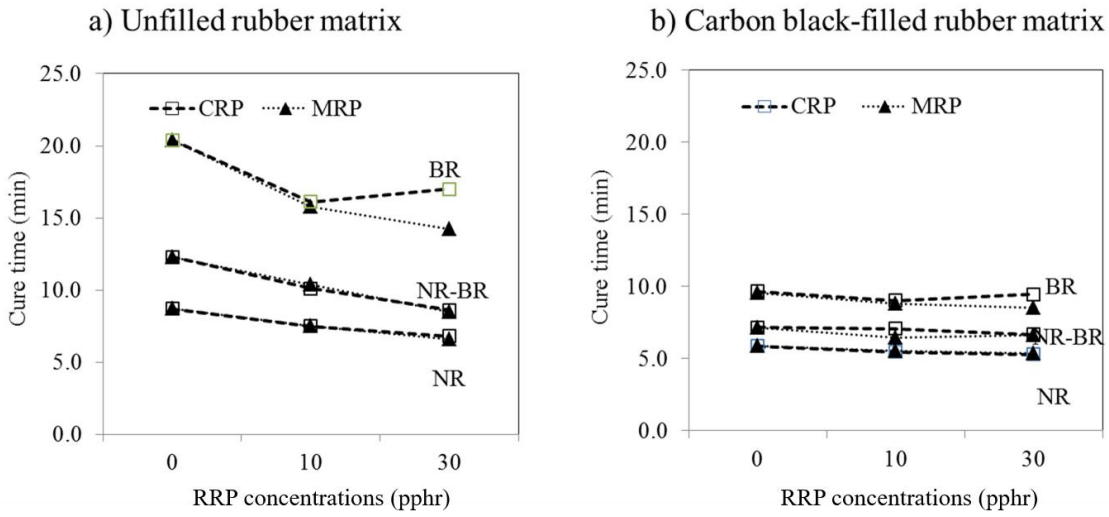

Figure 7-4 Comparison of cure time for MRP074 and CRP400 concentration of a) unfilled, and b) carbon black filled NR, BR and NR/BR compounds.

7.3.2 Mechanical properties

The addition of carbon black increased the tensile strength and modulus of NR, BR and NR/BR relative to the unfilled compound. Reinforcement of the rubber matrix by the carbon black restricted the mobility of the rubber network. The breakup and reformation of filler network within the rubber chain during the fracture process involved energy dissipation, often referred to as being part of the mechanical hysteresis [102]. Hence, increased hysteresis partially contributed to the enhancement of tensile strength of CB filled compounds.

Table 7-1 summarises the tensile properties of carbon black filled NR, BR and NR/BR containing MRP074 and CRP400 at 10 or 30 pphr. Carbon-black filled NR with 10 pphr MRP074 concentrations, displayed an 11% reduction of tensile strength, compared to 24% reduction for the unfilled rubber (Chapter 5), relative to compounds without MRP074. In

NR/BR blend compound, there is only a small decreasing trend in tensile strength for MRP074 compound compared to NR. The values in tensile strength of NR/BR, containing 10 (28 MPa) and 30 pphr of MRP074 (26 MPa), were comparable to the carbon-black filled NR (29 and 26 MPa for 10 and 30 pphr of MRP074 respectively). The tensile strength reduction due to the CRP400 filler was very pronounced with increases in CRP400 concentrations, compared to MRP074 filled NR and NR/BR. This indicates that tensile strength was influenced by the particle size of the filler in the rubber matrix. Larger particles of CRP400 acted as a critical stress-raiser that initiated fracture and lowered tensile strength [157]. Other factors, which also had influence on tensile strength, were filler dispersion, crosslinking density [172], surface area of filler and rubber filler interaction [166,192].

Table 7-1 Tensile and elongation at break properties, including standard deviation, of CB filled rubber containing CRP400 and MRP074.

	Tensile strength (MPa)	Modulus at 100 % elongation (MPa)	Elongation at break (%)
NR/0 (control)	33.0 ± 0.4	1.26 ± 0.02	690 ± 25
NR/10-CRP400	27.2 ± 1.1	1.32 ± 0.05	640 ± 20
NR /30-CRP400	22.0 ± 0.8	1.26 ± 0.06	580 ± 25
NR/10-MRP074	29.2 ± 1.1	1.32 ± 0.02	660 ± 15
NR/30-MRP074	26.1 ± 0.4	1.30 ± 0.06	610 ± 30
BR/0 (control)	13.5 ± 1.6	1.54 ± 0.04	520 ± 40
BR/10-CRP400	11.5 ± 0.6	1.40 ± 0.04	480 ± 15
BR/30-CRP400	08.5 ± 0.4	1.24 ± 0.01	420 ± 20
BR/10-MRP074	17.6 ± 0.4	1.42 ± 0.05	620 ± 35
BR/30-MRP074	15.3 ± 0.7	1.24 ± 0.03	610 ± 30
NR-BR/0 (control)	29.60 ± 1.5	1.40 ± 0.02	700 ± 20
NR-BR/10-CRP400	24.00 ± 0.7	1.43 ± 0.05	640 ± 25
NR-BR/30-CRP400	20.70 ± 0.5	1.32 ± 0.04	620 ± 30
NR-BR/10-MRP074	27.80 ± 0.5	1.39 ± 0.04	690 ± 35
NR-BR/30-MRP074	26.40 ± 0.3	1.41 ± 0.03	660 ± 15

In carbon-black filled BR, an increase in tensile strength and elongation at break (EB) can be observed at 10 pphr, with a subsequent decrease at 30 pphr of MRP074. The tensile strength

of CRP400 filled compound showed a reduction with increasing CRP400 concentration. Similar to unfilled BR (Chapter 5), the higher modulus of BR corresponded to higher apparent crosslink density followed by NR/BR and NR compounds. When incorporating up to 30 pphr of either RRP, sulphur migration (mentioned earlier) occurred causing a reduction of the M100.

Overall, at 30 pphr of RRP filler, reduction in tensile strength and EB was observed for carbon black filled NR, and NR/BR compounds. The competition between the reduction of crosslinking and stiffening [172] of both RRP filler explains the different trend behaviour of M100 for NR and NR/BR.

Table 7-2 displays the hardness and tear strength based on crescent tear pieces of RRP filled NR, BR and NR/BR blends in unfilled or CB-filled compounds. The hardness showed little change with the addition of up to 30 pphr concentrations of either CRP400 or MRP074. The reduction in crosslink density, attributed to the sulphur migration discussed earlier, decreased the hardness of the BR compound, particularly for CRP400 filled BR at 30 pphr concentrations. The crescent tear test, measured the maximum force required to propagate a 1 mm initial cut through the whole specimen to failure. The resistance to crack propagation in unfilled compounds was ranked NR>>NR/BR>BR. This may be attributed to the strain-induced crystallisation and 'crack tip blunting' behaviour [157] of NR during tearing.

In BR, the opposite trend to the tear strength of the NR and NR/BR compound was observed in Figure 7-5. The crack propagation resistance of BR increased with increasing MRP074 and CRP400 concentration in both unfilled and CB filled BR, within the test range of up to 30 pphr. The origin of the RRP is likely to be NR/BR CB filled compounds which are more rigid/stronger than the softer/weaker rubber matrices. Therefore, fracture tended to initiate at the weakest point (high stress concentration) and it is assumed that tear deviated along the matrix-RRP interface rather than through the RRP particles [46]. Pittolo and Burford [193] also showed that the tear strength of recycled material is dependent on both, the filler hardness and the filler-matrix bonding. Thus, the increase in tear strength suggests that interface interaction of RRP in BR is higher and the RRP particles exhibited higher hardness (more crosslinks) than in the NR matrix and this is more clearly observed in CB filled BR compounds.

In unfilled compounds, CRP400-BR had slightly lower tear strength compared to MRP074 containing BR at 30 pphr of MRP074. According to Mathew *et al.* [172], it is assumed that with smaller particles, there will be more filler particles present per unit volume to deflect or deviate (crack bifurcation), an advancing crack which contributes to the higher tear strength.

Table 7-2 Hardness and crescent tear strength for RRP filled NR, BR and NR/BR blend compounds; unfilled and CB filled compound.

	Hardness (Shore A) ±SD[+] Unfilled	Tear strength (kN/m) ±SD[+] Unfilled	Hardness (Shore A) ±SD[+] CB-30 pphr	Tear strength (kN/m) ±SD[+] CB-30 pphr
NR/0	32 ± 0.5	32.0 ± 0.9	48 ± 0.7	94.5 ± 23
NR/10-CRP400	33 ± 0.9	24.8 ± 1.6	50 ± 0.5	75.5 ± 16
NR/30-CRP400	35 ± 0.8	14.6 ± 2.1	50 ± 0.4	60.1 ± 13
NR/10-MRP074	34 ± 0.7	23.0 ± 3.1	50 ± 1.0	79.3 ± 14
NR/30-MRP074	36 ± 0.5	10.5 ± 1.7	50 ± 0.7	84.1 ± 09
BR/0	41 ± 0.3	4.7 ± 0.9	55 ± 0.5	14.6 ± 0.3
BR/10-CRP400	41 ± 0.7	7.1 ± 0.3	54 ± 0.7	16.9 ± 1.3
BR/30-CRP400	38 ± 0.9	7.2 ± 0.6	52 ± 0.5	35.9 ± 8.3
BR/10-MRP074	41 ± 0.4	6.9 ± 0.9	54 ± 0.7	16.4 ± 0.8
BR/30-MRP074	40 ± 0.8	8.8 ± 0.2	53 ± 0.7	25.4 ± 6.0
NR-BR/0	35 ± 0.5	12.4 ± 1.0	52 ± 0.6	69.4 ± 09.3
NR-BR/10-CRP400	35 ± 0.0	11.2 ± 1.2	52 ± 0.7	62.9 ± 11.8
NR-BR/30-CRP400	36 ± 0.9	11.3 ± 0.8	52 ± 0.7	61.5 ± 17.0
NR-BR/10-MRP074	36 ± 0.6	08.8 ± 0.8	52 ± 0.5	73.9 ± 11.2
NR-BR/30-MRP074	37 ± 0.7	09.8 ± 0.4	52 ± 0.7	66.0 ± 16.4

[+]standard deviation

Despite the weak interface interaction of MRP074 networks, an increase in crescent tear propagation strength for BR compound was probably due to a combination of factors such as:

- stronger bonding between the BR phase and crosslinked-MRP074
- greater tear deviation,
- probably a reduced crosslink density matrix

- some contribution of hysteresis within the filler.

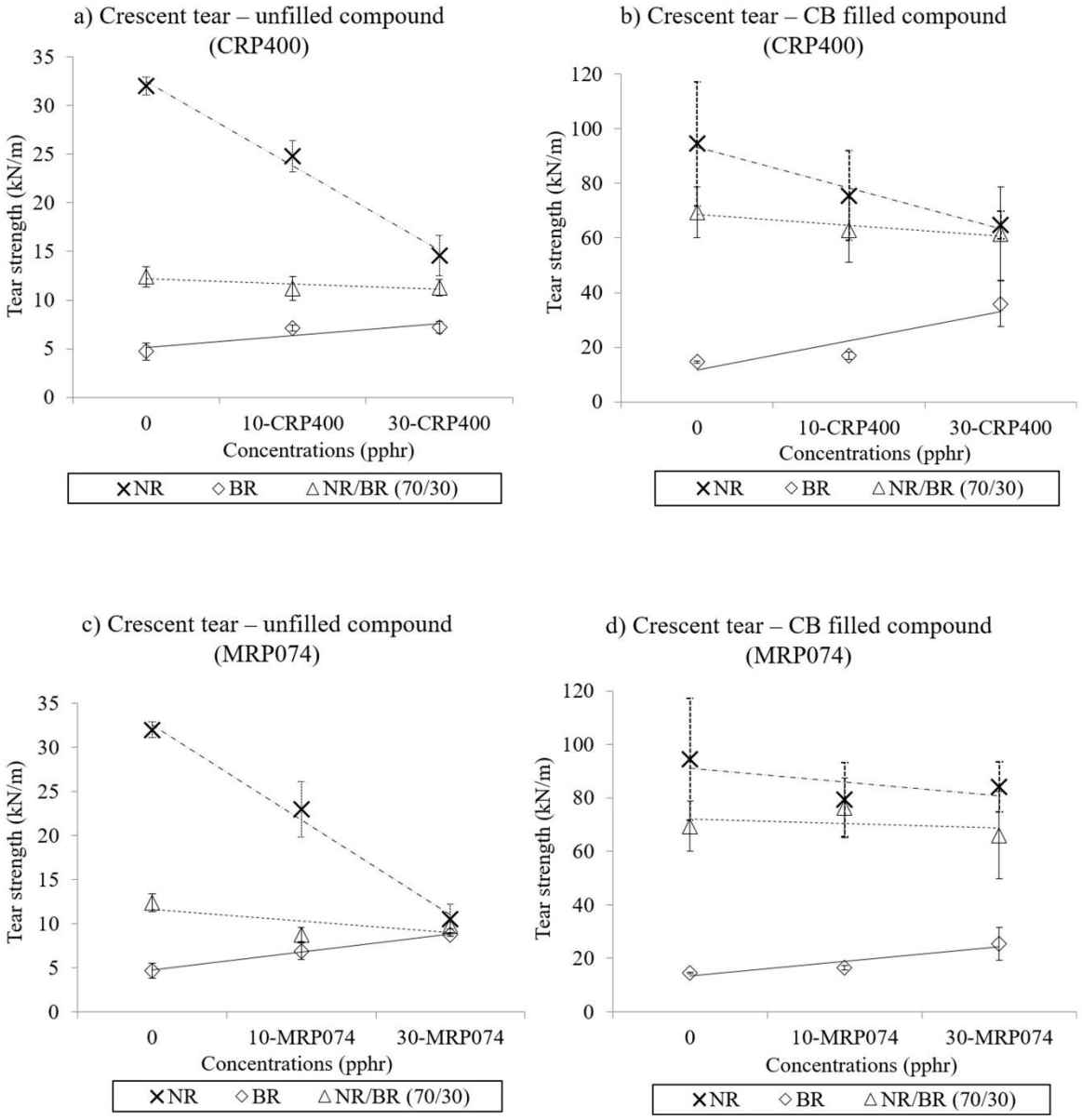

Figure 7-5 Crescent tear strength of unfilled and carbon-black filled NR, BR and NR/BR compound for (a)-(b) CRP400 and (c)-(d) MRP074 filled compound (Note: The Y-axis full scale in (a) and (c) is less than half that in (b) and (d)).

The addition of carbon black (CB) resulted in a heterogeneity in the rubber matrix. Hence, CB filled compounds displayed a higher scatter in the tear strength results compared to the unfilled compound. The addition of carbon black in NR and NR/BR control compounds produced wide scatter even without the MRP074 incorporation (Figure 7-5 (c) and (d)). This

requires the optimisation of the mixing procedure and the addition of small quantities of processing oils. Uniformly dispersed curatives, filler and other ingredients in the matrices need to be incorporated in the continuous phase to resist failure under various stress and strain conditions. These factors also need to be considered when incorporating MRP074 into any rubber matrix. Clarke *et al.* [194] concluded that a suitable mixing cycle with an optimum cure system could produce a fine textured morphology due to optimum filler/additives dispersion. This results in blends with higher strength, whereas the clustering in coarse morphology is more likely to introduce premature crack initiation and consequent early failure. A compromise in mechanical properties is usually a consequence of blending two rubbers. Blending NR with BR increases crack propagation. Despite the lower crack resistance in NR/BR blends compared to NR, BR has an excellent abrasion resistance, and blending with NR improved this property (see section 7.3.3).

The heterogeneity created by the carbon black filler, which acted as a barrier and led to the deviation of a crack growth path, retards the crack propagation of the NR, BR and NR/BR blend compounds. Similar to tensile strength, hysteresis partially contributed to the enhancement of tear strength performance of CB filled compounds, relative to unfilled rubber compounds. Other strengthening factors such as strain crystallisation, strength anisotropy and crack tip blunting are also reported [195,196]. This compensates for the tear strength reduction of unfilled NR and NR/BR compounds containing MRP074 and CRP400. The crack propagation resistance of NR/BR (70/30 ratio) appears to be slightly improved giving similar performance to NR compounds at an equivalent ratio of 10 pphr MRP074. The addition of carbon black to MRP074 filled compounds tended to improve tear resistance more than in CRP400 filled compounds, which contradicts the result from the unfilled materials. However, at 10 pphr concentrations, considering the large scatter in the tear strength results (Table 7-2), the effect of MRP074 was not significantly different compared to CRP400 in CB filled NR and NR/BR blend compounds.

According to Pittolo and Burford [193], tear strength increases with high filler-matrix adhesion and increases with filler hardness. For CB filled BR, the CB enhanced the interaction between CRP400 and the rubber matrix. The crosslinking of BR matrix was significantly reduced by the addition of RRP, but the crosslinking of the RRP particles increased. Higher sulphur migration occurred in CRP400 than in MRP074, due to its higher

surface area, which increased the hardness of the filler leading to a more tear deviation mechanism. This probably explains the higher tear strength at 30 pphr concentrations for CRP400 compared to MRP074 compounds.

Using equilibrium swelling data for the unfilled and filled rubber compounds, the extent of interaction between rubber and RRP was investigated. The Lorenz-Parks model equation [197] was used.

$$\frac{Q_f}{Q_g} = ae^{-z} + b \qquad \text{(Eq. 7-2)}$$

Where Q is the swelling index value as determined in Eq. 5-1 and the subscripts *f* and *g* refer to filled and gum compound, respectively. *z* is the weight fraction of filler in each compound and *a* and *b* are constants which depend on the filler surface 'activity' (chemical or physical surface activity describe the potential of reaction between filler-filler particles or polymers-fillers).

High value of *a* and low value of *b* could indicate strong polymer-filler interaction. This model does not take into account the effect of filler that could enhance the crosslinking efficiency of the curing agent. The Cunnen–Russel equation (Eq. 7-3), modified from Eq. 7-2, was then used [198]. V_{ro} and V_{rf} are the volume fractions of rubber in the solvent-swollen gum and filled compound, respectively.

$$\frac{V_{ro}}{V_{rf}} = ae^{-z} + b \qquad \text{(Eq. 7-3)}$$

The weight or volume fractions of filler will include the combination of CB and RRP in CB filled compound.

Another model to characterise rubber filler interaction is the Kraus model [199], as given in Eq. 7-4. As mentioned earlier, the carbon black affects the apparent crosslink density. The model suggested the use of V_{ro} of unfilled compounds which represent crosslinks that are not

influenced by the filler. A reduced filler-polymer adhesion will produce considerable increase in the apparent swelling of rubber.

$$\frac{V_{ro}}{V_{rf}} = 1 - \left[\frac{m\phi}{(1-\phi)}\right] \quad \text{(Eq. 7-4)}$$

Where,

$$m = 3C(1 - V_{ro}^{1/3}) + V_{ro} - 1 \quad \text{(Eq. 7-5)}$$

C is a constant characteristic of the filler but is independent of the solvent; ø is the volume fraction of filler in each compound. Higher *C* values indicates higher rubber-filler interaction. The Eq. 7-4 is in the form of a straight line, where the gradient, m, quantifies the extent of restriction of the rubber-filler interaction. Compound containing reinforcing fillers such as carbon black showed not only a good fit to the Kraus model but also a more effective interaction filler/rubber matrix which exhibited a negative higher slope [198,200]. V_{ro} and V_{rf} were determined using Eq. 7-6:

$$V_r = \frac{(w_2 - \phi w)\,\rho_p^{-1}}{(w_2 - \phi w)\,\rho_p^{-1} + A_s\,\rho_s^{-1}} \quad \text{(Eq. 7-6)}$$

Where, ρ is density with the subscripts *p* and *s* refering to polymer/rubber and solvent respectively, w was defined earlier in Chapter 5 (section 5.2.6), A_s = amount of solvent absorbed by sample.

Table 7-3 shows the V_{ro}/V_{rf} values of RRP in unfilled or CB filled NR, BR and NR/BR compounds. When the mobility within the rubber network is restricted due to some attachment of the filler surface and rubber matrix, V_{ro}/V_{rf} will decrease as filler concentration increases [198]. In this study, the ratio of V_{ro}/V_{rf} increased with increasing filler concentration for RRP in unfilled and CB filled matrix.

Table 7-3 V_{ro}/V_{rf} of RRP in unfilled and carbon black filled NR, BR or NR/BR compounds.

Compound (Unfilled)	V_{ro}/V_{rf}	CB-filled compound	V_{ro}/V_{rf}
Control	1	NR-CB	0.8099
NR-CRP400-10	1.0270 (10)	NR-CB-CRP400	0.8103 (10)
	1.1119 (30)		0.9160 (30)
NR-MRP074	1.0306 (10)	NR-CB-MRP074	0.8368 (10)
	1.1170 (30)		0.9311 (30)
BR-CRP400	1.0749 (10)	BR-CB-CRP400	0.8719 (10)
	1.5990 (30)		1.1084 (30)
BR-MRP074	1.0691 (10)	BR-CB-MRP074	0.8812 (10)
	1.2972 (30)		1.0320 (30)
NR/BR-CRP400	1.0529 (10)	NR/BR-CB-CRP400	0.8948 (10)
	1.1481 (30)		0.9925 (30)
NR/BR-MRP074	1.0342 (10)	NR/BR-CB-MRP074	0.8895 (10)
	1.1003 (30)		0.9719 (30)

Values in the parentheses are filler concentration (pphr)

This supports the earlier results (Figure 7-3), that at higher concentration of RRP, reduced crosslinking of the matrix caused higher solvent uptake. Figure 7-6 shows the Kraus plot of RRP for unfilled and carbon black filled NR, BR and NR/BR compounds. In unfilled compounds, RRP exhibited a positive slope. According to Kraus, if the ratio of $V_{ro}/V_{rf}>1$, the filler does not bond very well to the rubber matrix whereas strong interaction was predicted if $V_{ro}/V_{rf}<1$ was achieved. The ratio $V_{ro}/V_{rf}<1$ (exception for 30 pphr concentration in BR) for RRP CB filled NR, BR and NR/BR confirmed the role of CB for better adhesion of RRP filled compounds in comparison to unfilled compounds ($V_{ro}/V_{rf}>1$). However, deviations from the proposed linear Eq. 7-4 were observed at higher concentration for the CB filled compounds (Figure 7-6).

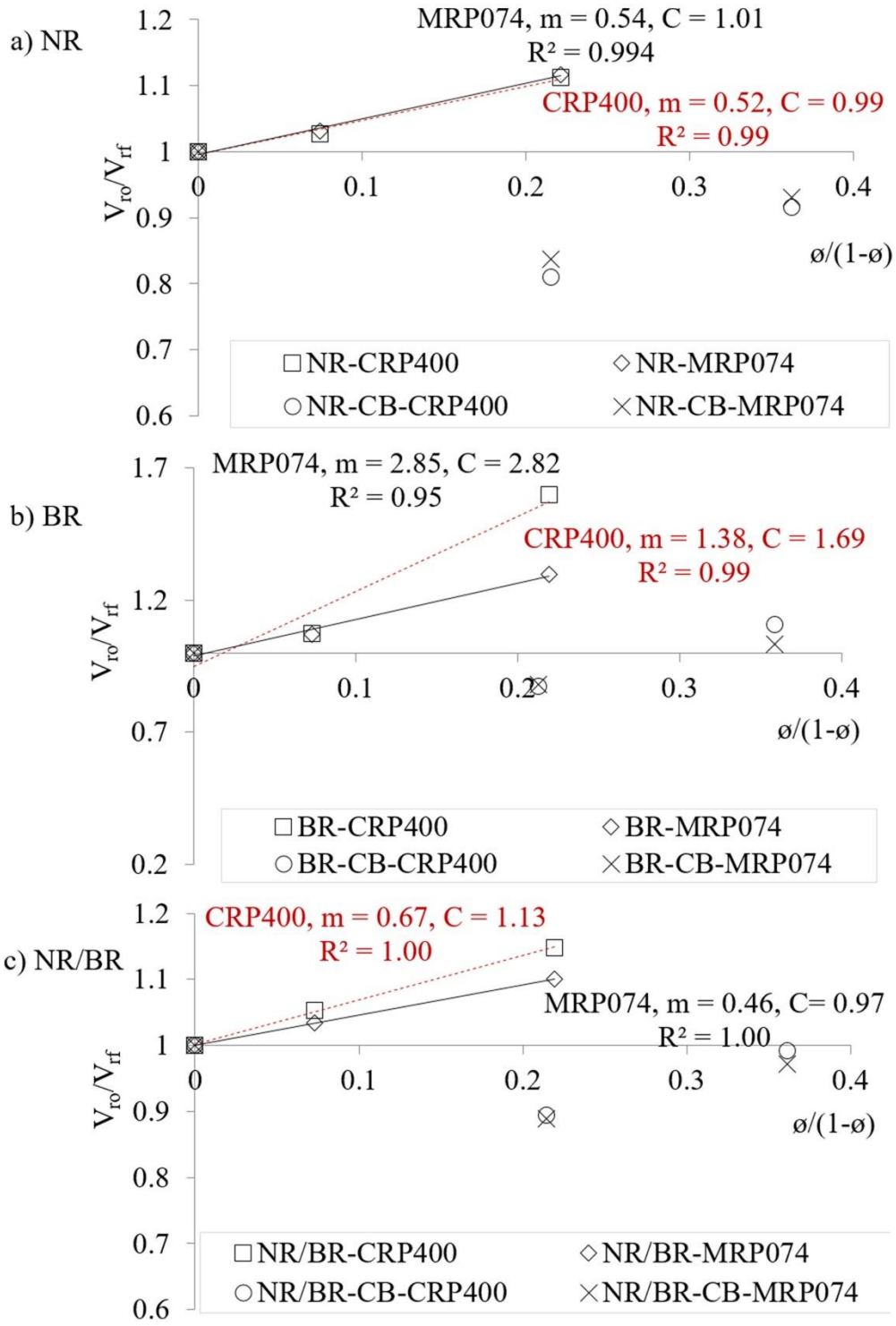

Figure 7-6 Kraus plot for unfilled or CB-filled NR, BR and NR/BR containing RRP filler.

Comparison of the gradient values of *a* for Lorenz-Park, Cunnen and Russel or m and C for the Kraus equation is shown in Table 7-4. Both Lorenz-Park and the Cunnen and Russel

equations indicate that CRP400 had better adhesion to NR, whereas MRP074 bonded with BR and NR/BR matrices. A similar trend was observed in BR for the Kraus equation but disagreement indicated by the *C* value showed that CRP400 exhibited better adhesion to NR/BR. There is a marginal difference in the *C* value with either of the RRP fillers in the NR matrix. The crescent tear strength (Table 7-2), within its experimental error for the unfilled compounds seemed to correspond to the rubber-interaction parameters given by the Kraus model. The highest value of *m* observed for MRP074 in BR compounds showed higher reinforcing ability compared to CRP400 and reflected in higher crescent tear strength especially at 30 pphr of MRP074. For NR/BR compounds, the highest value of *m* observed for CRP400 compared to MRP074 and also corresponded to the highest interaction parameter, *C* for the particular rubber matrix. Higher crescent tear strength was observed for CRP400 compared to MRP074 in NR/BR compound.

Table 7-4 Gradient values for Kraus, Cunnen and Russel, and Lorenz-Park equation for RRP in unfilled compound.

Compound (Unfilled)	Kraus equation		Cunnen and Russel equation	Lorenz-Park equation
	*m**	*C*	*a*	*a*
NR-CRP400	0.5164	0.99	-0.6018	-0.8050
NR-MRP074	0.5375	1.01	-0.6277	-0.8161
BR-CRP400	1.3833	1.69	-3.2636	-3.7159
BR-MRP074	2.8505	2.82	-1.6003	-2.0665
NR/BR-CRP400	0.6713	1.13	-0.7863	-1.1612
NR/BR-MRP074	0.4561	0.97	-0.5334	-0.7975

**m* represents the polymer-filler interaction parameter obtained from the gradient of the plot of V_{ro}/V_{rf} against $ø/(1- ø)$. (see Appendix E for *a* values from Lorenz-Park, and Appendix F for Cunnen and Russel equation)

Table 7-5 shows the gradient values of *a* for Lorenz-Park, Cunnen and Russel and *m* and *C*, for the Kraus equation, for RRP in CB filled compounds. Between the models, disagreement is observed on the performance of RRP filled materials in BR compounds. Although deviations from the straight line model for Kraus were observed (Figure 7-6), which were probably due to a change in degree of crosslink, which occurred during the sulphur migration

described earlier, the model supports the higher extent of interaction of CRP400 filled compound in BR and NR and MRP074 for NR/BR compounds. Nonetheless, the extent of interaction between CRP400 and MRP074 in NR and NR/BR is similar as indicated by the small difference in the *C* value compared to that in BR compounds. Similarly, the rubber-interaction parameters given by the Kraus model correspond to the crescent tear strength of RRP in CB filled compounds. Deviation occurred at 30 pphr of RRP concentration in particular unfilled or CB filled BR and NR/BR compounds, probably indicating the onset of dewetting and void formation [198].

Table 7-5 Gradient values for Kraus, Cunnen and Russel, and Lorenz-Park equation for RRP in CB filled compounds.

CB-filled compound	Kraus equation		Cunnen and Russel equation	Lorenz-Park equation
	m	*C*	*a**	*a*
NR-CRP400	-0.2791	0.82	0.4307	0.0296
NR-MRP074	-0.2315	0.79	0.3622	-0.0295
BR-CRP400	0.2361	0.81	-0.1200	-0.7322
BR-MRP074	0.0420	0.66	0.0592	-0.4856
NR/BR-CRP400	-0.0550	0.67	0.1416	-0.3938
NR/BR-MRP074	-0.1097	0.71	0.1991	-0.2962

*see Appendix E for *a* values from Lorenz-Park, and Appendix F for Cunnen and Russel equation

7.3.3 Abrasion resistance

The choice of the abrasion test method is critical for the performance evaluation of any new compound. In this work, the effect of MRP074 and CRP400 on abrasion resistance is only discussed for the CB filled compounds. DIN and Akron abrasion tests were conducted. The DIN abrader uses more severe frictional forces than the Akron abrader. Elsewhere, Martin *et al.* [184] demonstrated that the Akron abrasion test is more severe than experienced in normal tyre wear. The actual tyre wear may also involve fatigue, thermal degradation and oxidation [201]. Thus, laboratory tests may not replicate real world abrasion behaviour, especially for tyre applications due to various climate, road and driving conditions [184,202].

The following experiments demonstrated that the Akron abrasion test could indicate the strength of interactions between rubber and CB and RRP filler, particularly in NR/BR blends. A weak interaction or interface will provide a starting point for crack initiation and any further applied load or deformation will lead to rapid crack propagation/wear.

The abrasion resistance results of NR, BR and NR/BR vulcanisates with different MRP074 concentrations are displayed in Figure 7-7. The outstanding performance of BR can be seen in both abrasion tests, confirming previous reports [203]. The combination of both the excellent abrasion resistance of BR and good processing and fatigue of NR produces improved blends, especially for truck and passenger tyre applications.

Overall the trend in abrasion loss of MRP074 filled NR and BR is similar for both abrasion tests, but differs for NR/BR blends. For DIN and Akron abrasion tests, the volume loss increased with the increase in MRP074 concentrations, which may be attributed to the reduced crosslink density in NR [204]. There was a negligible increasing trend in volume loss for NR/BR compounds, using the DIN abrasion test on MRP074 filled compounds at 10 or 30 pphr concentrations. However, much higher increases in abrasion loss in Akron abrasion tests, at similar MRP074 concentrations, are shown in Figure 7-7 (b). The BR compound showed a small decrease in abrasion loss for both DIN and Akron abrasion indicating good bonding of MRP074 with BR compounds at 10 pphr. At 30 pphr of MRP074 concentrations, there was a small increase in the volume loss for both tests.

The addition of carbon black concentration of 50 pphr in NR/BR compounds improved the abrasion resistance of MRP074 filled materials, within the tested range of up to 30 pphr MRP074. This seems true for the Akron abrasion, but not for DIN abrasion test. The strong interface bonding between NR and BR is well documented [194] and plays an important part in the ability of blends to withstand deformation. However, the Akron abrasion test demonstrated that the interaction was not strong enough to sustain material integrity as indicated by higher losses with MRP074 at up to 30 pphr. The DIN abrasion test could not easily detect the changes in the matrix introduced by MRP074, particularly in CB filled NR/BR (Figure 7-7 (a)). This is due to Akron and DIN using different abrasion mechanisms. DIN offers predominantly a mixture of tensile-tearing and cutting (frictional rubbing) while Akron provides micro-scale tearing and fatigue assessment [160]. Although prediction from

laboratory measurements has yet to be achieved, Akron abrasion is reported [202] to correlate well with fatigue properties and is thus probably more useful in material evaluation.

The control compound containing 50-pphr CB showed higher volume loss compared to 30-pphr CB indicating that dispersion is also one of the factors affecting abrasion resistance. Carbon black properties (particle size, surface area, low/high structure and etc.), type of elastomer and mixing process variables are an important aspect for the improvement in carbon black dispersion which led to better abrasion resistance properties [205]. Improving abrasion resistance may also be possible through optimisation of the cure systems.

The weak interface in BR (Chapter 6) was only apparent at higher concentrations of MRP074 (30 pphr) in both DIN and Akron abrasion tests. Similarly, for NR/BR blends (where the interface interaction of MRP074 and matrix was not studied), it may be assumed that the weakness was again present and reflected in the Akron abrasion result. However, this was not revealed by the DIN abrasion test.

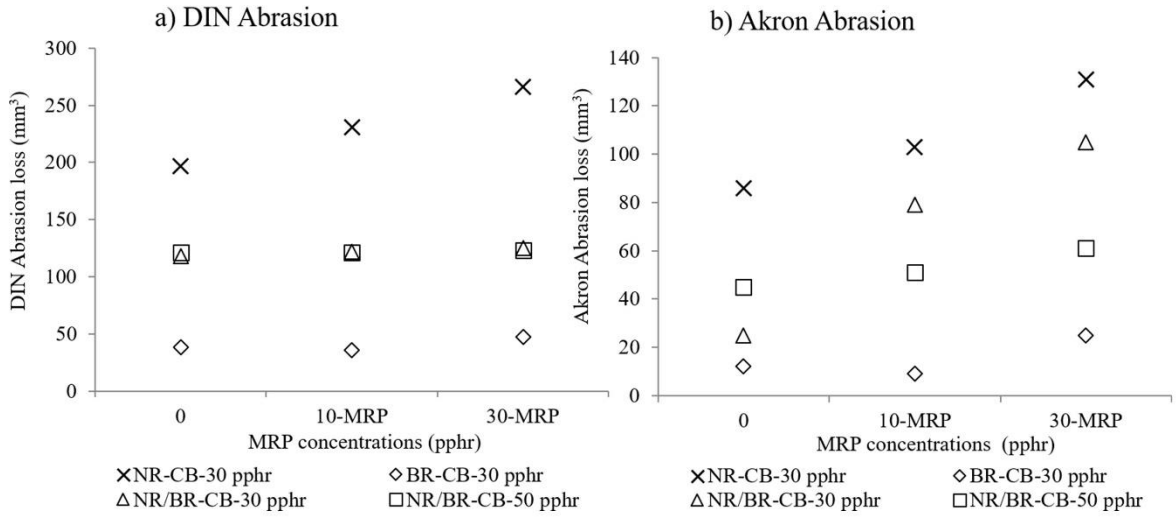

Figure 7-7 Comparison of (a) DIN and (b) Akron abrasion resistance tests of MRP074 carbon-black filled NR, BR and NR/BR compound (Note: The Y-axis full scale in (b) is less than half that in (a)).

7.3.4 Abrasion resistance performance of MRP074 versus CRP400 filled compound

The abrasion resistance results for NR, BR and NR/BR vulcanisates, with different CRP400 concentrations, are displayed in Figure 7-8. Similar to MRP074 filled NR compounds, there was an increasing trend in the volume loss for CRP400 filled NR, within the test range up to 30 pphr, for both DIN and abrasion tests.

Table 7-6 shows the comparison of DIN and Akron abrasion loss for MRP074 and CRP400. For NR and NR/BR blend compounds, the higher abrasion volume loss of finer MRP074, compared to larger CRP400 particles, infers that the structure of the rubber-filler interface was more important for the abrasion results than the size of the RRP. Due to the irregular structure of CRP400, the stronger filler-rubber matrix could reduce the abrasion rate compared to MRP400 compounds. A contrary result was found in MRP074 filled BR compounds, where a decrease in volume loss was observed at 10 pphr MRP074. Increasing volume loss was observed in BR as the concentration of CRP400 and MRP074 increased. As discussed in Chapter 5, sulphur migration was higher for CRP400 than for MRP074 due to its higher surface area. This caused a significant reduction in the crosslink density of the BR matrix, which resulted in better abrasion resistance for MRP074 filled compounds.

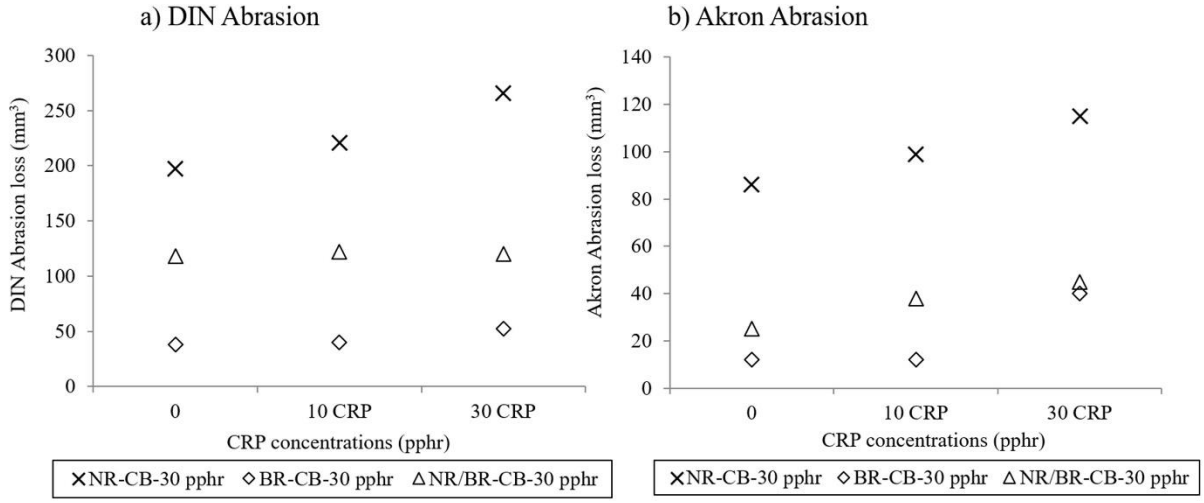

Figure 7-8 Comparison of (a) DIN and (b) Akron abrasion resistance tests of CRP400 carbon-black filled NR, BR and NR/BR compound (Note: The Y-axis full scale in (b) is less than half that in (a)).

As with the MRP074 filled compounds, DIN and Akron abrasion test gave a similar trend for NR and BR compounds and this differed for NR/BR blends containing CRP400. DIN abrasion showed a small increase in volume loss with almost negligible difference between 10 and 30 pphr concentrations relative to the control compound, while the Akron abrasion test showed a steady increase in the abrasion loss. The CRP400 compound had better abrasion resistance indicated by Akron testing compared to the MRP074 compound.

Table 7-6 Abrasion resistance of elastomers containing MRP074 or CRP400 using DIN and Akron abrasion testing.

Compound (pphr)	Abrasion volume loss (mm^3)		Compound (pphr)	Abrasion volume loss (mm^3)	
NR	DIN	Akron	BR	DIN	Akron
0	197	86	0	38	12
10-MRP074	231	103	10-MRP074	36	9
30-MRP074	266	131	30-MRP074	47	25
0	197	86	0	38	12
10 CRP400	221	99	10 CRP400	40	12
30 CRP400	266	115	30 CRP400	52	40
NR/BR (70/30)	DIN	Akron	NR/BR (70/30)	DIN	Akron
0	118	25	0	118	25
10-MRP074	122	79	10-CRP400	122	38
30-MRP074	125	105	30-CRP400	120	45

Ayyer *et al.* [151] reported that the cryogenic particles had higher surface area, due to higher content of finer particles (compared to ambient particles), at all the nominal particle sizes. Elsewhere [206], the rough textures of ambient particles exhibited higher surface area than cryogenic particles at similar particle size distributions. Different textures between MRP074 and CRP400 resulted from different methods of grinding, as described in a previous report [32]. This work uses MRP074 with a significantly smaller particle size compared to CRP400. Although the estimation of the total surface area based on a spherical smooth particle model suggested that MRP074 had greater surface area compared to an equivalent volume of CRP400, the analysis could have underestimated the irregular surfaces which were beyond the reach of 2D measurements, due to the microscopically rough surface of CRP400.

In various carbon black filled elastomers, according to Hong *et al.* [207], the rates of abrasion decreased with increasing surface area and with the developing structure of the filler. Although the CRP400 particles were much larger compared to MRP074, the irregular structure provided better interfacial adhesion between CRP400 and the CB filled rubber matrix, than the MRP074 filled compound. This also infers that the rough structure of CRP400 may have provided greater surface area than the MRP074 filled compound, which would explain the higher abrasion resistance of CRP400 filled NR and NR/BR than MRP074 filled compounds.

7.3.5 Fatigue-To-Failure Tester (FTFT)

Figure 7-9 shows the fatigue life of NR/BR CB filled compounds and the effect of MRP074 and CRP400 filler at 10 or 30 pphr concentrations, under fully relaxing conditions, a fixed strain of 100% and frequency of 5 Hz. A different fatigue machine was used to obtain the fatigue life of unfilled compound to that used for the carbon black filled compounds, thus the results of unfilled compound only allowed indicative comparison. The fatigue life of rubber compound is defined as kilocycles (kc) to failure under specified conditions. The fatigue life of unfilled NR/BR and the effect of MRP074 and CRP400 filler have been discussed in Chapter 5. A similar trend was observed for the effect of MRP074 and CRP400 on CB filled NR/BR compounds compared to the unfilled compounds. MRP074 filled NR/BR exhibited a higher fatigue life than CRP400 filler at 10 or 30 pphr concentrations.

Investigations using FTFT in comparison with DeMattia flex cracking (DMFC) were carried out by Roche *et al.* [116] on SBR compounds. They found that the FTFT test was very sensitive to poor dispersion in the rubber matrix, compared to DMFC. Dixon *et al.* [123] highlighted that FTFT tests showed significant effect of higher CB structure in finer particles than in coarser particle size for SBR compounds. The interpretation of the FTFT tests is not clear due to insufficient information since fatigue life is dependent on various factors as stated in Chapter 5.

Based on this research, the possible explanation is that the FTFT test is very sensitive towards inhomogeneities in the rubber matrix. A similar explanation, when comparing tensile and tear strength, given by Gibala *et al.* [157], could also apply. The relatively homogeneous

composition for MRP074 contained less stress raisers compared to CRP400 filled compounds. Filler particles that are larger than the typical flaw size act as stress raisers that initiate fracture which result in shorter fatigue life. Hence, any conditions such as poor dispersion could increase the agglomerate size and reduce the fatigue life. Other possible factors such as hysteresis loss [208] due to breakdown of filler-filler structure or rubber-filler interaction, SIC effect, stress-softening and heat build-up during cyclic loading could also contribute to the lower fatigue life of CRP400 filled compounds.

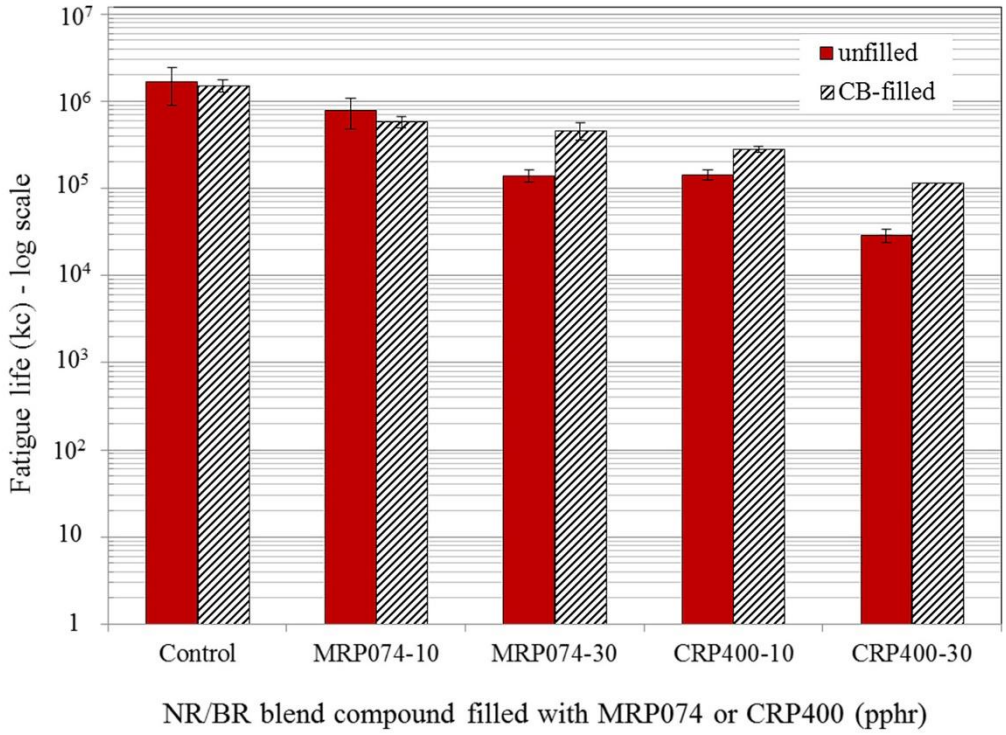

Figure 7-9 Fatigue life of NR/BR compound with 10 or 30 pphr of MRP074 and CRP400 (fully relaxing conditions, 100% strain, 5 Hz).

7.4 Summary

The reduction in tensile strength of RRP filled compounds was due to filler particles that were larger than the typical flaw size acting as stress raisers that initiated fracture, and also depended on the type of rubber matrix. The sulphur migration affected the crosslink density of MRP074 or CRP400 filled matrix and was reflected in the torque reduction and the lower apparent crosslinking density. Likewise the tear and abrasion resistance of compounds

containing MRP074 and CRP400 filled compound were lower than the control compound in NR and NR/BR blend compounds. Further optimisation of the design formulation such as cure systems modification and optimised carbon black concentrations may be possible for MRP074/CRP400 at higher concentrations with consequent enhancement in these key properties.

Crescent tear tests were used as an indication of crack propagation resistance in the rubber matrix. The effect of structure and weak interface interaction was confirmed by the lower tear strength in MRP074 filled compound, compared to CRP400 filled matrix, in both unfilled NR and NR/BR blend compounds. However, in BR, the opposite trend was observed. In these tests, the effect of hardness of the RRP and of adhesion between the filler and rubber matrix were also important. This is more clearly observed in BR compounds, than in NR, due to the lower contributing effect from the strain-induced crystallisation and higher sulphur migration. The migration caused more crosslinks in RRP and fewer crosslinks in the BR matrix. The crescent tear increased with RRP hardness indicating that there was relatively high interaction of RRP and the unfilled (no carbon black) BR matrix and is attributed to a tear deviation mechanism (the tear path is likely to proceed along the interface around the particles instead of a straight path through the particles i.e. perpendicular to the applied loading direction when a filler particle is encountered).

For the carbon black filled compounds, the weak interactions of MRP074 were not reflected in the tear strength results due to a high scatter in the data caused by the inhomogeneity and tear deviation by the carbon black filler. The carbon-black filler seemed to compensate for the weak matrix-filler interaction shown by the MRP074 filler. The CB enhanced the interaction between the CRP400 and rubber matrix. Higher sulphur migration occurred in CRP400 than in MRP074, due to its greater surface area, which increased the hardness of the filler leading to more tear deviation. This explains the higher tear strength at 30 pphr concentrations for CRP400 compared to MRP074 compounds. Kraus rubber-interaction parameters, compared to other models studied, corresponded to the crescent tear strength of RRP in unfilled and CB filled NR, BR or NR/BR compounds.

Higher volume losses for NR, and for higher concentrations of MRP074 (30 pphr) in BR, in both DIN and Akron abrasion tests were found. Despite the compensation of carbon black

filler in tear strength, the Akron test appeared to be able to characterise the possible weak interaction of MRP074 particularly in NR/BR blend matrices more effectively than in the DIN abrasion test. The DIN and Akron abrasion resistance tests give two contrary trends for the NR/BR blends, while for NR and BR, DIN and Akron test trends were similar. The CRP400 filled compound had better abrasion resistance, as indicated by Akron testing, compared to MRP074 filled NR and NR/BR blend compounds. The irregular structure of CRP400, related to its larger surface area, appears to be a more dominant factor than the particle size which contributed to better abrasion resistance than in MRP074 filled compounds. The abrasion resistance of the BR compound containing MRP074 filler however outperformed by comparison with the CRP400 filled compounds. In BR, due to higher migration of curatives, for the CRP400 compounds, a significant reduction in the crosslink density of the matrix was caused which resulted in better abrasion resistance for the MRP074 filled compound.

The superior abrasion resistance of BR compounds and carbon black concentration compensates for the abrasion loss in NR/BR blends containing 10 pphr of MRP074 and was comparable to NR compounds.

FTFT test are very sensitive towards inhomogeneities in the rubber matrices. MRP074 filled compounds are relatively ‘homogeneous’ and therefore contain minimal stress concentrations compared to CRP400 filled compounds. Filler particles that are larger than the typical flaw size acted as additional stress raisers that initiate fracture which resulted in shorter fatigue lives. Thus, significant reduction was found in the fatigue life of CRP400 by comparison with MRP074 filled NR/BR compounds at 10 or 30 pphr concentrations. The fatigue results produced different ranking at different strain/stress and frequency/strain rate levels. This showed that FTFT tests conducted at only one strain was insufficient to draw any conclusion of the overall compound performance.

Chapter 8 Fatigue crack growth and fracture morphology of RRP (Recycled Rubber Powder) filled NR/BR compound

8.1 Introduction

Previous results for tensile properties (Chapter 7) have shown that the addition of (micronised rubber particles) MRP074 may avoid significant deterioration in key mechanical properties (tensile and tear strength) compared to larger particles of (crumb rubber particles) CRP400. The interface study however, showed that the strength at the interface was relatively weak due to the microscopic smooth structure of MRP074 caused by the cryogenic method, used for its production. Reduction of tear strength of RRP filled NR [148] and NR/BR compounds (Chapter 7) were compensated by the addition of carbon black filler. Defects in the bulk materials, which may have originated from poor dispersion of fillers, ingredients such as zinc oxide, curatives or impurities during mixing or moulding, can weaken the rubber-filler interaction. Under various stress-strain conditions, micro-crack initiation, due to the inherent flaws, leads to crack propagation and eventually failure. Therefore, crack growth resistance is of great importance in determining the strength and durability of rubber products.

Quasi-static properties such as tensile strength, abrasion and tear resistance give simple and quick information which are often used for quality control of rubber compounds. However, these tests do not describe rubber performance in dynamic conditions. Wear loss in tyres or cracking in rubber mountings is usually associated with crack growth due to repeated cyclic stress. These types of failure under cyclic/repeated conditions are known as fatigue failure and occur well below the ultimate tensile strength of the material [109]. Suitable parameters for assessing material properties and their relation to lifetime performance in specific applications are required. The most practical approach is fracture mechanics where the crack growth rate is influenced by the tearing energy of the rubber material and independent of the shape of the test piece. The energy balance theory was first used in rubber tearing under static loading by Rivlin and Thomas [107] who derived their model from Griffith's criterion [209]. The tearing energy, alternatively thought of as "energy release rate", can be applied for cyclic loading [109] and is widely used as a criterion for fatigue crack growth rate in elastomers.

In many studies of recycled rubber materials using untreated or treated powder, only quasi-static mechanical properties are reported (See Chapter 3). Generally, few works have examined the fatigue properties and fracture morphology. In the fatigue life evaluations, some researchers [30,146] used DeMattia flex cracking (DMFC) for the crack growth rate measurements. Roche *et al.* [116] evaluated the effect of filler dispersion and rubber formulation on the fatigue crack growth behaviour of Styrene Butadiene Rubber (SBR). They reported that fracture mechanics based on the energy balance provides more precise information than the conventional standard fatigue methods (DMFC) or fatigue-to-failure tester (FTFT). Other authors [112,117,142] highlighted the contradictory performance of fatigue crack growth rates of rubber compounds at different tearing energies. The energy approach for the crack growth analysis could provide new information for RRP evaluation.

The fatigue fracture surface morphology, and the mechanism of fatigue crack growth for NR compounds have been comprehensively studied [84,173,210,211]. Tee *et al.* [212] showed that from 2004 up to the present, 49% of studies on fatigue of rubber focused on NR, 21% on SBR, 25% on other rubber types and only 5% on rubber blends. In this research, fatigue crack growth in NR/BR blend (70/30 compound) with MRP074 was compared to CRP400 using a fracture mechanics approach. Recycled Rubber Powder (RRP) refers to both MRP074 and CRP400 filler. The effect of either RRP at 10 pphr on the damage microstructure of NR/BR (70/30), and fatigue fracture surface morphology dependence on the fatigue crack growth (FCG) under different strain amplitudes were also studied. The fatigue crack growth performance of RRP-filled NR/BR compounds at different strain amplitudes is important as materials behave differently under different tearing energies [112].

8.2 Materials and specimens

8.2.1 NR/BR compound (70/30 ratio)

For FCG test, carbon black (CB)-filled NR/BR compounds containing either CRP400 or MRP074 at 0 or 10 pphr respectively were investigated. Rubber compounds were previously described in Chapter 7 (CB-filled compound). Single-edge notched tensile specimens (SENT), as shown in Figure 8-1, were used in the tests.

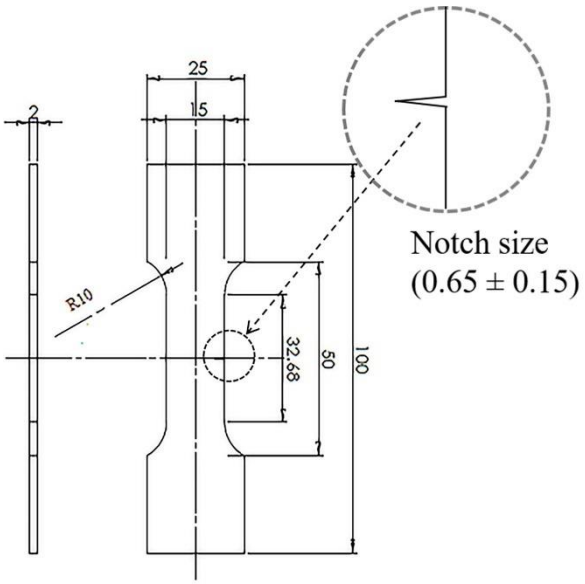

Figure 8-1 Single-edge notched tensile specimens (SENT) for fatigue crack growth test (Dimension in mm).

8.3 Experimental procedures

8.3.1 Fatigue crack growth (FCG) test

FCG tests were conducted on an Instron Electropuls 3000 with a 250 N load cell, at ambient conditions, using displacement control mode with a superimposed minimum load control. FCG tests were carried out on NR/BR carbon black filled compound (control) with 10 pphr of either MRP074 or CRP400 filler. Single-edge notch tensile (SENT) dumbbell shaped specimens had a rectangular cross-section of 15 x 2 mm thick, with 40 mm distance, between grips from the total specimen length of 100 mm. A pre-crack size of 1 mm has been commonly used by several researchers [213,214]. This pre-crack size is not appropriate for NR/BR filled carbon black since, at this length, the critical size has already been exceeded and there is no stable crack propagation, especially at higher dynamic strains. An initial crack of approximately 0.65 ± 0.15 mm was cut into the narrow edge of each rubber specimen using a sharp razor blade. The specimens were quasistatically stretched to 18 mm (~107% strain) maximum displacement to introduce a natural crack shape, prior to dynamic testing. The setup is shown in Figure 8-2. Three specimens per amplitude were then individually subjected to a sinusoidal excitation at a frequency of 5 Hz and 6, 9, 11 or 15 mm strain

amplitude which corresponds respectively to 40%, 59%, 71% or 96% dynamic strain. The equivalent average strain rate can be calculated as $\dot{\varepsilon} = 2\varepsilon t$, where $\dot{\varepsilon}$ is the equivalent strain rate, ε is the dynamic strain amplitude, and t is the time required per cycle. Thus the equivalent strain rates for 40%, 59%, 71% and 96% dynamic strain were 0.16 s^{-1}, 0.24 s^{-1}, 0.28 s^{-1}, 0.38 s^{-1} respectively. Due to cyclic stress-relaxation, and to avoid buckling of the rubber material, the targeted minimum load was fixed at 1 N with constant peak displacement using tri-modal control of the Instron WaveMatrix™ test software. The specimens were illuminated from both the front and the back with light emitting diodes (LED) to achieve a greater image contrast. The tests were periodically stopped at a specific number of cycles and the image of the crack was captured by a digital camera (computar®, MLH-10X). The post-treatment measurement of the crack length was conducted using ImageJ software [152] with semi-automatic ABSnake plugins [215]. The half crack contour lengths were measured at a specific number of cycles. For the first 3000-5000 cycles at each dynamic strain amplitudes, the measurements are not used for the *dc/dN*, due to the unstable crack growth at the beginning of the FCG test. The crack growth rate (*dc/dN*) from the stable crack growth region was obtained within the linear slope of the crack length, *c* plotted against the number of elapsed fatigue cycles.

Figure 8-2 Set-up of cyclic crack growth test determination.

8.3.2 Measurement of crack contour length, *c*

The observation of crack depth using a travelling microscope is time-consuming and technology has progressed to use automatic measurement techniques [212,216,217]. In this work, the observation of crack contour length was simplified using automatic frame grabbing by a camera (controlled by the analogue output of an Electropuls Fatigue machine) using Instron WaveMatrix™ Dynamic Testing Software and Dantec image capturing software. The resolution of the images was (1624 x 1202 pixels). Initial images using a ruler for calibration were taken prior to the analysis. The SENT specimen was slightly strained before the calibration images were captured. The crack contour length was measured using the captured images at different cycles-n and ImageJ software with semi-automatic ABSnake plugins. Sequential images from the initial crack length to failure were converted into stacks (layers of images) before the analysis was carried out. The half crack contour length was assigned as a region of interest (ROI) as shown in Figure 8-3.

The ROI was marked manually on the first and second image. Using the ROI propagate option of the software, the previous marker can be used for the subsequent images and adjusted according to the crack length. After completing the crack contour length ROI on all images, the software can automatically calculate the length using pixels and results can be exported to an excel file. The pixel length was then converted to ‘mm’ using an earlier calibration measurement.

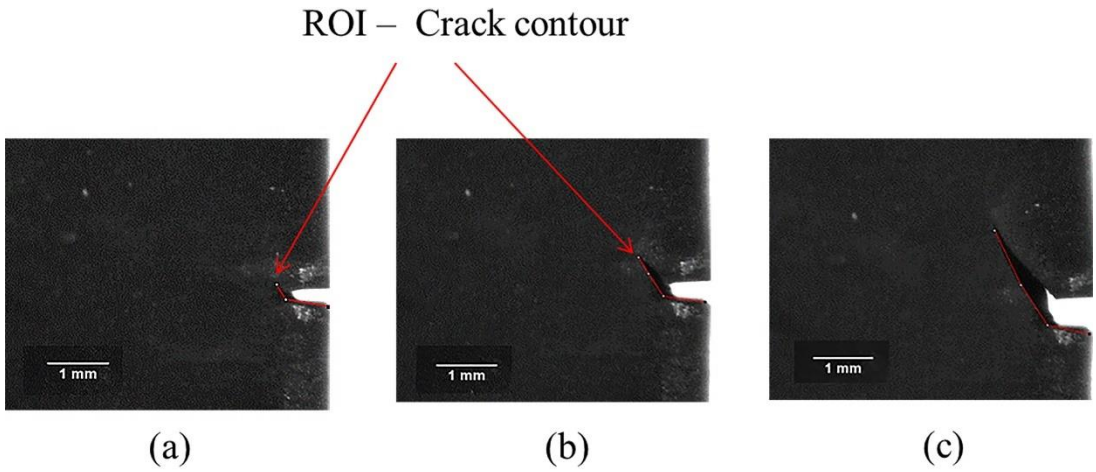

Figure 8-3 Crack contour length taken from the NR/BR control sample.

8.3.3 Determination of crack growth rate (*dc/dN*)

The measurement of the cyclic crack growth, using SENT specimen, depends on the cut length, thus a scatter in the results is unavoidable. The crack contour length displayed always represents the half of the measured contour length for carbon black filled rubber. Figure 8-4 shows the effect of notch length on the half crack contour length of NR/BR (70/30) blend at 15 mm strain amplitude (96% dynamic strain or average strain rate of 0.38 s^{-1}). Thus, a consistent crack length should be made where possible. Once the crack initiation occurs, the crack will grow at the stable propagation rate, followed by an unstable propagation region, and finally rapid propagation until rupture (Figure 8-4).

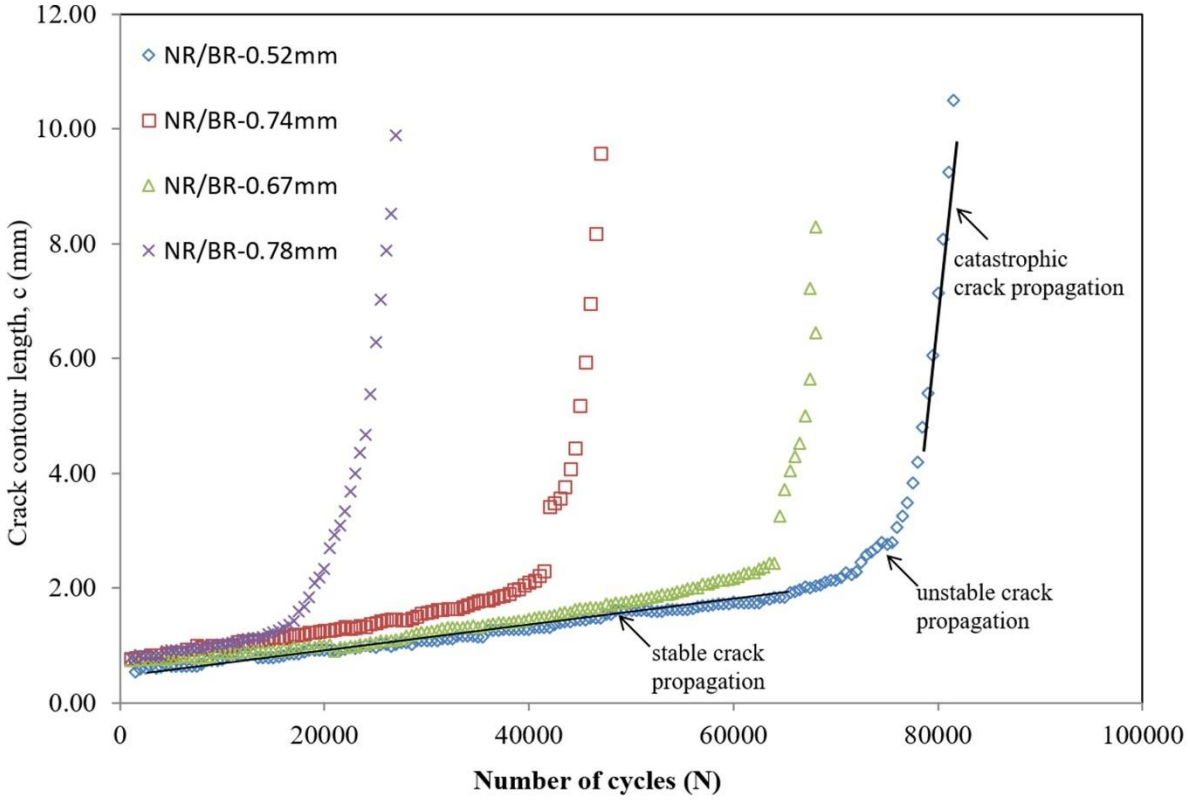

Figure 8-4 Crack contour length dependence on the initial notch length for NR/BR blend compounds at amplitude of 15 mm (96% dynamic strain or average strain rate of 0.38 s^{-1}).

Measurements of crack contour, *c* in section 8.3.2 were plotted against fatigue cycles, n, and crack growth rates (*dc/dN*) from the stable crack growth region were obtained from the linear

slope of *c* plotted against the number of elapsed fatigue cycles. Figure 8-5 shows the stable crack growth region of selected NR/BR samples and a linear fit of the crack contour length versus number of elapsed fatigue cycles.

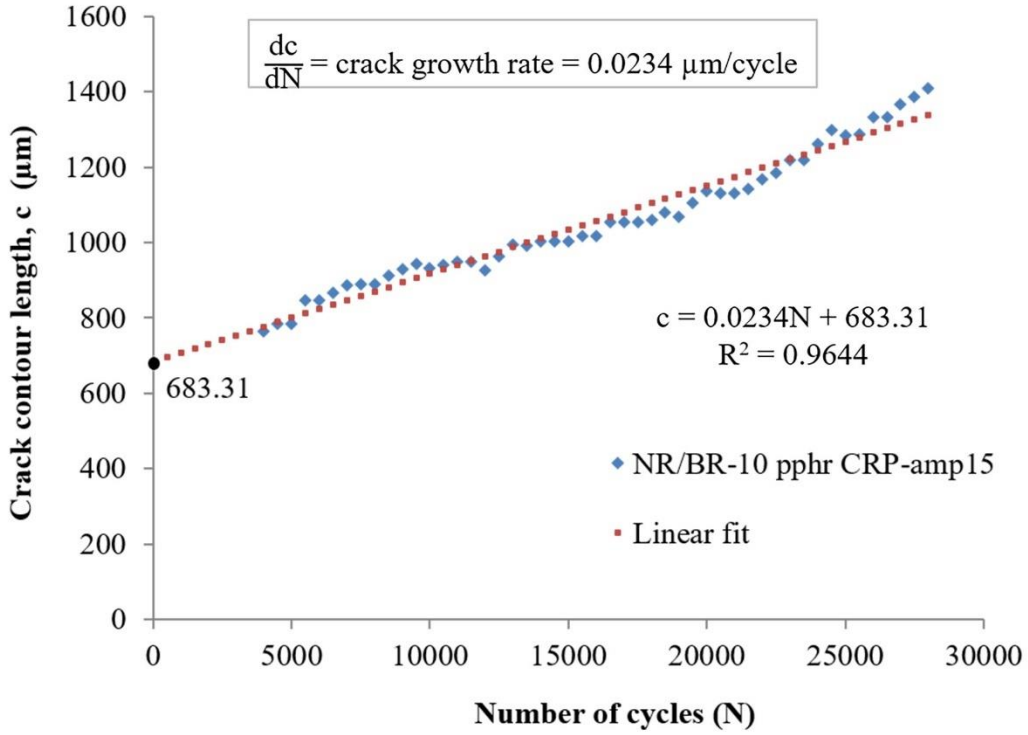

Figure 8-5 Crack contour length from stable crack propagation region and a linear fit to obtain the fatigue crack growth rate.

8.3.4 Fatigue crack growth – Tearing energy relation

Fracture behaviour is characterised by the relationship between crack growth rate, *dc/dN*, and tearing energy, T, which is recognised as a fundamental property of crack propagation in elastomers [108]. Tearing energy or strain energy release rate for SENT specimens under cyclic loading can be calculated using Equations 8-1 and 8-2 [109]:

$$T = 2kWc \qquad \text{(Eq. 8-1)}$$

$$k = \frac{\pi}{\sqrt{\lambda}} \qquad \text{(Eq. 8-2)}$$

$$\therefore T = \frac{2\pi}{\sqrt{\lambda}} W c \qquad \text{(Eq. 8-3)}$$

W is the strain energy density or stored energy at a distance from the crack (i.e. integral area under the retraction curve/cyclic unloading of the load-displacement curves (Figure 8-6) was divided by the volume of the specimen between the grips), *c* is the crack length, λ is the extension ratio and *k* is a constant, depending on the strain (Eq. 8-2).

Energy at the minimum strain level (W_{min}) was taken into account for *W* since the test was conducted under non-relaxing conditions (minimum load > 0, F_{min} = 1 N). *W* was measured using an un-notched specimen which was cycled under the same conditions as in the FCG test for each of the strain amplitudes tested.

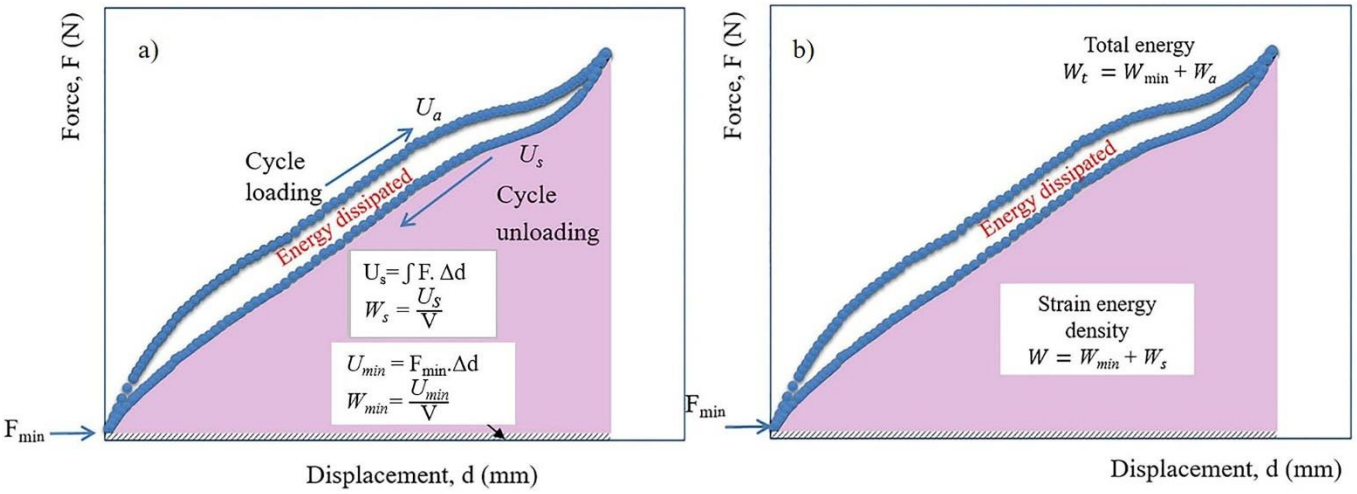

Figure 8-6 Loading and unloading cycle, where a) the total work done under loading cycle, U_a is equal to the sum of work done under unloading cycle, U_s and dissipated energy (energy lost) in force displacement curve b) Total energy and strain energy density determination.

Using the power-law relation (Eq. 3-3), (Eq. 8-3), the cyclic crack growth rate with tearing energy, T can be expressed as:

$$\frac{dc}{dN} = B\left(\frac{2\pi}{\sqrt{\lambda}}\, W\, c\right)^{F} \qquad \text{(Eq. 8-4)}$$

where B and F are material constants i.e. dependent on the type of rubber used. F is also known to depend on the material hysteresis and can be affected by both strain level and strain rate.

8.3.5 Hysteresis loss

The hysteresis loss/energy dissipated is defined as the difference between total work done obtained from integral area under the cyclic loading, (U_a) and cyclic unloading/retraction, (U_s) in a load *vs* displacement curve as shown in Figure 8-6(a). Total energy density, W_t, and strain energy density, W, were then determined using corresponding W_a and W_s i.e. work of deformation for a unit volume for cyclic loading and retraction curve plus the energy at the minimum strain level (W_{min}) (Figure 8-6(b)). Measurement of the hysteresis loss from the energy densities (total and strain energy) was then acquired using the same SENT specimen during the FCG test. All the energies measurements were obtained from a representative stress-strain hysteresis loop at the number of fatigue cycles closest to 50% of the service life for each specimen. Percentage of relative hysteresis H_r [%] = (W_t-W/W_t) x 100 and absolute hysteresis density, H_{ab}= (W_t-W) were determined using an average of the 3 measurements. The averages and the standard deviations of the total and strain energy density, and hysteresis density as absolute value and percentage of relative hysteresis of the total energy for three rubber compounds, for each level of strain amplitudes tested, were reported.

8.3.6 SEM morphology of fracture surfaces from FCG test

Fracture surface specimens were cut about 5 mm from the fracture surface and all specimens were gold coated to minimise electrical charging prior to analysis. The morphology of each crack fracture surface after FCG test was viewed using a JEOL JSM-6610 LV Scanning Electron Microscope (SEM), operating at 15 kV accelerating voltage.

8.4 Results and Discussion

8.4.1 Hysteresis loss under cyclic loading

The breakup and reformation of the filler network, within the rubber chain, during cyclic deformation involves energy dissipation, often suggested as being part of the mechanical hysteresis [102]. Reduction in crack growth rates in carbon black filled compounds than in unfilled rubber compound is partially due to increases in hysteresis and other factors such as CB reinforcement and strain induced crystallisation [99,101]. Here, unfilled rubber refers to a rubber compound with no added filler (CB, RRP or both). The fatigue life improvement is strongly dependent on the type and optimal concentration of the CB [80]. Hence, hysteresis is an important characteristic when evaluating fatigue properties in terms of deformation and crack growth behaviour [218]. The relationship of fatigue properties, critical J-Integral-values and hysteresis was studied by Kim and Jeong [219] for different types of carbon black in NR compounds. They used a similar tearing energy equation (Eq.3-1) to calculate the critical J-Integral-value for onset of a crack growth at the initiation of a pre-cracked dumbbell specimen observed using a digital motion camera. The fatigue life of the compound increases with the increase in the critical J-Integral-value and hysteresis. Carbon black (N650) filled NR containing larger aggregates (carbon black primary particles bonded together) has lower hysteresis compared to a compound with smaller particle size, and a higher surface area CB (N330) compounds. The hysteresis is also dependent on the temperature [220], pre-conditioning, frequency/strain rate and dynamic strain [91] thus the result can vary according to these factors due to the viscoelastic properties of the rubber. Other reinforcement factors such as strain induced crystallisation, strength anisotropy, crack deviation and crack tip blunting have also been reported [195,196] in fracture evaluation research.

The tri-modal function of the Instron WaveMatrix™ dynamic testing software allows a minimum load (in this case, set at 1 N) to be applied with a displacement controlled strain superimposed, taking account of the permanent set of the samples throughout the cyclic loading. Measurement of the hysteresis loss from the energy densities (total and strain energy) was then obtained using the same SENT specimen during the FCG test. Comparison between tearing energy calculated from W of notched and un-notched specimens at different dynamic strains amplitude or average strain rates for NR/BR blend control compound is demonstrated

in Figure 8-7. Virtually no differences in tearing energy were observed between un-notched and notched specimen. Hence, both relative and absolute hysteresis loss measurements, using strain energy density from the single-edge notched tensile (SENT) specimens, during the FCG test were used instead of a separate test using un-notched specimen. In addition, strain energy density dependent on testing conditions where the total energy densities decreased as the cycles accumulated, due to cyclic stress softening of the material [93]. Therefore, the use of both SENT specimen and energy measurement, obtained at the number of fatigue cycles closest to 50% of its service life, were expected to be more representative of hysteresis data compared to quasi-static tensile testing.

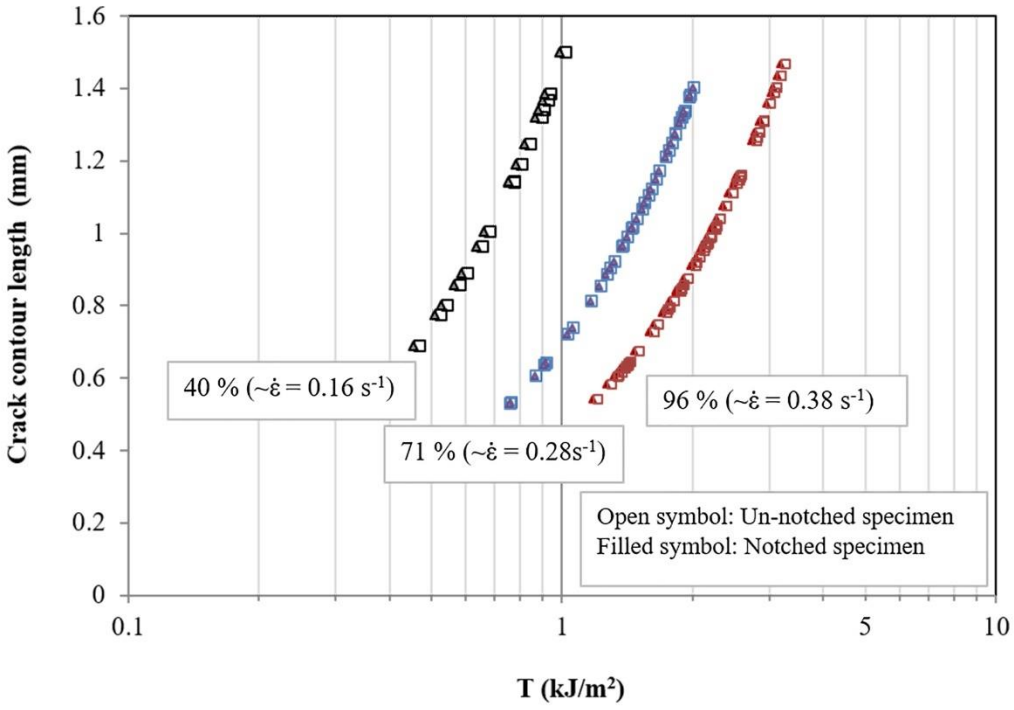

Figure 8-7 Comparison of stable propagation crack length *vs* tearing energy, where *W* was obtained from notched and un-notched specimens at different dynamic strains for NR/BR control compounds.

8.4.2 FCG of CRP400 and MRP074 NR/BR filled compounds

The effect of both MRP074 and CRP400 at 10 pphr concentrations on FCG characteristics of NR/BR blend compound is shown in Figure 8-8. Scatter in fatigue crack growth results is commonly observed due to fatigue being sensitive to various parameters (microstructure of

material/heterogeneity/different size of flaws, specimen fabrication, environmental conditions, etc.) which are difficult to control [221]. In addition, FCG rates using crack contour length shows more scatter compared to crack depth, but is more closely related to the increases in the crack surfaces and tearing energy [141]. Although the experimental data was scattered considerably, the R^2 of the fitting according Eq. 8-4 appeared adequate (> 80%), therefore it is reasonable to predict the dependent variables. A value of R^2 as low as 70% has been reported [216] for unfilled and filled NR due to the nature of the crack in rubber matrices. Both dynamic strain energy density [83,214] and hysteresis loss [222] parameters can be used to evaluate the crack growth resistance of rubber compounds. The FCG results related to these parameters are discussed in the following.

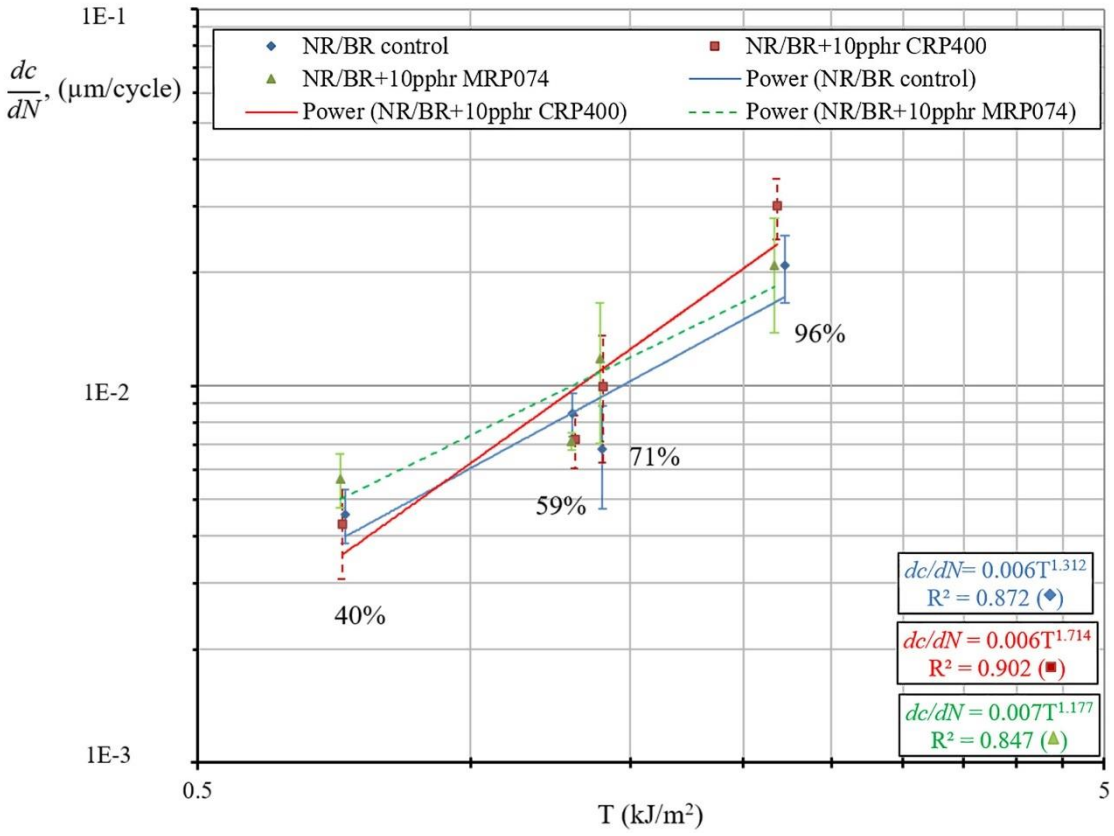

Figure 8-8 Fatigue crack growth comparison with control NR/BR compounds and different RRP at 10 pphr for 40%, 59%, 71% and 96% dynamic strain amplitudes.

At the lower tearing energy (40 % dynamic strain or average strain rate of 0.16 s^{-1}), the crack growth rate of CRP400 filled (10pphr) NR/BR compound did not appear to be significantly lower than the control compound due to the relatively high scatter in the results. However,

both CRP400 and NR/BR compounds exhibited lower crack growth than MRP074 filled compounds. Figure 8-9 and Table 8-1 show the total and strain energy densities for control, MRP074 and CRP400 filled NR/BR compounds under various strains. By examining the plots, considering the data scattering, there are virtually no differences between energy values for all compounds but Table 8-1 shows that at 40% or 59% dynamic strain amplitudes, CRP400 compounds exhibited lower strain energy densities compared to the control and MRP074 filled compounds within accepted experimental error. The lower strain energy density corresponded to a reduced energy available for crack propagation which would partially explain the lower crack growth of CRP400 filled NR/BR compounds at 40 or 59% dynamic strain.

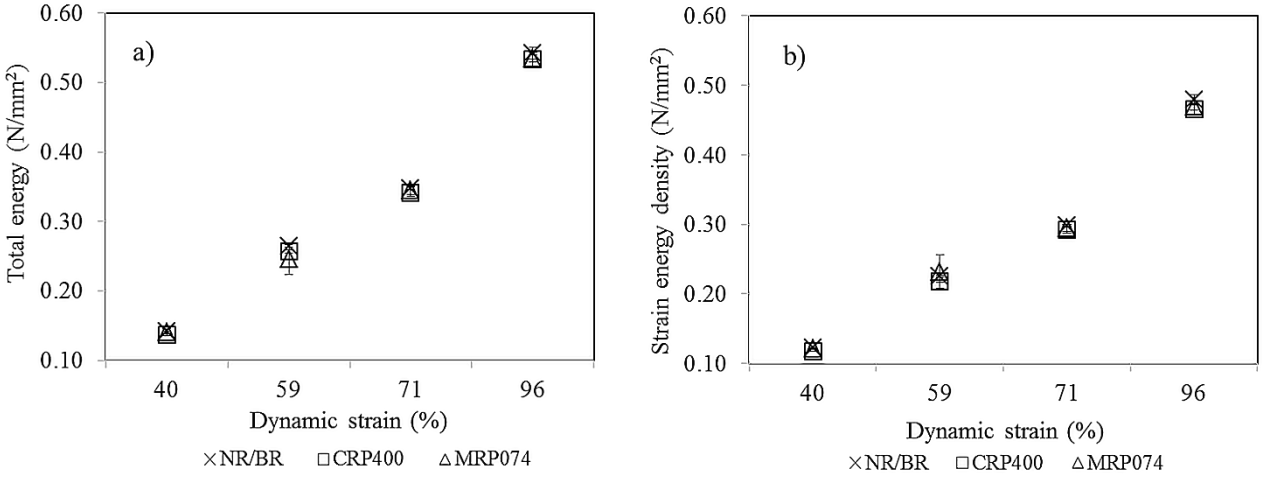

Figure 8-9 Total and strain energy density of NR/BR blend compounds (control and CRP400 and MRP074 filled compounds) at each level of dynamic strains tested.

The addition of filler has been shown to increase hysteresis [223] in a rubber matrix, with the extent depending upon the type and amount of filler. Higher hysteresis could reduce the energy available for crack propagation [80] and is important for rubber reinforcement. This indicates that fracture resistance of rubber is not only dependent on the strain energy density (crack driving force) but also on the energy dissipated around the crack tip [88].

Figure 8-10 shows the absolute and relative hysteresis loss for NR/BR and RRP filled compounds at each of the dynamic strain levels tested. The increase in dynamic strain increased the absolute hysteresis of the rubber network (Figure 8-10 (a)). At 40 % dynamic

strain, there was no significant influence on the absolute value of hysteresis loss of NR/BR control or both RRP filled NR/BR compounds. However, the relative hysteresis loss showed different trends. The possible explanation can be attributed to multiple energy dissipative mechanisms [80] that occurred around the crack tip. As expected, both RRP filled compounds had increased relative hysteresis loss due to the additional filler in the NR/BR compounds (Figure 8-10 (a)). The NR/BR control compound had higher relative crosslink density than the NR/BR phase of the RRP compounds as migration of curatives from the virgin compound to the RRP causing reduction in the crosslinking in both CRP400 and MRP074 filled matrix. The higher crosslinking could have reduced the ability of the rubber to dissipate energy through hysteresis.

Table 8-1 Total and strain energy density of NR/BR blend compounds (control and CRP400 and MRP074 filled compounds) from SENT specimens at each level of dynamic strains tested.

Dynamic Strain	NR/BR	NR/BR-CRP400	NR/BR-MRP074
	Total energy density, W_t (N/mm^2)		
40%	0.142 ± 0.003	0.137 ± 0.001	0.141 ± 0.001
59%	0.265 ± 0.002	0.257 ± 0.002	0.246 ± 0.022
71%	0.348 ± 0.002	0.341 ± 0.005	0.345 ± 0.006
96%	0.542 ± 0.009	0.534 ± 0.010	0.535 ± 0.005
	Strain energy density, W (N/mm^2)		
40%	0.123 ± 0.002	0.118 ± 0.0002	0.121 ± 0.0011
59%	0.225 ± 0.001	0.218 ± 0.001	0.232 ± 0.024
71%	0.298 ± 0.002	0.292 ± 0.005	0.295 ± 0.005
96%	0.479 ± 0.008	0.465 ± 0.008	0.469 ± 0.005

The CRP400 compound showed higher relative hysteresis loss compared to the MRP074 compound. The possible reasons include to the following factors:

- irregular surface of CRP400 compared to MRP074 as discussed in Chapter 7. The irregular surface of CRP400 filled compounds provided a stronger interface between the particles and the rubber matrix,
- some contribution of hysteresis within the CRP400 fillers and more contact with CB which created more internal friction contributing to higher relative hysteresis.

Combined effects of additional hysteresis for CRP400 compound could have reduced the crack growth rate.

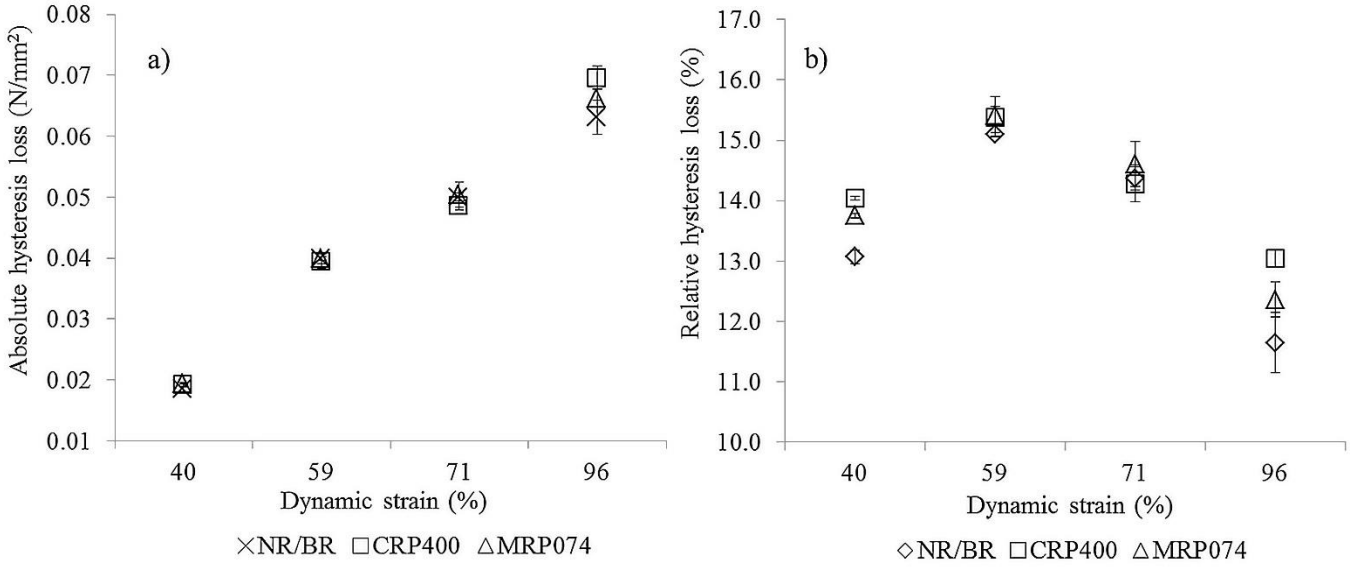

Figure 8-10 a) Absolute hysteresis loss and b) relative hysteresis loss of NR/BR blends with 10 pphr of CRP400 and MRP074 obtained from SENT specimens at each level of dynamic strains tested.

At 71% dynamic strain or equivalent strain rate of 0.28 s^{-1} (Figure 8-8), the FCG of NR/BR is lower compared to CRP400 and MRP074 filled compounds. A reduction in properties for RRP filled NR/BR compared to the NR/BR control compound have been reported in Chapter 7. The weak bonding between the matrix and RRP could have led to a weak interface for failure initiation. The migration of sulphur, apart from the weak bonding, has also been suggested as a cause for this reduction in properties in the mechanical and FCG tests. RRP might increase the stress concentration and reduced strength at the crack tip consequently resulting in the reduction of the SIC effect. Other factors affecting SIC can be the rubber

composition and experimental conditions such as various strain rates and temperatures [98]. The addition of carbon black shifts the onset of crystallisation to lower strains than in unfilled NR compounds [98,224]. There is an optimal crosslinking density or maximum strain for a maximum crystallinity in the rubber network. The morphology, chain mobility, volume or size of the crystallites could also influence the crack propagation.

An increase in absolute hysteresis loss due to introduction of RRP is expected, when part of the strain energy density is dissipated as heat, while the other part acts as a crack/fracture driving force [225]. Also, the relative hysteresis loss passed through a maximum then decreased with increasing dynamic strain amplitudes. At 50 or 71% dynamic strain, there was no significant difference between MRP074, CRP400 and control NR/BR values. The overlapping trends of the relative hysteresis loss for all compounds is not yet fully understood but could be attributed to the multiple dissipative processes occurring at the crack tip [80]. Additional dissipation may be attributed to the SIC effect. The SIC effect is believed to be higher at 71% compared to 59% dynamic strain since there is a large scatter and deviation of actual crack growth rates data from values predicted by the power law equation. SIC increased with increasing strain amplitude and increased the anisotropy of the material [84]. At higher strain during cyclic loading, strain induced crystallisation of NR will create an area at the crack tip which will prevent the crack growth in that direction. Higher SIC at the crack tip enhances crack tip blunting and branching [102]. The crack bifurcation into two or more smaller shared crack tips reduces the total tearing energy available for each individual crack [85,226].

At 96% dynamic strain, a lower relative hysteresis loss was observed for all tested samples compared to lower dynamic strains (e.g. 40%). During this stage, the molecular chain (filler-filler bonds and weak rubber-filler bonds) [91] was broken down and the chain mobility increased. As cycles continued, less energy was required for the breakdown of filler-filler and rubber-filler networks leading to reduced energy dissipation compared with lower dynamic strains. Another possible reason is that the relative hysteresis was dependent on the degree of crystallinity during cyclic loading and unloading [227]. The reduction of the SIC at 96% dynamic strain reduced the relative hysteresis loss (Figure 8-10 (b)).

At higher tearing energy levels (96 % dynamic strain), the crack growth rates changed to be ranked CRP400>MRP074>control NR/BR compound. There could be a competition between SIC and the crack growth. Higher crack growth rate reduced both the threshold tearing energy and the ability to crystallise [228] at the crack tip. By increasing the amplitude, it is suggested that the ultimate properties of the CRP400 decreased faster than in MRP074 which increased the crack growth rates of CRP400. This supports the strength dependence of the crack growth rate on the energy release rate at higher strain [228]. In addition, weak bonding between the RRP filler and rubber matrix created more microvoid sites which initiated fatigue failure. These microvoids are believed [46] to increase in size with increasing dynamic strain amplitudes and contribute to higher crack growth rate of RRP filled matrix.

CRP400 filled NR/BR showed significant absolute hysteresis loss at 96% dynamic strain. Similarly, CRP400 filled compounds exhibited higher relative hysteresis loss compared to MRP074 or control filled NR/BR. Higher hysteresis dissipates heat and increases the neighbouring network temperature which can accelerate molecular chain rupture and suppress the SIC effect [229] at the crack tip. A lower relative hysteresis loss for NR/BR or with MRP074 filler probably reflects a better transmission of the stress from matrix to the neighbouring particles. Further investigation is needed to confirm this assumption.

8.4.3 Evolution of fatigue crack growth

The pathway of crack growth from SENT specimen under cyclic loading for carbon-black filled NR, BR and NR/BR compounds has been documented by Hamed *et al.* [196]. Crack path coordinates were replicated using the photograph of the crack growth commencing from the cut edge under cyclic stress mode. The authors highlighted the ‘up-down alternating’ cracking pattern and crack branching occurrences. There is also a tendency for crack propagation into longitudinal paths parallel to the loading direction. This direction causes a stop or delay in the crack growth propagation in the rubber compound. They [196] pointed out that there is a critical pre-crack size that controls the propagation path. Several researchers [85,111] proposed that one crack with higher energy release will propagate or become part of larger cracks, while the smaller cracks with lower energy release will stop growing.

Lee and Moet [230] qualitatively related damage microstructure surfaces to three stages of FCG curves from the stable propagation region until fracture at 20% strain for NR/BR blend compounds (50/50). From the fracture topography, they concluded that microcracks and crack tip roughening were involved in the damage and crack resistance mechanisms, respectively, prior to mechanical failure. In this study, the fatigue fracture morphology relation with the FCG was applied as well and extended under different amplitudes. Many published articles focused on the NR fracture surfaces; however, there has been less research on the mechanism of crack growth in NR/BR blends. Hence, the damage microstructure of NR/BR control and the effect of RRP (MRP074 or CRP400), focused at 10 pphr concentrations, was examined.

There are many factors [228] which affect the direction of the crack path including: strain crystallisation for crystallising elastomer, anisotropy of the material strength [84,111], strain amplitude, inhomogenities and ratio of the energy release rates [111]. It is beyond the scope of this thesis to consider all these factors due to limited time and facilities constraints. The crack pathway reported is based on observation throughout the experiments and discussions included present research findings and published work of others. The schematic development of the crack growth is shown in Figure 8-11 (NB: terminology for stages differ from that at page 47 (Chapter 3). The pathway of cracking of rubber is complex: The schematic picture is rarely the universal pathway for a rubber compound. In the stage I-stable crack propagation zone, the evolution of the crack growth was initiated from a crack tip and begins with a thin crack along the surface (sharp cracks) appear from the crack tip. Similar observation was reported by Hainsworth [231].

The sharp thin layer of crack bifurcates either inclining up or down the applied loading. As the strain cycles continued, no crack growth occurred on the initial crack tip, while stable crack propagation was observed from the growth of the sharp thin crack line. The local stress concentration was higher at the crack tip [117]. It was observed for all samples (control, MRP074 and CRP400 filled compounds) that the uniform crack depth through the thickness did not occur if the main molecular chains at the crack tip did not fracture. The chain-breaking process ahead of the crack tip is governed by the bond strengths and the alignment or crosslink of the molecular chains [228]. Since NR is dominant in NR/BR blends, due to the effect of SIC, the formation of crystal zones ahead of the crack tip blunted the crack tip.

Crack tip blunting often occurs in a highly deformed material [226] during cyclic loading. This is the characteristic of strain-induced crystallisation NR [118]. BR on the other hand has lower ability to SIC than NR in uniaxial strained conditions [169] and did not show evidence of SIC at 23°C [170]. The SIC effect appeared to enhance the molecular chain around the vicinity of the crack tip. The evidence of SIC, from the X-ray diffraction investigations carried out by several authors during static deformation, have been reviewed by Huneau [98].

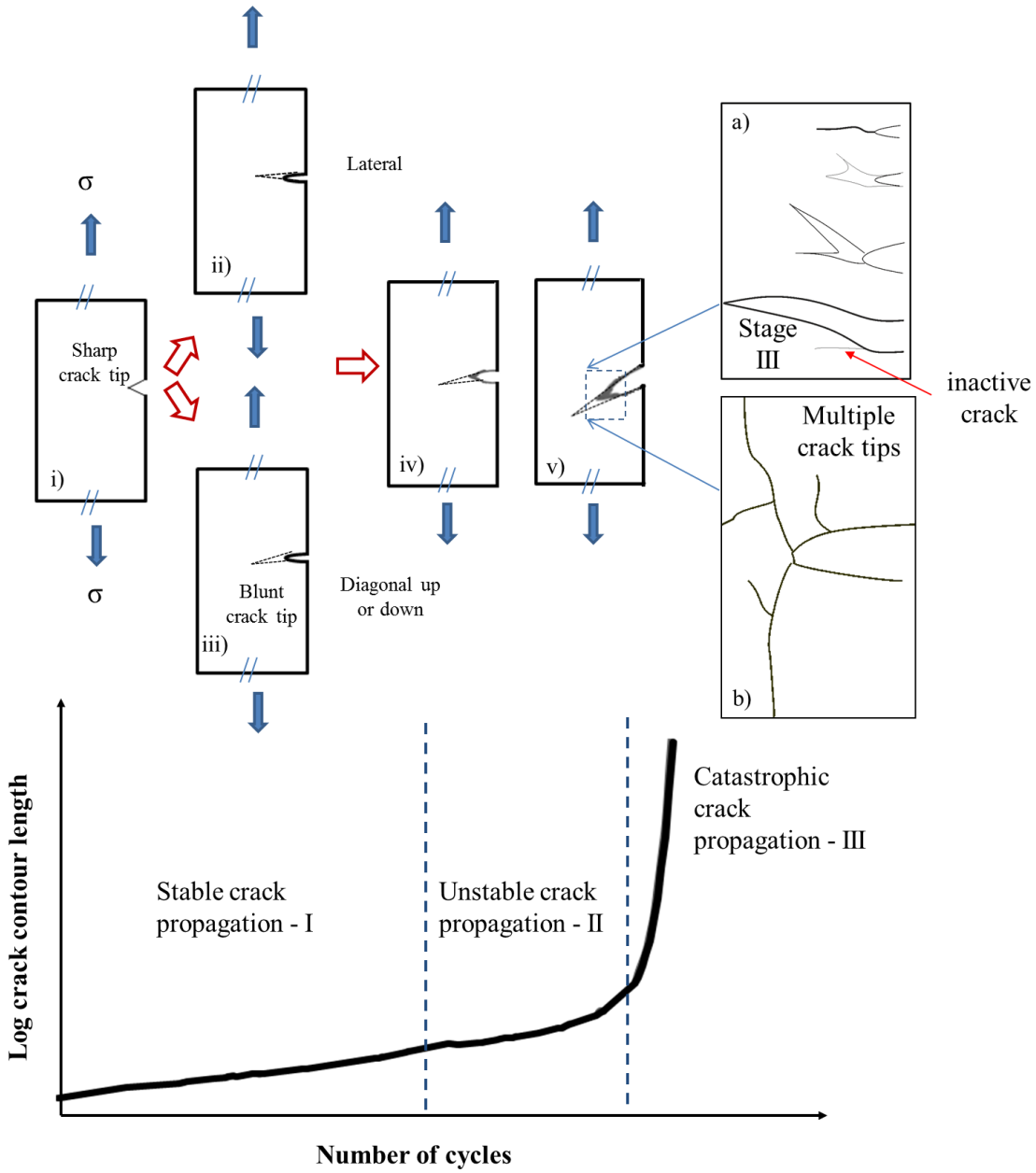

Figure 8-11 Schematic representation of crack growth in RRP filled NR/BR for a carbon black filled compound (30 pphr concentrations) under fatigue crack growth evolution (side view of the crack tip).

Depending on the characteristic of the flaws, temperature, strain amplitude or strength anisotropy under cyclic loading conditions, the transformation from stable crack propagation to the unstable region will occur once the ligaments or main molecular chains were fractured. The main crack advances through the thickness of the sample and links to the original thin crack along the surface which propagates with fatigue cycles (Figure 8-11 (v)). During the transition, the main crack will propagate depending on the ratio of the energy release rate at the front crack tip and also the previously mentioned factors. When fracture resistance at the crack tip is higher (often in the case of a shorter crack tip), the direction of crack growth will be diverted towards the weak plane [196] of the applied loading.

The influence of RRP on the crack path depends on the interfacial adhesion between the rubber filler matrix and hardness of the RRP [156]. The crack propagation path could be through the particles or along the matrix-particle interface. Kumar [46] has shown that due to the weak bonding between the rubber-recycled particles, the crack propagation path is likely to proceed along the interface around the particles than through the particles. Although the crack propagation path was not studied, due to the stronger interface between CRP400 and the rubber matrix compound, it required a longer crack path to debond at the matrix-filler interface compared to MRP074 compound. This results in higher relative hysteresis found in CRP400 NR/BR compounds compared to MRP074 and control NR/BR filled compounds.

As discussed in the FCG section, the higher hysteresis loss at higher strain reduced the ability of SIC for CRP400 filled compounds and resulted in less strength anisotropy compared to MRP074 and NR/BR control compound. Hence the crack growth was more towards the perpendicular direction to the applied loading (forward cracking). As for MRP074 and the control compound, an inclined path of the crack propagation was observed due to the higher anisotropy at the crack tip caused by the SIC effect [84,111]. The schematic of the effect of SIC on the crack propagation path is shown in Figure 8-12.

Cracks in an inclined direction will continue to propagate at a slower rate in the transition region (unstable crack propagation) compared with the forward direction which partly explains the performance of crack growth of CRP400 filled NR/BR at higher strains. During stage II, crack bifurcation or branching normally occurred. In unfilled NR/BR for RRP filled compound, less bifurcation is seen compared to the CB filled compound. The second crack

tip appeared which will have delayed the first main crack tip (Figure 8-11 (a)). At this stage, the second crack tip would have taken control (possible higher energy release rate) and propagated faster than the main crack tip. When both of the crack tips appear to have similar crack length, competition between both of the crack tips occurred. The dominant crack will continue to progress while the less dominant will remain inactive. As the crack progresses, more crack bifurcation was observed but only one crack tip was dominant to proceed with the crack growth and propagate across the specimen until fracture (stage III).

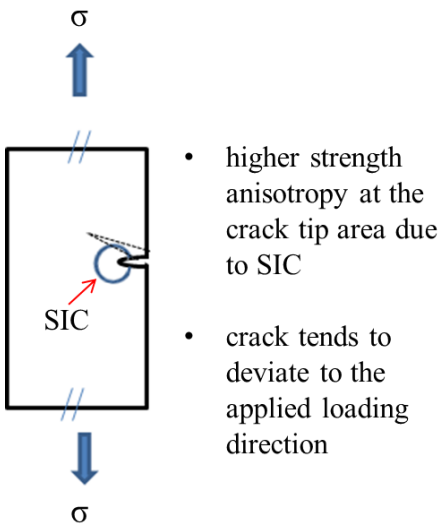

Figure 8-12 Effect of SIC on the strength anisotropy at a crack tip.

The complexity arises in carbon black filled rubbers with more secondary or tertiary cracks from the main crack or when another new crack tip would emerge. Therefore multiple crack tips would grow (Figure 8-11 (b)) and deviate when they coincide with filler obstacles and a strong interface. More multiple crack tips are believed to appear with higher carbon black concentration and stronger interfaces. It is also suggested that the multiple crack tips are due to extensive strain-induced anisotropy particularly at the tip of the crack [226,232]. In this study, the crack bifurcation was greater in 30 pphr concentrations of CRP400 compared to MR074 or control compounds as shown in Figure 8-13. The performance of FCG for 30 pphr concentrations of either RRP (MRP074 and CRP400) in unfilled and CB filled NR/BR compounds however was not studied due to time constraints.

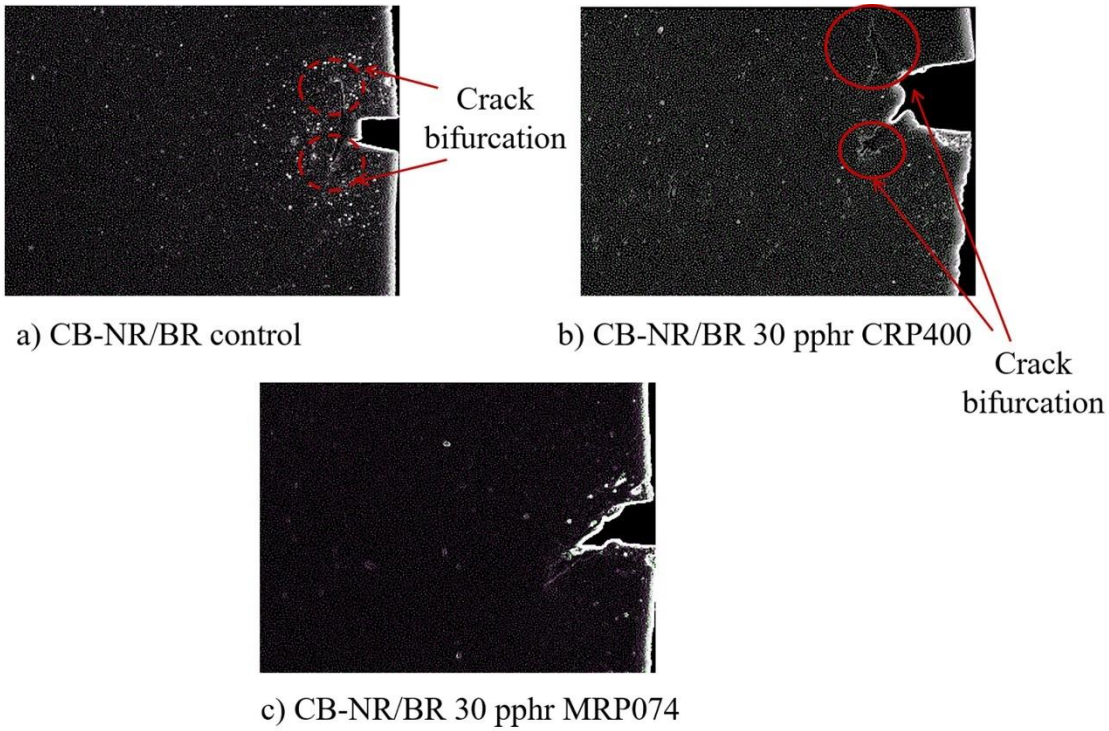

Figure 8-13 Crack bifurcation in a) NR/BR control blend compound b) 30 pphr concentration of CRP400 or c) 30 pphr MRP074 (fatigue cycles about 100,000 cycles under 71% dynamic strain).

8.4.4 Morphology of fracture surfaces from FCG tests at different tearing energies

Evaluation of the fracture surface at microscopic scale after fatigue failure is important for identification of the crack growth regime, location of crack initiation and possible flaws information. Crack growth mechanisms and microscopic examination of fracture surfaces from fatigue tests have been reported for NR [84,173,174,225,226]. The sample formulations, method of testing, and focused interest were different in each case. Nevertheless, some observations and similar fracture mechanisms occurring on the fracture morphology of NR were also seen to take place in NR/BR (70/30) blend compound due to the dominant factor of NR and its unique properties of SIC. Le Cam *et al.* [210] described the microscopic rough 'twisted knots' at the stable crack propagation zone as 'wrenching' due to stretched ligaments which break and shrink. For unfilled NR, at low and higher tearing energy, Weng *et al.* [225] used the term 'surface peeling and buckling' and 'ligaments breakage' respectively to describe the cracking morphology. The microstructure of the fatigue damage changes at

different strain amplitudes [84] and is also dependent on factors such as velocity of crack growth [84,175], strain rates, strain crystallisation [174] (polymer type), environmental factors (oxygen, ozone, ultraviolet-light, etc.) and mechanical (stretching, triaxial stresses) [135] conditions.

The crack roughness is a characteristic of the crack growth rate [226]. The higher ratio of macroscopic rough to smooth fracture surface indicates stronger resistance to crack growth. Quantitative measurement of roughness is not currently a simple task due to variation of fracture depths and irregular cracking structures. Hence, in this thesis, qualitative observation was made at different tearing energies to understand the relation of roughness and crack resistance mechanism in NR/BR blends and the effect of CRP400 and MRP074.

In an earlier study (Chapter 5) on morphology of fracture samples from FTFT, it was shown that the two distinct features (rough and macroscopically smooth textures) were present in NR or NR/BR blend compounds. A difference in this study is that the proportion of 'rough surfaces' largely dominates the surface failure of NR/BR but is less dominant in NR compounds. This section offers some important insights into crack propagation at the crack tip up to failure where from the FTFT the location of the crack initiation is unknown.

8.4.4.1 Lower tearing energy (FCG test)

At lower dynamic strain amplitudes (40% or $\dot{\varepsilon}$~0.16 s^{-1}) or tearing energy, the crack fracture morphology during the FCG tests showed different crack propagation regions: (a) stable crack propagation (b) unstable crack propagation and (c) catastrophic propagation zone (Figure 8-14). In tests, the 'V' shape near to the crack tip featured a shallow valley which consisted of a striation of overlapping microscopic rough 'twisted knots'. This 'V' shape reflected the inclined direction of the crack path and 'A' in Figure 8-14 corresponds to the crack tip area where the main fracture of chains/ligaments took place.

A higher magnification of the fracture morphology, under lower tearing energy is depicted in Figure 8-15. Beurrot *et al.* [174] attributed the fracture "leaves" shape to the short deviated cracks developed from the main crack path or known as 'crack branching phenomena', during fatigue crack propagation, for carbon black filled NR. The microscopically rough

structure reflects the breaking and retraction of the ligaments [173,231]. Under constant strain amplitude, depending on the threshold energy of the rubber, the repeated deformation process probably contributed to the 'build up/overlapping' layered structure when the cycles continued. This could explain why the striation morphology ('zig-zag' striation or 'up and down' pattern cracks proposed by Flamm *et al.* [84] and Hamed *et al.* [196]) was not apparent at lower tearing energy. This 'twisted knots' layered structure contributed to the microscopic roughness at the crack tip. The microstructure corresponded to the stable crack propagation of the FCG testing. Between these layers, a distinct cracking line was observed which probably indicated breaking of some of the molecular chains. Weng *et al.* [225] proposed coalescence of microvoids to form crazes for unfilled NR at lower tearing energy. This partially explains the cracking line. In this study, two types of microscopic roughness are proposed. In the first type, at lower tearing energy, microscopic roughness was attributed to the layered structure 'twisted knots' before the molecular chains/ligaments ruptured at the crack tip. The second type of microscopic roughness is attributed to the crack branching or bifurcation after the rupture of molecular/ligaments at the crack tip. As crack lengths increased, the crack bifurcation or branching became more obvious with a wide gap of tearing (highlighted with dotted line) as shown in Figure 8-14.

Once the dynamic catastrophic tearing energy had been exceeded, for CB filled, catastrophic failure was delayed compared to unfilled rubber compounds. The presence of carbon black filler provides additional attachment sites for the network broken ligaments/chains [102]. In the unstable crack propagation (II), the crack growth was much faster and crack lines appeared to be much broader and rougher on a macroscopic scale.

Before final fracture (F), transition from microscopically rough to smooth surface was observed. The 'fracture leaves' structure can still be observed before the final fracture. There is also a small area of striation morphology which probably indicates relatively higher crack growth rates before the final fracture. This type of microstructure is more obvious at higher tearing energies [173,175].

8.4.4.2 Higher tearing energy (FCG test)

Figure 8-16i and ii shows the SEM images of fracture samples for NR/BR blend compounds after fatigue crack growth with stable crack propagation (I), the transition region (unstable) (II), and the catastrophic region (III) under a strain amplitude of 15 mm (96% dynamic strain). At higher tearing energies, crack growth and ligament break-up are much faster than at lower amplitudes. Thus, shortly after the ligaments break-up (area of 'V' shape), the roughening crack tip is reduced resulting in much broader fracture leaves. This corresponds to a competition between higher crack growth rate and the effect of SIC as discussed earlier.

Increase in strength anisotropy due to the SIC effect at higher dynamic strain influenced the crack growth which caused a tendency to deviate or bifurcation/branching [228]. Crack diversion or bifurcation was observed and increased with the number of cycles. Deeper cracking lines behind the fracture 'leaves' were visible compared to the preceding crack (Figure 8-16i (b) compared to (a)). Crack diversion, highlighted by the red dotted line, was observed at stage II and before the lamellar striation (Figure 8-16ii(c)). Microcracks/voids are more obvious at higher strain amplitudes and thus are in agreement with Flamm *et al.* [84].

In the catastrophic region (Figure 8-16ii (c) and (d)), there is an area with considerable striation morphology and highly elongated lamellar features before the final fractures were observed. Several areas of striation patches were also visible. The increasing tearing energy appears to have increased the crack growth rate and the striation sizes. The distance 'd' between two striations increases from approximately 20-40 μm to 50-60 μm as approaching to the failure region (Figure 8-16ii (d)) which follow a similar trend on striation morphologies as reported by Ruellan *et al.* [211]. This type of fracture morphology has also been observed in NR under severe loading by others [84,173]. The characterisation of 'striation morphology' are still unclear but a full discussion of these characteristics is beyond the scope of this study.

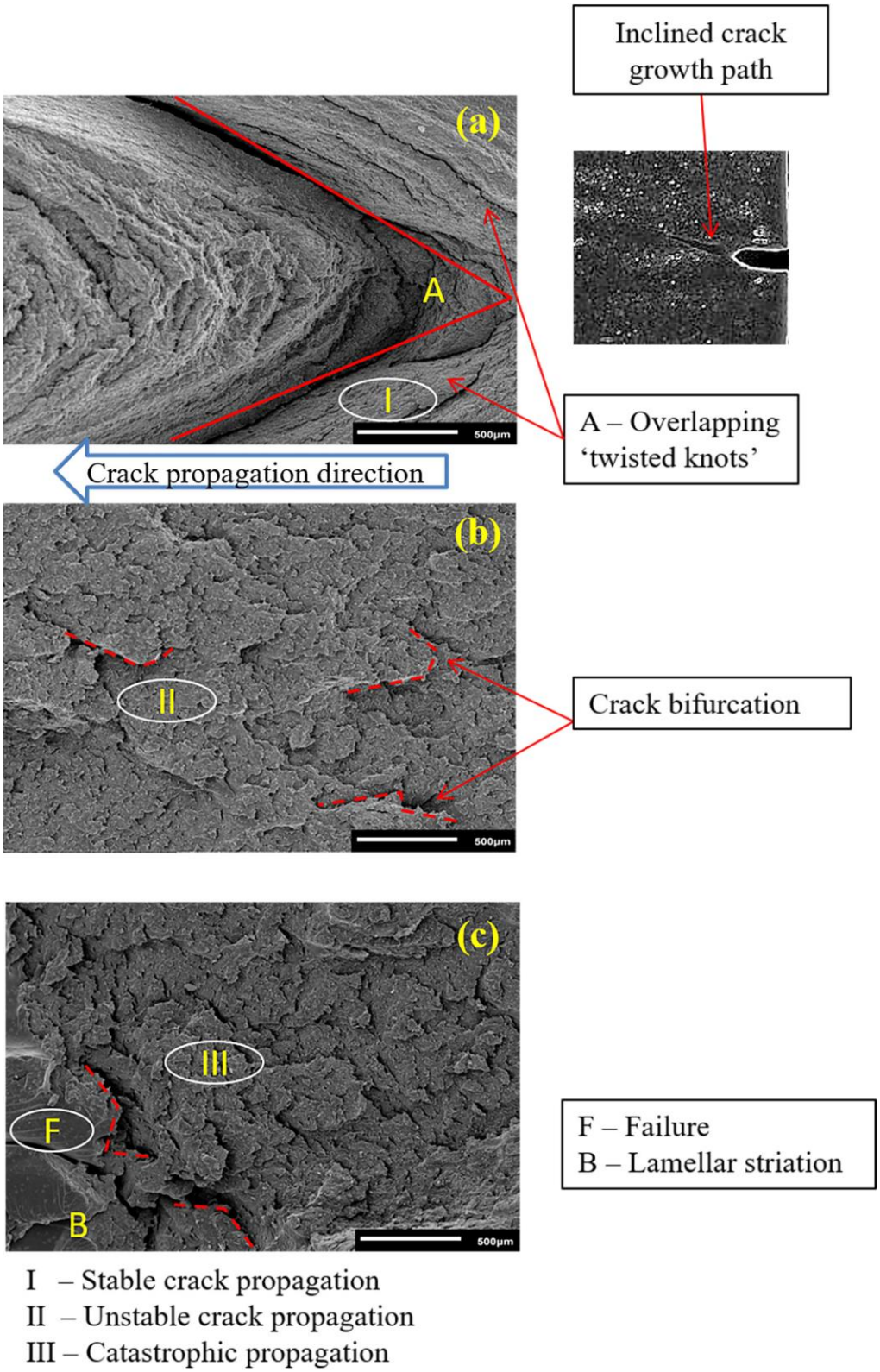

Figure 8-14 Fracture morphology at 6 mm (40% dynamic strain) strain amplitude for NR/BR blend compounds showing different crack propagation regions (a) stable crack propagation (b) unstable crack propagation and (c) catastrophic propagation zone.

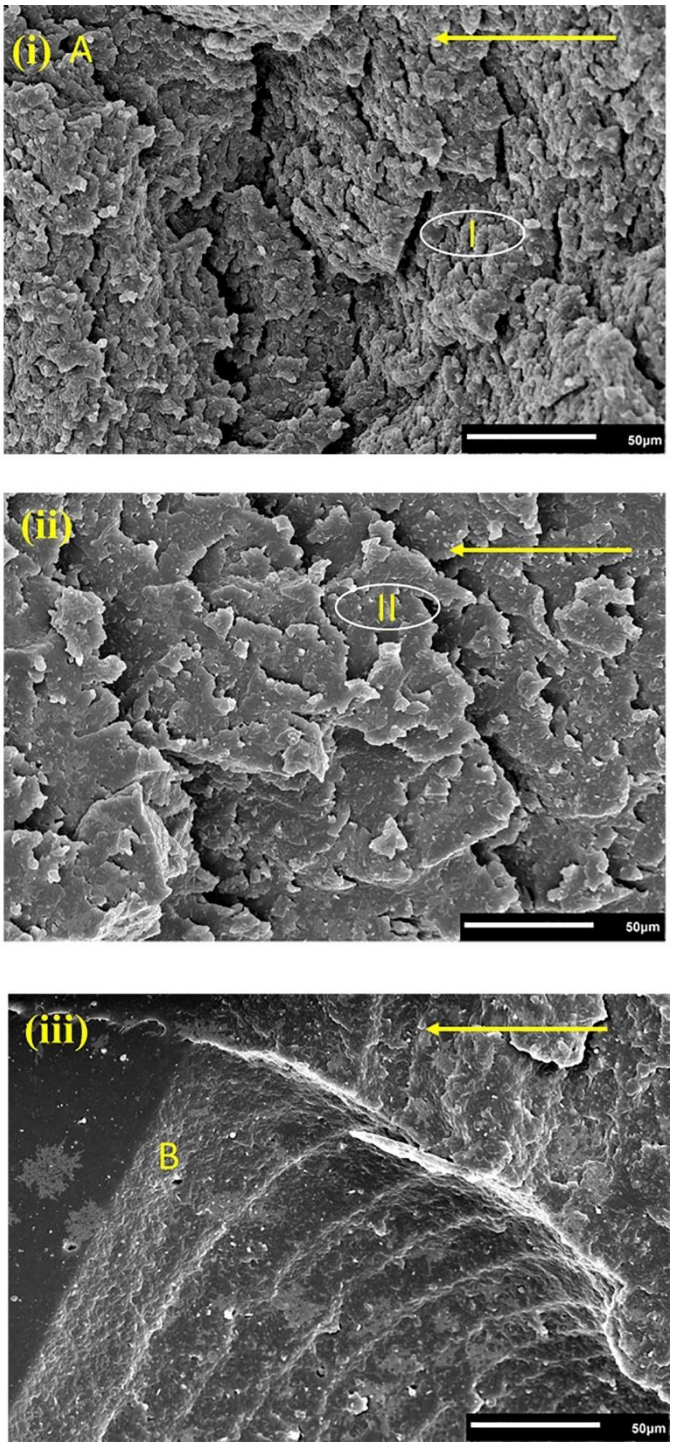

Figure 8-15 A higher magnification for Figure 8-14 (i) Stable crack propagation zone (A) (ii) unstable crack propagation iii) striations before final fracture (B) (A and B located in Figure 8-14 (a) and (c)) Horizontal arrow indicates the crack propagation direction.

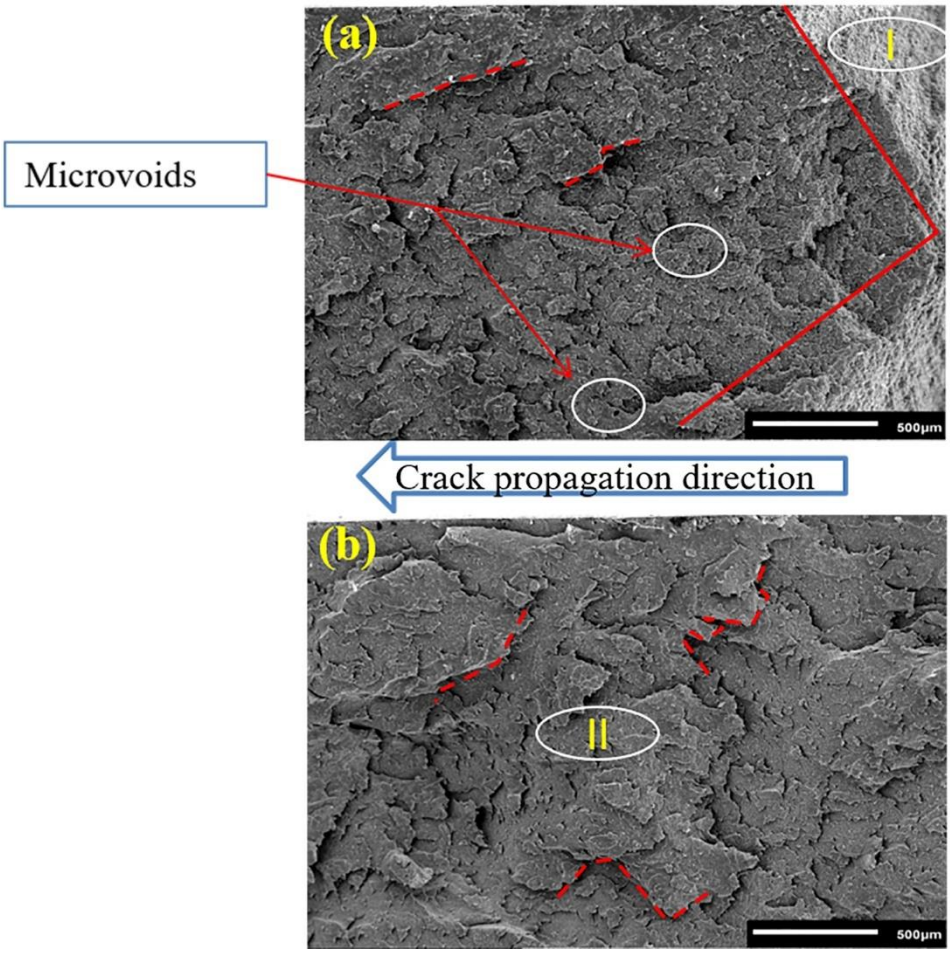

Figure 8-16i Fracture morphology at 15 mm (96% dynamic strain) strain amplitude for NR/BR blend compounds showing different crack propagation regions (a) stable crack propagation (b) transition.

8.4.4.3 CRP400 and MRP074 filled NR/BR compounds

It is recognised [102, 226] that the inclusion of particulate fillers, such as carbon black, promotes tear deviation and crack bifurcation and thus increases fracture surface roughness in comparison to gum/unfilled rubber compound. Figures 8-17 and 8-18 show the effect of CRP400 and MRP074 at 10 pphr concentration on the fracture morphology of fatigue crack growth for NR/BR blend compounds at 6 mm strain amplitude (40% strain). The addition of RRP increases the roughness of the fracture surface relative to that of the CB filled NR/BR compound without RRP filler, which is in apparent contrast to Figure 8-14.

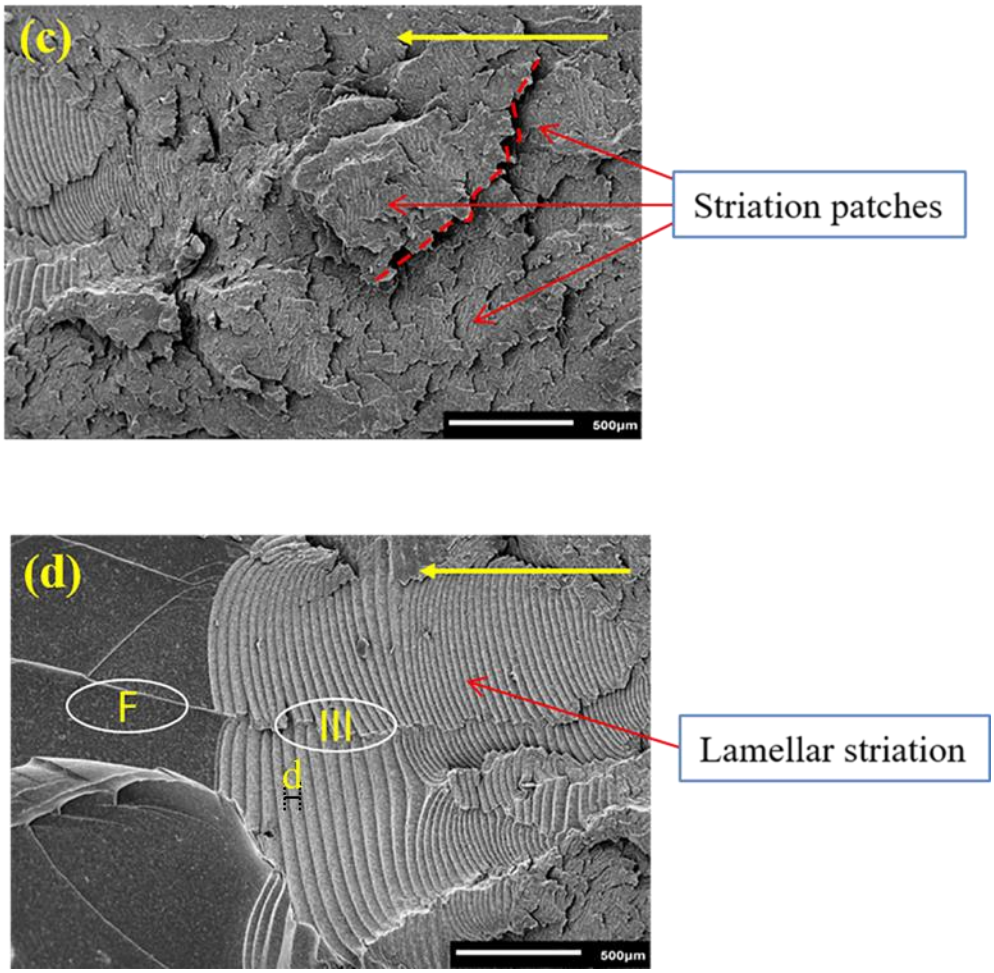

Figure 8-16ii Fracture morphology at 15 mm (96% dynamic strain) strain amplitude for NR/BR blend compounds showing different crack propagation regions (c) and (d) catastrophic propagation zone.

In the early discussion, CRP400 filled compound has lower crack growth rates at a lower tearing energy. From a microscopic viewpoint, more rough fracture surfaces were observed with CRP400-filled compound compared to the control and MRP074-filled compound. The microscopic rougher surfaces corresponded to more crack bifurcation in agreement with the study by Asare [85]. The crack bifurcation and diversion were reflected on the fracture surfaces as an uneven rough 'undulating' structure. More 'undulating' structure and greater cracking depth is observed for CRP400 than MRP074 filled compounds. The creation of rough crack surfaces/additional surface area around the irregular particles of CRP400 (Figure 6-5) in contrast to MRP074 (Figure 6-4), would require additional energy resulting in slower

crack growth rates, and the longer crack path contributed to higher relative hysteresis as discussed in section 8.4.2.

More microvoids are visible for both RRP fillers (Figure 8-19) than in the control NR/BR compound (Figure 8-14). The embedded CRP400 particles and layers around the CRP400 particles, compared to clear "voids" for MRP074, support the previous assumption of strong bonding between the particles and rubber matrices, and longer crack paths than for MRP074 filler.

The fracture surfaces at a higher strain amplitude (96% dynamic strain) for CRP400 and MRP074 compounds are shown in Figures 8-20 and 8-21 respectively. There is no obvious 'V' shape at the crack tip fracture surfaces which corresponds to the forward crack pathway. The crack growth was much faster as indicated by broader 'fracture leaves', in contrast to Figures 8-17 (a) and 8-18 (a), after the molecular chains at the crack tip were fractured. As stated earlier, weak bonding between the RRP filler and rubber matrix likely creates more microvoid sites and increase in size with increasing dynamic strain amplitudes [84] for RRP (MRP074 and CRP400) filled compound. This could have increased the stress concentration and hence reduced strength at the crack tip reflecting indistinct 'V' shape. Before final fracture, the striation morphology observed for the control compound was also visible in RRP filled compounds.

The striation morphology patterns were distorted and some were detached. The detachment and distortion were substantial in CRP400 filled compounds. This is probably due to extensive crack bifurcation and diversion around the CRP400 particles. Severe crack bifurcation was expected with the larger particle size of CRP400 and stronger interface compared to MRP074. When crack bifurcation occurs, one crack exhibits higher energy release rate and will advance or become part of a larger crack. Cracks which have the lower energy release rate will stop growing [85,111]. This will leave several crack lines as their "footprint" in the fracture morphology. Fracture images of crack bifurcation before final fracture corresponding to several crack lines behind the fracture 'leaves' can be seen in Figure 8-22 which confirmed the previous explanation.

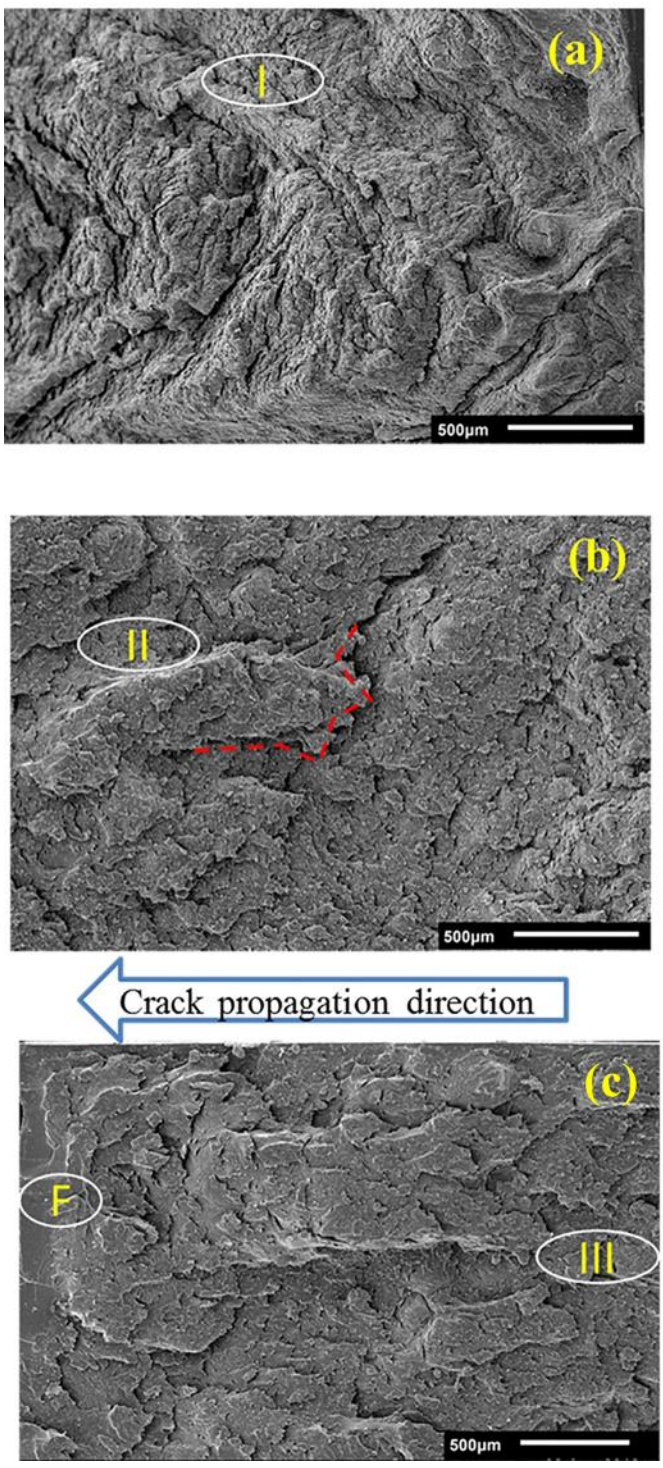

Figure 8-17 Fracture morphology at 6 mm strain amplitude (40% strain) for CRP400 filled-NR/BR blend compound showing different crack propagation regions (a) stable crack propagation (b) transition and (c) catastrophic propagation zone.

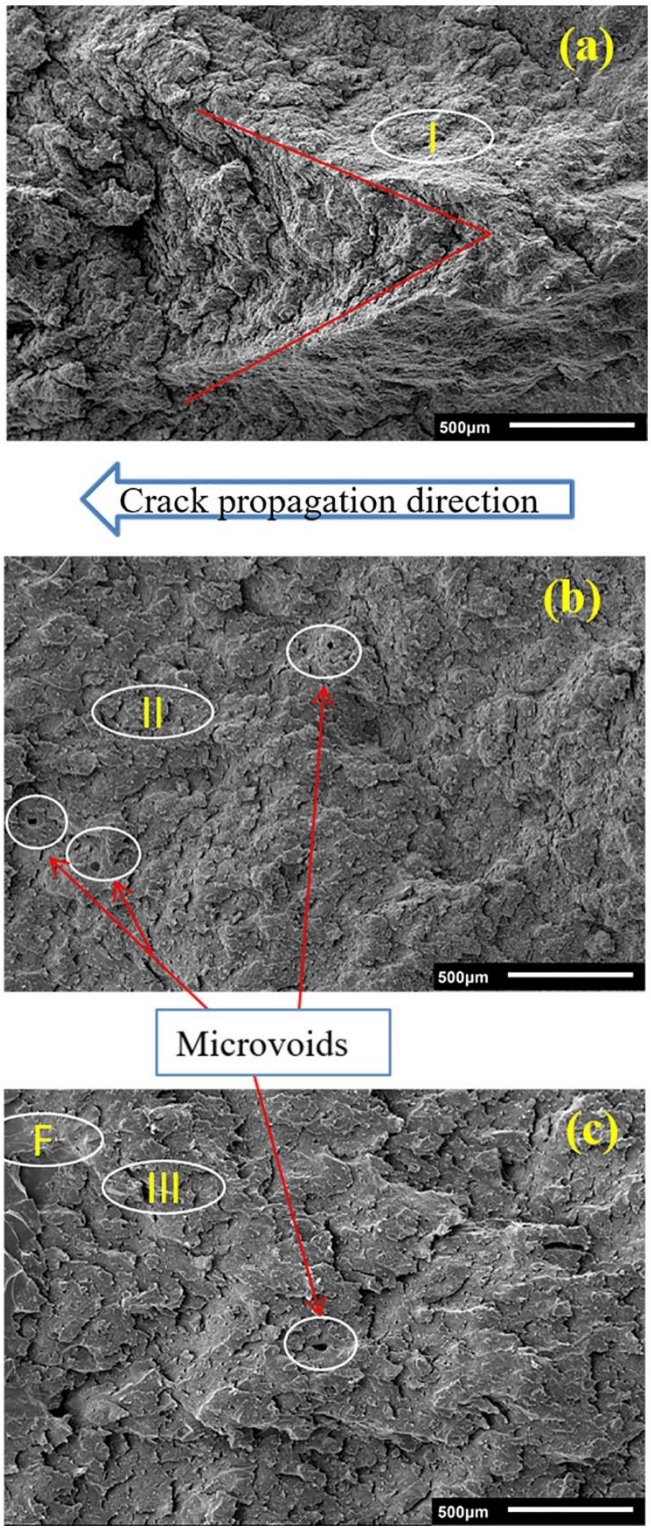

Figure 8-18 Fracture morphology at 6 mm (40% strain) strain amplitude for an MRP074 filled-NR/BR blend compound showing different crack propagation regions (a) stable crack propagation (b) transition and (c) catastrophic propagation zone.

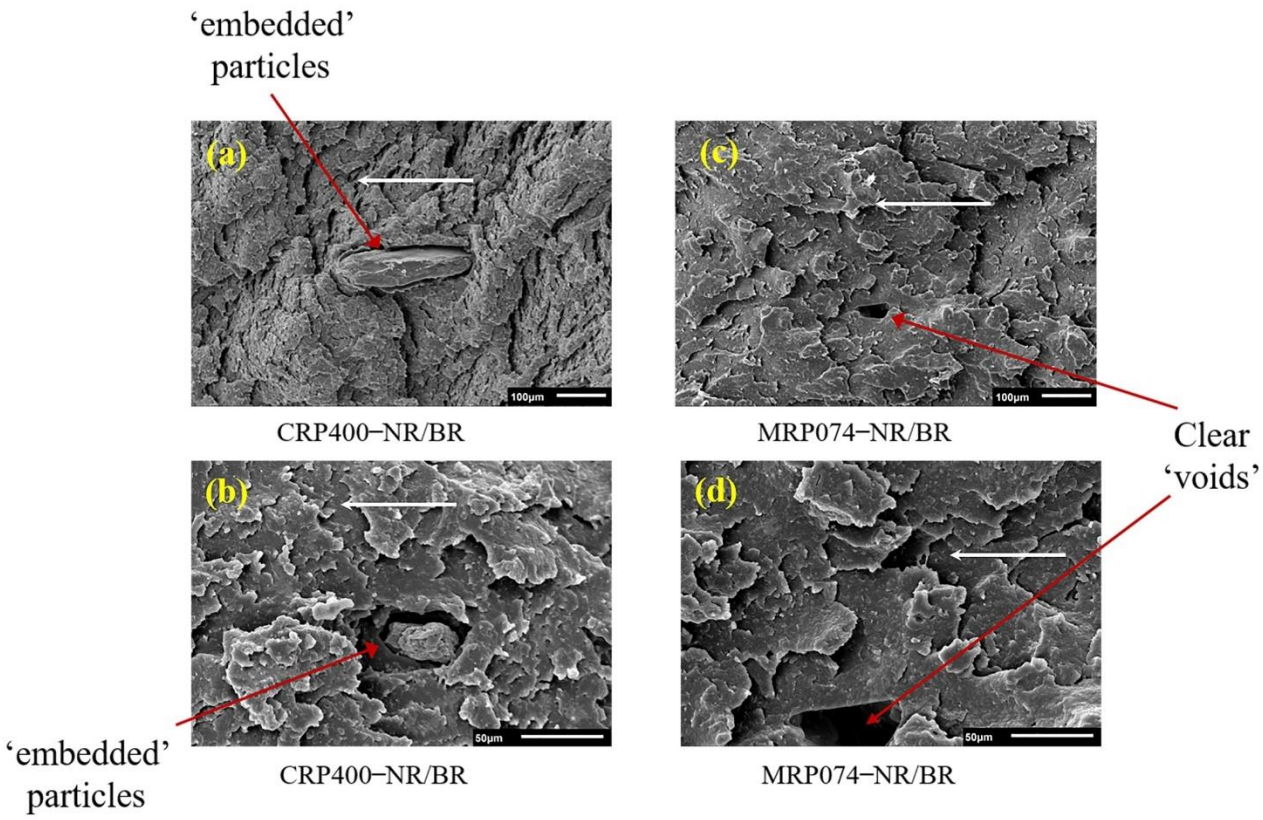

Figure 8-19 Microvoids in (a), (b) CRP400–NR/BR and (c), (d) MRP074–NR/BR compounds at 40% strain amplitude for different magnifications (arrow indicates crack propagation direction).

The schematic diagram on Figure 8-23 shows the fracture surface of an NR/BR compound and the effect of 30 pphr concentration of MRP074 and CRP400 after FCG testing at 71% strain amplitude before final fracture. Similarly, this is not a generalised microstructure for fatigue fracture of RRP filled compounds given the dependency on tearing energies, filler concentration and flaw size. The microstructure was microscopically rougher with the addition of CRP400 than MRP074 and the control filled compound. This is due to more bifurcation and branching occurring with the CRP400 filled compound. More depth of cracking was observed which reflects an 'undulating' structure.

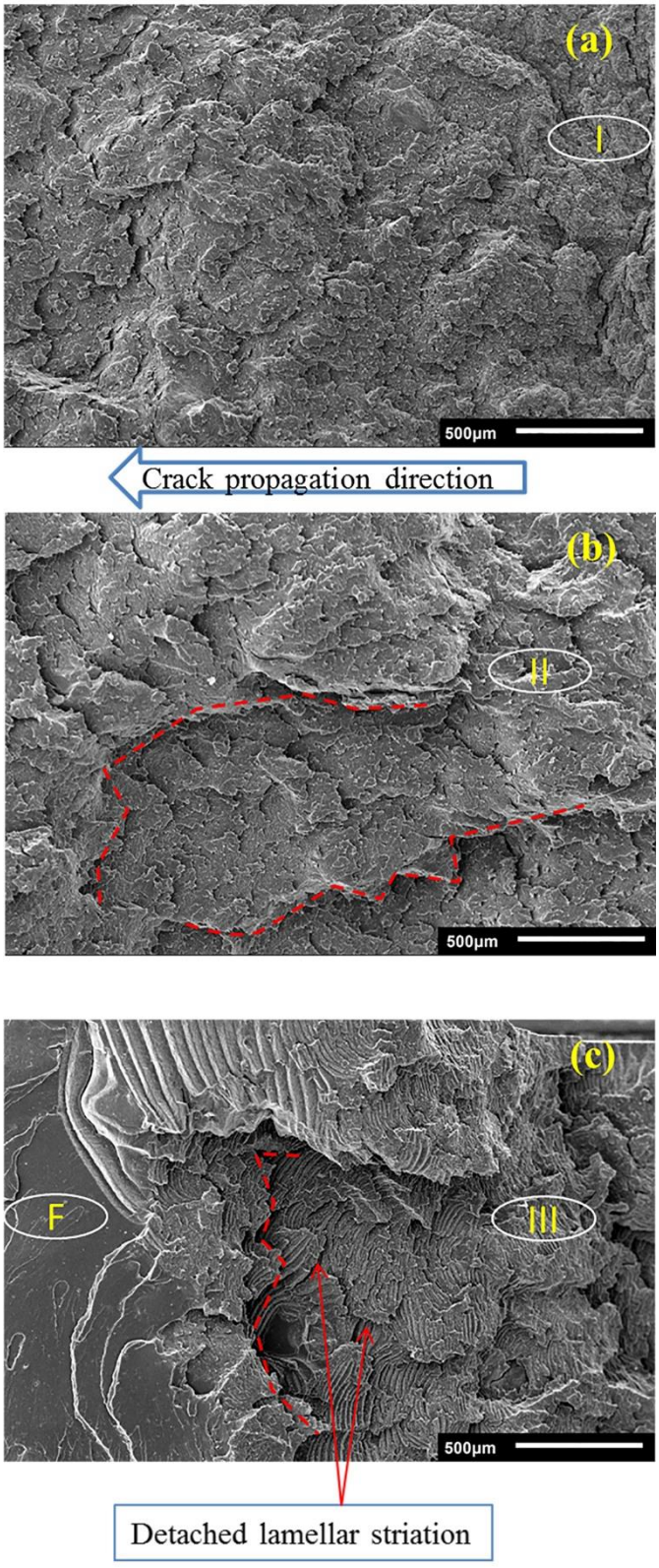

Figure 8-20 Fatigue fracture morphology of a 10 pphr CRP400 filled NR/BR blend at amplitude 15 mm (96% strain) (a) stable crack propagation , b) transition and (c) catastrophic region.

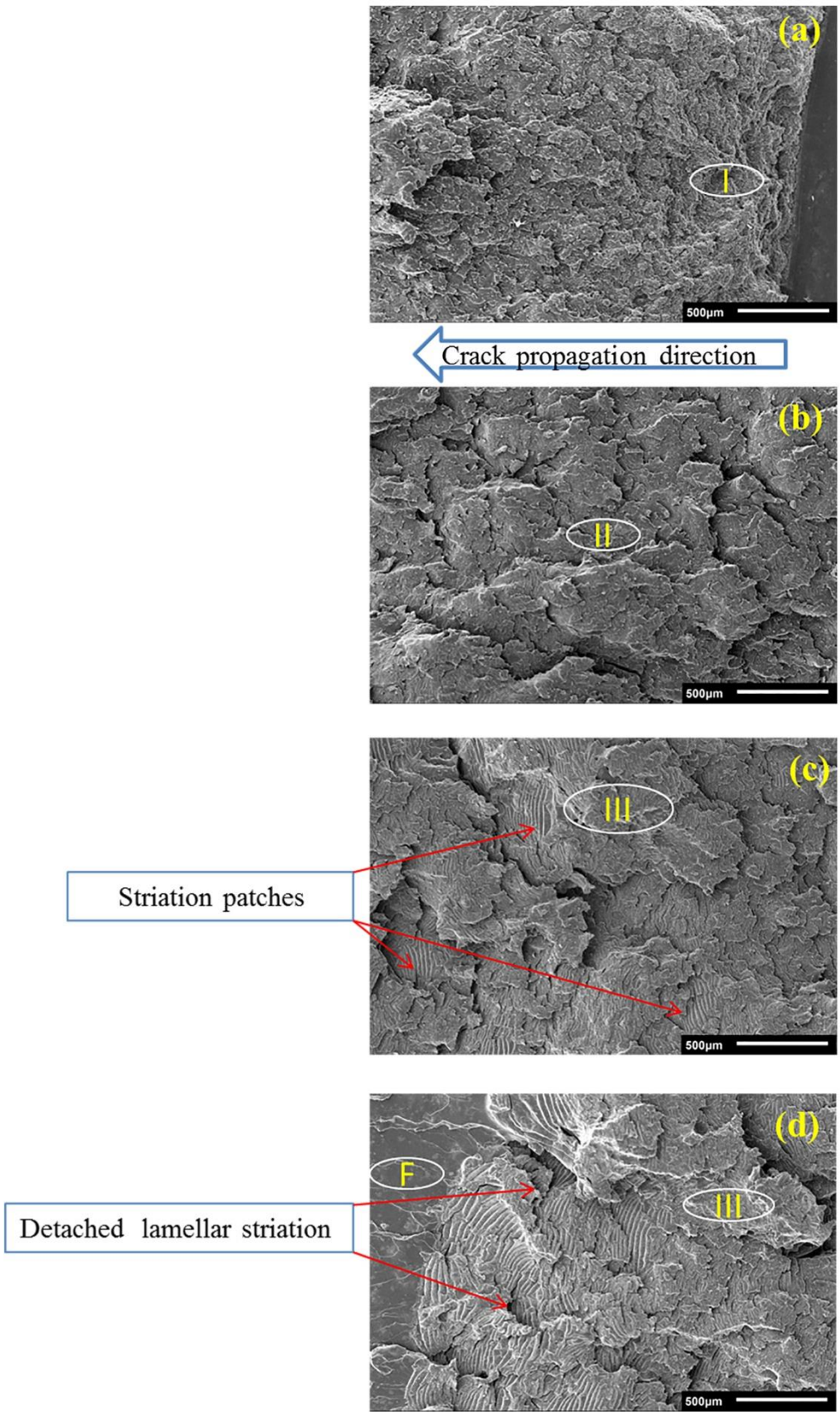

Figure 8-21 Fatigue fracture morphology of a 10 pphr MRP074 filled NR/BR blend at amplitude 15 mm (96% strain) (a) stable crack propagation, b) transition and (c) and (d) catastrophic region.

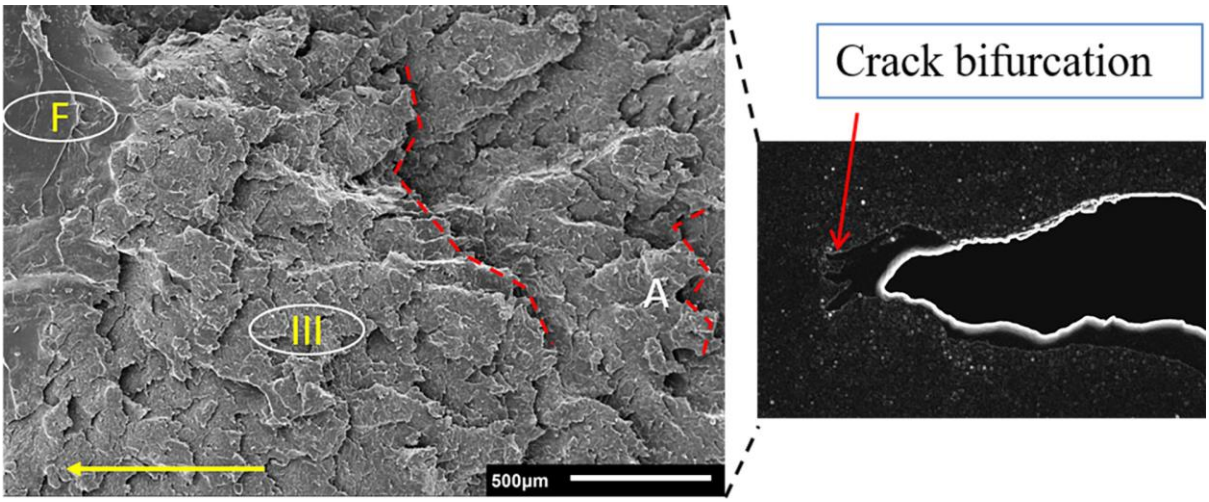

Figure 8-22 FCG fracture morphology of a 10 pphr MRP074 filled NR/BR blend at amplitude 9 mm (59% dynamic strain) showing crack bifurcation corresponding to several crack lines behind the fracture 'leaves' before final fracture (Horizontal arrow-crack propagation direction); F-failure, III-catastrophic crack propagation region.

With similar concentrations at 30 pphr in the CRP400 filled compound, the striation morphology appeared to be partially inhibited. The addition of 30 pphr MRP074 reduced the features to patches of spiral rib striations whereas in the CRP400, the features are almost non-existent. The possible explanation is that more obstacles and more bifurcation/branching occurred reducing the velocity of the crack growth before final failure. Further investigation is needed to confirm this assumption.

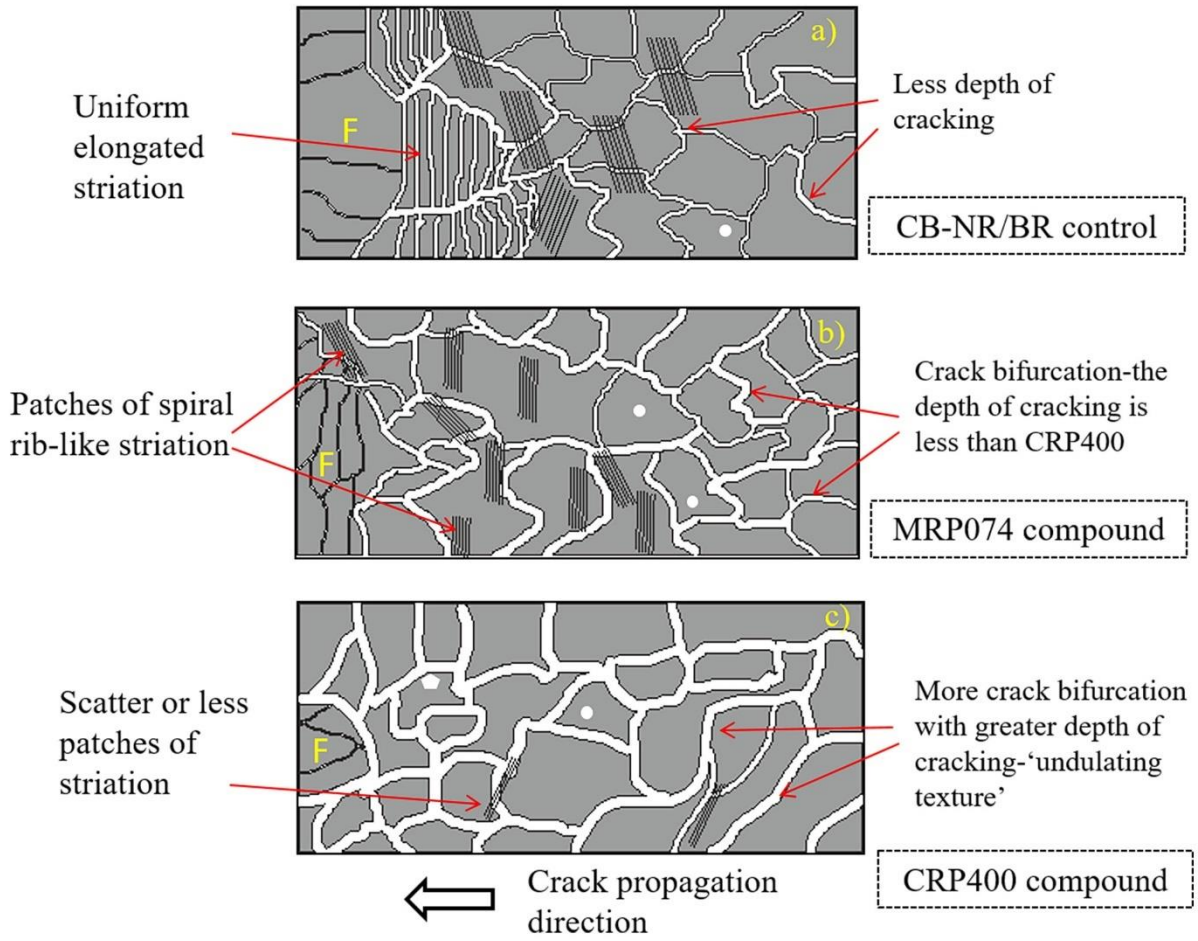

Figure 8-23 Schematic of microstructure of crack fracture surfaces after FCG at a dynamic strain of 71% in the catastrophic crack propagation region for a) CB-NR/BR control b) 30 pphr MRP074 filled CB-NR/BR c) 30 pphr CRP400 filled CB-NR/BR compounds (F-failure).

8.5 Summary

By using the tri-modal function of the Instron WaveMatrix™ dynamic testing software, a minimum load was applied to avoid sample buckling in FCG testing. A displacement controlled strain was superimposed, compensating for a permanent set of the samples throughout the experiments. Hence, both relative and absolute hysteresis loss measurements, using strain energy density from the SENT specimen, during FCG test were possible and produced more representative of hysteresis data for the samples tested.

At lower tearing energy (40% dynamic strain), the CRP400 filled compound showed a slightly lower crack growth rates compared to NR/BR control compound. Fracture resistance of rubber is not only dependent on the strain energy density (crack driving force) but also energy dissipated around the crack tip. The irregular surface of CRP400 provided greater surface area and stronger interface between the particles and rubber matrix. There was a longer crack path around CRP400 particles and hence more new surface energy compared to either smaller, microscopically smooth MRP074 or control filled NR/BR compounds. The possible combined effects included differences in crosslink density, inhomogeneities due to filler addition, and relatively weak rubber-filler bonding and all could contribute to the relative hysteresis loss.

At 71% dynamic strain, however, it seems that the irregular structure of CRP400 did not play an important role as there were no significant differences in the relative hysteresis loss. In addition, there were negligible differences in the dynamic energy (total and strain energy density). The increases in dynamic strain will have increased the absolute hysteresis of the rubber network. The relative hysteresis loss showed different trends which is probably attributed to multiple mechanisms occurring around the crack tip. SIC increased with increasing strain amplitude and caused increased anisotropy of the material strength. Higher SIC at the crack tip enhanced crack tip blunting and branching which contributed to considerably higher scatter of the fatigue crack growth rates. Fatigue crack growth of NR/BR is slightly lower compared to CRP400 or MRP074 filled compounds (71% and 96% dynamic strain). Weak bonding between the RRP filler and rubber matrix created more microvoid sites which initiated fatigue failure. These microvoids are believed to increase in size with increasing dynamic strain amplitudes and probably contributed to higher crack growth of the RRP filled matrix. The SIC effect reduction could be another factor, where the RRP increased the stress concentration and reduced strength at the crack tip.

The ultimate tensile properties of the CRP400 decreased faster, than in MRP074 compounds which increased the crack growth rates. This supports the suggestion of strength dependence of the crack growth rate on the energy release rate at higher strains. Higher absolute and relative hysteresis is slightly detrimental to the fatigue crack growth of CRP400 filled compounds. This probably indicates better transfer of heat to the surrounding network in CB filled MRP074 than CRP400 filled compounds at higher strain (96% dynamic strain). The

higher temperature changes the material properties in general and could suppress the SIC effect and accelerate rupture of the molecular chain around the crack tip. The combination of higher strength and other factors (SIC and lower relative hysteresis) for NR/BR compounds contributed to the lower slope (power-law exponent) of the energy release rate *vs* crack growth relationship.

At similar pre-crack length, the crack propagation path indirectly reflected the strength of the material. With higher anisotropy due most likely to the SIC effect, the crack deviation and bifurcation would have delayed the crack growth rates of the rubber material.

The crack fracture morphology at different tearing energies provides a valuable insight into the fatigue mechanisms of NR/BR blend control and CRP400 or MRP074 filled compounds. Partial conclusions of this study are as follows.

a) At lower tearing energy, the lower crack growth rate showed layered structure of "twisted knots". The microscopic rough structure reflected the breaking and retraction of the molecular chains/ligaments. The crack could not propagate until the molecular chains at the crack tip ruptured. The 'V' shape on the microstructure of the fracture surfaces might reflect the SIC effect at the crack tip and have caused the inclined direction of the crack pathway to the applied loading.

b) Two types of microscopic roughness were observed. First, roughness at the crack tip corresponding to the stable crack propagation stage. Secondly, more roughness at the unstable cracks propagation which was due to crack bifurcation or deviation.

c) At higher tearing energy, broader 'fracture leaves', and striation morphology before final fracture, was observed.

d) Fracture images of crack bifurcation before final fracture corresponded to several crack lines behind the fracture 'leaves'. The crack bifurcation and deviation was reflected as uneven rough 'undulating' shapes on the fracture surfaces or three-dimensional structure which required more energy to create compared to microscopically smooth flat fracture surfaces.

The microstructure gave valuable information on fatigue crack growth mechanisms. Crack tip blunting and crack bifurcation or deviation at the crack tip are clearly an important aspect of resistance against crack propagation. However, they cannot be an explanation for the overall performance covering the total fatigue life. Total fatigue life also comprises of fatigue initiation from various sources of flaws and crack propagation within the bulk materials. Differences in the microstructure at various tearing energies also showed the dependency of the crack growth microstructure on the tearing energies.

Chapter 9 Conclusions and Future work

9.1 Conclusions

The addition of either Micronised Rubber Powder (denoted as MRP074~74 μm nominal diameter) or Crumb Rubber Powder (CRP400~400 μm nominal diameter) recycled rubber particles affects the crosslink density of unfilled and carbon black (CB) filled matrices and was observed in ΔM reduction (ΔM = maximum torque (M_H) - minimum torque (M_L)) as well as in the change in apparent crosslinking density. The reduction of crosslink density has been observed by Gibala and Hamed [171] in Styrene Butadiene Rubber, who found, that sulphur migrated from the virgin compound to the ground rubber tyre matrix. The reactivity or solubility towards curatives and accelerators of Natural Rubber (NR), Butadiene Rubber (BR) or NR/BR (70/30 blend ratio) rubber matrices, and the particle surface area of CRP400 or MRP074, each affect the degree of sulphur migration. The increased solubility of curatives in BR, relative to NR, probably allows more diffusion of curatives from virgin BR to the recycled rubber powder (RRP-CRP400 and MRP074) phase than does NR, which may explain a pronounced reduction in both ΔM and apparent crosslink density particularly at higher CRP400 concentrations.

For quasi-static tensile tests, the tensile failure of RRP filled materials is dependent on the filler size and type of matrix. For NR or NR/BR blend compounds, filler particles that are larger than or equal to the typical flaw size act as stress raisers that initiate fracture resulting in lower tensile strength. The larger CRP400 particles resulted in lower tensile strength than the smaller MRP074 at similar filler concentrations in either unfilled or carbon black filled compounds. In low strain induced crystallising BR, the opposite was observed. For the unfilled compounds, the addition of 10 or 30 pphr (parts per hundred rubber) of CRP400 did not have a significant effect on the tensile strength. In contrast, for MRP074, the tensile strength of BR compound increased as the MRP074 concentration increased. In CB filled BR, an increase in tensile strength was observed at 10 pphr with a subsequent decrease at 30 pphr of MRP074 which suggests an optimal concentration somewhere between this values.

A more regular shaped surface topology of MRP074 when compared with CRP400 was identified using Transmission Electron Microscopy (TEM) micrographs. The weak

interaction at the interface between MRP074 particles and the rubber network matrix was visualised as polystyrene ‘voids’ around particles, using the TEM ‘network visualisation’ technique. The weak interaction was defined in this work as less rubber chains interaction between the rubber and filler that could restrict the mobility of the rubber molecules on the filler surfaces. This confirmed the lower physical bonding of the MRP074 networks to the rubber matrix.

Hysteresis partially contributes to the enhancement of tear performance of CB filled compounds relative to unfilled rubber compounds by reducing energy available for crack propagation. Other strengthening factors such as strain induced crystallisation (SIC), strength anisotropy, crack deviation and crack tip blunting are also reported [195,196]. Despite the reduction in the crosslinking density of the matrix, increased crack deviation could probably compensate for the tear strength reduction of NR and NR/BR compounds containing MRP074 and CRP400 fillers particularly at 10 pphr concentration where no significant change occurred.

The crescent tear strength test was able to characterise the possible weak interaction of MRP074 in unfilled NR and NR/BR blend matrices. The effect of structure and the weak interface interaction was confirmed by the lower tear strength in MRP074 filled matrices compared to CRP400 filled matrices in both unfilled NR and NR/BR blend compounds. For the carbon black filled compound, the weak interactions of MRP074 were not reflected in the tear strength results due to a high scatter in the data, caused by the inhomogeneity and tear path deviation, when the carbon black filler was present. The carbon-black filler seems to compensate for the weak matrix-filler interaction shown by MRP074 filler.

In the crescent type tear strength tests, the effect of hardness of the RRP and the adhesion between the filler and rubber matrix are also important. This is more clearly observed in BR compounds than in NR due to the lower contributing effect from the strain induced crystallisation and higher sulphur migration. The migration caused more crosslinks in RRP and fewer crosslinks in the BR matrix. The crescent tear strength increased with RRP hardness indicating that there is a relatively high interaction of RRP and unfilled (no carbon black filler) BR matrices. This is attributed to a tear path deviation mechanism according to Pittolo and Burford [193]. The Kraus model predicts the extent of interaction between the

rubber and the RRP filler in unfilled compounds and this corresponds to the crescent tear result.

In CB filled BR, the CB enhances the interaction between the CRP400 and the rubber matrix. Higher sulphur migration occurred in CRP400, than in MRP074, due to its greater surface area which increased the hardness of the filler leading to more tear path deviation mechanisms. This explains the higher tear strength at 30 pphr concentrations for CRP400 compared to MRP074 compounds. V_{ro} and V_{rf} are the volume fractions of rubber in the solvent-swollen gum and filled compounds, respectively. The ratio V_{ro}/V_{rf} <1 (with the exception for 30 pphr concentration in BR) for RRP CB filled NR, BR and NR/BR confirmed the role of CB for better adhesion of RRP filled compounds in comparison to unfilled compounds (V_{ro}/V_{rf} >1). The Kraus parameter showed that for CB filled NR or NR/BR, there is only a marginal difference in the extent of interaction between either of the RRPs. Deviations from the proposed linear model were observed at higher RRP concentrations.

The Akron abrasion resistance test appears to be able to characterise the possible weak interaction of MRP074 particularly in NR/BR blend matrices more effectively than the DIN abrasion test. The DIN and Akron abrasion tests give two contrary trends for the NR/BR blends, while DIN and Akron trends were similar for NR and BR.

The abrasion resistance of the BR compound containing MRP074 filler outperformed the CRP400 filled compound. In BR, due to higher migration of curatives into the CRP400 phase, there was a significant reduction in the crosslink density of the matrix which resulted in higher abrasion resistance for the MRP074 filled compound.

The Fatigue-to-Failure Tests (FTFT) was very sensitive to inhomogeneities in the rubber matrix. The smaller MRP074 filled compound is relatively ‘homogeneous’ and therefore contains minimal stress concentrations compared to CRP400 filled compounds. Filler particles that are larger than the typical flaw size act as additional/major stress raisers that initiate fracture and lead to shorter fatigue lives. The fatigue performance for un-notched specimens, using FTFT at 100% strain, appeared to correlate with the FCP test at higher strains. The FTFT conducted at only one strain was thus insufficient to draw any conclusion about the overall compound performance. This fatigue test is likely to produce different

results at different strain/stress levels. Some of the other factors such as the dependency of frequency/strain rate and temperature were not examined in this research.

By using the tri-modal control, a displacement controlled strain was superimposed to compensate for permanent set of the samples throughout the experiments. Virtually no differences in tearing energy from the energy densities were observed between un-notched and notched specimen. Hence, both relative and absolute hysteresis loss measurements, using strain energy density from the single-edge notched tensile (SENT) specimens, during the FCG test were used instead of separate test using un-notched specimen. In addition, strain energy density dependent on testing conditions where the total energy densities decreased as the cycles accumulated, due to cyclic stress softening of the material [93]. Therefore, the use of both SENT specimen and energy measurement, obtained at the number of fatigue cycles closest to 50% of its service life, were expected to be more representative of hysteresis data compared to quasi-static tensile testing.

For a lower tearing energy, CRP400 filled compounds showed no significant difference in the crack growth rates compared to the NR/BR control compounds due to the relatively high scatter in the results. However, it exhibited lower crack growth rate than MRP074 compounds. The irregular surface of CRP400 provided greater surface area for bonding and a stronger interface between the particles and rubber matrix. This created a longer crack path around CRP400 particles and hence increased surface energy compared to the smaller, microscopically smooth MRP074 and control filled NR/BR compounds. Higher absolute and relative hysteresis loss, at lower tearing energy for CRP400 appears to decrease the crack growth rates of the CRP400 filled NR/BR compounds. The NR/BR control compounds had high crosslink density whereas in both CRP400 and MRP074 filled matrices the migration of curatives from the virgin compounds to the RRP caused reduction in the crosslinking of the rubber matrices. The higher crosslinking could have impaired the ability of the rubber to dissipate energy through hysteresis.

The opposite results were observed at higher tearing energies. At higher tearing energy levels (96% dynamic strain), the crack growth rates changed to be ranked CRP400>MRP074>control NR/BR compound, where CRP400 exhibited the highest crack growth followed by MRP074 and the control NR/BR compound. The combination factors

such as strength, SIC and lower relative hysteresis for NR/BR compounds contributed to the lower slope (power-law exponent) of the energy release rate *vs.* crack growth relationship.

The weak bonding between the RRP filler and rubber matrix appeared to create more microvoid sites which initiated fatigue failure. These microvoids were believed to increase in size with increasing dynamic strain amplitudes and contributed to the higher crack growth rate of the RRP filled matrix. Reduced SIC could be another factor, where the RRP increased the stress concentration so reducing the strength at the crack tip. Differences in relative hysteresis loss showed that additional energy dissipation, due to multiple new crack surfaces at the crack tip, contributed to the FCG of the RRP compounds. At a higher tearing energy, the combination of higher absolute and relative hysteresis loss were slightly detrimental to the crack growth rates of the CRP400 compound. This probably indicates better transfer of heat to the surrounding network in CB filled MRP074 than in the CRP400 compounds, which explains the more rapid crack growth rate of CRP400 CB filled NR/BR compounds.

More crack deviation (tortuosity) and bifurcation was observed in CRP400 filled compounds compared to MRP074 filled NR/BR. The crack bifurcation and deviation corresponded to deeper crack lines behind the fracture ‘leaves’ and was reflected as an uneven rough ‘undulating’ shape on the fracture surfaces, or three-dimensional structures, which require more energy to create when compared to microscopically smooth flat fracture surfaces.

The crack fracture morphology at different tearing energies provided valuable insight into the fatigue crack growth mechanisms of the NR/BR blend control and CRP400 and MRP074 filled compounds. Crack tip blunting, and crack bifurcation or deviation, at the crack tip were clearly an important aspect of the resistance to the crack propagation. However, they cannot explain the overall performance of the total fatigue life. Total fatigue life comprises of (a) fatigue initiation from various sources of flaws, (b) crack propagation within the bulk materials, and (c) final catastrophic crack growth. Fracture morphologies for NR/BR and RRP filled compound had different fracture surface topography at various tearing energies, which showed the dependency of the crack growth microstructure on tearing energies. The morphology at crack initiation, propagation and final fracture stages have been established. Understanding the crack growth mechanisms using SENT samples enabled identification of

the crack initiation location, and possibly the cause of failure, in the FTFT or for other engineering rubber products exposed to fatigue loading.

The limitations of this study are due to the finite duration and facilities constraints. Quasi-static testing is not sufficient to analyse and predict the RRP performance for rubber matrices especially in dynamic applications. The different rankings were determined for MRP074 or CRP400 filler using conventional rubber test standards and fracture mechanics tests. Although the mean CRP400 particle size was about a factor five larger in one dimension than MRP074, the CRP400 compound exhibited lower crack growth rates in the technically important low strains/tearing energies regions. The "rougher" surface/more irregular shape of CRP400 particles appeared to be a more important factor than the particle size of MRP074 for the FCG performance especially at lower strains.

All the above findings offer a different approach in evaluating RRP for application in the elastomeric matrix.

9.2 Recommendation for future work

There are many factors [228] which affect the direction of the crack path, including strain crystallisation for crystallising elastomer, anisotropy of the material strength [84,111], strain amplitude and ratio of the energy release rates [111]. The goal and scope of this thesis did not permit consideration of all these factors due to the limited duration and facilities constraints. The following areas have been identified for future investigation:

1) Investigate mechanical and fatigue crack growth at different temperatures. Increase in temperature increases molecular chain mobility, and so can reduce hysteresis loss in rubber matrices [219]. Studies have shown [105,233] that the dependency of cyclic crack growth on strain rates effect was different for specific types of elastomer. Hence, future work may also be extended to study the effect of frequency/strain rates on fatigue/cyclic crack growth for non-crystallising and strain induced crystallising rubbers filled RRP compound.

2) Investigate the effect of RRP in elastomers under different tearing energies using pure shear test pieces. Doing this will eliminate the dependence on the initial cut length and might also reduce the scatter in the fatigue data.

3) Investigate the FCP comparison on the effect of RRP concentration under relaxing and non-relaxing conditions (varied minimum strain levels) since studies [83,232] have reported an increase in the fatigue life of rubbers with increasing levels of the minimum stress [83,234].

4) The fatigue trend for un-notched specimen using fatigue-to-failure test at 100% strain seems to correlate with the FCP test at higher strains. It would be interesting to investigate the performance of RRP in elastomers at different levels of fatigue strains using FTFT.

5) The results in Chapter 5 and Chapter 7 indicated that the performance of MRP074 outperformed the CRP400 filled compound in tensile strength and abrasion resistance for BR compound. The fatigue crack growth test was limited to carbon black filled NR/BR compound (70/30 ratio) as the material of study. Therefore, future work required to study the effect of MRP074 and CRP400 on fatigue crack growth rates for carbon black filled non-strain induced crystallising rubber compounds.

6) The micronised form of cryogenic particles lack the surface topology to achieve good adhesion. Chemical or physical treatment of MRP074 could be considered for better interface adhesion between the particles and matrix. The effect of carbon black with a much higher structure could probably provide an additional area to allow further penetration/entrapment of polymer chains for MRP074 filler in order to compensate the weak interaction of microscopically smooth surfaces. This area should be investigated.

7) Use of fractal dimension [235] to quantity aggregation of fillers/RRP in rubber matrices to quantify dispersion effects on the physical properties of rubber compound.

8) To study the effect of MRP074 in FCP tests using an optimal carbon black concentration for mechanical properties enhancement.

9) Evaluate abrasion resistance and fatigue crack growth rates for rubber compound having similar hardness or crosslinking densities. This would isolate other variables that appear to affect the measured properties.

10) Explore if coating of MRP074 and CRP400 particles could lead to enhanced fatigue lives when they are incorporated into commercial rubber compounds.

References

1. Rajan, V.V., Dierkes, W.K., Joseph, R., and Noordermeer, J.W.M., *Science and technology of rubber reclamation with special attention to NR-based waste latex products.* Progress in Polymer Science, 2006. **31**(9): pp. 811-834.
2. Ramarad, S., Khalid, M., Ratnam, C.T., Chuah, A.L., and Rashmi, W., *Waste tire rubber in polymer blends: A review on the evolution, properties and future.* Progress in Materials Science, 2015. **72**: pp. 100-140.
3. Ahmed, R., van de Klundert, A., and Lardinois, I., *Rubber waste options for small-scale resource recovery urban solid waste series 3.* Netherlands: WASTE, 1996.
4. *Natural Rubber Statistics 2016*. [accessed on 10 March 2019]; Available from: http://www.lgm.gov.my/nrstat/nrstats.pdf.
5. Van Beukering, P.J.H. and Janssen, M.A., *Trade and recycling of used tyres in Western and Eastern Europe.* Resources, Conservation and Recycling, 2001. **33**(4): pp. 235-265.
6. Forrest, M. *Overview of the world rubber recycling market*. Recycling and Re-use of Waste Rubber [accessed; Available from: http://www.smithersrapra.com/SmithersRapra/media/Sample-Chapters/Recycling-and-Re-use-of-Waste-Rubber.pdf.
7. Papp, F.P., *Optimizing the use of micronized rubber powder made from end-of-life tire material.* Rubber World, 2012. **246**(5): pp. 16-27.
8. Saiwari, S., *Post-consumer tires back into new tires: de-vulcanization and re-utilization of passenger car tires.* PhD thesis, 2013, University of Twente. Netherlands.
9. Blumenthal, M., *What's new with ground rubber?: Tire recycling update.* Biocycle: Journal of Composting & Organics Recycling, 1998. **39**(3): pp. 40-44.
10. Klingensmith, W. and Baranwal, K., *Recycling of rubber: An overview.* Rubber World, 1998. **218**(3): pp. 41-46.
11. Amari, T., Themelis, N.J., and Wernick, I.K., *Resource recovery from used rubber tires.* Resources Policy, 1999. **25**(3): pp. 179-188.
12. Grigoryeva, O., Fainleib, A., Starostenko, O., Danilenko, I., Kozak, N., and Dudarenko, G., *Ground tire rubber (GTR) reclamation: Virgin rubber/reclaimed GTR (RE) vulcanizates.* Rubber Chemistry and Technology, 2004. **77**(1): pp. 131-146.

13. Yehia, A.A., Mull, M.A., Ismail, M.N., Hefny, Y.A., and Abdel‐Bary, E.M., *Effect of chemically modified waste rubber powder as a filler in natural rubber vulcanizates.* Journal of Applied Polymer Science, 2004. **93**(1): pp. 30-36.
14. Sreeja, T.D. and Kutty, S.K.N., *Cure characteristics and mechanical properties of natural rubber/reclaimed rubber blends.* Polymer - Plastics Technology and Engineering, 2000. **39**(3): pp. 501-512.
15. Kim, J.K. and Burford, R.P., *Study on powder utilization of waste tires as a filler in rubber compounding.* Rubber Chemistry and Technology, 1998. **71**(5): pp. 1028-1041.
16. Rattanasom, N., Poonsuk, A., and Makmoon, T., *Effect of curing system on the mechanical properties and heat aging resistance of natural rubber/tire tread reclaimed rubber blends.* Polymer Testing, 2005. **24**(6): pp. 728-732.
17. De, D. and De, D., *Processing and material characteristics of a reclaimed ground rubber tire reinforced styrene butadiene rubber.* Materials Sciences and Applications, 2011. **2**(05): pp. 486-496.
18. Abraham, F., Clauss, G., and Alshuth, T. *Testing and simulation of the influence of glass spheres on fatigue life and dynamic crack propagation of elastomers*. in *Constitutive Models for Rubber Proceddings*. 2005. Balkema.
19. *Latest World Rubber Industry Outlook now available from IRSG*. [accessed on 10 March 2019]; Available from: http://www.rubberstudy.com/news-article.aspx?id=5147&b=earlier-news.aspx.
20. Martínez, J.D., Puy, N., Murillo, R., García, T., Navarro, M.V., and Mastral, A.M., *Waste tyre pyrolysis–a review.* Renewable and Sustainable Energy Reviews, 2013. **23**: pp. 179-213.
21. *Tyre cross section*. [accessed 2015]; Available from: http://www.mecordsindia.com/images/chafer-fabric-used-tyre.jpg.
22. [accessed on 11 June 2015]; Available from: http://www.continental-tyres.co.uk/www/tyres_uk_en/themes/van-tyres/winter-tyres/why-winter-tyres.html.
23. *Racing Tyres & Road Tyres – Differences*. [accessed on 15 July 2015]; Available from: https://www.tyre-shopper.co.uk/news/the-excitement-of-racingon-the-track-and-at-the-pit-station.
24. ETRMA. *End-of-life Tyre Report 2015*. [accessed on 5 February 2019]; Available from: http://www.etrma.org/tyres/ELTs.

25. ETRMA. *Guidance on the use of Vulcanised-rubber Pseudo Substances in IMDS declarations of tyres* 2013 [accessed on 5 February 2019]; Available from: http://www.etrma.org/.
26. *"The tyre grip"*. [accessed on 20 July 2015]; Available from: http://www.dimnp.unipi.it/guiggiani-m/Michelin_Tire_Grip.pdf.
27. Jansen, S.T.H., Schmeitz, A.J.C., Maas, S., Rodarius, C., and Akkermans, L., *Study on some safety-related aspects of tyre use*. 2014: TNO.
28. Zhao, J. and Ghebremeskel, G.N., *A review of some of the factors affecting fracture and fatigue in SBR and BR vulcanizates.* Rubber Chemistry and Technology, 2001. **74**(3): pp. 409-427.
29. Maridass, B. and Gupta, B.R., *Recycling of waste tire rubber powder-devulcanization in a counter rotating twin screw extruder.* Kautschuk Gummi Kunststoffe, 2003. **56**(5): pp. 232-236.
30. Bandyopadhyay, S., Dasgupta, S., Agrawal, S.L., and Mandot, S.K., *Use of recycled tyre material in NR/BR blend based tyre tread compound: Part II (with ground crumb rubber).* Progress in Rubber, Plastics and Recycling Technology, 2006. **22**(4): pp. 269.
31. Bandyopadhyay, S., Dasgupta, S., Mandal, N., Agrawal, S.L., Mandot, S.K., Mukhopadhyay, R., Deuri, A.S., and Ameta, S.C., *Use of recycled tyre material in natural rubber based tyre tread cap compound Part I:(with ground crumb rubber).* Progress in Rubber, Plastics and Recycling Technology, 2005. **21**(4): pp. 299-317.
32. Dierkes, W., *Untreated and treated rubber powder*, in *Rubber Recycling*, De, S.K., Isayev, A., and Khait, K., Editors. 2005. p. 127-154.
33. Karger-Kocsis, J., Mészáros, L., and Bárány, T., *Ground tyre rubber (GTR) in thermoplastics, thermosets, and rubbers.* Journal of Materials Science, 2012. **48**(1): pp. 1-38.
34. Sienkiewicz, M., Kucinska-Lipka, J., Janik, H., and Balas, A., *Progress in used tyres management in the European Union: A review.* Waste Management, 2012. **32**(10): pp. 1742-1751.
35. Myhre, M. and MacKillop, D.A., *Rubber recycling.* Rubber Chemistry and Technology, 2002. **75**(3): pp. 429-474.
36. Sweet, A., *Management of End of Life Tyres.* (Firecone Report), NZ, Ministry for The Environment, www. mfe. govt. nz, 2004.

37. Shulman, V.L., *Tyre recycling.* WASTE: A handbook of waste management and recycling. Elsevier, Amsterdam, The Netherlands, 2011: pp. 297-320.
38. ETRMA. *European Tyre & Rubber Industry*. Statistic Edition 2016 2016 [accessed on 3 January 2019]; Available from: http://www.etrma.org/.
39. ETRMA. *European Tyre & Rubber Industry*. Statistic Edition 2015 [accessed 2016]; Available from: http://www.etrma.org/.
40. Shaw, D., *Why is recycled rubber not used in tyres?* European Rubber Journal, 2011(September/October): pp. 34-37.
41. Jacob, C. and De, S.K., *Powdered rubber waste in rubber compounds*, in *Rubber Recycling*, De, S.K., Isayev, A., and Khait, K., Editors. 2005. p. 213-246.
42. Khait, K., *New solid-state shear extrusion pulverization process for used tire rubber recovery.* Rubber World, 1997. **216**(2): pp. 38.
43. Bilgili, E., Arastoopour, H., and Bernstein, B., *Analysis of rubber particles produced by the solid state shear extrusion pulverization process.* Rubber Chemistry and Technology, 2000. **73**(2): pp. 340-355.
44. Fernández-Berridi, M.J., González, N., Mugica, A., and Bernicot, C., *Pyrolysis-FTIR and TGA techniques as tools in the characterization of blends of natural rubber and SBR.* Thermochimica Acta, 2006. **444**(1): pp. 65-70.
45. Adhikari, B., De, D., and Maiti, S., *Reclamation and recycling of waste rubber.* Progress in Polymer Science, 2000. **25**(7): pp. 909-948.
46. Kumar, P., *Investigating the recycled rubber granulate-virgin rubber interface.* PhD thesis, 2007, Queen Mary University of London.
47. Fan, P. and Lu, C., *A Study on Functionalization of Waste Tire Rubber Powder Through Ozonization.* Journal of Polymers and the Environment, 2011. **19**(4): pp. 943-949.
48. Zhang, X., Zhu, X., Liang, M., and Lu, C., *Improvement of the properties of ground tire rubber (GTR) ‐ filled nitrile rubber vulcanizates through plasma surface modification of GTR powder.* Journal of Applied Polymer Science, 2009. **114**(2): pp. 1118-1125.
49. Fuhrmann, I. and Karger-Kocsis, J., *Promising approach to functionalisation of ground tyre rubber-photochemically induced grafting: Short communication.* Plastics, Rubber and Composites, 1999. **28**(10): pp. 500-504.

50. Dierkes, W., *Surface activated rubber crumb: A new development in rubber recycling.* Journal of Elastomers and Plastics, 1996. **28**(3): pp. 257-278.
51. Rooj, S., Basak, G.C., Maji, P.K., and Bhowmick, A.K., *New route for devulcanization of natural rubber and the properties of devulcanized rubber.* Journal of Polymers and the Environment, 2011. **19**(2): pp. 382-390.
52. Thaicharoen, P., Thamyongkit, P., and Poompradub, S., *Thiosalicylic acid as a devulcanizing agent for mechano-chemical devulcanization.* Korean Journal of Chemical Engineering, 2010. **27**(4): pp. 1177-1183.
53. Mandal, S.K., Alam, N., and Debnath, S.C., *Reclaiming of ground rubber tire by safe multifunctional rubber additives: I. Tetra benzyl thiuram disulfide.* Rubber Chemistry and Technology, 2012. **85**(4): pp. 629-644.
54. Isayev, A., Chen, J., and Tukachinsky, A., *Novel ultrasonic technology for devulcanization of waste rubbers.* Rubber Chemistry and Technology, 1995. **68**(2): pp. 267-280.
55. Tukachinsky, A., Schworm, D., and Isayev, A.I., *Devulcanization of waste tire rubber by powerful ultrasound.* Rubber Chemistry and Technology, 1996. **69**(1): pp. 92-103.
56. Levin, V.Y., Kim, S.H., Isayev, A.I., Massey, J., and Von Meerwall, E., *Ultrasound devulcanization of sulfur vulcanized SBR: Crosslink density and molecular mobility.* Rubber Chemistry and Technology, 1996. **69**(1): pp. 104-114.
57. Levin, V.Y., Kim, S.H., and Isayev, A.I., *Vulcanization of ultrasonically devulcanized SBR elastomers.* Rubber Chemistry and Technology, 1997. **70**(1): pp. 120-128.
58. Lee, S.H., Hwang, S.H., Kontopoulou, M., Sridhar, V., Zhang, Z.X., Xu, D., and Kim, J.K., *The effect of physical treatments of waste rubber powder on the mechanical properties of the revulcanizate.* Journal of Applied Polymer Science, 2009. **112**(5): pp. 3048-3056.
59. Farris, R.J. Powder processing techniques to recycle rubber tires into new parts from 100% reclaimed rubber powder/crumb. Vol. 40. 2001: Chelsea Center for Recycling and Economic Development, University of Massachusetts Lowell.
60. Morin, J.E., Williams, D.E., and Farris, R.J., *A novel method to recycle scrap tires: High-pressure high-temperature sintering.* Rubber Chemistry and Technology, 2002. **75**(5): pp. 955-968.

61. Bilgili, E., Dybek, A., Arastoopour, H., and Bernstein, B., *A new recycling technology: compression molding of pulverized rubber waste in the absence of virgin rubber.* Journal of Elastomers and Plastics, 2003. **35**(3): pp. 235-256.
62. Gugliemotti, A., Lucignano, C., and Quadrini, F., *Production of rubber parts by tyre recycling without using virgin materials.* Plastics, Rubber and Composites, 2012. **41**(1): pp. 40-46.
63. Kojima, M., Tosaka, M., Ikeda, Y., and Kohjiya, S., *Devulcanization of carbon black filled natural rubber using supercritical carbon dioxide.* Journal of Applied Polymer Science, 2005. **95**(1): pp. 137-143.
64. Clauzade, C., *End-of-life tires in electric arc furnaces: An industrial success story*. 2006, ALIAPUR, Lyon, France.
65. Cole, W.F., *Performance of green, tire derived, recovered carbon black.* Rubber World, 2010. **241**(5): pp. 20-25.
66. Norris, C. and Bennett, M., *The Recovery of Silica from End-of-Life-Tyres-Pyrolysis as alternative source of silica filler*, in *KGK rubberpoint*. 2015.
67. Stevenson, K., Stallwood, B., and Hart, A.G., *Tire rubber recycling and bioremediation: a review*. Bioremediation Journal, 2008. **12**(1): pp. 1-11.
68. Li, Y., Zhao, S., and Wang, Y., *Microbial desulfurization of ground tire rubber by Thiobacillus ferrooxidans.* Polymer Degradation and Stability, 2011. **96**(9): pp. 1662-1668.
69. Saiwari, S., Dierkes, W.K., and Noordermeer, J.W.M., *Comparative investigation of the devulcanization parameters of tire rubbers.* Rubber Chemistry and Technology, 2014. **87**(1): pp. 31-42.
70. Yazdani, H., Karrabi, M., Ghasmi, I., Azizi, H., and Bakhshandeh, G.R., *Devulcanization of waste tires using a twin‐screw extruder: The effects of processing conditions.* Journal of Vinyl and Additive Technology, 2011. **17**(1): pp. 64-69.
71. Flory, P.J. and Rehner Jr, J., *Statistical mechanics of cross‐linked polymer networks I. Rubberlike elasticity.* The Journal of Chemical Physics, 1943. **11**(11): pp. 512-520.
72. Kumnuantip, C. and Sombatsompop, N., *Dynamic mechanical properties and swelling behaviour of NR/reclaimed rubber blends.* Materials Letters, 2003. **57**(21): pp. 3167-3174.

73. Bandyopadhyay, S., Agrawal, S.L., Ameta, R., Dasgupta, S., Mukhopadhyay, R., Deuri, A.S., Ameta, S.C., and Ameta, R., *An overview of rubber recycling.* Progress in Rubber, Plastics and Recycling Technology, 2008. **24**(2): pp. 73.
74. Myhre, M., Saiwari, S., Dierkes, W., and Noordermeer, J., *Rubber recycling: chemistry, processing, and applications.* Rubber Chemistry and Technology, 2012. **85**(3): pp. 408-449.
75. Maridass, B. and Gupta, B.R., *Effect of carbon black on devulcanized ground rubber tire—Natural rubber vulcanizates: Cure characteristics and mechanical properties.* Journal of Elastomers and Plastics, 2006. **38**(3): pp. 211-229.
76. Isayev, A.I., Liang, T., and Lewis, T.M., *Effect of particle size on ultrasonic devulcanization of tire rubber in twin-screw extruder.* Rubber Chemistry and Technology, 2014. **87**(1): pp. 86-102.
77. Myhre, M.J. and MacKillop, D.A., *Modification of crumb rubber to enhance physical properties of recycled rubber products.* Rubber World, 1996. **214**(2): pp. 42-46.
78. Maridass, B. and Gupta, B.R., *Effect of extruder parameters on mechanical properties of revulcanized ground rubber tire powder.* Polimery, 2007. **52**(6): pp. 456-460.
79. Beatty, J.R., *Some fatigue properties of rubber blends.* Journal of Elastomers and Plastics, 1979. **11**(2): pp. 147-167.
80. Mars, W.V. and Fatemi, A., *Factors that affect the fatigue life of rubber: A literature survey.* Rubber Chemistry and Technology, 2004. **77**(3): pp. 391-412.
81. Chitale, A.K. and Gupta, R.C., *Product design and manufacturing*. 2011: PHI Learning Pvt. Ltd.
82. Kraus, G., *Reinforcement of elastomers by carbon black.* Rubber Chemistry and Technology, 1978. **51**(2): pp. 297-321.
83. Abraham, F., *The influence of minimum stress on the fatigue life of non strain crystallising elastomers.* PhD thesis, 2002, Coventry University.
84. Flamm, M., Spreckels, J., Steinweger, T., and Weltin, U., *Effects of very high loads on fatigue life of NR elastomer materials.* International Journal of Fatigue, 2011. **33**(9): pp. 1189-1198.
85. Asare, S., *Failure of Rubber Components under Fatigue.* PhD thesis, 2013, Queen Mary University of London.
86. Hamed, G.R., *Energy dissipation and the fracture of rubber vulcanizates.* Rubber Chemistry and Technology, 1991. **64**(3): pp. 493-500.

87. Harwood, J.A.C. and Payne, A.R., *Hysteresis and strength of rubbers.* Journal of Applied Polymer Science, 1968. **12**(4): pp. 889-901.
88. Persson, B.N.J., Albohr, O., Heinrich, G., and Ueba, H., *Crack propagation in rubber-like materials.* Journal of Physics: Condensed Matter, 2005. **17**(44): pp. R1071.
89. Qazvini, N.T., Mohammadi, N., Jalali, A., Varasteh, A., and Bagheri, R., *The fracture behavior of rubbery vulcanizates: I. Single component versus blend systems.* Rubber Chemistry and Technology, 2002. **75**(1): pp. 77-82.
90. Tsunoda, K., *The Role of Visco-elasticity on the Crack Growth Behaviour of Rubber.* PhD thesis, 2001, Queen Mary University of London.
91. Kar, K.K. and Bhowmick, A.K., *High‐strain hysteresis of rubber vulcanizates over a range of compositions, rates, and temperatures.* Journal of Applied Polymer Science, 1997. **65**(7): pp. 1429-1439.
92. Kar, K.K. and Bhowmick, A.K., *Hysteresis loss in filled rubber vulcanizates and its relationship with heat generation.* Journal of Applied Polymer Science, 1997. **64**(8): pp. 1541-1555.
93. Mullins, L., *Softening of rubber by deformation.* Rubber Chemistry and Technology, 1969. **42**(1): pp. 339-362.
94. Diani, J., Fayolle, B., and Gilormini, P., *A review on the Mullins effect.* European Polymer Journal, 2009. **45**(3): pp. 601-612.
95. Payne, A.R., *Strainwork dependence of filler‐loaded vulcanizates.* Journal of Applied Polymer Science, 1964. **8**(6): pp. 2661-2686.
96. Fröhlich, J., Niedermeier, W., and Luginsland, H.-D., *The effect of filler–filler and filler–elastomer interaction on rubber reinforcement.* Composites Part A: Applied Science and Manufacturing, 2005. **36**(4): pp. 449-460.
97. Tosaka, M., Murakami, S., Poompradub, S., Kohjiya, S., Ikeda, Y., Toki, S., Sics, I., and Hsiao, B.S., *Orientation and crystallization of natural rubber network as revealed by WAXD using synchrotron radiation.* Macromolecules, 2004. **37**(9): pp. 3299-3309.
98. Huneau, B., *Strain-induced crystallization of natural rubber: a review of X-ray diffraction investigations.* Rubber Chemistry and Technology, 2011. **84**(3): pp. 425-452.
99. Lindley, P.B., *Relation between hysteresis and the dynamic crack growth resistance of natural rubber.* International Journal of Fracture, 1973. **9**(4): pp. 449-462.

100. Lindley, P.B., *Non-relaxing crack growth and fatigue in a non-crystallizing rubber.* Rubber Chemistry and Technology, 1974. **47**(5): pp. 1253-1264.
101. Donovan, J.A., *Strain Crystallization and Failure of Elastomers.* Japan Rubber Association magazine, 2002. **75**(6): pp. 239-245.
102. Hamed, G.R., *Molecular aspects of the fatigue and fracture of rubber.* Rubber Chemistry and Technology, 1994. **67**(3): pp. 529-536.
103. Candau, N., Chazeau, L., Chenal, J.-M., Gauthier, C., Ferreira, J., Munch, E., and Rochas, C., *Characteristic time of strain induced crystallization of crosslinked natural rubber.* Polymer, 2012. **53**(13): pp. 2540-2543.
104. Mars, W.V. and Fatemi, A., *A literature survey on fatigue analysis approaches for rubber.* International Journal of Fatigue, 2002. **24**(9): pp. 949-961.
105. Lake, G.J. and Lindley, P.B., *Cut growth and fatigue of rubbers. II. Experiments on a noncrystallizing rubber.* Journal of Applied Polymer Science, 1964. **8**(2): pp. 707-721.
106. Gdoutos, E.E., *Fracture mechanics: an introduction*. Vol. 123. 2006: Springer Science & Business Media.
107. Rivlin, R.S. and Thomas, A.G., *Rupture of rubber. I. Characteristic energy for tearing.* Journal of Polymer Science, 1953. **10**(3): pp. 291-318.
108. Gdoutos, E.E., Schubel, P.M., and Daniel, I.M., *Determination of critical tearing energy of tyre rubber.* Strain, 2004. **40**(3): pp. 119-125.
109. Gent, A.N., Lindley, P.B., and Thomas, A.G., *Cut growth and fatigue of rubbers. I. The relationship between cut growth and fatigue.* Journal of Applied Polymer Science, 1964. **8**(1): pp. 455-466.
110. Samsuri, A. and Mat Piah, M.B., *Cyclic crack growth measurement using using split-tear test piece.* Journal of Rubber Research, 2004. **7**(2): pp. 115-126.
111. Gent, A.N., Razzaghi-Kashani, M., and Hamed, G.R., *Why do cracks turn sideways?* Rubber Chemistry and Technology, 2003. **76**(1): pp. 122-131.
112. Halladay, J.R. and Krakowski, F.J., *The use of fatigue crack propagation testing in rubber compound development.* Rubber World, 2009. **239**(4): pp. 28-31.
113. Lake, G.J., *Mechanical fatigue of rubber.* Rubber Chemistry and Technology, 1972. **45**(1): pp. 309-328.
114. Young, D.G., *Application of fatigue methods based on fracture mechanics for tire compound development.* Rubber Chemistry and Technology, 1990. **63**(4): pp. 567-581.

115. Lake, G.J. and Lindley, P.B., *The mechanical fatigue limit for rubber.* Journal of Applied Polymer Science, 1965. **9**(4): pp. 1233-1251.
116. Roche, N. and Perier, L., *Influence of Elastomers Formulation on Fatigue Crack Growth Properties.* Procedia Engineering, 2013. **66**: pp. 705-712.
117. Ellul, M.D., *Mechanical fatigue*, in *Engineering with Rubber, How to Design Rubber Components*, Gent, A.N., Editor. 1992, Hanser: New York. p. 139-176.
118. Lake, G.J. and Thomas, A.G., *Strength.* Engineering with Rubber, How to Design Rubber Components", Munich: Carl Hanser Verlag, 1992.
119. Young, D.G., *Dynamic property and fatigue crack propagation research on tire sidewall and model compounds.* Rubber Chemistry and Technology, 1985. **58**(4): pp. 785-805.
120. Stevenson, A., in *Rubber and Plastic News*. 1988. p. 42.
121. Ponnamma, D., Maria, H.J., Chandra, A.K., and Thomas, S., *Rubber nanocomposites: latest trends and concepts*, in *Advances in elastomers II*, Visakh, P.M., Sabu Thomas, Chandra, A.K., and Mathew, A.P., Editors. 2013, Springer. p. 69-107.
122. Hamed, G.R., *Reinforcement of rubber.* Rubber Chemistry and Technology, 2000. **73**(3): pp. 524-533.
123. Dizon, E.S., Hicks, A.E., and Chirico, V.E., *The effect of carbon black parameters on the fatigue life of filled rubber compounds.* Rubber Chemistry and Technology, 1974. **47**(1): pp. 231-249.
124. Auer, E.E., Doak, K.W., and Schaffner, I.J., *Factors affecting laboratory cut-growth resistance of cold SBR tread stocks.* Rubber Chemistry and Technology, 1958. **31**(1): pp. 185-201.
125. Nie, Y., Wang, B., Huang, G., Qu, L., Zhang, P., Weng, G., and Wu, J., *Relationship between the material properties and fatigue crack-growth characteristics of natural rubber filled with different carbon blacks.* Journal of Applied Polymer Science, 2010. **117**: pp. 3441-3447.
126. Studebaker, M.L. and Beatty, J.R., *The oxidative hardening of SBR.* Rubber Chemistry and Technology, 1972. **45**(2): pp. 450-466.
127. Coran, A.Y., *Vulcanization,* in *Science and Technology of Rubber (Third Edition)*. 2005, Elsevier. p. 321-366.

128. Kim, S.G. and Lee, S.-H., *Effect of crosslink structures on the fatigue crack growth behavior of NR vulcanizates with various aging conditions.* Rubber Chemistry and Technology, 1994. **67**(4): pp. 649-661.
129. Scott, G., *A review of recent developments in the mechanisms of antifatigue agents.* Rubber Chemistry and Technology, 1985. **58**(2): pp. 269-283.
130. Hamed, G.R., *Materials and Compounds—Chapter 2*, in *Engineering with rubber, How to design rubber components*, Gent, A., Editor. 1992, Carl Hanser Verlag: Munich. p. 11-34.
131. Datta, R.N., Huntink, N.M., Datta, S., and Talma, A.G., *Rubber vulcanizates degradation and stabilization.* Rubber Chemistry and Technology, 2007. **80**(3): pp. 436-480.
132. Dweik, H., Abu-Lafi, S., and Scott, G., *The Antioxidant and Antifatigue Activity of Phenothiazine Oxide in Natural Rubber.* Bethlehem University Journal, 2001: pp. 10-19.
133. Baldwin, J.M. and Bauer, D.R., *Rubber oxidation and tire aging-a review.* Rubber Chemistry and Technology, 2008. **81**(2): pp. 338-358.
134. Hamed, G.R. and Zhao, J., *Tensile behavior after oxidative aging of gum and black-filled vulcanizates of SBR and NR.* Rubber Chemistry and Technology, 1999. **72**(4): pp. 721-730.
135. Legorju-Jago, K. and Bathias, C., *Fatigue initiation and propagation in natural and synthetic rubbers.* International Journal of Fatigue, 2002. **24**(2): pp. 85-92.
136. Hu, X., Li, Y., and Liu, X. *Experimental studies of thermal aging effects on the tensile and tearing fracture behavior of carbon black filled rubbers*. in *ICF13*. 2013.
137. Huntink, N.M., *Durability of rubber products.* PhD thesis, 2003, University of Twente.
138. Lake, G.J., *Ozone cracking and protection of rubber.* Rubber Chemistry and Technology, 1970. **43**(5): pp. 1230-1254.
139. Ramesan, M.T., Alex, R., and Khanh, N.V., *Studies on the cure and mechanical properties of blends of natural rubber with dichlorocarbene modified styrene–butadiene rubber and chloroprene rubber.* Reactive and Functional Polymers, 2005. **62**(1): pp. 41-50.

140. Kim, H.J. and Hamed, G.R., *On the reason that passenger tire sidewalls are based on blends of natural rubber and cis-polybutadiene.* Rubber Chemistry and Technology, 2000. **73**(4): pp. 743-752.
141. Wunde, M. and Klüppel, M., *Influence of phase morphology and phase morphology and filler distribution in NR/BR and NR/SBR blends on fracture mechanical properties.* Rubber Chemistry and Technology, 2016. **89**(4): pp. 588-607.
142. Ghosh, P., Stocek, R., Gehde, M., Mukhopadhyay, R., and Krishnakumar, R., *Investigation of fatigue crack growth characteristics of NR/BR blend based tyre tread compounds.* International Journal of Fracture, 2014. **188**(1): pp. 9-21.
143. Menon, A.R.R., Pillai, C.K.S., Jin, W.S., and Nah, C., *Fatigue resistance of silica-filled natural rubber vulcanizates: comparative study of the effect of phosphorylated cardanol prepolymer and a silane coupling agent.* Polymer International, 2005. **54**(4): pp. 629-635.
144. Karabork, F. and Akdemir, A., *Friction and wear behavior of styrene butadiene rubber-based composites reinforced with microwave-devulcanized ground tire rubber.* Journal of Applied Polymer Science, 2015. **132**(33): pp. 42419.
145. Muhr, A.H. and Roberts, A.D., *Rubber abrasion and wear.* Wear, 1992. **158**(1-2): pp. 213-228.
146. Han, S.-C. and Han, M.-H., *Fracture behavior of NR and SBR vulcanizates filled with ground rubber having uniform particle size.* Journal of Applied Polymer Science, 2002. **85**(12): pp. 2491-2500.
147. Burford, R.P. and Pittolo, M., *Characterization and performance of powdered rubber.* Rubber Chemistry and Technology, 1982. **55**(5): pp. 1233-1249.
148. Phadke, A.A., Chakraborty, S.K., and De, S.K., *Cryoground rubber-natural rubber blends.* Rubber Chemistry and Technology, 1984. **57**(1): pp. 19-33.
149. Kumar, P., Fukahori, Y., Thomas, A.G., and Busfield, J.J.C., *Recycled rubber: The rubber granulate-virgin rubber interface.* Rubber Chemistry and Technology, 2007. **80**(1): pp. 24-39.
150. Stoček, R., Gehde, M., Michael, H., and Maňas, S., *Determination of fatigue behaviour and crack propagation of filled vulcanized rubber.* Material Science and Technology, 2008. **4**: pp. 105-112.

151. Ayyer, R., Rosenmayer, T., Schreiber, W., and Colton, J., *Effects of micronized rubber powders on structure and properties of polypropylene composites.* Waste and Biomass Valorization, 2013. **4**(1): pp. 65-71.
152. *ImageJ*. [accessed 2016]; Available from: https://imagej.nih.gov/ij/.
153. Leung, C., *Development of a Composite Material using Rubber Crumb.* MSc thesis, September 2007, University of Plymouth. Plymouth.
154. Datta, S., Stoček, R., Kuřitka, I., and Sáha, P., *Determination of compounding formulation of cured rubber by reverse engineering.* Polymer Engineering & Science, 2015. **55**(6): pp. 1450-1458.
155. *Tire Investment, Recovery and Extension Act of 2007, House of Representatives HR5103, US Government* 2008 [accessed 2016]; Available from: https://www.congress.gov/bill/110th-congress/house-bill/5103/text.
156. Burford, R.P. and Pittolo, M., *Mode of crack propagation in rubber-crumb-filled polymer composition.* Journal of Materials Science Letters, 1987. **6**(8): pp. 969-971.
157. Gibala, D., Thomas, D., and Hamed, G.R., *Cure and mechanical behavior of rubber compounds containing ground vulcanizates: part III. Tensile and tear strength.* Rubber Chemistry and Technology, 1999. **72**(2): pp. 357-360.
158. Swor, R.A., Jensen, L.W., and Budzol, M., *Ultrafine recycled rubber.* Rubber Chemistry and Technology, 1980. **53**(5): pp. 1215-1225.
159. Phadke, A.A. and De, S.K., *Use of cryoground reclaimed rubber in natural rubber.* Conservation & Recycling, 1986. **9**(3): pp. 271-280.
160. Halim, M.H., *Truck tyre tread rubber: compounding and abrasion resistance.* PhD thesis, 1990, Loughborough University.
161. Bonfanti, A., *Study of the fracture behavior of natural rubber and polybutadiene based compounds: structure to properties correlation.* Master degree, 2014, Politecnico Di Milano.
162. Ghosh, P., Mukhopadhyay, R., Kankroli, R., and Stoček, R., *Durability prediction of NR/BR and NR/SBR blend tread compounds using Tear Fatigue Analyser.* Kautschuk Gummi Kunststoffe, 2016.
163. Sarkawi, S.S., Dierkes, W.K., and Noordermeer, J.W.M., *Elucidation of filler-to-filler and filler-to-rubber interactions in silica-reinforced natural rubber by TEM Network Visualization.* European polymer journal, 2014. **54**: pp. 118-127.

164. Kamaruddin, S., *Long-term mechanical properties of rubber.* PhD thesis, 2013, University of Southampton.
165. Smith, C.L., *Basic confocal microscopy.* Current protocols in neuroscience, 2011: pp. 2.2.1-2.2.13.
166. Sae-oui, P., Sirisinha, C., and Thaptong, P., *Utilization of limestone dust waste as filler in natural rubber.* Journal of Material Cycles and Waste Management, 2009. **11**(2): pp. 166-171.
167. Gibala, D., Laohapisitpanich, K., Thomas, D., and Hamed, G.R., *Cure and Mechanical Behavior of Rubber Compounds Containing Ground Vulcanizates. Part II—Mooney Viscosity.* Rubber Chemistry and Technology, 1996. **69**(1): pp. 115-119.
168. Batchelor, G.K. and Green, J.T., *The determination of the bulk stress in a suspension of spherical particles to order c 2.* Journal of Fluid Mechanics, 1972. **56**(3): pp. 401-427.
169. Gent, A.N. and Zhang, L.Q., *Strain‐induced crystallization and strength of elastomers. I. cis‐1, 4‐polybutadiene.* Journal of Polymer Science Part B: Polymer Physics, 2001. **39**(7): pp. 811-817.
170. Kang, M.K., Jeon, H.-J., Song, H.H., and Kwag, G., *Strain-induced crystallization of blends of natural rubber and ultra high cis polybutadiene as studied by synchrotron X-ray diffraction.* Macromolecular Research, 2016. **24**(1): pp. 31-36.
171. Gibala, D. and Hamed, G.R., *Cure and mechanical behavior of rubber compounds containing ground vulcanizates. Part I-Cure behavior.* Rubber Chemistry and Technology, 1994. **67**(4): pp. 636-648.
172. Mathew, G., Singh, R.P., Lakshminarayanan, R., and Thomas, S., *Use of natural rubber prophylactics waste as a potential filler in styrene–butadiene rubber compounds.* Journal of Applied Polymer Science, 1996. **61**(11): pp. 2035-2050.
173. Le Cam, J.-B. and Toussaint, E., *The mechanism of fatigue crack growth in rubbers under severe loading: the effect of stress-induced crystallization.* Macromolecules, 2010. **43**(10): pp. 4708-4714.
174. Beurrot, S., Huneau, B., and Verron, E., *In situ SEM study of fatigue crack growth mechanism in carbon black‐filled natural rubber.* Journal of Applied Polymer Science, 2010. **117**(3): pp. 1260-1269.

175. Munoz, L., Vanel, L., Sanseau, O., Sotta, P., Long, D., Odoni, L., and Guy, L., *Fatigue crack growth dynamics in filled natural rubber.* Plastics, Rubber and Composites, 2012. **41**(7): pp. 273-276.

176. Agarwal, K., Setua, D.K., and Sekhar, K., *Scanning electron microscopy study on the influence of temperature on tear strength and failure mechanism of natural rubber vulcanizates.* Polymer Testing, 2005. **24**(6): pp. 781-789.

177. Pal, P.K. and De, S.K., *Studies of Polymer-Filler Interaction, Network Structure, Physical Properties, and Fracture of Silica-and Clay-Filled EPDM Rubber in the Presence of a Silane Coupling Agent.* Rubber Chemistry and Technology, 1983. **56**(4): pp. 737-773.

178. Schuster, R.H., Meier, J., and Klüppel, M., *The role of interphase in filler partition in rubber blends.* Kautschuk Gummi Kunststoffe, 2000. **53**(11): pp. 663-674.

179. Ma, J.-H., Zhang, L.-Q., and Wu, Y.-P., *Characterization of filler-rubber interaction, filler network structure, and their effects on viscoelasticity for styrene-butadiene rubber filled with different fillers.* Journal of Macromolecular Science, Part B:Physics, 2013. **52**(8): pp. 1128-1141.

180. Cook, S., Cudby, P.E.F., and Tinker, A.J. *Direct observation of crosslink distribution in vulcanized blends through visualizing the networks*. in *142nd Fall Meeting of the Rubber Division*. 1992. Nashville, TN: Rubber Division, ACS.

181. Cook, S., Cudby, P.E.F., Tinker, A.J., and Bomal, Y. *Network visualisation of elastomer vulcanizates*. in *156th Fall Meeting of the Rubber Division*. 1999. Orlando, FL: ACS.

182. Tinker, A.J., in *Blends of Natural Rubber-Novel techniques for blending with speciality polymers*, Tinker, A.J. and Jones, K.P., Editors. 1998, Chapman and Hall: London. p. 8-20.

183. Ladouce-Stelandre, L., Bomal, Y., Flandin, L., and Labarre, D., *Dynamic mechanical properties of precipitated silica filled rubber: Influence of morphology and coupling agent.* Rubber Chemistry and Technology, 2003. **76**(1): pp. 145-159.

184. Martin, P.J., Brown, P., Chapman, A.V., and Cook, S., *Silica-reinforced epoxidized natural rubber tire treads-performance and durability.* Rubber Chemistry and Technology, 2015. **88**(3): pp. 390-411.

185. Burford, R.P. and Pittolo, M., *Fracture morphology of rubber compounds containing recycled rubber powder.* Journal of Materials Science Letters, 1983. **2**(8): pp. 422-424.

186. Ten Brinke, A., *Silica reinforced tyre rubbers.* PhD thesis, 2002, University of Twente.
187. Ismail, H., Salleh, S.Z., and Ahmad, Z., *Fatigue and hysteresis behavior of halloysite nanotubes‐filled natural rubber (SMR L and ENR 50) nanocomposites.* Journal of Applied Polymer Science, 2013. **127**(4): pp. 3047-3052.
188. Zaimova, D., Bayraktar, E., Miskioglu, I., Katundi, D., and Dishovsky, N., *Manufacturing of New Elastomeric Composites: Mechanical Properties, Chemical and Physical Analysis*, in *Composite, Hybrid, and Multifunctional Materials*, Tandon, G., Editor. 2015, Springer.
189. Groves, S.A., *Crosslink density distributions in NR/BR blends: effect of cure temperature and time.* Rubber chemistry and technology, 1998. **71**(5): pp. 958-965.
190. Fei, Z., Long, C., Qingyan, P., and Shugao, Z., *Influence of carbon black on crosslink density of natural rubber.* Journal of Macromolecular Science, Part B, 2012. **51**(6): pp. 1208-1217.
191. Muniandy, K., Ismail, H., and Othman, N., *Effects of partial replacement of rattan powder by commercial fillers on the properties of natural rubber composites.* BioResources, 2012. **7**(4): pp. 4640-4657.
192. Fukahori, Y., *Carbon black reinforcement of rubber (1): general rules of reinforcement.* International Polymer Science and Technology, 2004. **31**(8): pp. 11-17.
193. Pittolo, M. and Burford, R.P., *The mechanical properties of rubber compounds containing soft fillers.* Journal of Materials Science, 1984. **19**(10): pp. 3330-3336.
194. Clarke, J., Clarke, B., and Freakley, P.K., *Relationships between mixing method, microstructure and strength of NR: BR blends.* Rubber Chemistry and Technology, 2001. **74**(1): pp. 1-15.
195. Reincke, K., Grellmann, W., Lach, R., and Heinrich, G., *Toughness optimization of SBR elastomers–use of fracture mechanics methods for characterization.* Macromolecular Materials and Engineering, 2003. **288**(2): pp. 181-189.
196. Hamed, G.R., Kim, H.J., and Gent, A.N., *Cut growth in vulcanizates of natural rubber, cis-polybutadiene, and a 50/50 blend during single and repeated extension.* Rubber Chemistry and Technology, 1996. **69**(5): pp. 807-818.
197. Lorenz, O. and Parks, C.R., *The crosslinking efficiency of some vulcanizing agents in natural rubber.* Journal of Polymer Science, 1961. **50**(154): pp. 299-312.

198. Da Costa, H.M., Visconte, L.L.Y., Nunes, R.C.R., and Furtado, C.R.G., *Mechanical and dynamic mechanical properties of rice husk ash–filled natural rubber compounds.* Journal of applied polymer science, 2002. **83**(11): pp. 2331-2346.

199. Kraus, G., *Swelling of filler‐reinforced vulcanizates.* Journal of Applied Polymer Science, 1963. **7**(3): pp. 861-871.

200. Mathew, G., Singh, R.P., Nair, N.R., and Thomas, S., *Recycling of natural rubber latex waste and its interaction in epoxidised natural rubber.* Polymer, 2001. **42**(5): pp. 2137-2165.

201. Grosch, K.A., *Rubber abrasion and tire wear.* Rubber Chemistry and Technology, 2008. **81**(3): pp. 470-505.

202. Mathew, N.M. and De, S.K., *Scanning electron microscopy studies in abrasion of NR/BR blends under different test conditions.* Journal of Materials Science, 1983. **18**(2): pp. 515-524.

203. Arayapranee, W., in *Abrasion Resistance of Materials*, Adamiak, M., Editor. 2012, InTechOpen. p. 147-166.

204. Rattanasom, N. and Chaikumpollert, O., *Crack growth and abrasion resistance of carbon black‐filled purified natural rubber vulcanizates.* Journal of Applied Polymer Science, 2003. **90**(7): pp. 1793-1796.

205. Mutagahywa, B.M., *Carbon black dispersion in rubber assessment methods and process studies.* PhD thesis, 1984, Loughborough University.

206. Holland, G.W., Hu, B., and Holland, S., *Surface area measurement of ground rubber using the BET surface area analyzer.* Rubber World, 1994. **210**(2): pp. 29-33.

207. Hong, C.K., Kim, H., Ryu, C., Nah, C., Huh, Y.-i., and Kaang, S., *Effects of particle size and structure of carbon blacks on the abrasion of filled elastomer compounds.* Journal of Materials Science, 2007. **42**(20): pp. 8391-8399.

208. Harwood, J.A.C., *Hysteresis in rubbers and its influence on strength.* Journal of Applied Chemistry, 1967. **17**(11): pp. 333-338.

209. Griffith, A.A., *AA Griffith, Philos. Trans. R. Soc. London, Ser. A 221, 163 (1920).* Philos. Trans. R. Soc. London, Ser. A, 1920. **221**: pp. 163.

210. Le Cam, J.-B., Huneau, B., Verron, E., and Gornet, L., *Mechanism of fatigue crack growth in carbon black filled natural rubber.* Macromolecules, 2004. **37**(13): pp. 5011-5017.

211. Ruellan, B., Le Cam, J.-B., Robin, E., Jeanneau, I., Canévet, F., Mauvoisin, G., and Loison, D., *Fatigue crack growth in natural rubber: The role of SIC investigated through post-mortem analysis of fatigue striations.* Engineering Fracture Mechanics, 2018.

212. Tee, Y.L., Loo, M.S., and Andriyana, A., *Recent advances on fatigue of rubber after the literature survey by Mars and Fatemi in 2002 and 2004.* International Journal of Fatigue, 2018. **110**: pp. 115-129.

213. Reincke, K., Grellmann, W., and Heinrich, G., *Investigation of mechanical and fracture mechanical properties of elastomers filled with precipitated silica and nanofillers based upon layered silicates.* Rubber Chemistry and Technology, 2004. **77**(4): pp. 662-677.

214. Dong, B., Liu, C., and Wu, Y.-P., *Fracture and fatigue of silica/carbon black/natural rubber composites.* Polymer Testing, 2014. **38**: pp. 40-45.

215. *ABSnake plugins*. [accessed 2016]; Available from: http://imagejdocu.tudor.lu/doku.php?id=plugin:segmentation:active_contour:start.

216. Poisson, J.L., Orlando, V., and Muhr, A.H. *The impact of strain history on crack growth of rubber*. in *Tire Technology Expo Conference* 2018. Hannover, Germany.

217. Tavares, P.J., Viriato, N.S., and Moreira, P.M.G.P. *An Automated Method for the Measurement of Fatigue Crack Progression*. in *Key Engineering Materials*. 2014. Trans Tech Publ.

218. Zarrin‐Ghalami, T. and Fatemi, A., *Material deformation and fatigue behavior characterization for elastomeric component life predictions.* Polymer Engineering & Science, 2012. **52**(8): pp. 1795-1805.

219. Kim, J.-H. and Jeong, H.-Y., *A study on the material properties and fatigue life of natural rubber with different carbon blacks.* International Journal of Fatigue, 2005. **27**(3): pp. 263-272.

220. Wang, M.-J., *The role of filler networking in dynamic properties of filled rubber.* Rubber Chemistry and Technology, 1998. **72**(2): pp. 430-448.

221. Bolotin, V.V., *Mechanics of fatigue*. Vol. 11. 1999: CRC Press.

222. Dong, B., Liu, C., Zhang, L., and Wu, Y., *Preparation, fracture, and fatigue of exfoliated graphene oxide/natural rubber composites.* RSC Advances, 2015. **5**(22): pp. 17140-17148.

223. Payne, A.R., *Hysteresis in rubber vulcanizates.* Journal of Polymer Science:Polymer Symposia, 1974. **48**(1): pp. 169-196.
224. Marano, C., Boggio, M., Cazzoni, E., and Rink, M., *Fracture phenomenology and toughness of filled natural rubber compounds via the pure shear test specimen.* Rubber Chemistry and Technology, 2014. **87**(3): pp. 501-515.
225. Weng, G., Yao, H., Chang, A., Fu, K., Liu, Y., and Chen, Z., *Crack growth mechanism of natural rubber under fatigue loading studied by a real-time crack tip morphology monitoring method.* RSC Advances, 2014. **4**(83): pp. 43942-43950.
226. Papadopoulos, I., *Predicting the fatigue life of elastomer components.* PhD thesis, 2006, Queen Mary University of London.
227. Van Der Horst, M., McGill, W.J., and Woolard, C.D., *The tensile properties of strain‐crystallizing vulcanizates. II. Stress relaxation and hysteresis.* Journal of Applied Polymer Science, 2006. **101**(4): pp. 2423-2430.
228. Lake, G.J., *Fatigue and fracture of elastomers.* Rubber Chemistry and Technology, 1995. **68**(3): pp. 435-460.
229. Dong, B., Liu, C., Lu, Y., and Wu, Y., *Synergistic effects of carbon nanotubes and carbon black on the fracture and fatigue resistance of natural rubber composites.* Journal of Applied Polymer Science, 2015. **132**(25).
230. Lee, M.P. and Moet, A., *Analysis of fatigue crack propagation in NR/BR rubber blend.* Rubber Chemistry and Technology, 1993. **66**(2): pp. 304-316.
231. Hainsworth, S.V., *An environmental scanning electron microscopy investigation of fatigue crack initiation and propagation in elastomers.* Polymer Testing, 2007. **26**(1): pp. 60-70.
232. Busfield, J.J.C., Ratsimba, C.H., and Thomas, A.G., *Crack growth and strain induced anisotropy in carbon black filled natural rubber.* Journal of Natural Rubber Research, 1997. **12**(3): pp. 131-141.
233. Young, D.G., *Fatigue crack propagation in elastomer compunds: Effects of strain rate, temperature, strain level, and oxidation*. Vol. 59. 1986. 809-825.
234. Cadwell, S.M., Merrill, R.A., Sloman, C.M., and Yost, F.L., *Dynamic fatigue life of rubber.* Industrial & Engineering Chemistry Analytical Edition, 1940. **12**(1): pp. 19-23.

235. Summerscales, J., Guild, F.J., Pearce, N.R.L., and Russell, P.M., *Voronoi cells, fractal dimensions and fibre composites.* Journal of Microscopy, 2001. **201**(2): pp. 153-162.

APPENDIX A – Particle size analysis of dispersed RRP in rubber matrix using imageJ [152]

1. Draw a straight line along the scale bar or calibration scale of an image and select Analyse> Set scale measurement
2. Select Process > Filters > Gaussian blur to reduce *noise*
3. Select Process > Binary > Option to uncheck box for 'black background' to set a black image (count 255) on a white background (count 0)
4. Manual thresholding an original picture to a binary image (black and white, image)

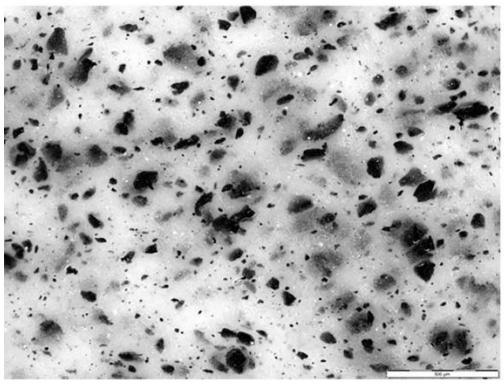

Original picture (set to 8-bit image type)

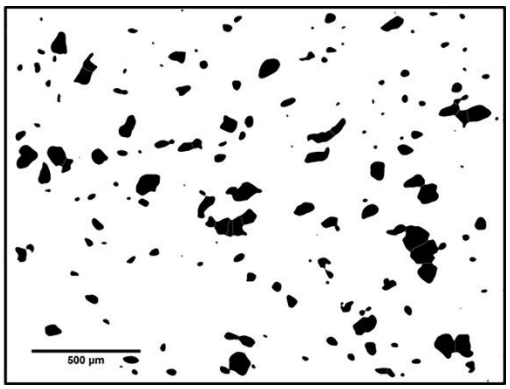

Binary image

5. Select Analyse > Set measurements to select the required parameter such as area and shape descriptors. For example *Circ.* (circularity): 4π*area/perimeter^2. A value of 1.0 indicates a perfect circle. As the value approaches 0.0, it indicates an increasingly elongated shape (https://imagej.nih.gov/ij/docs/guide/146-30.html)
6. Select Process > Make binary > watershed (if necessary to separate 'touching' particles)
7. Select Analyse > Analyse particles, set a limit, in this case 100 μm^2 to avoid any stray pixels on the image and excludes image on edges
8. Based on circular equivalent area irrespective of any shape appearing in the region of interest. An approximate diameter of the particle size (d) was calculated using, $d = 2\sqrt{(A/\pi)}$, where the image particle area (A) automatically measured by the imageJ software.
9. The particle size diameter data was then analysed using the Microsoft Excel data analysis (cumulative frequency and a histogram).

APPENDIX B – Outline of rubber compounds preparation

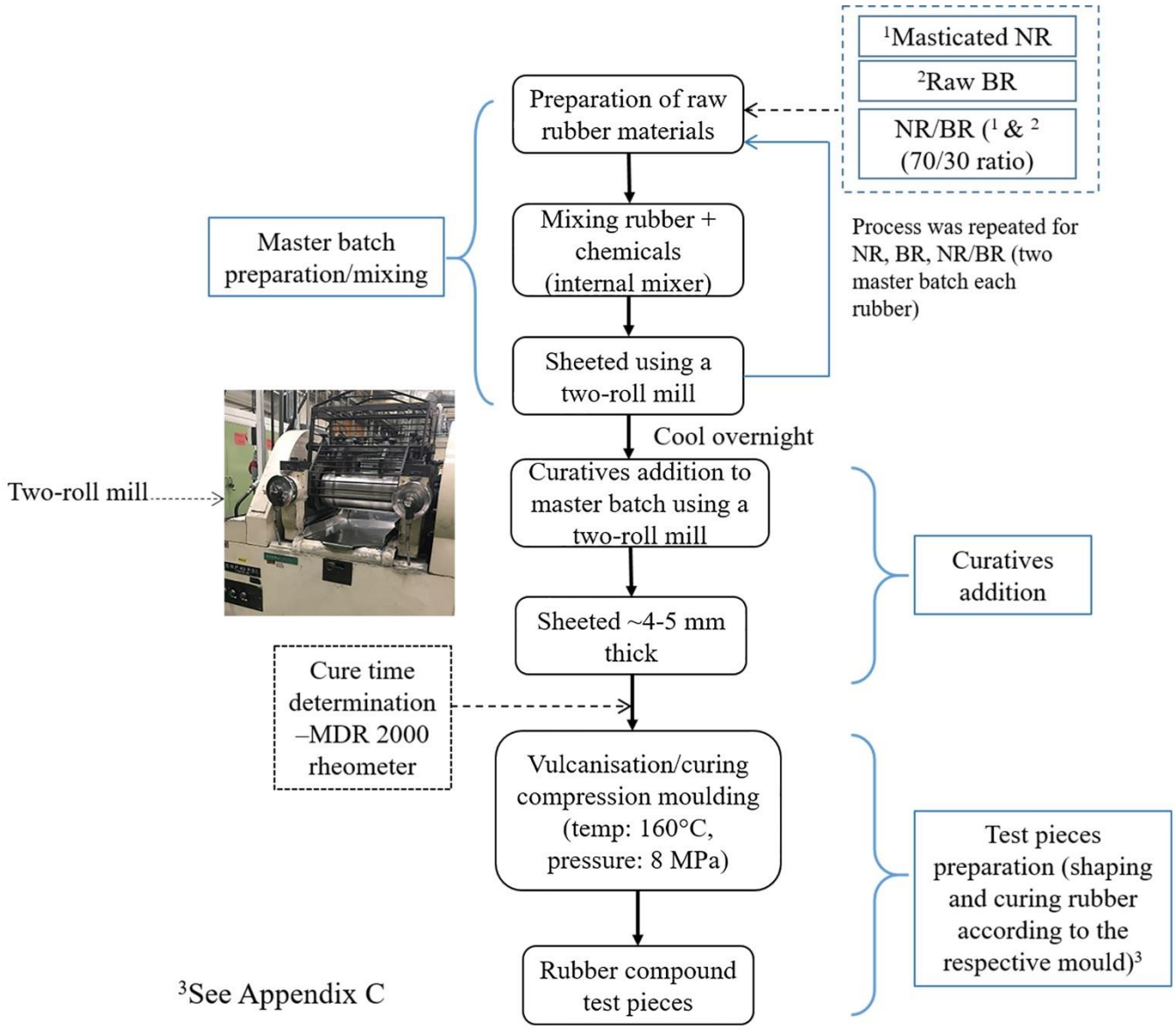

APPENDIX C – Rubber moulds and specimen dimensions

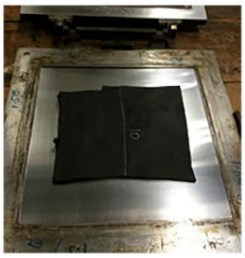

Rubber slab/sheet mould
Sample dimension:
229 x 229 x 2 mm thick

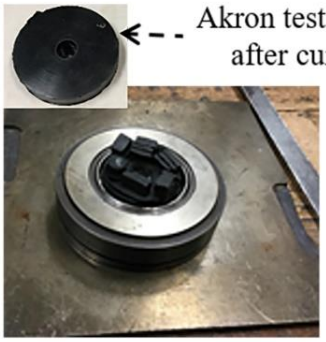

Akron abrasion mould
Sample dimension:
64 mm dia x 12.5 mm thick
Centre hole (12.7 mm dia)

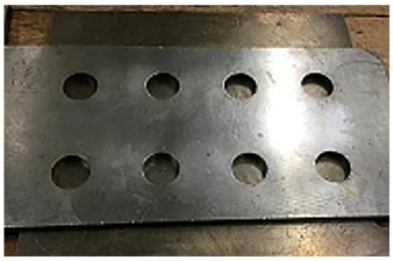

Hardness mould
Sample dimension:
25 mm dia x 6 mm thick

Image analysis test piece
mould
Sample dimension:
13 mm dia x 6 mm thick

DIN abrasion mould
Sample dimension:
15 mm dia x 8 mm
thick

APPENDIX D – Cure curves graph of NR, BR or NR/BR (reference from page 98)

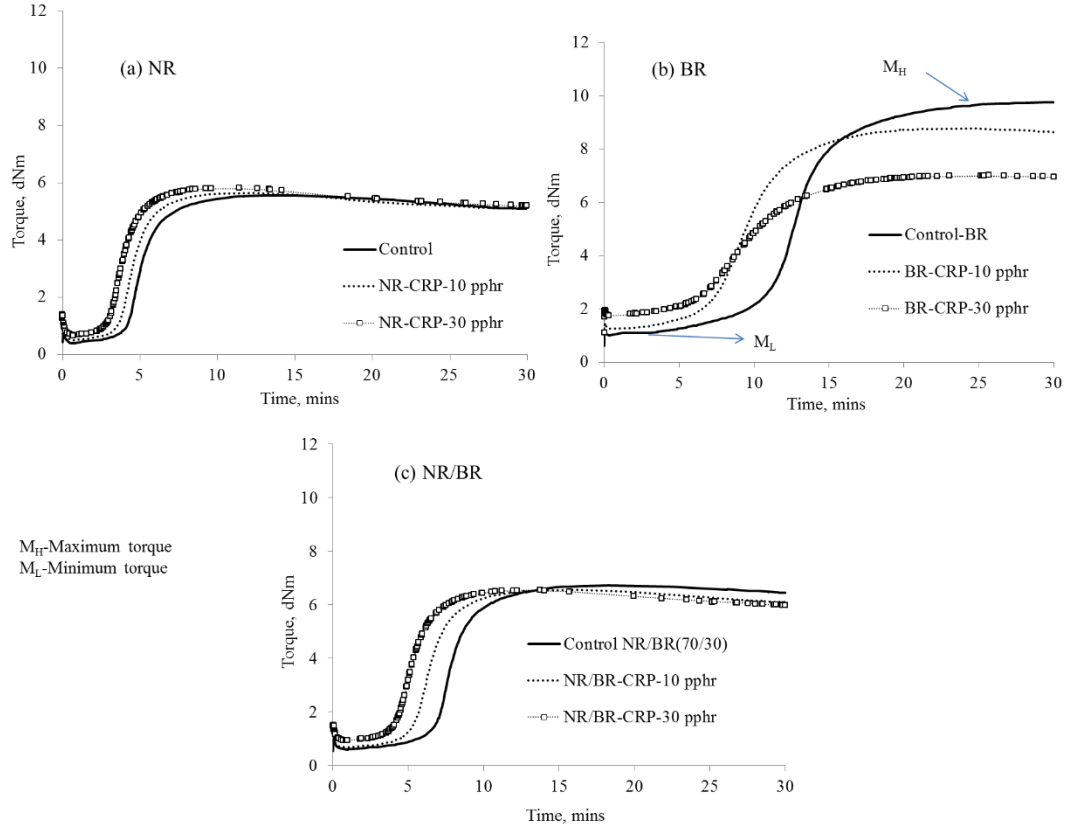

I. Cure curves of unfilled NR, BR or NR/BR containing 10 or 30 pphr of CRP400

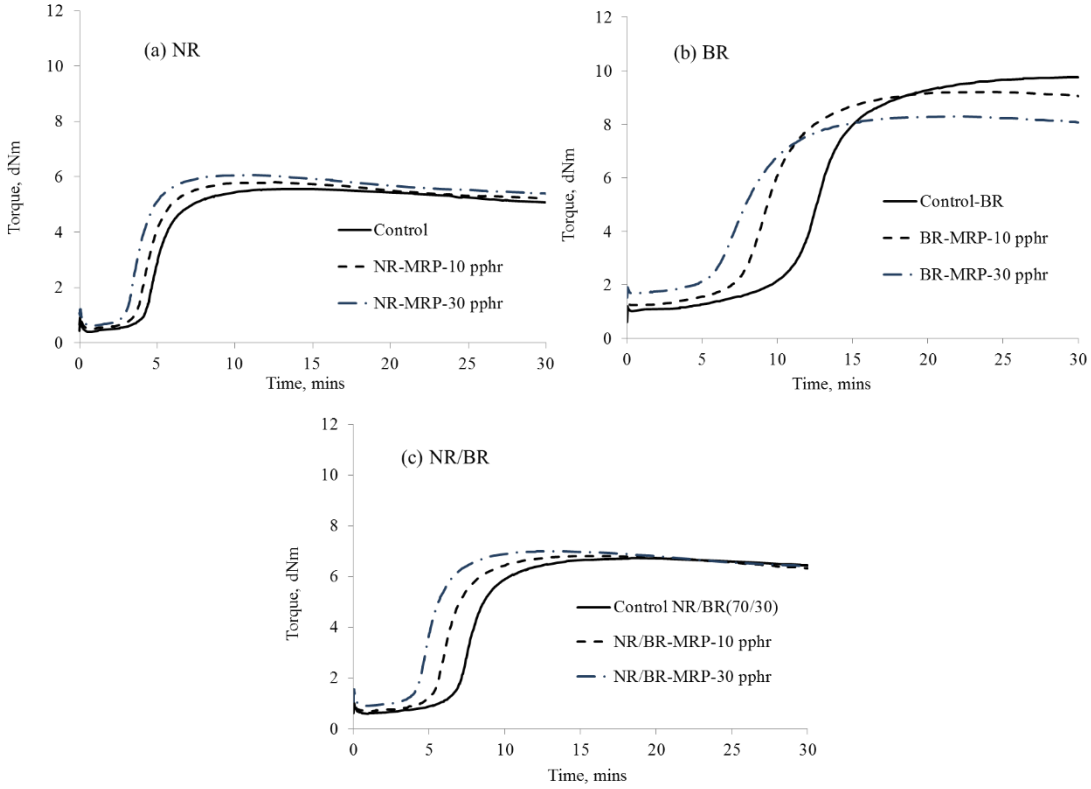

II. Cure curves of unfilled NR, BR or NR/BR containing 10 or 30 pphr of MRP074

III. Basic cure characteristics of unfilled NR, BR or NR/BR blends filled with CRP400 or MRP074

Mix	NR			BR			NR/BR		
	t_{s2}	t_{95}	Δ torque, (M_H-M_L), dNm	t_{s2}	t_{95}	Δ torque, (M_H-M_L), dNm	t_{s2}	t_{95}	Δ torque, (M_H-M_L), dNm
	(min:sec)								
0	4:47	8:43	5.17	11:24	20:22	8.74	7:23	12:19	6.13
CRP-10	4:17	7:31	5.15	8:11	16:05	7.52	6:00	10:07	5.88
CRP-30	3:40	6:46	5.16	8:25	17:00	5.27	4:53	8:34	5.61
MRP-10	4:14	7:30	5.32	8:22	15:49	7.98	5:55	10:22	6.13
MRP-30	3:34	6:34	5.45	6:54	14:11	6.61	4:43	8:31	6.10

t_{95} – Time at 95% of the maximum torque rise

t_{s2} – Time for torque to rise 2 units above M_L

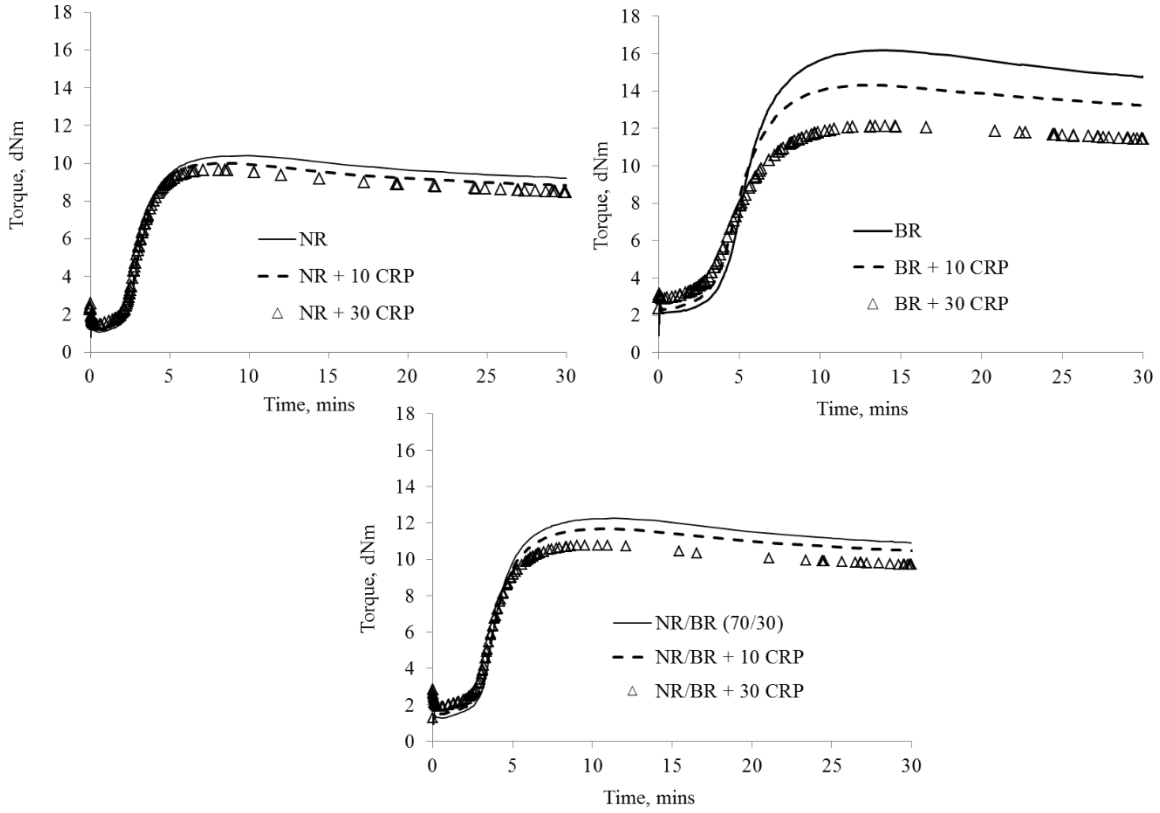

IV. Cure curves of carbon-filled NR, BR or NR/BR containing 10 or 30 pphr of CRP400

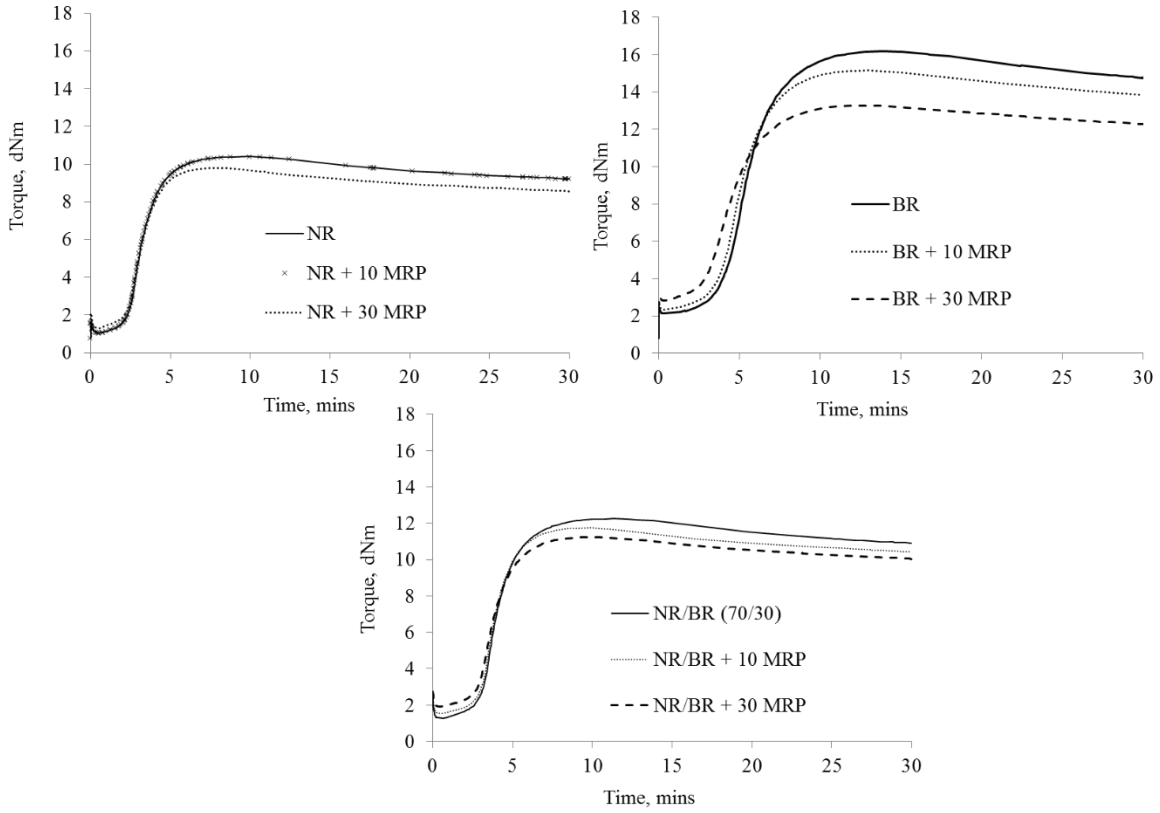

V. Cure curves of carbon-filled NR, BR or NR/BR containing 10 or 30 pphr of MRP074

VI. Basic cure characteristics of carbon-filled NR, BR or NR/BR blends containing CRP400 or MRP074

Mix	NR			BR			NR/BR		
	t_{s2}	t_{95}	Δ torque, (M_H-M_L), dNm	t_{s2}	t_{95}	Δ torque, (M_H-M_L), dNm	t_{s2}	t_{95}	Δ torque, (M_H-M_L), dNm
	(min:sec)								
0	2:39	5:52	9.35	4:02	9:34	14.06	3:16	7:10	10.97
CRP-10	2:37	5:28	8.83	3:45	9:01	12.0	3:14	7:04	10.18
CRP-30	2:35	5:18	8.20	3:40	9:28	9.22	3:08	6:41	8.88
MRP-10	2:41	5:33	9.02	3:52	8:49	12.82	3:14	6:28	10.21
MRP-30	2:38	5:21	8.48	3:19	8:31	10.45	3:10	6:39	9:33

t_{95} – Time at 95% of the maximum torque rise

t_{s2} – Time for torque to rise 2 units above M_L

APPENDIX E – Lorenz-Park equation - The parameter *a*, obtained from gradient of the plot Q_f/Q_g *vs* e^{-z}

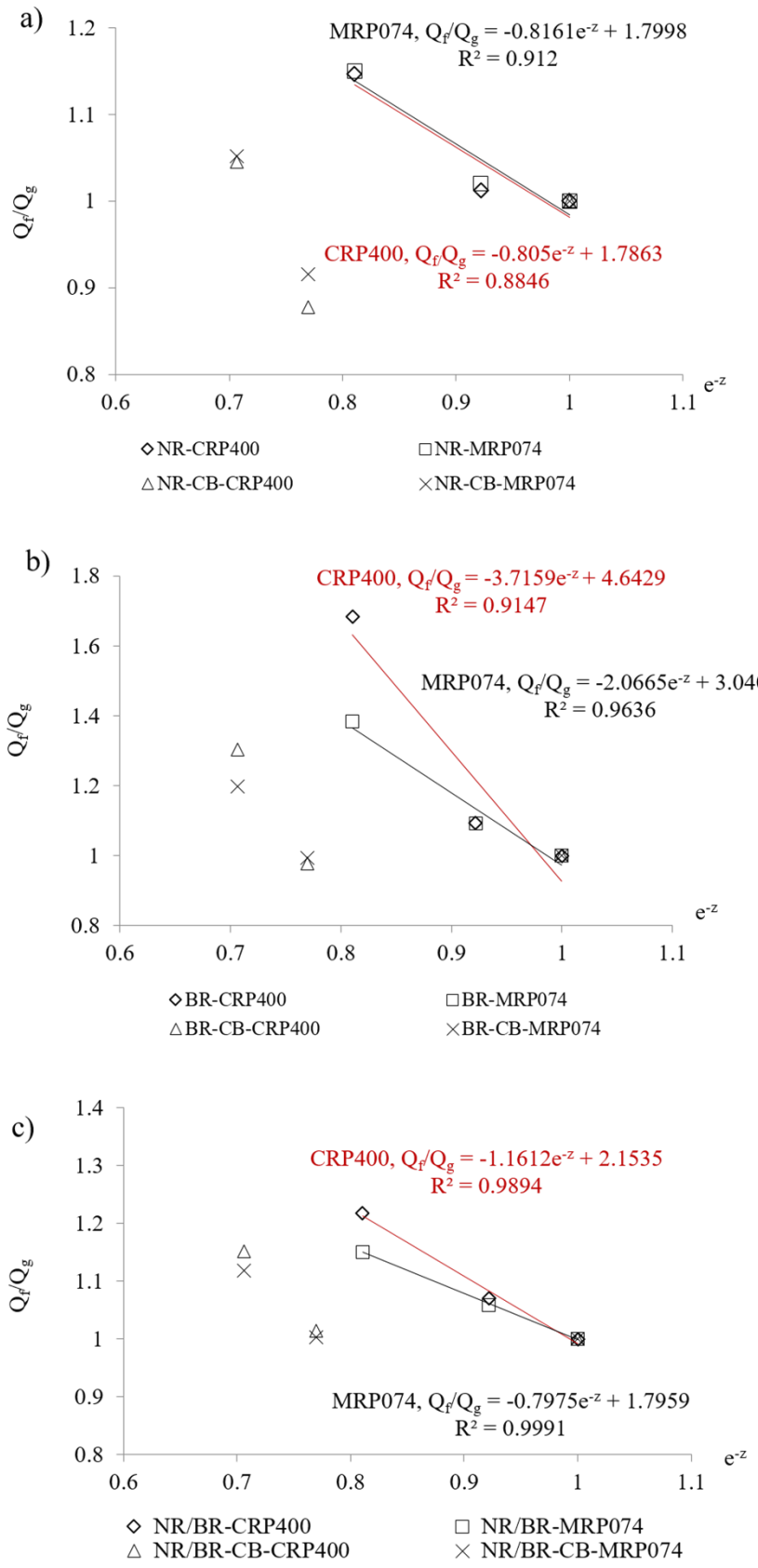

RRP-unfilled and RRP-CB-filled compound

a) NR
b) BR
c) NR/BR

Notes: A deviation from a straight line of Eq. 7.2, occurred at higher concentrations of RRP in carbon-black filled compound, probably indicating the onset of dewetting and void formation.

APPENDIX F – Cunnen and Russel equation - The parameter *a*, obtained from gradient of the plot V_{ro}/V_{rf} *vs* e^{-z}

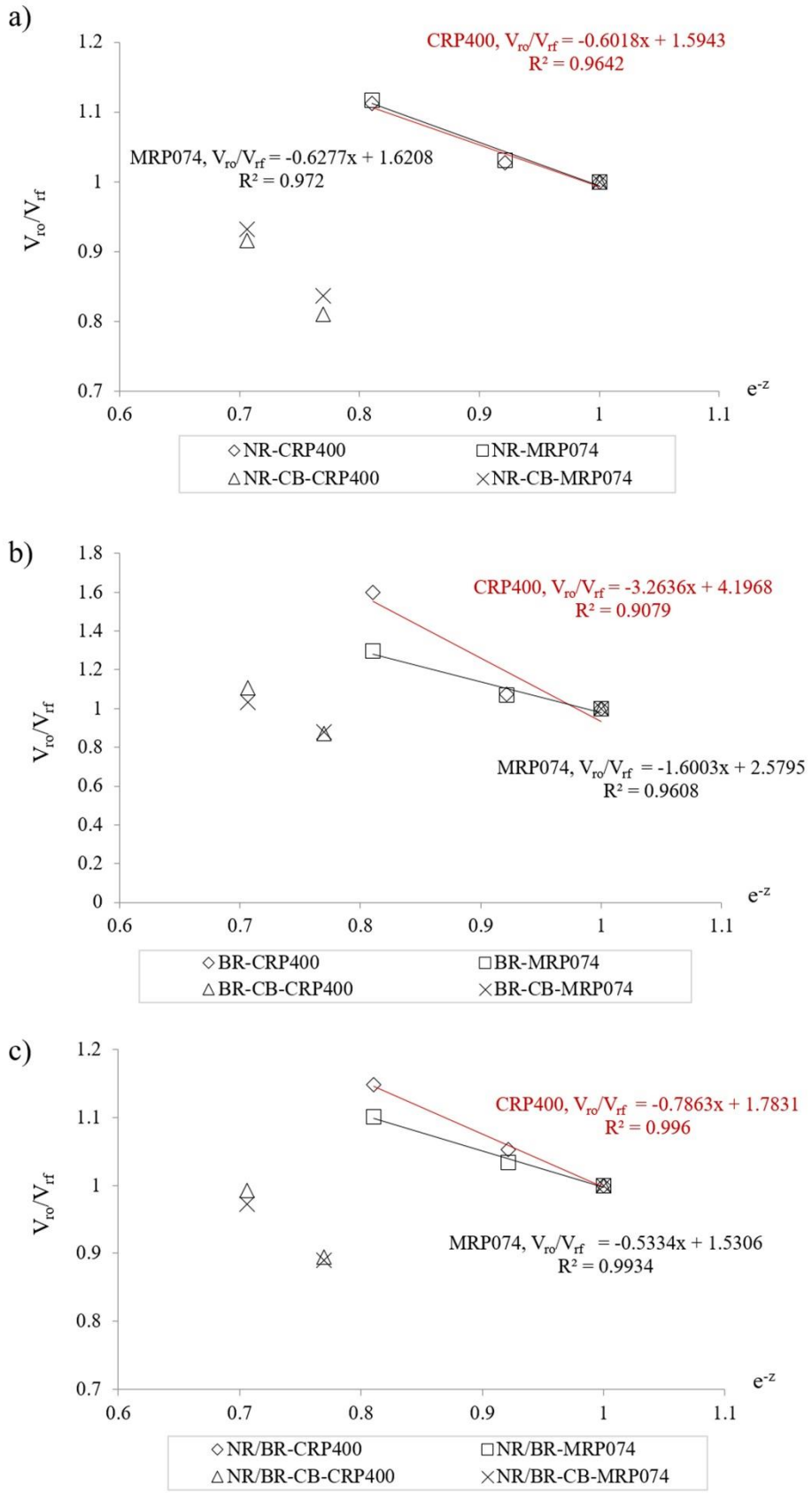

RRP-unfilled and RRP-CB-filled compound

a) NR
b) BR
c) NR/BR

Notes: A deviation from a straight line of Eq. 7.2, occurred at higher concentrations of RRP in carbon-black filled compound, probably indicating the onset of dewetting and void formation.